



UiT The Arctic University of Norway

Faculty of Health Sciences

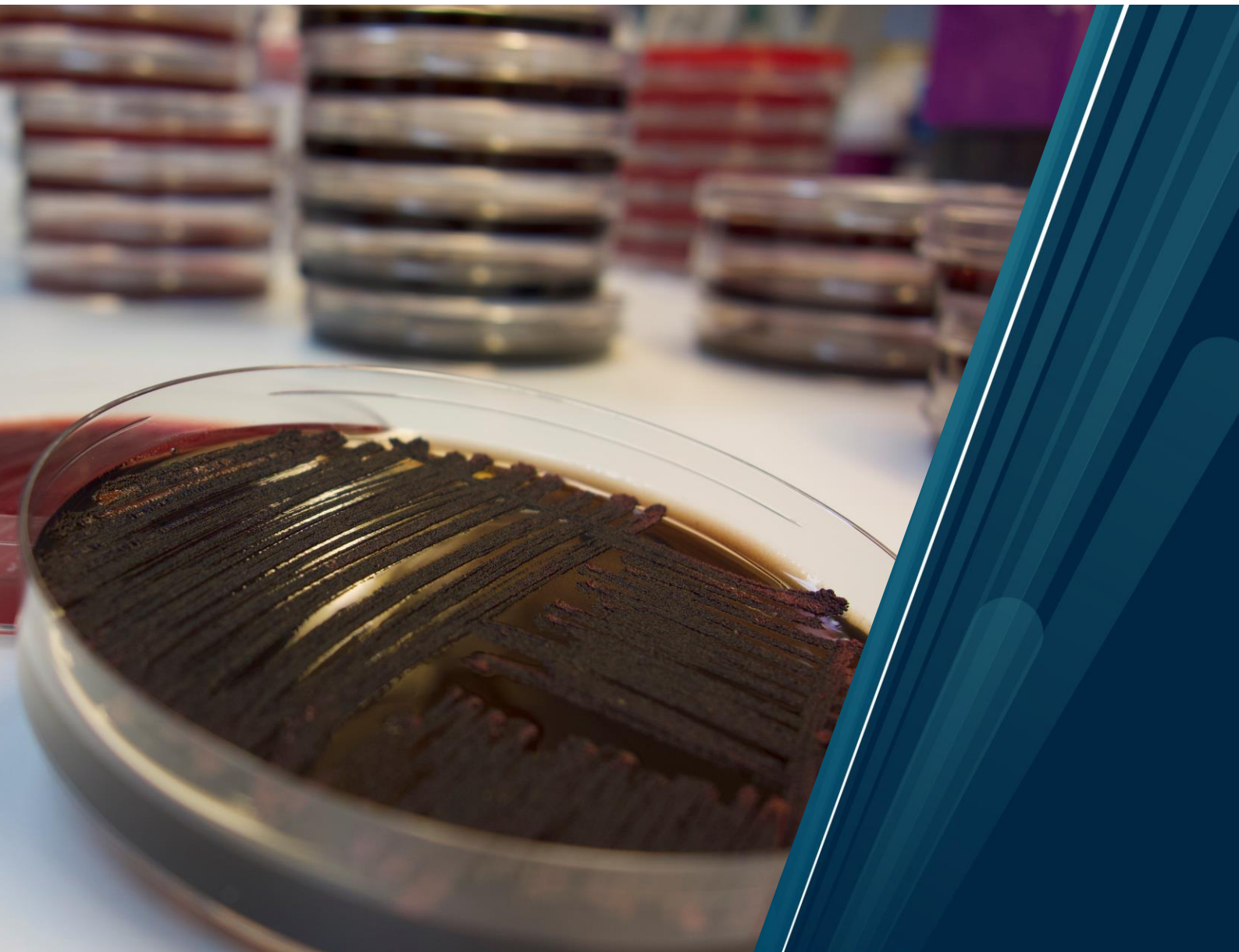
Department of Medical Biology

## **Antimicrobial activity and mode of action**

Examples from natural products, peptides, and peptidomimetics

Eric Juskewitz

A dissertation for the degree of Philosophiae Doctor, June 2022



*A dissertation for the degree of Philosophiae Doctor*

## **Antimicrobial activity and mode of action**

### **Examples from natural products, peptides, and peptidomimetics**

**Eric Juskewitz**



**June 2022**

The work for this thesis was carried out from November 2017 to June 2022 at the Host-Microbe Interactions research group, Department of Medical Biology, Faculty of Health Sciences, UiT – The Arctic University of Norway. The work was part of the DigiBiotics project funded by the Research Council of Norway (via the Centre for Digital Life Norway) and the AntiBioSpec project funded by UiT – the Arctic University of Norway

# Table of Contents

Table of Contents .....	i
List of Tables.....	iii
List of Figures .....	iii
Acknowledgements .....	iv
Abstract .....	v
List of publications.....	vi
List of abbreviations.....	vii
1 Introduction .....	1
1.1 The challenge.....	1
1.1.1 Infectious diseases.....	1
1.1.2 Antimicrobial resistance.....	2
1.1.3 A brief history of the antimicrobial discovery void .....	2
1.2 The fundamentals .....	3
1.2.1 Drug development.....	3
1.2.2 Antimicrobials.....	6
1.2.3 Resistance mechanisms .....	11
1.3 The solution .....	13
1.3.1 Alternative antimicrobial therapeutics .....	13
1.3.2 New antimicrobial compound classes of interests .....	15
1.3.3 Reinvigorating antimicrobial R&D.....	18
1.4 Research aim.....	19
1.5 Structural outline .....	21
2 Methodology for a biological mode of action study .....	22
2.1 Introduction .....	22
2.2 Research Design .....	22

2.3	Antimicrobial activity screening based on the minimal inhibitory concentration (MIC)	23
2.4	Antibiofilm testing.....	24
2.5	MOA profiling using promoter-reporter biosensors.....	25
2.6	Membrane related assay .....	26
2.6.1	Membrane integrity analysis .....	27
2.6.2	Membrane potential quantification .....	28
2.7	Time-kill curves.....	29
2.8	General methodological considerations.....	30
2.9	Summary.....	32
3	Summary of main results.....	33
3.1	Paper I.....	33
3.2	Paper II .....	34
3.3	Paper III .....	35
3.4	Paper IV .....	36
4	Discussion .....	37
4.1	The natural product lulworthinone — aggregation and delocalisation .....	38
4.2	Amphipathic barbiturates — a promising scaffold.....	42
4.3	Antimicrobial peptides — surface coating as a potential application .....	45
4.4	DigiBiotics.....	48
4.5	Why MOA studies .....	51
4.6	Summary.....	52
5	Future prospects .....	53
6	Conclusion.....	54
	References .....	56

## **Paper I- Paper IV**

## List of Tables

Table 1. Variation of molecule/cell ration within the assay cascade .....	31
---	----

## List of Figures

Figure 1. Timeline of antimicrobial discovery and introduction for clinical use.....	3
Figure 2. The general drug development pipeline and compound triage.....	4
Figure 3. Phenotype-based vs. target-based drug discovery .....	6
Figure 4. Main molecular targets for antimicrobials.....	6
Figure 5. Peptidoglycan synthesis with highlighted antibiotic targets.....	8
Figure 6. Structural cell envelope difference between Gram-positive and Gram-negative bacteria .....	10
Figure 7. Main resistance mechanism against antimicrobials.....	11
Figure 8. Common secondary structures in antimicrobial peptides .....	16
Figure 9. Potential molecular interactions of AMPs .....	17
Figure 10. Deliverables of the DigiBiotics project .....	19
Figure 11. DigiBiotics workflow and assay cascade.....	32
Figure 12. Molecular structure of lulworthinone (1) and its degradation product (2) .....	33
Figure 13. FtsZ delocalisation in <i>B. subtilis</i> 2020 after treatment with 1 x MIC lulworthinone .....	34
Figure 14. General chemical structure of the natural products eusyntylamides and the amphipathic barbiturates .....	35
Figure 15. Overview of the small cationic peptide library investigated in paper IV .....	36

Cover photo: *P. aeruginosa* ATCC 27853 on blood agar; photo: Theresa Wagner

## Acknowledgements

Since I started my PhD position in November 2017, my journey in the Arctic has been better and more adventurous than I ever could have imagined. First and foremost, I would like to express my gratitude to my supervisors, Johanna U. Sollid, Ekaterina Mishchenko and Jeanette Hammer Andersen. My most profound appreciation goes to my main supervisor Johanna, for all the guidance and encouragement a mentee could wish for. Thank you for giving me personal space to develop myself, listen to my problems, and brighten up Friday morning meetings. I want to give a special thanks to my second supervisor, Ekaterina. I really appreciated all your valuable time, insights, and help. You are truly one of the kindest people I know. Furthermore, I want to acknowledge Jeanette for all your contributions, comments, and the ability to ground myself, so things got done.

To thrive, one needs a good environment, and my friends and colleagues at the HMI research group provided the best I could hope for. Special thanks to the fantastic engineers Mikal Fitsum and Kjersti Julin for their excellent support. I enjoyed the open exchange of scientific ideas, the companionship and sharing the sweet things in life. Thank you, Hermoine and Nina, for being such dear friends - sharing all the coffee and hikes through my journey.

I want to thank the whole DigiBiotics team. It has been a pleasure to be a part of such a big and diverse team. A special thanks to Phil and Marte for spending many hours talking about science, life, and everything in between. To Digital Life Norway for funding my project and providing a plethora of opportunities for scientific training. Especially for the chance to conduct an industry internship at GlucoSet AS. To the DLN Junior Resource Group - Emil, Maria, Marte and Simona - thank you for all the good times and chuckles in the name of duty!

My friends, I thank you for all the company – which made my time in the Arctic worth living. Without you, Tromsø would have been darker than just the polar night. My family, thank you for your support in all the years – even though we were separated by distance, we were never apart. To my amazing Susanne, thank you for conquering the Arctic with me and being the sun whenever I needed it.

Tromsø, June 2022

*Eric Juskewitz*

## Abstract

Infections caused by bacteria are the third leading cause of death worldwide. Antimicrobials are used to treat and prevent those infections and enabled the development of the modern healthcare system as we know it. However, those achievements are threatened by the global emergence of antimicrobial-resistant bacteria. There is an obvious need for developing new antimicrobials. Natural environments, like the Arctic Ocean, offer largely underexplored biodiversity with promising natural antimicrobial products. This thesis investigates marine and marine-inspired molecules for their antibacterial properties and potential applications.

In **paper I**, a new dimeric naphthopyrone containing a sulphate group was isolated from a marine fungus in the family *Lulworthiaceae*. The compound was produced in high quantities and tested against a panel of clinical bacterial isolates. The molecule exhibited strong antibacterial activity against methicillin-resistant *Staphylococcus aureus*, with a MIC of 1.56  $\mu\text{g/mL}$ . The molecule also displayed moderate antiproliferative activities ( $\text{IC}_{50}$  15.5-32  $\mu\text{g/mL}$ ) against three human cell lines. Degradation of lulworthinone under acidic conditions was observed.

**Paper II** investigated the antibacterial mode of action of lulworthinone. The molecule showed a membrane-targeting mode of action, which led to the dissipation of the membrane potential. Further assays indicated that the antibacterial activity is based on self-aggregation, which was not reported for other naphthopyrones. The delocalisation of cell division protein FtsZ indicated a malfunction of the whole cell division apparatus.

In **paper III**, a series of amphipathic barbiturates – mimicking the natural products eusyntyelamides – were investigated for their antibacterial properties. The peptides showed activity (MIC 2-8  $\mu\text{g/mL}$ ) against a panel of 30 multi-drug resistant clinical isolates. The mode of action study showed a membranolytic effect. The guanidine barbiturate **7e** demonstrated *in vivo* efficacy in a neutropenic peritonitis model.

**Paper IV** determined the potential application of antimicrobial peptides as surface coatings for medical devices. High concentrations of the peptides could be covalently and homologously bound to the model surface. The cyclic peptide analogues exhibited strong anticolonization effects against *S. epidermis* RP62A. This paper offers proof of concept for using antimicrobial peptides as surface coatings.

## List of publications

This thesis is based on the following publications, cited by roman numerals.

### Paper I

Jenssen, Marte, Philip Rainsford, **Eric Juskewitz**, Jeanette H. Andersen, Espen H. Hansen, Johan Isaksson, Teppo Rämä, and Kine Ø. Hansen. '**Lulworthinone, a New Dimeric Naphthopyrone From a Marine Fungus in the Family Lulworthiaceae With Antibacterial Activity Against Clinical Methicillin-Resistant Staphylococcus Aureus Isolates**'. *Frontiers in Microbiology* 12 (2021): 2862. <https://doi.org/10.3389/fmicb.2021.730740>.

### Paper II

**Juskewitz, Eric**, Ekaterina Mishchenko, Vishesh K. Dubey, Marte Jenssen, Martin Jakubec, Philip Rainsford, Johan Isaksson, Jeanette H. Andersen, and Johanna U. Ericson. '**Lulworthinone: In Vitro Mode of Action Investigation of an Antibacterial Dimeric Naphthopyrone Isolated from a Marine Fungus**'. *Marine Drugs* 20, no. 5 (May 2022): 277. <https://doi.org/10.3390/md20050277>.

### Paper III

Paulsen, Marianne H., Magnus Engqvist, Dominik Ausbacher, Trude Anderssen, Manuel K. Langer, Tor Haug, Glenn R. Morello, Laura E. Liikanen, Hans-Matti Blencke, Johan Isaksson, **Eric Juskewitz**, Annette Bayer, and Morten B. Strøm. '**Amphipathic Barbiturates as Mimics of Antimicrobial Peptides and the Marine Natural Products Eusynstyelamides with Activity against Multi-Resistant Clinical Isolates**'. *Journal of Medicinal Chemistry* 64, no. 15 (12 August 2021): 11395–417. <https://doi.org/10.1021/acs.jmedchem.1c00734>.

### Paper IV

Karlsen, Eskil André, Wenche Stensen, **Eric Juskewitz**, Johan Svenson, Mattias Berglin, and John Sigurd Mjøen Svendsen. '**Anti-Colonisation Effect of Au Surfaces with Self-Assembled Molecular Monolayers Functionalised with Antimicrobial Peptides on S. Epidermidis**'. *Antibiotics* 10, no. 12 (December 2021): 1516. <https://doi.org/10.3390/antibiotics10121516>.



## List of abbreviations

ADMET	Absorption, distribution, metabolism, excretion, toxicity
AMP	Antimicrobial peptide
AMR	Antimicrobial resistance
CLSI	Clinical Laboratory Standards Institute
CFU	Colony-forming unit
ECM	Extracellular matrix
EMA	European Medicines Agency
FACS	Fluorescence-activated cell sorter
FCM	Flow cytometry
FDA	Food and Drug Administration
FSC	Forward scatter
HTS	High-throughput screening
LPS	Lipopolysaccharide
LTA	Lipoteichoic acid
MIC	Minimum inhibitory concentration
MOA	Mode of action
MRSA	Methicillin-resistant <i>Staphylococcus aureus</i>
NP	Natural product
OM	Outer membrane
PG	Peptidoglycan
PD	Pharmacodynamics
PK	Pharmacokinetics
SAR	Structure-activity relationship
SSC	Sideward scatter
SME	Small and medium-sized enterprises
TKC	Time-kill curve
USD	US dollar
WHO	World Health Organisation

# 1 Introduction

Infections caused by antimicrobial-resistant (AMR) bacteria were the third leading cause of death worldwide in 2019 [1]. Antimicrobials are becoming less effective due to the rapid spread of antimicrobial resistance among bacteria. Meanwhile, the drug discovery pipeline for developing new antimicrobial drugs is running dry, and new treatment options primarily being altered versions of new drugs. Bacteria rapidly adapt to the new versions of old drugs, since the resistance mechanism is already “known”. Therefore, we need new chemical classes or molecules with new modes of action (MOAs) [2]. This research aims to find new antimicrobials and define their MOAs against clinically relevant bacteria. The first chapter will introduce the study by discussing the background and context, followed by the research problem, the research aims, objectives and questions, the significance, and limitations.

## 1.1 The challenge

### 1.1.1 Infectious diseases

With the introduction of antibiotics, ailing patients could be treated and recover from infectious diseases. Together with antiseptic procedures, sanitation and hygiene, antimicrobial treatment led to a vast reduction in the mortality rates due to bacterial infection. This marked the start of modern medicine. Nowadays, surgery, chemotherapy or organ transplantation are unthinkable without the preventive use of antimicrobials [3].

During his Nobel prize lecture in 1945 [4], Sir Alexander Fleming warned that bacteria could become resistant to antimicrobial drugs. His prediction proved correct: every implementation of a new antimicrobial has been followed by the emergence of resistance to it. The development of AMR is an evolutionary process, vastly accelerated by the selective pressure applied by an overwhelming use of antimicrobials. Now, the achievements of modern medicine are at risk due to the rise of AMR.

### 1.1.2 Antimicrobial resistance

The World Health Organization (WHO) released its first global surveillance report on AMR in 2014 [5], predicting that AMR will profoundly influence global health and the economic sector. First estimates suggest that 300 million people will die prematurely because of AMR-related bacterial infections by 2050 [6].

To address this emerging threat, the WHO published a list of antibiotic-resistant "priority pathogens" to guide and promote antibiotic research and development [7]. This list harbours a coterie of the hardest to treat multi-drug resistant bacteria called the ESKAPE group (*Enterococcus faecium*, *Staphylococcus aureus*, *Klebsiella pneumoniae*, *Acinetobacter baumannii*, *Pseudomonas aeruginosa*, and *Escherichia coli*) [8]. These bacteria pose particular threats in healthcare settings (hospitals, nursing homes and patients with ventilators or blood catheters). An estimated 1.27 million deaths were attributable to AMR in 2019 [1]. Of those deaths, the ESKAPE group was responsible for ~73 %. This highlights the importance of developing drugs targeting those pathogens.

### 1.1.3 A brief history of the antimicrobial discovery void

In the era of antibiotic discovery, the Waksman platform – screening soil actinomycetes – identified the main classes of antibiotics (aminoglycosides, beta-lactams, chloramphenicols, macrolides and tetracyclines) in a short period in the 1940s (Figure 1). The golden age ended in the 1960s (as the first signs of AMR were detected [9]) when the low-hanging fruits of commonly present antibiotics had been used up, and several antimicrobials were consistently rediscovered. Around this time, synthetic antimicrobials entered the space (e.g., fluoroquinolones) and synthetic chemistry was able to introduce drug analogues that converted narrow-spectrum compounds working against Gram-positive species into broad-spectrum antimicrobials (erythromycin – azithromycin, penicillin – ampicillin) [10].

Parallel to increasing AMR, the development of cures was downsized. The pharmaceutical industry responded to market forces and the perceived abundance of antimicrobials by shutting down or cutting back antimicrobial discovery programs. This resulted in a big discovery void of new chemical classes between 1987 (lipopeptides [11]) and 2020 (teixobactins [12], halicins [13], and diazabicyclooctane [14]).

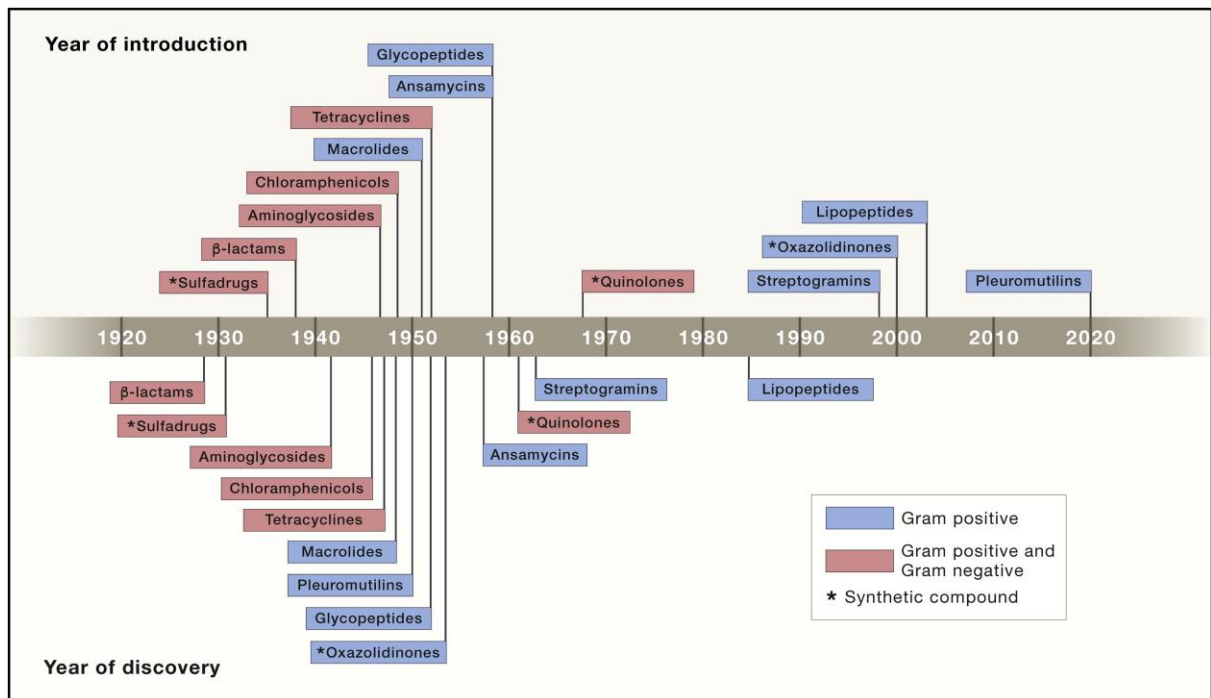


Figure 1. Timeline of antimicrobial discovery and introduction for clinical use; permission by Elsevier: Lewis (2020)

With the rise of AMR, it got increasingly difficult and costly to develop new drugs. From the discovery to market, developing a drug takes 10-12 years [15], costs around 1.3 billion USD for research and development [16], [17], and 250-500 million USD to keep the drug on the market in the first five years [18], [19]. Companies face all those hurdles while antimicrobial misuse (overuse in animal husbandry, free over counter purchases, incorrect usage, and lax regulations) speeds up AMR development and shortens the market window for a drug [20].

## 1.2 The fundamentals

### 1.2.1 Drug development

In contrast to the rapid spread of AMR, drug development is a long process where each step leads to a better understanding of the compounds and filters out compounds with undesired properties (Figure 2). This process is called rational drug design, and it needs roughly 10,000 compounds to develop one drug [14], [21].

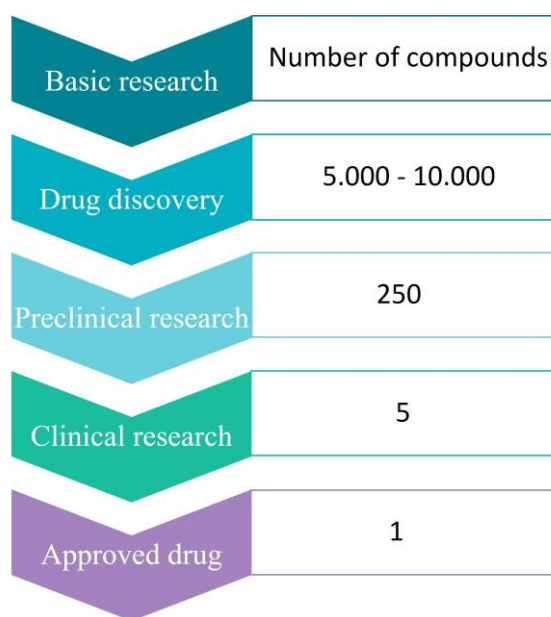


Figure 2. The general drug development pipeline and compound triage; based on Petrova et al. (2014)

The early drug discovery step starts with selecting a target disease and identifying potential drug targets. Afterwards, molecules are screened against the target to identify active hit compounds. Those hit compounds are investigated for their MOA and molecular targets *in vitro* and *in vivo*. If a molecule shows desirable properties, it can be further adapted with medicinal chemistry and advance in the pipeline as a lead compound.

In the preclinical step, the pharmacokinetics and pharmacodynamics properties, as well as the efficacy of the lead compound are determined. Animal studies evaluate the leads adsorption rate, distribution in the body, metabolic activity, excretion, and toxicity (ADMET). Key indicators are the maximum safety level of the drug in the host and potential side effects. The process development step determines the most cost-efficient way of manufacturing the lead compound afterwards. To maximise bioavailability in the host, the following formulation development estimates the best way to formulate the drug (tablets, capsules, etc.). If the drug is deemed safe for use in humans, applications for human trials are filed with the regulators (e.g., the European Medicines Agency (EMA) or the American Food and Drug Administration (FDA)).

In the clinical development step, the drug is administered to increasing numbers of humans. In phase 1, the drug is tested on volunteers (20–100) to assess drug dosing without compromising safety. Phase 2 determines the drug efficacy in a small cohort of diseased patients (100–500).

Phase 3 clinical trials (1.000–5.000 patients) are longitudinal studies to identify long-term safety issues and side effects [21].

In the product approval and launch phase, the manufacturer seeks approval from the regulatory bodies to enter the market. While being marketed, it is common to conduct phase 4 trials, where drug efficacy and safety are determined for minority patient groups (e.g., pregnant women or children) [22].

### **Target-based vs phenotype-based discovery**

Drug discovery is based on two main approaches (see Figure 3). The original approach, phenotype-based discovery, starts with a drug-like compound that undergoes phenotypic assays to determine potential therapy areas and pharmacology. After the initial whole-cell phenotypic screening, the drug target will be elucidated and followed up by MOA and safety profile studies. This approach has two significant advantages, (i) the ability to discover first-in-class drug moieties and (ii) the molecule can show drug efficacy in native cell or tissue environments [23], [24]. If the targets are unknown, the identification requires subsequent effort and time, creating a significant bottleneck for antibiotic discovery and development [25].

A paradigm shift came with new techniques (e.g., omics, high-throughput screening (HTS), bioinformatics). Drug screening shifted to identify disease-related targets first and screen for compounds afterwards. This target-based approach can unravel how a drug should interact with the target of interest [26]. As a result, vast compound libraries could now be screened for a specific molecular interaction in a less expensive HTS. This approach enabled a fast identification of best-in-class drug moieties [27].

While the target-based discovery has a generally good track record in developing new drugs with improved potency and safety profiles, it seems to fail for antibiotics [26], [28], [29]. There are still many knowledge gaps about how antimicrobials interact with bacteria, especially how they penetrate the cell envelope [26]. Payne *et al.* (2015) [28] recommended reverting to phenotypic-based assays to avoid those pitfalls. This approach also benefits from advances in high-throughput formats, automatization and computerisation of the screening processes [30].

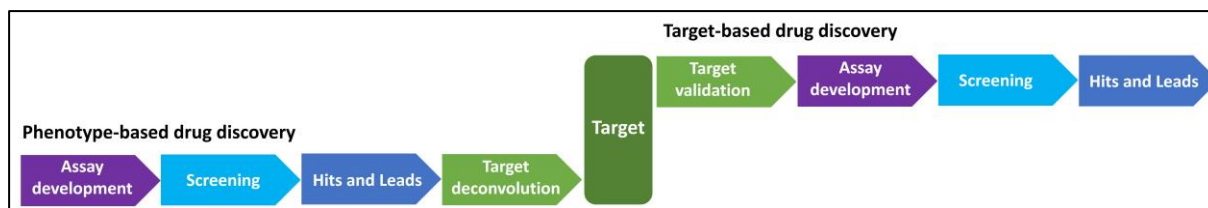


Figure 3. Phenotype-based vs. target-based drug discovery; based on Terstappen et al. (2007)[31]

## 1.2.2 Antimicrobials

Antimicrobial treatment seeks to interfere with pathogenic bacteria without damaging the host. This concept is called selective toxicity. To achieve this goal, bacterial structures or metabolic pathways need to be identified that are different or absent in the host [32]. The most common and researched targets for direct-acting agents are shown in Figure 4.

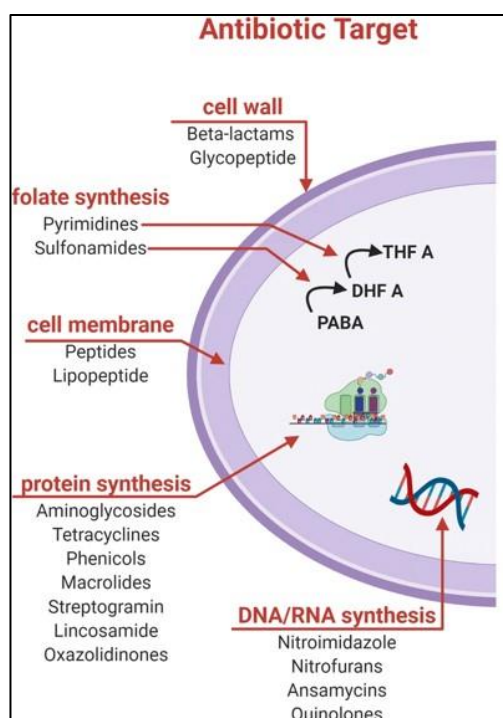


Figure 4. Main molecular targets for antimicrobials; permission by Springer Nature: Cardoso et al. (2021)[33], modified

## **Nucleic acids synthesis**

The synthesis of nucleic acids is necessary to transform cellular information from genes (DNA) to molecular blueprints (mRNA). This is a long and complex process that offers many inhibition targets. For example, quinolones inhibit DNA gyrase, which facilitates the supercoiling and packing of bacterial DNA [34], while rifampicin blocks the bacterial RNA polymerase [35]. However, mammalian cells are safe from such antimicrobials as they use different enzymes.

## **Protein synthesis**

Protein synthesis is a crucial part of cell activity. Information from mRNA is translated into molecules by joining amino acids together in the ribosome. Bacterial ribosomes are good distinct targets, as they differ from eukaryotic ones. Aminoglycosides interrupt the translation process at the ribosome, resulting in misfolded cytotoxic peptides [36].

## **Metabolic activity**

The metabolism is defined as the sum of all energy-creating reactions. Anti-metabolites mimic natural compounds involved in these processes and bind to the enzymes, rendering them ineffective. For example, trimethoprim mimics p-aminobenzoic acid — which is vital for folic acid synthesis — preventing bacterial multiplication. Humans do not produce folic acids but take them up with food [37].

## **Cell envelope**

The cell envelope is simultaneously a promising target and strong adversary for antibiotic treatment. It is a highly complex system, and as multiple MOAs target this system, it will be discussed in more detail. Bacterial cell envelopes possess structural elements (e.g., cell wall or the outer membrane) that eukaryotes lack. Furthermore, the bacterial surface is negatively charged instead of neutral in the case of eukaryotes. Both aspects are conserved among bacterial species, which offers potential broad-spectrum activity for antimicrobials [3], [38], [39].



**Cell wall** The cell wall is a rigid, porous structure made from peptidoglycan (PG), a polysaccharide backbone linked via peptide side bridges. Its essential role is to resist osmotic pressure, and it offers anchor points for various proteins and polymers [40]. This vast network of molecules cannot be assembled within the cell. Therefore, the subunits (also named lipid II) need to be transported to the outside, where they are joined together [41], [42].

This is where most antimicrobials (beta-lactams, carbapenems, cephalosporins, glycopeptides) interfere with the bacteria. They can hinder the assembly of the PG polymers (transglycosylation (Figure 5 black frame); inhibited by nisin [43], teicoplanin [44]) or inhibit the crosslinking (transpeptidation (Figure 5 blue frame); inhibited by penicillin [45], vancomycin [46]) of PG backbone parts. PG is regularly weakened before cell division, so further stimulating the intrinsic PG digestion by activating autolysins may be required. Together, the PG is weakened enough for the bacterial cell to lyse. This highlights why cell wall active antimicrobials work primarily on living and dividing bacteria [47], [48].

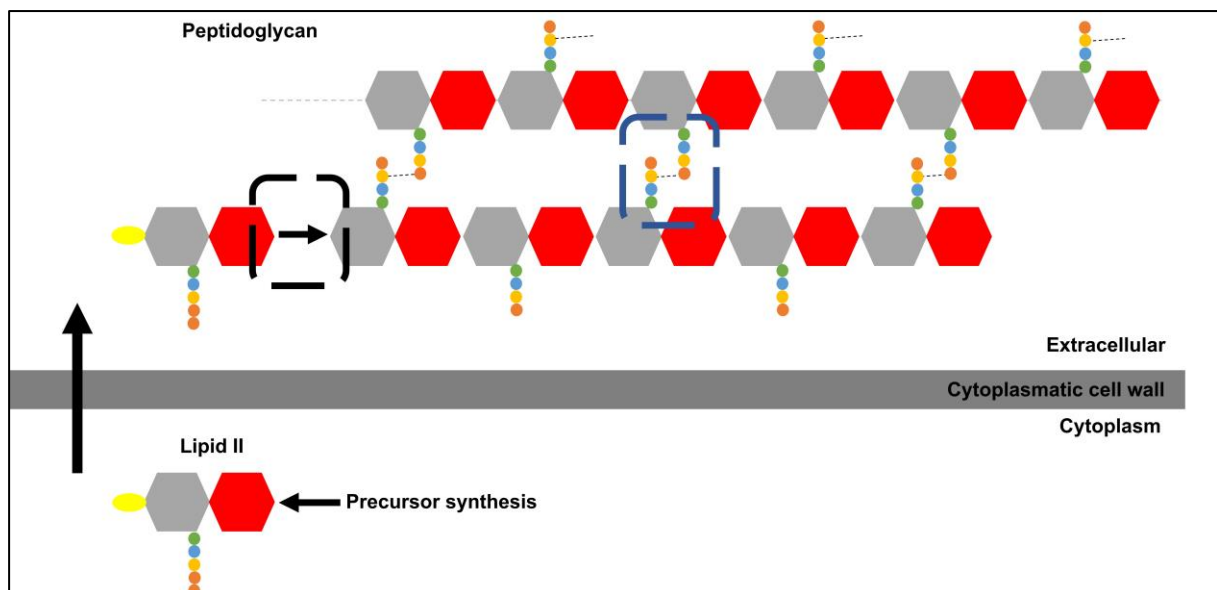


Figure 5. Peptidoglycan synthesis with highlighted antibiotic targets; based on Coyle et al. (2018) [49]

***Cell membrane*** The cell membrane controls the transport of molecules in or out of the cell. The membrane consists of a phospholipid backbone and proteins. Phospholipids contain a hydrophilic head and a hydrophobic tail; both create an amphipathic character. Assembling multiple phospholipids next to each other in aqueous environments leads to lipid bilayer formation [39].

While phospholipids form the main fabric of membranes, proteins provide the main functions. Membrane proteins are involved in molecule transport, enzymatic activities, signal transduction, cell-cell recognition, intercellular joining, or attachment to the cytoskeleton and extra-cellular matrix. Combined, proteins and phospholipids create a beneficial physiochemical environment for multiple cellular processes [50], [51].

The homeostasis of molecule concentrations within and outside of the cell is a fragile system. The difference between high and low concentrations of a molecule creates an energy gradient. Membranes are selective, and while small nonpolar molecules can pass through, charged molecules are less likely to traverse them. Those molecules need membrane-spanning transporter proteins. The transport is either passive (diffusion along the concentration gradient) or active (transport against the gradient under energy consumption). Those transporters create an imbalance of anions and cations on the membrane and create an electrical voltage – the membrane potential. The membrane potential acts like a battery and influences all transport of molecules in bacteria [50].

Antimicrobials can target phospholipids (disrupting the membrane architecture and functionality), proteins (conformation or localisation), and alter the membrane potential. Examples are the lipopeptides like daptomycin or polymyxins B and E. They mainly bind the membrane and increase permeability, leading to leakages of cytosolic compounds. Membrane active compounds do not bind to a specific target. They have the potential to be active against dormant or slow-growing bacteria, and cause low resistance development due to their multiple targeted MOAs, favourable pharmacokinetics, and potential to serve as a chemosensitizer for other antimicrobials [39].

## Gram-positive or Gram-negative bacteria — know your enemy

There are two distinct clades of bacteria, Gram-positive and Gram-negative. The cell envelope morphology and structure in both clades are fundamentally different (Figure 6).

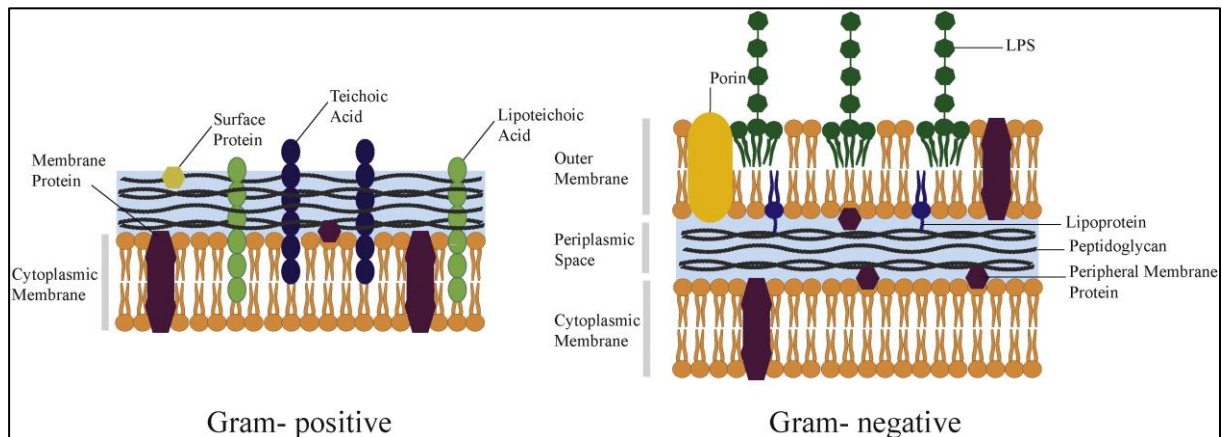


Figure 6. Structural cell envelope difference between Gram-positive and Gram-negative bacteria; permission by Elsevier: Epand et al. (2016)

**Gram-positive** Gram-positive bacteria are surrounded by a layer of PG around ten of nanometres thick. Their PG contains additional compounds called teichoic acids. Both subgroups of wall teichoic acids and lipid teichoic acids are covalently bound to the PG or membrane, respectively. The main functions are to provide stability of the PG (anchor function) and maintain a negative surface charge to attract cations [42].

**Gram-negative** Gram-negative bacteria are surrounded by two membranes, the cytoplasmic membrane and the outer membrane. The outer membrane (OM) contains lipopolysaccharides (LPS). Generally, PG is too porous to be a significant barrier for antimicrobial diffusion, but the outer membrane limits diffusion heavily. This gives Gram-negative bacteria an inherent advantage over their Gram-positive brethren. The hydrophobic bilayer restricts penetration of hydrophilic compounds and is a nearly impenetrable barrier. Antimicrobials need to diffuse through pores in the OM to reach their cellular target. As the pores are relatively substrate unspecific, single mutations can convey resistance to multiple antimicrobials at once. Furthermore, compounds that manage to leak across the OM can quickly be expelled by multidrug-resistant pumps before reaching their cellular target. [3]

### 1.2.3 Resistance mechanisms

Bacteria have developed multiple resistance mechanisms to overcome antimicrobial pressure:

- (i) modification or destruction of antimicrobials,
- (ii) efflux pumps to counter antimicrobial uptake,
- (iii) restriction of membrane permeability to inhibit the diffusion of antimicrobials,
- (iv) target modification to mask antimicrobial binding sites, and
- (v) development of alternative pathways to evade metabolic mimicry [52]–[54] (Figure 7).

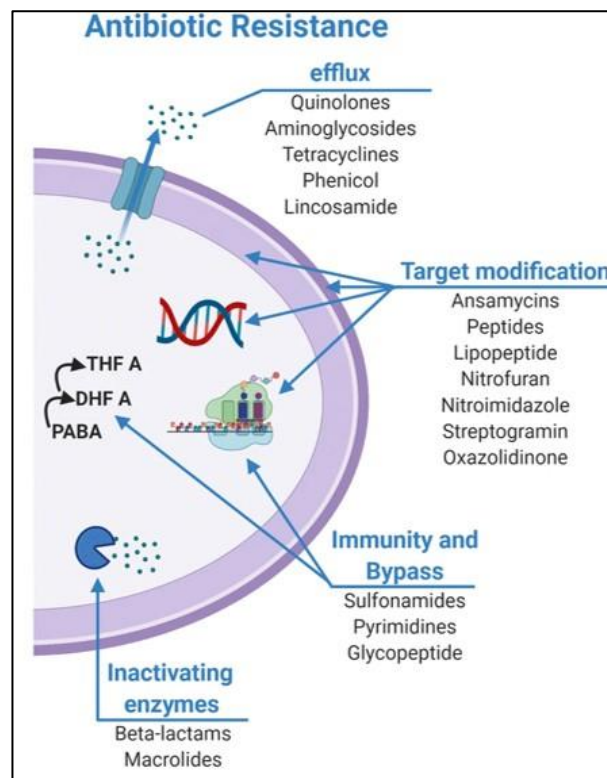


Figure 7. Main resistance mechanism against antimicrobials; permission by Springer Nature: modified from Cardoso et al. (2021) [33]

Besides their intrinsic resistance mechanisms (e.g., the adaption of membrane permeability, efflux pumps, and the presence of the outer membrane [52]), bacteria can also avoid treatment by tolerating antimicrobials or biofilm formation.

Antimicrobials induce various forms of cell damage. To survive the exposure, bacteria need to upregulate their damage repair functions. This is often a race against time. Subpopulations which are expressing those stress responses already can react to the lethal insult in sufficient time. This stochastic survival is termed antimicrobial tolerance [55]. An extreme form of

tolerance is the formation of persister cells. Here the cells enter spontaneously a dormant non-dividing state. While the antimicrobial eradicates the majority of the population, the persisters can emerge after the antibiotic stress receded which results in a relapsing infection [56].

Another way to counteract antibiotic stress is the formation of biofilms. Biofilms are mostly sessile bacterial communities formed on surfaces. The bacteria are encompassed by an extracellular matrix (ECM) which consists of polymers (exopolysaccharides), extracellular DNA, and proteins [57]. Biofilms protect against alterations in osmolarity or pH, mechanical and shear forces, and also block antimicrobials and the host defence system from accessing the bacterial cells [58]. This allows bacteria to withstand harsh conditions and provides resistance up to 1000-fold the MIC of the antimicrobial [59].

### **Resistance development**

Bacteria can acquire AMR in two major ways. Either they undergo genetic mutations themselves or acquire resistance genes from other bacteria. Developing a chromosomal mutation that leads to resistance is mostly a slow process. Even though mutations frequently happen in bacteria, it is serendipity if one leads to changes countering antimicrobials and mainly leads to resistance against a single antimicrobial. Without the presence of the specific antimicrobial, those mutations lead to a decreased fitness of the bacterium. Species members can outcompete the mutant, and the resistance can be lost within the population [52].

More problematic is the acquisition of resistance genes from the environment via horizontal gene transfer. Mobile genetic elements like plasmids or transposons can be easily exchanged between bacteria. Those gene elements often convey multiple resistance genes at once and lead to a rapid spread of AMR within an environment [60]. Especially in the health care sector — an environment with high antimicrobial use and therefore selective pressure — resistance genes are prevalent and exchanged fast [61].

## 1.3 The solution

The current efforts to tackle the AMR crisis can be grouped into (i) alternative antimicrobial therapeutics, (ii) the search for new antimicrobials, and (iii) the restructuring of the drug discovery and development pipeline. Theuretzbacher *et al.* (2020) [28] identified 407 active projects in the preclinical pipeline that developed new antibacterial options in a global survey. Most projects focus on non-traditional treatment approaches, and 70 % aim at new bacterial targets.

### 1.3.1 Alternative antimicrobial therapeutics

#### Antibodies

The immune system uses antibodies to neutralize pathogens. They are also able to neutralise bacterial virulence factors. Most antibodies in the clinic or development focus on toxins of *S. aureus*, *B. anthracis*, *C. botulinum*, *C. difficile*, and *P. aeruginosa*. Antibodies targeting other virulence factors (e.g., biofilm modulators, cellular attachment) have yet to be proven successful [62].

#### Anti-virulence agents

Alternative to targeting the pathogens directly, anti-virulence agents aim to inhibit the activity or production of virulence factors. Those treatments have no influence on bacterial growth but disarm bacteria and render them harmless. Potential targets include adhesion, biofilm formation, quorum sensing, siderophores, toxins, or persister formation. Since most virulence factors are species or strain-specific, the treatment currently has a narrow spectrum of activity [63], [64].

#### Bacteriophages

Phage therapy has been known for decades but has gained traction with the rise of AMR and modern techniques. The current development focuses on phages producing lysins and targeting *E. coli*, *P. aeruginosa* and *S. aureus* infections. Phages are considered safe as they do not target mammalian cells. As phages are specific for particular bacterial species (or subspecies), they

have a narrow activity spectrum. They are mainly used to treat patients with rare pathogens [63], [65], [66].

### **Microbiome-modulating therapies**

A deeper understanding of the human microbiome enabled the manipulation of host-pathogen interactions [67]. Current approaches involve restoring a healthy gut microbiome or engineering probiotics to produce antibiotic inactivators, AMPs or absorbers for bacterial toxins. Due to the great variety of microbiome compositions, the preclinical models still lack predictive power and hamper effective dosing in patients [63], [65].

### **Potentiators**

The antimicrobial drug activity can be enhanced by using potentiator molecules. Most of those molecules are not antimicrobial but enable other drugs to be more effective. The current focus is on potentiators that inhibit bacterial defences (e.g., beta-lactamase inhibitors), expand the treatment spectrum of activity (narrow to broad-spectrum) or protect against nephrotoxicity (e.g., caused by colistin, aminoglycosides) [65]. Furthermore, the potentiator approach offers the possibility of repurposing old and exhausted antibiotics [68].

### **Repurposed drugs**

An alternative to discovering new molecules is the repurposing of known drugs. Drugs approved for other diseases have not been tested for their antibacterial potential per se. The discovery of potential hit compounds from existing drug libraries benefits from a considerable body of knowledge. It can speed up the development process by ~50 %. Successful drug repurposing could save more than one billion USD in development costs [69], [70]. This approach has already shown to be a viable option against several ESKAPE bacteria. [71]–[73]

## **Vaccines**

Vaccines enable preemptive protection in the population and decrease the total incidence of infections. Vaccines against AMR bacteria would lower the public demand for antimicrobials. Currently, there are two vaccines available targeting AMR bacteria (Hib against *Haemophilus influenzae* and PCV7 against *Streptococcus pneumoniae* [74]). Unfortunately, due to the high genetic diversity within the ESKAPE bacteria group, no vaccines could target the pathogenic bacteria effectively so far [75]. As a result, only 11 new vaccines are in clinical trials. They have an even lower predicted success rate than antimicrobials [66], [76].

### **1.3.2 New antimicrobial compound classes of interests**

Efforts to promote antimicrobial discovery in the last decades resulted in an increase of molecules with a high level of diversity in the current pipeline. Besides progress for alternative approaches, the search for new direct-acting antimicrobials is still the primary research focus. Most direct-acting molecules present either new classes, targets or MOAs [77]. The majority of those compounds originated from or mimic natural products (NPs), with a focus on antimicrobial peptides (AMPs) [2].

## **Natural products**

Natural products (NPs) offer a trove of untapped potential, as organisms had millions of years to develop and refine metabolites and their functions. They provide a good starting point for drug discovery. The discovery boom in the golden era has shown that many antimicrobial compounds exist. Their scaffolds could be adapted to become more feasible for use in humans (e.g., penicillin-ampicillin [78]). Unfortunately, the finite number of antimicrobials (especially broad-spectrum) from easy-to-cultivate soil bacteria is known by now [9].

In order to reinstate a Waksman-style drug discovery platform, projects need to look at microbes that have been underexploited. The ocean is an under-explored environment. Most of the oceans' biodiversity remains undiscovered due to inaccessibility, sample limitations, and low cultivability of the organisms. Bioprospecting initiatives (like MarBio [79], Marbank [80], or the Marine Biodiscovery Centre [81]) address the problems as they sample new environments (e.g., the Arctic), use new sampling techniques, and use new tools for genome



mining and heterologous pathway expression [9]. Overall, NPs offer a good starting point for drug discovery as their MOAs and molecular scaffolds are well tested over time.

### Antimicrobial peptides

Due to their central roles in the innate immune system of all multicellular organisms, AMPs have been considered potential novel antimicrobials since their discovery in 1980 [82]. The advantages of AMPs are their broad-spectrum activity, including most major Gram-negative and Gram-positive bacteria, their bactericidal and rapid action, low potential for resistance development, and their lack of immunogenicity [83].

AMPs are composed of < 100 amino acids and harbour a net charge between +2 and +9. They contain cationic amino acids (e.g., arginine or lysine) along with hydrophilic residues. The arrangement of residues within the molecule or in the secondary-structure gives them an amphipathic character [84]. Common secondary structures ( $\alpha$ -helix,  $\beta$ -sheet, looped, extended, and mixed) are shown in Figure 8 a-e.

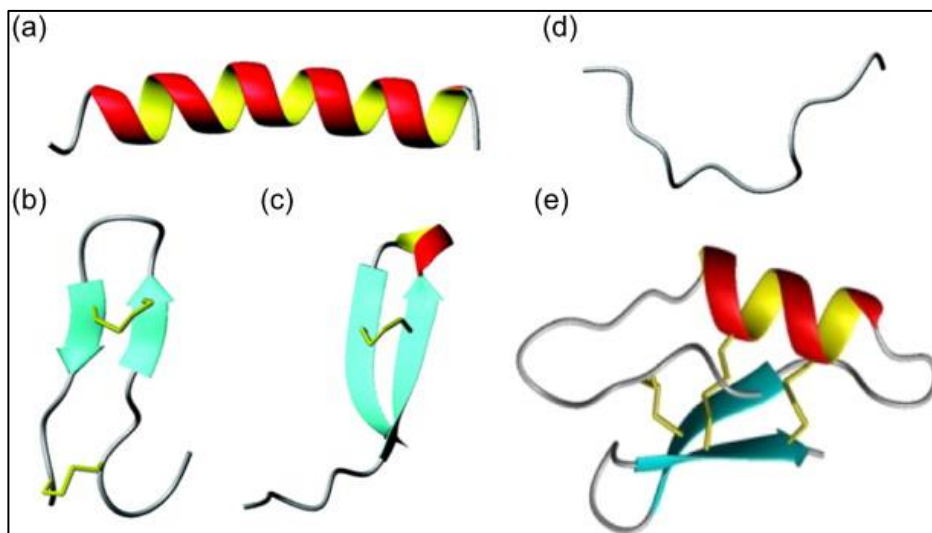


Figure 8. Common secondary structures in antimicrobial peptides; Ong et al. (2014) [85]

AMPs have shown to have one or more MOAs. AMPs have a membrane-targeted MOA classically, but other MOAs (including inhibition of DNA, RNA and protein synthesis) also occur [76] (see Figure 9). Furthermore, it has been shown that they can have anti-cancer, anti-biofilm or immunomodulating properties, which makes them a promising drug class in general [86]. It is still unknown whether the multiple functions of AMPs are independent or not.

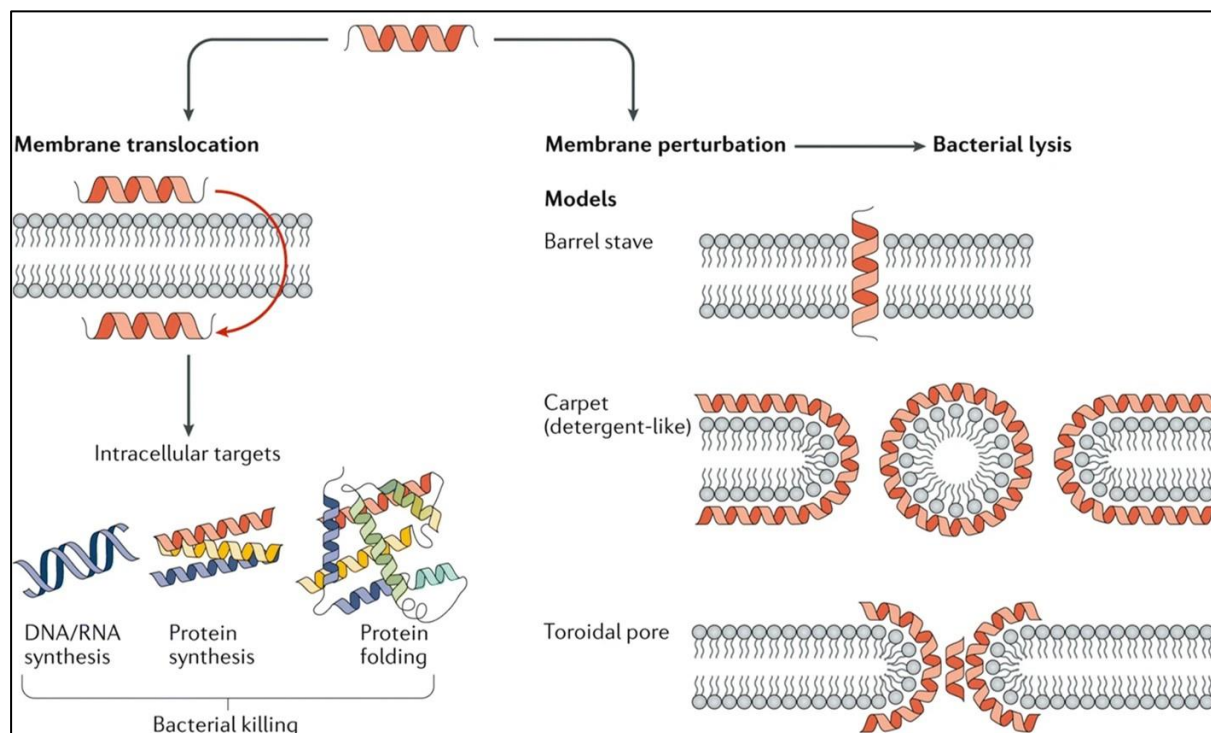


Figure 9. Potential molecular interactions of AMPs: permission by Springer Nature, Cardoso et al. (2021), modified

Most AMPs have an amphipathic character that promotes a strong electrostatic interaction with bacteria's negatively charged surface layer [87]. The bacterial membrane is considered the main target for AMPs as they increase permeability and disrupt bacterial membrane integrity. This causes leakage of cell content, which is followed by cell death. A number of models of AMP interaction with the membrane have been proposed (aggregation [88], barrel-stave [89], carpet [90], sinking raft [89], toroidal pore formation [91]; some shown in Figure 9). All models predict interaction with the physical properties of the membrane instead of biological targets. This makes them interesting antimicrobials as rearranging the physical properties of the whole membrane is hard to achieve.

Besides polymyxin B [92], colistin [93], tyrothricin [94], gramicidin S [95] and vancomycin [96], AMPs often fail preclinical studies due to low stability, bioavailability, and high *in vivo* toxicity. Therefore, it is crucial to strengthen the mechanistic understanding of the AMPs and their targets [83].

The structure and functions of AMPs are used to develop improved versions of natural products. The resulting molecular mimics are known as peptidomimetics. Peptidomimetics capitalize on the structural features of AMPs (e.g., amphipathicity, peptide backbone composition, charge, hydrophobicity, side chains) while incorporating residues with other biophysical properties (e.g., non-standard amino acids, exclusion of  $\alpha$ -amino acids in the peptide backbone). The change of biophysical properties often enhances *in vivo* stability and lowers toxicity while resembling the activities of usual AMPs [87], [97].

### **1.3.3 Reinvigorating antimicrobial R&D**

Drug development is a general risky endeavour as just 5 % of all products make it to the market [20]. The standard business model of charging high prices and selling large volumes - does not work for antimicrobials. As a result, there has been a steady decline in pharmaceutical companies investing in antimicrobial research. Currently, there are three big companies (GlaxoSmithKline, Merck, Pfizer) [98] left in the field, and they account for 4 out of 42 antimicrobials under development [20]. These commercial decisions threaten the global ability to research, develop and produce new antibiotics for society. Besides academic ventures, the key players keeping the pipeline alive are small and medium-sized enterprises (SMEs).

### **DigiBiotics**

To supply the global drug development pipeline, public-funded initiatives were formed. Governments have acknowledged the schism between the commercial model of pharma companies and the urgent need for new antimicrobials. As a result, the Norwegian Research Council and Digital Life Norway funded the DigiBiotics project in 2017. DigiBiotics is a drug discovery project that aims to analyse understudied chemical classes by combining the activities of multiple work packages: bioprospecting (WP1), synthetic chemistry (WP2), structure confirmation using optical (WP3) and NMR (WP4) spectroscopy, molecular dynamic modelling (WP5), and microbiology (WP6). The rationale was to develop marine-inspired hit

compounds that target bacterial infections and are active on the cell envelope. The deliverables of the project are depicted in Figure 10.

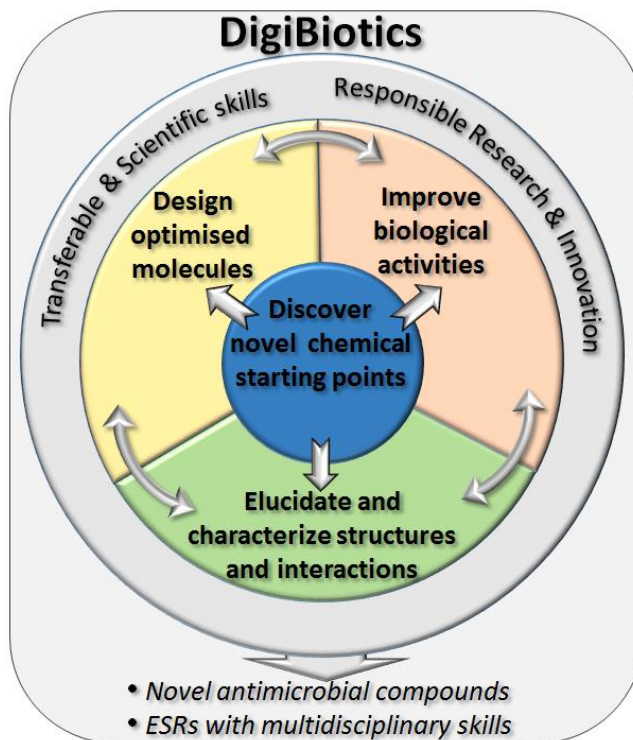


Figure 10. Deliverables of the DigiBiotics project

## 1.4 Research aim

The constant development of new antimicrobial drugs with renewed MOAs is needed for infection control. Recent antimicrobial research is directed towards small drug molecules (< 1 kDa). These molecules have the potential to be effective against unique and underexplored targets like bacterial membranes or protein-protein interactions on cell surfaces [99], [100].

The pharmaceutical industry avoided the research of those molecules, especially AMPs, due to challenging ADMET properties [101]. Therefore, the molecules are considered undesirable and were precluded from the classical design-analyse-improve cycle. This presents a problem as the antimicrobial drug development pipeline is dry and needs new drug candidates to develop possible treatments [3].

As a result, the current knowledge about small drug molecules is inadequate for the pharmaceutical industry to pursue them as potential drug leads. Academic efforts are needed to supplement the drug development process and investigate those compounds. Providing further knowledge could make those molecules feasible for industry research.

#### **1.4.1.1 Research Aim, objectives, and question**

Given the lack of knowledge on small drug molecules, this study aimed to identify and determine new antibacterial compounds by screening and mode of action studies. The following objectives were defined:

Objective #1 – Identify antimicrobial hit compounds against clinically relevant bacteria.

Objective #2 – Determine the molecular MOA of the hit compounds.

Objective #3 – Explore potential applications for small drug compounds.

To reach the proposed research objectives, the following research questions were addressed.

RQ #1 – What small compound classes can be relevant to test for?

RQ #2 – What is the MOA of each identified hit?

RQ #3 – How can those hit compounds be exploited?

#### **1.4.1.2 Research significance and limitations**

This study will contribute to the body of knowledge on antimicrobial compounds by investigating and characterising underexplored chemical classes and their modes of action. This will help address the current shortage of hit compounds for the drug development pipeline and explore potential new drug targets.

The empirical results reported herein should be considered in light of some limitations.

First, as the last part of the DigiBiotics pipeline, the access to potential antimicrobials depended on the preceding work packages, bioprospecting (WP1) and organic synthesis (WP3). The

bioprospecting work package was heavily influenced by the serendipity of finding compounds and producing feasible amounts of the compound for the MOA studies.

Second, the screening methodology was a labour-intensive task. It was a considerable bottleneck for screening the peptide libraries provided by WP3.

Third, the employed methods are based on *in vitro* conditions, simplified computational models, and artificial membranes. Any antimicrobial activity needs to be validated further in fitting *in vivo* models (e.g., mouse tight model, peritonitis model).

Fourth, as drug development is a commercial endeavour, there might be existing research that is not publicly available about the studied compound classes.

## **1.5 Structural outline**

In Chapter One, the context of the study has been introduced. The research objectives and questions have been identified, and the value of such research is argued. Furthermore, the limitations of the study have also been discussed

Chapter Two discusses the research design and the applied *in vitro* methods for screening and MOA determination in detail. The advantages and limitations of each method are highlighted.

In Chapter Three, a summary of significant findings from each publication is provided.

Chapter Four provides a general discussion of the results and a broader context. The rationale behind each screening campaign, the MOA, potential applications, and limitations are given for each investigated molecule/molecules group. Furthermore, the DigiBiotics pipeline is reviewed in the scope of current endeavours to fight AMR and the benefits of MOA studies are highlighted.

In chapter Five, future prospects and potential studies are outlined.

Chapter Six provides the conclusions of this thesis, summarising the key findings in relation to the research objectives and questions.

## **2 Methodology for a biological mode of action study**

### **2.1 Introduction**

This study aimed to screen for antimicrobial molecules and determine their mode of action. This chapter presents the methodology which was employed during the study. The workflow followed a screening assay cascade using phenotype-based methods. In the light of this, the research design and choice of microbiological methods are explained. Furthermore, the limitations of each employed method are given. Finally, a summary of this chapter is presented.

### **2.2 Research Design**

Research aims to create sustainable and reproducible knowledge. This approach is based on the key assumptions that (i) there are natural causes for things around us, (ii) evidence from the natural world can be used to learn and explain those causes, and (iii) that there is consistency in those causes [102]. In this study, the research design follows the tradition of positivism. Here, the progress of science is purely based on observable data — obtained from observations and experiments — which will lead to new scientific truths [103].

Following this natural science tradition, experimental research is the main contributor to scientific evidence. The data will contribute to the body of knowledge with a deductive approach as it adds new data to existing hypotheses. Once a hypothesis is generated, other explanations are still taken into consideration. The employed scientific methods were based on the comparison of control groups (no variable is manipulated) vs experimental groups (a specific variable is manipulated) in strictly limited environments (laboratories). This approach allowed observing causation (cause and effect) between variables [104]. Different methods exhibiting the same phenomenon were combined, and the experimental design was kept as simple as possible. Additionally, the experiments were based on random sampling to ensure representative data samples and generalizability.

All collected data were quantitative (numbers-based). Descriptive and inferential statistics were used to interpret the scientific evidence [105]. Each experiment consisted of at least three biological replicates, with a minimum of three technical replicates each, to ensure the validity of the statistics. Following the investigations, the data were stored according to the FAIR principles (findable, accessible, interoperable, reusable [106]) and analysed via given software on equipment or with the statistical software R 4.1.0.

The workflow followed a screening assay cascade – starting with assessing antimicrobial properties, MOA estimations via biosensors and ending with an in-depth analysis to confirm the MOA. Every method has its inevitable limitations, which must be considered when interpreting the data. All microbiological techniques are discussed in the following, and limitations are highlighted.

### 2.3 Antimicrobial activity screening based on the minimal inhibitory concentration (MIC)

Phenotypic screening based on growing bacterial cultures allows the identification of hit compounds regardless of their MOA. This whole-cell screening has the advantage of selecting compounds that can penetrate and kill/prevent the growth of bacteria. In industrial high-throughput settings, thousands of molecules are tested with a fixed concentration (e.g., 10-20  $\mu\text{M}$  [107]) in 384-1536 well formats. The MIC of a hit compound is evaluated later [108].

Due to the relatively small compound libraries used in the study, the screening was combined with antimicrobial susceptibility testing. Here, microbial survival was evaluated as an endpoint measurement of visible growth after 24 hours. The assay was conducted in a micro-broth approach containing a two-fold dilution series (ranging from 0.5-256  $\mu\text{g/mL}$ ) in a 96-well format.

The screening process was split into two parts to focus the research effort and reduce manual labour. First, the MICs of the molecules were determined for common lab strains (*B. subtilis* 168 / ATCC 23857, *S. aureus* ATCC 9144, *E. coli* ATCC 25922, and *P. aeruginosa* ATCC 27853). If they showed promising MICs (e.g.,  $\text{MIC} \leq 16 \mu\text{g/mL}$ ), they were further tested against bacteria from the ESKAPE group (for a complete overview, see Table 2, **paper III**). The procedure followed the guidelines of the Clinical Laboratory Standards Institute (CLSI) [109] and included quality assurance strains and reference antimicrobials. The MIC values are currently the best available parameter to estimate the activity of an antimicrobial, both for deciding on treatment in the clinic and as an indicator for drug development.

Despite the standardisation of the method, it has its limitations. MICs do not represent *in vivo* efficacy. Antimicrobial activity within the host is influenced by many parameters (e.g., tissue penetration, concentration over time, host factors). Berlinger and Hancock (2021) [110] showed that adopting a more physiologically relevant *in vivo* test environment can influence



MIC values. Furthermore, the MIC value does not indicate the physiological state of cells. As the assay is based on visible cell growth, a compound could be bacteriostatic or bactericidal at the observed concentration [111]. Variation in methodology (e.g., change in inoculum or incubation time) can lead to considerable divergence of MICs. Furthermore, due to population dynamics within the sample, each MIC value can differ  $\pm$  one dilution step in each observation [112].

Nonetheless, MICs represent the current "gold standard" for determining antimicrobial activity. The experiments can be easily performed, offer the opportunity for automatisation – which also increases the reproducibility, and have a fast return of results (18-24 hours) [113]. Changing the setup would make new MIC values incomprehensible to the existing vast body of data.

## 2.4 Antibiofilm testing

Bacterial biofilms are estimated to cause > 60 % of hospital infections [114] as they adhere to medical equipment and promote infections in the patients. Compared to planktonic growing bacteria, biofilms increase protection against the immune system and antibiotic treatment (10-1000 x MIC [59]). Therefore, antimicrobial compounds are also screened for biofilm-eradication or -inhibition properties [115].

The assays used in this study are based on the staining of biofilms with Crystal Violet (CV). In a 96-well format, biofilm-forming bacteria (e.g., Gram-positive: *S. epidermidis* RP62A/ATCC 35984, or Gram-negative: *P. aeruginosa* PAO1) are cultivated in the presence of the antimicrobial in a two-fold concentration range (0.2-100  $\mu$ g/mL).

The biofilm formation inhibition assay quantifies the onset of biofilm formation. Here, the bacteria are grown in the presence of the compound for 24 hours. The compound is deemed inhibitory if the biofilm formation is impeded below the MIC value. The biofilm eradication assay investigates if the molecule can disperse established biofilms. The bacteria are grown for 24 hours in media to develop a biofilm. Afterwards, the growth medium is discarded and substituted with media containing the compound. In both assays, the media is discarded after the incubation, and the biofilm is stained with CV. After the staining, the biofilm can be quantified by optical density measurement [116].

The CV staining methods are convenient and easy to perform experiments. However, whilst *S. epidermidis* can form biofilms on the bottom of the 96-well plate, the assay needs additional equipment for *P. aeruginosa* cultivation. *P. aeruginosa* forms biofilm at the liquid-air interphase (swimming on top) [117]. This biofilm can easily be lost while handling the plates (e.g., substituting media, washing steps, and staining). Using MBEC biofilm inoculators or PEG-lids [118] resulted in a uniform biofilm formation. They enabled further handling similar to the *S. epidermidis* plates.

Following the incubation, media evaporation was observed in the wells framing the 96-well plate. This phenomenon is called the "Edge-Effect" [119] and can be countered by sealing plates with parafilm. The sealing creates an anaerobic environment that can simulate a more relevant clinical setting (host-like) – or in the case of *P. aeruginosa* PAO1 stimulate biofilm formation [120].

The CV staining methods offer an easy and low-cost option to assess initial biofilm formation and prevention capabilities in a medium-throughput format [121]. Biofilm active compounds can be further analysed for influence on metabolic activity and mechanical stability in more sophisticated dynamic models [122].

## **2.5 MOA profiling using promoter-reporter biosensors**

In the phenotypic-based drug discovery, the MOA of the antimicrobial is unknown, which poses a bottleneck for downstream MOA discovery. To address this issue, promoter-reporter based biosensors (e.g., luminescence or fluorescence) are used to map how an antimicrobial affects cellular targets and generates an MOA profile [25]. As a result, MOAs linked to major cellular pathways [123], heat shock, and oxidative stress [124] can be identified.

Antibiotic stress can selectively induce promoters in cells, which leads to a differential mRNA expression. Comparing the transcription of the promoters can provide a quantifiable phenotype following the exposure to antimicrobial stressors. This response can inform the MOA profile compared to reference antimicrobials with known targets [125]. So far, the most comprehensive and genome-wide reference compendium for mRNA expression profiling exists for *B. subtilis* [126] and *E. coli* [127], [128].

In this thesis, a library of eight *B. subtilis* 168 biosensors was used. The biosensors contained promoters that were fused to the luciferase reporter gene. The assay covered promoters for the biosynthesis of DNA (*yorB*), RNA (*belD*), proteins (*yheI*), cell wall and membrane (*ypuA*, *liaI*), fatty acids (*fabHB*), folic acid (*panB*), and included a viability control (*liaG*) reacting to antimicrobial stress in general [123]. The biosensors were grown in media with a concentration range of 0-8 x MIC of antimicrobial molecules or reference antibiotics, respectively.

The employed biosensors allowed the monitoring of essential pathways and could unravel off-target effects without knocking out essential genes [124]. The automated high-throughput setup offered a reproducible and fast real-time resolution when assessing the impact of antimicrobial stress (even at sub-MIC levels) on global gene expression. By comparing deviations to the wild type and other constructs, predictions for new antimicrobial molecules were assessed [128].

The method also comes with limitations. Any antimicrobial exclusively targeting Gram-negatives, or other Gram-positives, could not be detected. As of the end of this study, only *B. subtilis*-based biosensors were available for the DigiBiotics discovery pipeline. It has also been shown that these biosensors do not detect certain kinds of inhibitors with well-defined MOAs [129]. The *B. subtilis* biosensors could not detect tRNA synthase inhibitors, some PG synthesis inhibitors and membrane damaging agents. Urban *et al.* (2007) proposed similar gaps for types of protein biosynthesis inhibitors. To cover those gaps, MOA profiling could be supported by complementary techniques like transcriptomics [130], proteomics [131], or bacterial cytological profiling [132].

Nonetheless, the chosen biosensors offered an easy-to-use, viable, and low-cost model system to get a general indication of MOAs. Analysing MOAs on a pathway level enabled an HTS approach. Furthermore, a potential induction of multiple promoters at once can indicate combinational MOAs or off-target effects [126].

## 2.6 Membrane related assay

The bacterial membrane is essential for the survival and metabolic status of the cell. Membrane-active agents have two major MOAs: (i) they can interfere with several targets disrupting the functional integrity, or (ii) influence membrane-embedded proteins and the membrane potential, causing the inhibition of metabolic processes and leakage of cytosolic content [133]. The following assays were conducted to determine which MOA the compounds exhibited.

### 2.6.1 Membrane integrity analysis

Cellular or membrane integrity is one criterion for distinguishing between viable and dead bacterial cells [134]. To investigate the antimicrobial compounds' membranolytic properties, a method based on bioluminescence was used. Here, *B. subtilis* or *E. coli* producing intracellular luciferase were cultivated in a substrate (D-luciferin) containing media. If the membrane was destroyed, enzyme and substrate would react together and produce bioluminescence. The signal was relative to the degree of membrane disruption. If the membrane was disrupted, the signal would increase until internal ATP storage was depleted and dropped shortly afterwards. If the signal decreased over time, it indicated non-lethal membrane perturbations [135]. When compounds inhibit bacterial growth at non-permeabilising concentrations, their MOA will likely include interactions with the membrane or cellular targets [136].

Bacterial membranes are complex systems, and it is challenging to investigate single targets without disturbing the whole system. Model membrane systems (e.g., liposomes, vesicles, nanodiscs) can be used to investigate direct-acting effects on the lipid bilayers [137], [138]. Those artificial membranes offer the opportunity to investigate single membrane components (e.g., lipid compositions, membrane structure, drug-lipid interactions) [137], [139]. Alas, those physical systems provide an oversimplified version of the membrane. As many drugs target proteins, including membrane proteins in model systems is crucial. Membrane proteins are relatively unstable and denature once extracted from the membrane. To thoroughly investigate the functional properties of a membrane protein, it needs to be embedded in a membrane [137]. Thus, using a biological membrane model offers a more comprehensive overview of the range of possible drug interactions.

The assay is limited to a whole population resolution level. It is impossible to differentiate between potential subpopulations (e.g., viable vs permeabilised cells). This can be achieved by using flow cytometry and fluorescent dyes (e.g., propidium iodide or SYTO 9) [136]. However, those assays require an inoculation period for dye staining. In comparison, the assay in this study offers real-time monitoring of the drug-response dynamics. This factor is crucial for investigating fast-acting compounds like AMPs.

In conclusion, the assay can investigate membranolytic properties in real-time, is easy and cheap to conduct, and the 96-well format can potentially be automated.

## 2.6.2 Membrane potential quantification

To evaluate if antimicrobial compounds influence the metabolic state of bacteria, changes in the membrane potential were investigated. The membrane potential is a suitable indicator of cell metabolism, as it is the primary physical driving force for processes on/through the membrane.

Flow cytometry (FCM) offers opportunities to assess multiple cellular properties at once by measuring light and fluorescence scattering. Light scatter signals (forward scatter (FSC) and sideward scatter (SSC)) provide information about cell morphology. At the same time, fluorescent dyes can be used to monitor cellular functions or metabolic activity. FCM allows the investigation of whole bacterial populations and the detection of subpopulations within a sample. Subpopulations can be detected via morphological parameters (e.g., filamenting cells, cell debris, or aggregates) or metabolic states (e.g., live/dead staining, membrane potential). Thus, FCM offers a multiparametric analysis tool at the single-cell level to determine antimicrobial MOAs [140]–[142].

This study used a fluorescent dye to quantify the membrane potential of *S. aureus* ATCC 29213 in the presence of an antimicrobial at various concentrations. The green-fluorescent dye 3,3'-Diethyloxacarbocyanine iodide (DiOC<sub>2</sub>(3)) is transported into the cell if the membrane potential is active. After transportation, it embeds itself into the membrane. There, the dye self-aggregates and its fluorescence spectrum shifts from green to red. By quantifying the ratio of red to green fluorescence, changes in membrane potential can be analysed [143].

It is essential to choose suitable fluorescent dyes. Bacteria can be inherently resistant to staining. Dyes can bleed together via spectral overlap or sterically hinder each other [144]. In our case, DiOC<sub>2</sub>(3) needed an extensive pilot study as detection parameters (signals detection and strength) vary for each bacterial species – and rendered it not applicable for some (*B. subtilis* 168).

Nonetheless, the combination of potential-dependent staining and FCM offered an easy to conduct, cheap, high-throughput analysis of the membrane potential. It is a convenient and safe method to analyse whole bacterial cells ranging from single cells to populations.

## 2.7 Time-kill curves

Interactions of bacteria and drug molecules within the host are complex and variable systems. Therefore, information about pharmacodynamic (PD, concentration-dependent) and pharmacokinetic (PK, time-dependent) parameters is needed to inform patient dosing regime, prevention of drug-resistant bacteria, and drug development [145].

The most commonly used PK/PD parameter is the MIC. As the MIC is determined with fixed drug concentrations over a specified period of time (18-24 hours), it is a static parameter providing limited information. The antimicrobial effect *in vivo* results from dynamic changes in drug concentrations at the effect side. Therefore, data on changes in bacterial growth/kill rates in different drug concentrations over time are needed to represent those dynamics [146].

PD models are based on dose-response relationships. Here, time-kill curves (TKCs) were used to investigate the complexity of those interactions. TKCs provide more in-depth information than MIC about the nature of the inhibiting effect (bacteriostatic or bactericidal) and PD/PK [147]. Microbial growth or killing could be monitored as functions of drug concentration over time.

This study followed the standardised methods provided by the CLSI [148]. Here, bacteria were cultivated in a two-fold concentration range between 0-4 x MIC and bacterial survival was determined at time intervals from 0-5 hours. Bacterial survival was calculated by counting living cells (CFU/mL) after 24-hour cultivation on agar plates. Compounds were deemed bactericidal if a 1000-fold reduction of CFUs could be achieved.

TKCs are an easy and cost-efficient method to reflect a more variable *in vivo* setting than the static MIC [146]. Baquero and Levin (2021) [111] discussed that the most significant advantage of TKCs is they account for population heterogeneity. The high-density inoculum consists of subpopulations of diverse ages and physiological states. As antimicrobials can act at different concentrations with different effects [149], [150], the TKC accounts for a plethora of those combinations. Therefore, TKCs offer a comprehensible view of potential interaction/activities within the whole population.

This method does have limitations. As TKC reflect an increasing number of subpopulations, it still can not cover all possibilities. The CFU-based estimation of population numbers does not include persister cells (as they might not be detectable due to their slow growth rate) and cells forming aggregates (as they are located together and result in one indistinguishable colony). In

addition, the standard method is time-consuming and requires a large amount of consumables. High-throughput approaches have been proposed [151], which have their own limitations. Standard TKCs cannot mimic fluctuating drug concentrations (metabolism or adsorption in the host). Those dynamics are addressed in newer iterations of the method. Dynamic TKCs investigate changing antibiotic concentrations over prolonged time periods. In *S. aureus* varying drug concentrations and incubation (> 24 hours) showed significantly different antibiotic activities [152]. To further investigate PK/PD relations, more elaborate models (e.g., hollow fibre [153] or including body fluids [154]) are available.

MIC-only-based PK/PD integration cannot display the heterogeneity in bacterial populations. Therefore, more detailed PK/PD parameter estimation methods are needed [145]. The standard TKC offers a simple, economical, and easy to operate method to directly describe the interaction between drug and pathogen.

## 2.8 General methodological considerations

In cell-based assays, compounds are typically serially diluted before being added to microtiter plates. During many preparation steps, the interaction between compound and surfaces (e.g., microtiter plates, pipette tips, reaction tubes) can lead to a loss in compound or carryover [155]. AMPs, for example – due to their positive charges – are prone to adhere to common lab equipment made of glass or polystyrene. To avoid experimental inaccuracy, it is advised to handle AMP in polypropylene and cationic-adjusted growth media [156].

Most antimicrobial drugs target metabolically active cells. Slow-growing or dormant cells can avoid treatment and re-emerge after antibiotic treatment [141]. This can lead to distorted results when methods based on endpoint measurements are used. To avoid those pitfalls, the screening cascade should either include techniques with single-cell resolution (FCM or microscopy) or longitudinal studies (TKC) [157],[158].

The combination of multiple assays led to the variability of experimental parameters (inoculum density, number of molecules per membrane phospholipid, etc.). This awareness is essential when interpreting data, especially results that differ in effect or magnitude. Efforts to reduce variability as much as possible were implemented to the best of our knowledge (an example of variability is presented in Table 1 for **paper II**).

Experiment	Bacterial strain	Cell density (CFU/ml) <sup>A</sup>	Volume inoculum (μl)	Cells added (n)	x MIC	μg/mL	μM <sup>B</sup>	Assay volume (μl)	Molecules (n)	Molecules/Cell
Promotor-biosensor assay	<i>B. subtilis</i> 168	1.00E+08	45	4.50E+06	8	64	86.34	50	2.60E+15	5.78E+08
		1.00E+08	45	4.50E+06	4	32	43.17	50	1.30E+15	2.89E+08
		1.00E+08	45	4.50E+06	2	16	21.59	50	6.50E+14	1.44E+08
		1.00E+08	45	4.50E+06	1	8	10.79	50	3.25E+14	7.22E+07
		1.00E+08	45	4.50E+06	0.5	4	5.40	50	1.62E+14	3.61E+07
		1.00E+08	45	4.50E+06	0.25	2	2.70	50	8.12E+13	1.81E+07
		5.00E+07	180	9.00E+06	4	32	43.17	200	5.20E+15	5.78E+08
		5.00E+07	180	9.00E+06	2	16	21.59	200	2.60E+15	2.89E+08
Membrane integrity assay	<i>B. subtilis</i> 168	5.00E+07	180	9.00E+06	1	8	10.79	200	1.30E+15	1.44E+08
		5.00E+07	180	9.00E+06	0.5	4	5.40	200	6.50E+14	7.22E+07
		1.00E+06	1000	1.00E+06	4	25.00	43.17	1000	2.60E+16	2.60E+10
		1.00E+06	1000	1.00E+06	2	12.50	21.59	1000	1.30E+16	1.30E+10
Membrane potential assay	<i>S. aureus</i> ATCC 29213	1.00E+06	1000	1.00E+06	1	6.25	10.79	1000	6.50E+15	6.50E+09
		1.00E+06	1000	1.00E+06	0.5	3.13	5.40	1000	3.25E+15	3.25E+09
		1.00E+06	1000	1.00E+06	0.25	1.56	2.70	1000	1.62E+15	1.62E+09
		1.50E+08	500	7.50E+07	1	8	10.79	1000	6.50E+15	8.67E+07
Microscopy	<i>B. subtilis</i> 168 <i>B. subtilis</i> 2020	1.50E+08	500	7.50E+07	1	8	10.79	1000	6.50E+15	8.67E+07
		1.00E+06	750	1.00E+06	4	32.00	43.17	1500	3.90E+16	3.90E+10
Time-kill curves	<i>B. subtilis</i> 168	1.00E+06	750	1.00E+06	2	16	21.59	1500	1.95E+16	1.95E+10
		1.00E+06	750	1.00E+06	1	8	10.79	1500	9.75E+15	9.75E+09
		1.00E+06	750	1.00E+06	0.5	4	5.40	1500	4.87E+15	4.87E+09
		1.00E+06	750	1.00E+06	0.25	2	2.70	1500	2.44E+15	2.44E+09

Table 1. Variation of molecule/cell ration within the assay cascade; <sup>A</sup> Cell density estimated for OD<sub>600</sub> 1.0 = 5\*10<sup>8</sup> CFU/ml; <sup>B</sup> lulworthinone Mw 741.22 g/mol



## 2.9 Summary

This chapter discussed the screening assay cascade methods used to determine the MOA of antimicrobial compounds. As this work is part of two bigger drug discovery projects, complementary assays were done by other work packages. An overview of all methods used is displayed in Figure 11. As a result of the combined research effort, it was possible to analyse 25 antimicrobial molecules. The following result chapter will highlight the findings of each paper based on those findings.

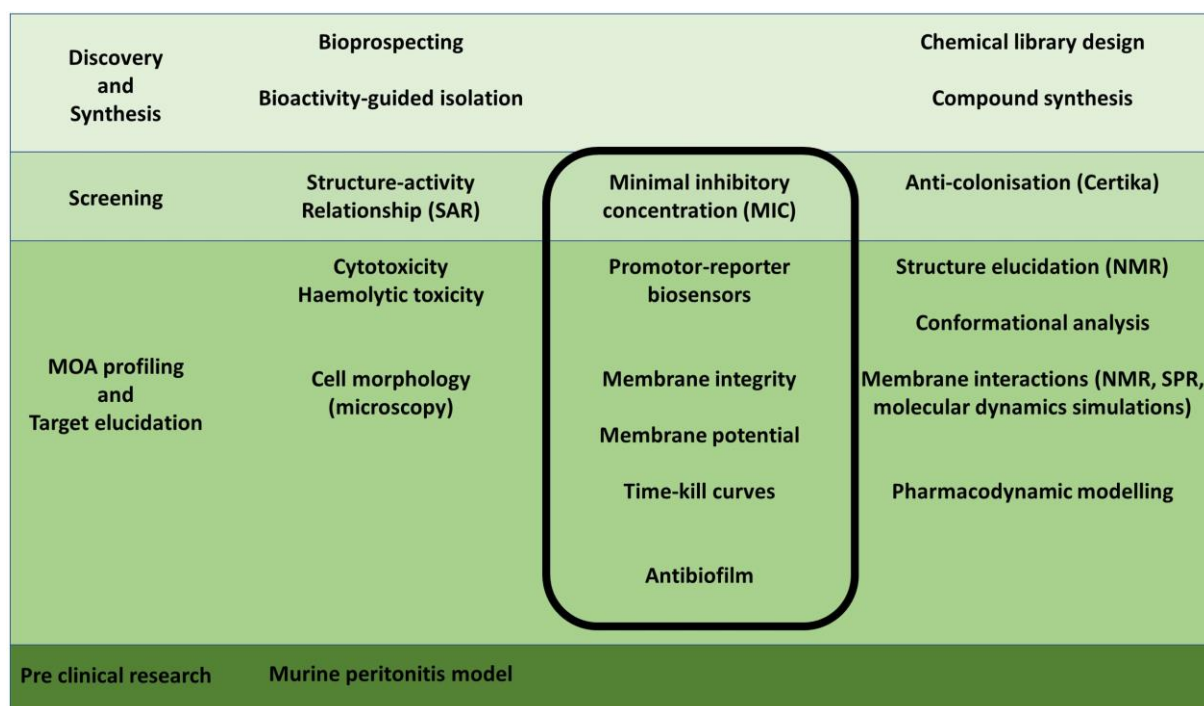


Figure 11. DigiBiotics workflow and assay cascade, highlighted in black are the phenotype-based assays described in this thesis.

### 3 Summary of main results

#### 3.1 Paper I

##### **Lulworthinone, a New Dimeric Naphthopyrone From a Marine Fungus in the Family Lulworthiaceae With Antibacterial Activity Against Clinical Methicillin-Resistant *Staphylococcus Aureus* Isolates**

Lulworthinone (**1**) was isolated from an obligate marine fungus from the order of *Lulworthiales*. The natural product showed antimicrobial activity against Gram-positive reference strains *S. aureus*, *S. agalactiae*, and five clinical MRSA isolates with MICs ranging from 1.56-12.5  $\mu\text{g/mL}$ .

Furthermore, the molecule had antiproliferation properties against three human cell lines: a melanoma cell line (A2058,  $\text{IC}_{50} = 15.5 \mu\text{g/mL}$ ), a hepatocellular carcinoma cell line (HepG2,  $\text{IC}_{50} = 27 \mu\text{g/mL}$ ), and a non-malignant lung fibroblast cell line (MRC5,  $\text{IC}_{50} = 32 \mu\text{g/mL}$ ).

The fungus produced the molecule in high yields ( $\sim 45 \text{ mg/mL}$ ). NMR and HRMS elucidated the structure as a dimeric naphthopyrone. Acidic isolation or test environments led to a degradation of the molecule (**2**). NMR indicated a potential aggregation of lulworthinone but not for the degradation product.

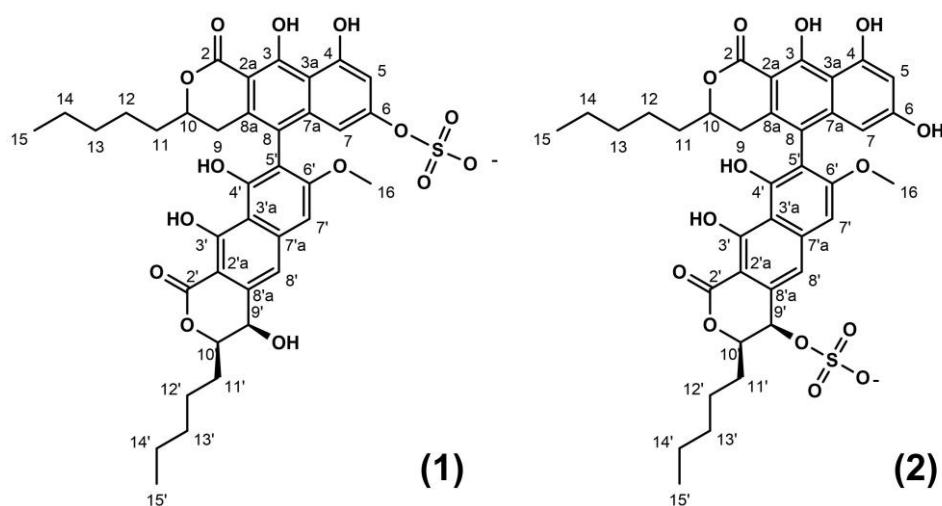


Figure 12. Molecular structure of lulworthinone (1) and its degradation product (2)

## 3.2 Paper II

### Lulworthinone: *In Vitro* Mode of Action Investigation of an Antibacterial Dimeric Naphthopyrone Isolated from a Marine Fungus

The antibacterial activity of lulworthinone against MRSA prompted a follow-up mode of action study. Biosensors indicated a cell wall/membrane targeting MOA profile of the molecule. Combined results of artificial and biological membrane models showed that lulworthinone does not interfere with the structural membrane integrity. At the same time, already small amounts of lulworthinone ( $\geq 0.25 \times \text{MIC}$ ) dissipated the membrane potential of *S. aureus* 29213.

The loss of membrane potential has been shown to influence cell division proteins. Here we could show that the key protein FtsZ was delocalised. The presence of the compound leads furthermore to an increase in cell size/volume and cell chain formation. Surface plasmon resonance (SPR) and dynamic light scattering revealed that the antibacterial activity is linked to the ability of lulworthinone to form aggregates.

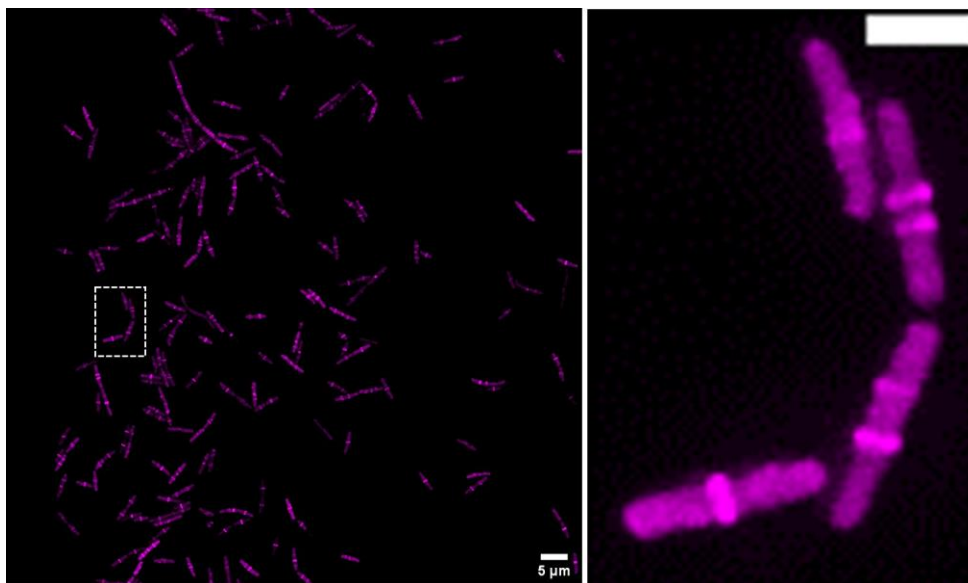


Figure 13. FtsZ delocalisation in *B. subtilis* 2020 after treatment with 1 x MIC lulworthinone

### 3.3 Paper III

#### Amphipathic Barbiturates as Mimics of Antimicrobial Peptides and the Marine Natural Products Eusynstyelamides with Activity against Multi-Resistant Clinical Isolates

The natural products eusynstyelamides follow the pharmacophore model of AMPs. Here, peptides mimicking their structure – two cationic side chains and two lipophilic side chains attached to a barbiturate scaffold – are investigated for their structure-activity relationships (SAR) and MOA. Two peptide series containing either two amines or guanines as cationic groups in combination with varying lipophilic side chains were tested. Both series displayed improved antibacterial activity (2-8  $\mu\text{g/mL}$ ) against common lab strains and clinical isolates from the ESKAPE group compared to the natural product (MIC of 6.25-12.5  $\mu\text{g/mL}$  against *S. aureus* ATTC 9144 and 20 - > 50  $\mu\text{g/mL}$  for MRSA ATCC 33591 [159]).

The lead compound **7e** (containing guanine) was further investigated. The murine neutropenic peritonitis model showed a significant reduction of viable bacterial cells of clinical *E. coli* and *K. pneumoniae* isolates. Simulations indicated incorporation of **7e** in the membrane in a low-energy "W"-like conformation. MOA studies proposed membranolytic properties of the compounds. The current peptidomimetic scaffold can easily be modified in respect of variation in cationic and lipophilic groups.

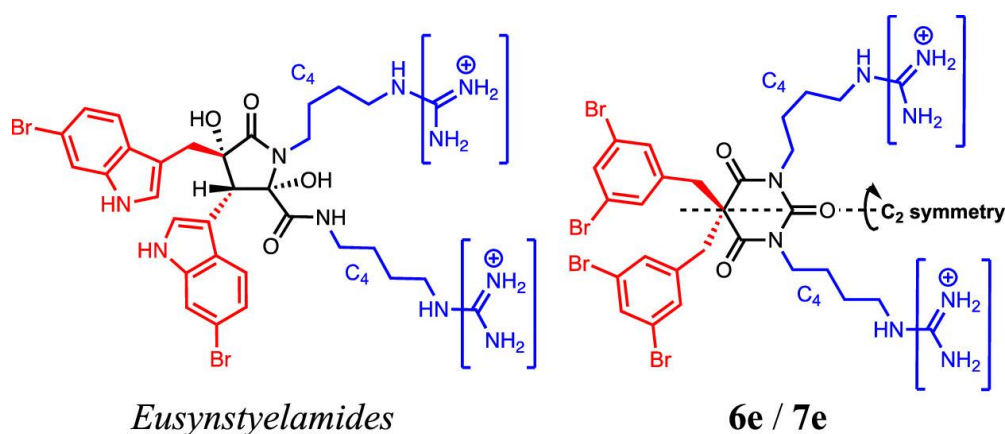


Figure 14. General chemical structure of the natural products eusynstyelamides and the amphipathic barbiturates

### 3.4 Paper IV

#### Anti-Colonisation Effect of Au Surfaces with Self-Assembled Molecular Monolayers Functionalised with Antimicrobial Peptides on *S. Epidermidis*

Medical devices containing anticolonisation surfaces can combat healthcare-associated infections. This study investigated the efficacy of antimicrobial peptides covalently attached to a golden surface. The molecules were successfully connected to the surface via a copper-catalysed [3 + 2] azide-acetylene coupling (CuAAC). The surfaces exhibited a dense and uniform coverage with peptides.

The tested peptide library showed a wide range of antibacterial efficacy. The library investigated four different parameters: (i) the exchange of tryptophan residues for bulkier biphenylalanine led to an increase in efficacy, (ii) cyclisation – and steric confinement – of the peptides led to a favourable activity against Gram-positives and a reduction in Gram-negatives, (iii) tethering the peptides with a chemical linker on the surface influenced the MIC marginally, and (iv) while longer peptide tethers resulted in less bacterial colonisation on the surfaces, the cyclic peptide **2d** – directly attached to the surface – showed a 6-log reduction in bacterial colonisation.

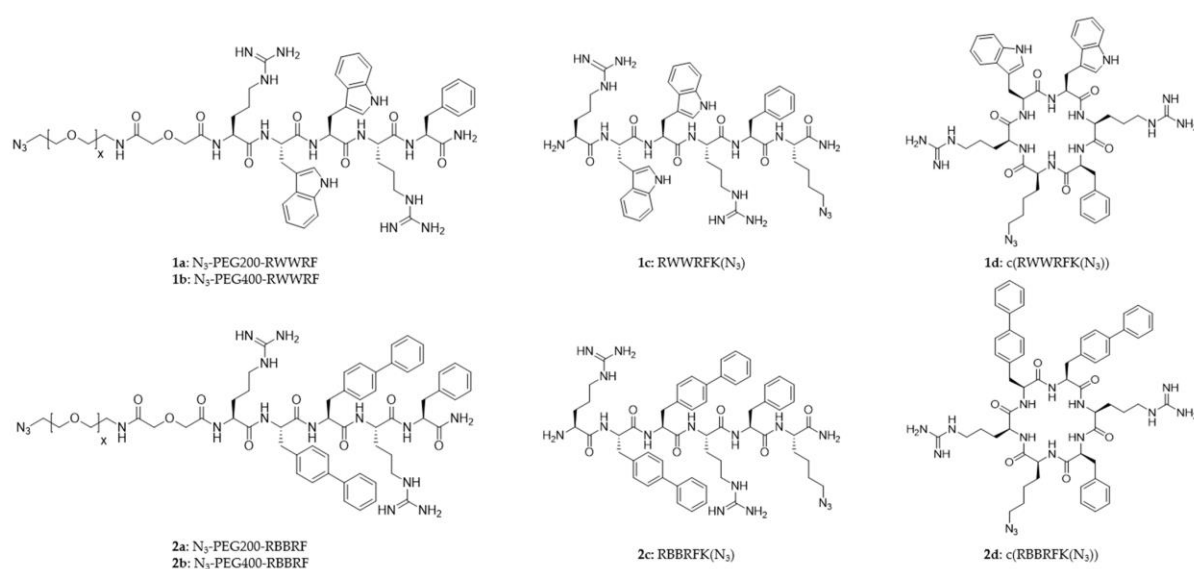


Figure 15. Overview of the small cationic peptide library investigated in **paper IV**

## 4 Discussion

The overuse and misuse of antimicrobials lead to a substantial increase in antimicrobial resistance. This is of public concern as most modern medicine areas rely on antibiotics. Unfortunately, the current drug development pipeline cannot produce enough innovative antimicrobial agents to outcompete the rise of resistance. Therefore, we need to fill the drug development pipeline with antimicrobial molecules from new chemical classes or with new MOAs [160].

This study was part of two related drug discovery projects - AntiBioSpec and DigiBiotics. The goal was to identify new antimicrobial compounds from the marine environment and determine their MOAs. In addition, the potential application of AMPs as a surface coating was investigated. The projects were based on multiple work packages to achieve this goal, each investigating molecules from a different scientific perspective while forming a pipeline workflow. This work reports the microbiological perspective.

The research-based discovery pipeline identified multiple hit compounds, most of them active against the clinically significant ESKAPE group. MOA studies indicate membrane-targeted activity in all cases. Some compounds displayed promising properties for further drug development (hit-to-lead phase) or application on medical devices. The main results are discussed in the **papers I-IV**. The findings in a more general context will be addressed in the following chapter.

## 4.1 The natural product lulworthinone — aggregation and delocalisation

**Screening** **Paper I** presents the results of a phenotypic screening campaign. The campaign investigated the underexplored biodiversity of marine microorganisms found in the Arctic. The bioactivity guided isolation of natural products was performed on 20 strictly marine microorganisms [161].

In the case of lulworthinone, the dereplication step showed an unusual elemental composition. The combination of a dimeric structure, the presence of a sulphate group, and a high yield prompted the isolation of the bioactive compound. NMR-aided searches in molecule structure databases identified the compound as a dimeric naphthopyrone. Antimicrobial susceptibility testing revealed activity against a range of Gram-positive bacteria (*B. subtilis*, *S. agalactiae*, *S. epidermidis* and *S. aureus*), including several clinical MRSA strains (MIC 1.56–6.25 µg/mL). Several naphthopyrones have been discovered, and most are active against MRSA [162]–[166]. This indicates that the naphthopyrone scaffold could be a privileged structure [167]. Based on those findings, it was decided to research lulworthinone and establish an MOA profile.

**MOA** **Paper II** investigated the MOA of lulworthinone. An array of promotor-based biosensors covering major cellular pathways was used to screen for a potential MOA. Two biosensors indicated a cell envelope directed MOA. The promotor expressing *ypuA* is regulated by the sigma factor SigM and senses environmental stress [168]. It indicates cell wall biosynthesis inhibition or cell envelope stressing agents (e.g., vancomycin, polymyxin B and beta-lactams) [169]. The promotor expressing *liaI* is under the regulation of the two-component system LiaS/R and senses cell wall-active antibiotics that interfere with the lipid II cycle or perturb the cytoplasmatic membrane (e.g., AMP, bacitracin, and vancomycin). [170], [171]

Following this indication, multiple assays investigated the cell envelope integrity. Using NMR and artificial membranes [172], the permeation of water and ions through a lipid bilayer was analysed. No significant increase in permeation could be detected upon lulworthinone treatment. This ruled out a daptomycin-like increase of permeability, mainly based on interactions with phospholipids [173].

Using a biological model system, no significant cell wall or membrane integrity changes were detected. This indicates that lulworthinone exhibits no cell wall lysing properties like vancomycin or beta-lactams [47], [174]. Those results led to the investigation of the bacterium's cell viability and metabolic state.

A significant decrease in the membrane potential was shown at already low concentrations of lulworthinone. This points towards a negative influence on the cell energy production and physiological state, possibly leading to bacterial death. It is worth mentioning that concentrations of 0.25-0.5 x MIC led to a lag-phase of the population in the TKC (**paper II**, Figure 9). We speculate that cultures cultivated in concentrations below MIC can adapt their cell surface to the antimicrobial pressure of lulworthinone and survive afterwards.

Morphological studies via microscopy detected fewer bacteria in treated samples and the formation of cell chains. The appearance of the cell chains led to two hypotheses: (i) stress-induced cell chaining or (ii) improper cell division.

Cell chaining is known in *B. subtilis* as a phenotypic change from single motile cells to sessile chains. This effect is connected to the early onset of biofilm production and survival against environmental stress. Therefore, the observed aberrant morphology could indicate a general stress response to lulworthinone [175]–[177].

The cell division apparatus is a complex machinery offering multiple angles of attack [178] and recently moved into focus for antimicrobial drug development [179]. Cell division is initiated by polymerising FtsZ into a mid-cell ring structure (Z-ring), forming a scaffold for the division apparatus [178]. The positioning of the Z-ring is regulated by the Min protein system [180], cytoskeletal elements like MreB [181], and the anchor protein of FtsZ – FtsA [182]. All three structures are anchored or tethered to the membrane.

It was previously shown that MinD and FtsA tether themselves to the membrane by burrowing their amphipathic helix at their C-terminus into the bilayer [182], [183]. Membrane potential loss inhibits this tethering and leads to the delocalisation of most proteins involved in cell division. This led to the inhibition or reduction of septal localisation of the Z-ring [184]. Similarly, the presence of lulworthinone led to the delocalisation of FtsZ (Figure 8, **paper II**) or the formation of multiple Z-rings per cell. Those results align with the effects first described by Strahl and Hamoen (2010) [184] through dissipation of the membrane potential.



Additionally, it has been shown that FtsA mutants in *E. coli* and *B. subtilis* grow filamentously due to ineffective cell division [185]. Therefore, we suggest that membrane potential dissipation is the primary bactericidal effect of lulworthinone. The division apparatus is prokaryote-specific and offers an attractive drug target, especially as the crucial protein FtsZ is conserved among bacteria species [179], [186].

**Aggregation** In **paper I**, NMR indicated a possible self-aggregation of lulworthinone via its sulphate group. This group moves from C6-C9' in the scaffold in an acidic environment, and aggregation was no longer detectable. Following those indications, we observed self-aggregation of the molecule via SPR and DLS. We demonstrated that lulworthinone's antibacterial activity is linked to aggregation, and the calculated PD curve pointed towards colloidal aggregation.

Colloidal aggregates (CAs) form concentration-dependent, stable, spherical particles (50-1000 nm). They are known for non-specific reversible protein adsorption and inhibition [187], [188]. Due to their non-specific interactions with proteins, they can generate false-positive hits in HTS and are considered pan-assay interference compounds (PAINS) [189]. Based on their non-drug like activity, CAs are discarded as potential lead compounds. They are an example of the high attrition rates in early drug discovery.

**Applications** Although considered artefacts of the drug discovery process, colloidal aggregates are investigated for their unique properties. Their ability to stabilise proteins or polymers in aggregates opened the possibility of using CAs as potential drug delivery vehicles [190]–[192]. Colloidal aggregation offers a concentration-dependent carrier system in the hundreds of nanometres range that can transport drug molecules to previously inaccessible parts of the body [192].

Furthermore, lulworthinone targets mainly Gram-positive bacteria - including MRSA. As CAs are supposed to inhibit surface proteins unspecifically, it raises the question if there is a preferred surface protein family. Due to the concentration-dependent aggregation of lulworthinone, the target proteins could be enriched and further characterised [190], [193]. This would offer more insight into potential treatment options against MRSA.

**Limitations** In general, the MOA studies were hindered due to the bottleneck of compound supply. The compound yield of ~45.5 mg/L was outstandingly high for a fungus - other fungi

from the campaign yielded 0.02-14.1 mg/mL [161]. However, it took > 2 months to isolate this amount of compound, which was still not enough for all downstream assays.

Regarding PAINS, the screening campaign could have included safety precautions. As PAINS are known in HTS settings, a counter screen involving detergents (e.g., Triton X-100 or Tween-80) could have been easily implemented [188]. This would help to identify potential aggregators in the screening step. After the structure elucidation, electronic PAINS filters can help further flag possible artefacts. It should be noted that there are no definite properties to distinguish PAINS from drugs, but filters can be used as a precaution to generate awareness of an eventual probability [189].

The case of lulworthinone has highlighted that potential antimicrobial compounds are hidden in the complex biodiversity of the Arctic. The determination of the MOA investigated two targets for drug development – the membrane potential and the cell division machinery. We propose the MOA is based on membrane interaction and the following membrane potential dissipation. Unfortunately, aggregation-based activity is – at least currently – undesirable for drug development. Nonetheless, colloidal aggregation gains more interest itself as a potential drug delivery system.

## 4.2 Amphipathic barbiturates — a promising scaffold

**Screening and SAR Paper III** summarised the approach to identify hit compounds by screening a synthetic peptide library. The makeup of the library is based on a previously discovered natural products class – eusynstyelamides [159], [194], [195]. The compounds combined two cationic groups (either amine or guanidine) and two lipophilic groups attached to a central ring. This amphipathic character resembles the pharmacophore of AMPs. Generating peptidomimetics of eusynstyelamides, the influence of the two cationic groups (amine or guanidine) in combination with different bulky lipophilic groups was characterised. Antimicrobial susceptibility testing indicated broad-spectrum activity against common lab strains and clinical isolates from the ESKAPE group.

The chemical modification of the scaffold led to increased antimicrobial properties, and the main conclusions are in accordance with the literature. The antimicrobial activity increased with the lipophilicity of the side chains – but so did the haemolytic toxicity [196]–[198]. The guanidine series decreased the MIC by ~4-fold compared to the amines. Intriguingly, the electron distribution within the aromatic parts of the lipophilic side chains seemed to influence interaction with the bacterial membrane. At the same time, electron-withdrawing aromatic fluorines decreased haemolytic toxicity [199]. The guanidine series showed more haemolytic toxicity than the amine series but were less toxic against human cell lines (HepG2 & MRC-5). These results highlight the complex interplay between the different cationic and lipophilic side chains and their influence on antibacterial activity, haemolytic toxicity, and human cell cytotoxicity.

**MOA** The broad-spectrum guanidine barbiturate **7e** (3,5-di-Br) showed overall highest activity against clinical isolates and was selected for an *in vivo* pilot study. The murine peritonitis model – a standard model to study antimicrobial chemotherapy – was used to evaluate preclinical drug efficacy and safety [200]. The molecules were well tolerated up to 2.8 mg/kg with a maximally tolerated dose of 7 mg/kg in the mice. Treatment with **7e** led to a 90-98% reduction of the bacterial load. This indicates an antibacterial activity *in vivo* without rapid inactivation by the host.

To gain insights into the molecular dynamics of the barbiturates, conformational structures and membrane interactions were simulated. According to density functional theory-based geometry, there were three stable low energy configurations of **7e**. All three differed in the orientation of the lipophilic side chains. The orientation of an upward "W" was the energy

lowest configuration (Figure 6, **paper III**). Molecular dynamics simulations used a model of an inner membrane from *E. coli* to investigate the interaction between the molecules and membrane. For **7e**, the model predicts: (i) a fast insertion in the membrane, (ii) molecules remains within the membrane, and (iii) the molecule adapted the "W" conformation. The insertion was generally expected due to electrostatic interactions and activities of AMPs [201].

The predicted membranolytic activity of **7e** was investigated together with **6e** as an example of amine barbiturates. The activity of both molecules was compared between cell viability and membrane integrity assays.

For Gram-positives, both compounds revealed a strong and fast bactericidal effect which correlated with disruption of the membrane. In the case of **7e**, the membrane was destroyed < 2 seconds. The destruction was related to MIC values and showed increasing killing rates above the MIC. The Gram-positive model demonstrated a "typical" membrane disruptive MOA. The peptidomimetics permeabilised the cytoplasmatic membrane, leading to a fast bactericidal killing [202].

Gram-negatives showed a different picture. Even though the general viability decreased similar to Gram-positives, membranolytic activities, especially for **7e**, were less pronounced and delayed. Those findings indicate (i) the outer membrane of Gram-negatives offers protection against the peptidomimetics, and (ii) the peptidomimetics may have a secondary killing effect as the viability still decreased.

The outer membrane has proven to be the biggest challenge in treating Gram-negative infections [3]. Compounds can pass passively through the membrane or via porins in the membrane [203]. Both compounds – **6e** and **7e** – showed a delayed effect. A porin-based transport is unlikely as the barbiturates violate most "rules of permeation" [204]–[206]. This indicates a general prolonged time needed for permeation through the membrane.

The cell viability is still decreased, similar to the Gram-positive model. This indicates a secondary MOA. Besides permeabilisation or pore formation, AMPs have been shown to translocate into the cytoplasm and interfere with cytoplasmatic septum formation, cell-wall synthesis, nucleic acid synthesis, and protein synthesis [207]. All those MOAs cause a rapid killing, and would agree with the results. Additional studies focusing on potential intracellular targets could elucidate the activity against Gram-negatives further.

**Applications** The development of AMP-based therapies has encountered multiple challenges. Due to their stability, bioavailability, efficacy and toxicity problems, AMPs struggle to succeed in the clinic [84]. The barbiturate structure offers an easily adjustable scaffold for further optimisation studies. This is an essential factor in overcoming the problems mentioned above. Furthermore, the ease of synthesis has favourable implications for reducing cost and upscaling the production of the compounds.

The amphipathic barbiturates offer, compared to the natural products [194], [159], increased antimicrobial activity. Significantly, the activity against colistin-resistant bacteria – one of the drugs of last resort – must be highlighted here. Combined with the general lack of novel antimicrobial classes against Gram-negatives, the barbiturate scaffold addresses unmet clinical needs [208]. It should be further investigated in the Hit-to-Lead phase.

**Limitations** The barbiturate library investigated the naturally occurring cationic groups combined with multiple bulky lipophilic side chains. For the next iteration of barbiturates, it might be feasible to consider the Lipinski "rules of five" [209] and "rules of permeation" [205], [206], [210] for constructing the library. Addressing those rules offers a guideline to optimise the natural leads and should improve the activity against Gram-negatives and antimicrobial uptake [3].

Pore formation of AMPs depends on the lipid/peptide ratio on the membrane [207]. In the current test setup of the membrane integrity assay, the bacterial inoculum is 1000-fold increased compared to the MIC assay. Therefore, potential membranolytic activity against Gram-negatives was probably not observed due to the increased amount of target and the slower diffusion rate of the molecule through the outer membrane.

The peptide library has shown the potential to optimise natural drug leads regarding antimicrobial activity. The molecule **7e** showed the most promising broad-spectrum activity, even against colistin-resistant clinical isolates. With the first promising preclinical data from the *in vivo* studies, it would be prudent to move into the Hit-to-lead phase of the drug discovery process. Here, further downstream processes can benefit from the easy to modify chemical structure of the barbiturates.

### 4.3 Antimicrobial peptides — surface coating as a potential application

**Screening** Paper IV also investigated a small peptide library based on the small cationic AMP pharmacophore [211]. The goal was to use the peptides to create an anti-colonisation surface against bacteria. All peptides adhere to the general pharmacophore for an AMP, an amphipathic structure generated by the segregation of two cationic and three lipophilic groups on the scaffold.

At first, the influence of three parameters on intrinsic antimicrobial activity was tested: (i) the bulkiness of lipophilic amino acids, (ii) attaching polyethylene glycol (PEG) linkers (short/long), or (iii) the cyclisation of the peptides.

The peptides showed a mixed spread of intrinsic antimicrobial activity. In general, the peptides were more active against Gram-positives than Gram-negatives. Replacing tryptophan with the bulkier and more lipophilic biphenylalanine increased the antimicrobial activity. This effect was expected and is in accordance with the literature [212], [213].

PEG-linkers will be used to tether the peptides to the surfaces. Here, the influence on antimicrobial activity of short (Mw 200) and long (Mw 400) PEG linkers attached to the peptide were investigated. In both cases, the peptide activity was reduced. The activity loss could indicate a reduction of binding affinity due to sterical hindrance of the AMP by the PEG-tail. The tail could either wrap around the molecule or hinder membrane passage [214].

The cyclisation of peptides has been reported to enhance antibacterial activity due to increased amphipathicity, leading to increased membrane interactions [215]. Furthermore, cyclic peptides are less prone to degradation [216] and increase salt resistance [217]. To see if conformational freedom of peptide influences the antimicrobial effect, one peptide of each series (containing either tryptophan or biphenylalanine) was cyclised. The cyclic peptides were more effective against Gram-positives, but not for Gram-negatives. Those results are in contradiction to results priorly reported [215]. This discrepancy might be caused due to differences in media (MHB instead of LB) and strains (*E. coli* ATCC 29522 and *P. aeruginosa* ATCC 27853 instead of *E. coli* DH5 $\alpha$ ).

**MOA** It has been shown that AMPs covalently bound to a surface are still lethal. The most influential known parameters are the surface type, coupling strategy, usage of chemical spacers, peptide concentration and orientation [218]. Multiple solid surface types (e.g., glass [219],

[220], metal [221], [222], plastic [223], [224], or self-assembled monolayers (SAM) [225] are under investigation for coating with AMPs. The peptide immobilisation can be carried out randomly (binding pre-synthesised peptides in random orientation to the surface) or in a controlled manner (constructing peptides on the surface). The controlled immobilisation is preferable to ensure the availability of the active AMP motives [226], [227].

In **paper IV**, the peptides were immobilised on an Au-SAM surface via click chemistry [228]. In combination with ToF-SIMS [229], a successful and evenly distributed homogenous peptide coverage of the surface could be proven. The successful immobilisation of all peptides enabled the investigation of the influence of PEG-linkers/spacers on anti-colonisation activity.

The bactericidal activity of immobilised peptides is dependent on the conformational freedom to form secondary structures. Some AMPs can be directly immobilised on a surface. They are active if they can adapt their secondary structure (e.g.,  $\alpha$ -helix or  $\beta$ -sheets) [230], [231]. Other AMPs (e.g., LL-37 [221], KLAL, MK5E [232]) need more room and flexibility to express their antimicrobial activity. Here, using a spacer enables flexibility and lateral movement for antibacterial activity. In those cases, increased spacer length correlates with enhanced activity [232]. PEG is commonly used as a linker to tether AMP to the surface. PEG intrinsic properties (anionic, hydrophilic and flexible [233]–[235]) make it an excellent antifouling agent. Here, it additionally helps by preventing non-specific peptide binding to the surface.

The antiproliferation assay [236] revealed an interesting anti-colonisation pattern in **paper IV**. As seen in the intrinsic antimicrobial activity, biphenylalanine containing peptides had a stronger effect than the tryptophan ones. A minor increase in activity could be shown with growing spacer length (on surface < PEG 200 < PEG 400) in both series. Surprisingly both cyclic peptides directly immobilised on the surface demonstrated strong anti-colonisation effects (**1d** ~256-fold; **2e** ~1\*10<sup>6</sup>-fold).

As highlighted by Bagheri *et al.* (2009) [232], the general membrane-associated MOA of AMPs [237], [238] does not seem to be influenced by the spacer. If specific binding to the target is needed (e.g. nisin selective binding of lipid II [43]), the spacer might influence the activity. The extent to which the MOA of the cyclic peptides benefits from direct immobilisation needs to be further investigated.

**Application** The primary MOA of AMPs is directed towards the membrane. This offers the opportunity to immobilise AMPs on the surface of medical devices to prevent bacterial

contamination and biofilm formation [133]. Binding AMPs covalently to a surface exploits their advantages (e.g., broad-spectrum activity, low resistance development) while countering their disadvantages (e.g., short-term stability, cytotoxicity, and bioavailability) [218]. Furthermore, surfaces treated with AMPs have proven their long-term stability and resistance to environmental conditions. It has been shown that they withstand extended washing, heat treatment, changing pH values, and ultrasonic treatment [224]. Combined with antifouling surfaces (e.g., PEG), AMP treated surfaces offer opportunities to lessen the burden of device-associated infections [239], [240].

**Limitations** Immobilising an AMP decreases the antimicrobial activity up to 100-fold compared to soluble molecules [59], [232], [241]. Therefore, the lack of available molecules might impede concentration-dependent killing MOAs, like pore formation. The spatial distance toward the target has to be considered as well. As shown by Bagherie *et al.* (2009) [232], antimicrobial activity is dependent on spacer length. The usage of PEG spacers ( $M_w \leq 400$ ) eradicated antimicrobial activity for Gram-negatives. It seems that the peptide tethers are too short to span the LPS and interact with the membranes.

In a more general setting, AMP coated surfaces need contact with the bacteria. Molecules from either the host or bacteria (e.g., serum, blood pellets, ECM) could mask the surface and lead to an inactivation of the antimicrobial properties. To counteract this possibility, it is considered beneficial to combine bactericidal AMP surfaces with antifouling surfaces [59].

This small peptide library has shown a potential application for AMPs. As AMPs struggle in clinical development (e.g., due to low stability, cytotoxicity, bioavailability and short half-time), binding them covalently to a surface can mitigate some disadvantages. Medical devices with surface-bound AMPs have been shown to reduce bacterial colonisation 3-4-fold [242]. They can help to combat bacterial infections and reduce antibiotic usage, especially in the case of the cyclic peptides **1d** and **2d**, which demonstrated a surprisingly strong anti-colonisation effect compared to their MICs. Follow up studies may reveal more about the relationship between MIC values and anti-colonisation outcomes.



## 4.4 DigiBiotics

**Call to action** The rise of AMR and the lack of antimicrobial molecules in the development pipeline led to a call to action from the WHO [243] and the European Commission [244]. To reinvigorate the field, public-funded projects should step in and cover for the lack of early drug discovery projects from the industry. Norway answered the call by coordinating research efforts with the Joint Programming Initiative on Antimicrobial Resistance (JPIAMR) [245] and funding multiple national projects via the Digital Life Norway framework [246]. The DigiBiotics project was financed with ~24 million NOK [247].

The main goal of DigiBiotics was to find new antimicrobials from or inspired by the marine environment. To enable a robust screening campaign, the project defined core drug properties – similar to a target product profile (TPP). To meet the challenge of AMR, the molecules needed to be active against bacteria of the ESKAPE group and have a cell envelope targeted MOA.

Every chemical library was pre-selected and tailored to adhere to the TPP. To ensure membrane activity, each library was based on the pharmacophore of AMPs. The previous knowledge of AMPs at UiT laid the foundation for the construction of the libraries. Additionally, bioprospecting was included to broaden the influx of compounds for the pipeline.

**Roadmap** It needs a lot of time and effort to develop the next generation of antimicrobials. To ensure a robust antimicrobial discovery pipeline, it is more important than ever to have stricter concepts about the screening process, assays needed to reach Go/No-Go thresholds and how to proceed after initial hit compound validation. Recently, Miethke et al. (2022) [248] have proposed a roadmap to enhance and sustain current trends in discovery and development. Fortunately, DigiBiotics already adhered to most aspects concerning the early discovery steps.

The workflow should be generally based on standardised assays to establish a reliable screening campaign. Following those predefined test setups decreases reproducibility problems and yields a more robust hit compound series.

The screening process should be combined with MIC determination. The antimicrobial molecules can demonstrate their activity against existing resistance mechanisms by including contemporary clinical isolates in the screening. This data elevates a hit compound – as it confirms activity in whole cells and clinical relevance. The combination can speed up the screening process and enables faster downstream analysis. This aspect has been shown in **papers I and III**. The activity against ESKAPE bacteria prompted follow up studies.

Indications of the MOA, molecular targets and toxicity accelerate the hit discovery further. Any chemical modification for ADMET properties will benefit from this knowledge. Therefore, assays elucidating those areas should be included as early as possible. This speeds up the discovery process and can result in an early Go/No-Go decision for further development. This approach was used during the thesis. In the cases of lulworthinone, the aggregation-based MOA made it undesirable for further drug development. In contrast, the membranolytic MOA and *in vivo* pilot study highlighted the potential of the amphipathic barbiturate **7e** as a lead compound.

Here is where academia and public funding mostly ends. Resources necessary to move a molecule from Hit-to-lead increase immensely and are mostly not covered in the academic budget. This phase needs a diverse scientific team with expertise in microbiology, bioinformatics, pharmacokinetics, analytical, computational, and medicinal chemistry that is out of scope for purely academic research [248]. Academic groups either have to collaborate with translational research centres (like the Helmholtz Centre for Infection Research [249] or the Translational Research Institute Australia [250]) or partner with the industry to progress further. The last decades have led to a diverse network to invigorate antimicrobial development. By building more capacity within a project it increases the chance to attract funding (REPAIR Impact Fund [251], AMR action fund [252], DISARM and PASTAUER act [253], [254]), generating spin-offs (e.g., incubators like INCATE [194], AICUBATOR [195]), getting help from NGOs (GARDP [257], CARB-X [258]), and collaborate with other companies (BEAM Alliance [259]).

**The academic setting** As highlighted above, a broad spectrum of expertise is needed for drug development. This is out of scope for purely academic research groups and requires a wide net of collaborations. While DigiBiotics is a network of research groups with diverse expertise, it is still based on fundamental research. Downstream processes like medicinal chemistry, *in vivo* experiments, and in-depth PK/PD studies are rarely possible in an academic setting and need substantial funding.

Furthermore, it is hard to sustain competence in academia. As academia is a fluid system of PhDs, Post Docs and PIs, competence will be built and lost frequently. It is hard to achieve in-depth knowledge compared to an industrial setting. While research groups usually focus on specific molecular targets, mechanisms, or organisms – pharmaceutical companies use whole platforms for investigation. To combine the need for public-funded research with long-term

stability, public translational research centres might be the solution. A national centre would focus research efforts and offer stability and know-how for projects. This could improve the outcome and sustainability of knowledge for publicly-funded research [248], [260].

The DigiBiotics project has shown that early drug discovery can be effective in academia. Within the project's scope, marine or marine-inspired compounds were characterised, and new tools for MOA studies were developed. Besides this thesis's described work, the pipeline published ten papers, and each associated PhD is close to graduation. To translate the research further, it is necessary to engage in research agreements within a more extensive framework — public or private — to develop a market-ready drug.

## 4.5 Why MOA studies

Many EMA/FDA approved drugs are without known MOAs or targets [261], [262]. This raises the question of why spend resources and time investigating MOAs. Drug development is a complex, lengthy, and expensive process with a high uncertainty that the drug will succeed [263]. To guide the process and enable decisions, as many facts as possible must be known. Knowledge about the MOA offers significant pieces of information.

First, the MOA is informative about the biology behind the antimicrobial activity. This was shown for lulworthinone and the barbiturates. Each molecule provides new insights into a target molecule and related biological processes. The interactions between the drug and target give data on potential resistance development, applications, or even secondary targets. Furthermore, each drug is also a tool for potential follow up studies to investigate the target extensively.

Secondly, the MOA informs the drug development process. Understanding the MOA helps to predict, evaluate, and understand the clinical effects of the molecule. The information directs efforts for chemical modifications. As shown for the barbiturates, a drug can be optimised regarding activity on the target (effectivity) and the patient (ADMEtox). This adds an immense value to the individual sample molecule and fights the attrition rate in the pipeline [264]. Furthermore, MOA and target validation can lead to the development of follow-on drugs. Each discovery helps to decode mechanisms and facilitates advances in medicinal chemistry [265].

Thirdly, the MOA helps advise about the drug's clinical usage and potential regulations. Knowledge about the MOA helps generate a safety and efficacy profile of the molecule. This enables better dosing of the compound (stability, half time, effective dose etc.), informs about the potential application, and helps to predict side effects within the human body.

## 4.6 Summary

This chapter provided an overview of each researched compound class, discussed the rationale behind the screening campaigns and investigated the putative MOAs. The natural product lulworthinone showed a membrane-active MOA — dissipating the membrane potential and dysregulation of the cell division apparatus. The activity was linked to the aggregation of the molecule, which makes it undesirable for drug development but opens potential applications as a drug carrier system. The marine-inspired amphipathic barbiturates showed a broad-spectrum activity against bacteria of the ESKAPE group. The antimicrobial activity is linked to membranolytic properties in Gram-positives, but effects in Gram-negatives indicate a secondary MOA. The promising pilot study *in vivo* and the easily adjustable scaffold make compound **7e** an attractive candidate for further investigations. The AMP pharmacophore was additionally investigated for potential application as a coating for medical devices. The covalent attachment of cyclic peptide **2d** led to a 6-log reduction in bacterial colonisation, highlighting AMP-coated surfaces' potential benefit in the medical setting.

Furthermore, the framework of academic drug discovery was discussed in the example of Digibiotics, and the benefits of MOA studies were highlighted.

## 5 Future prospects

The results obtained within this study should be followed up in further studies. This chapter will propose opportunities for future research.

First, antimicrobial activity was shown for multiple naphthopyrones. However, to our knowledge aggregation was never linked to their activity. This opens the question of whether the antibacterial effect is based on the naphthopyrone scaffold or colloidal aggregation. This conundrum is especially intriguing as lulworthinone aggregation is based on the sulphate groups not present in other molecules and their placement. To elucidate the relationship, other known naphthopyrones can be tested for activity in the presence of detergents. Furthermore, as the sulphate group seems to be the primary facilitator for aggregation, its role should be further investigated with crystallisation or in conformational and molecular dynamic models to understand the molecular interactions better [266]–[268].

Second, few drug molecules from the discovery pipeline show activity in *in vivo* assays or in clinical trials. This is not surprising, as the laboratory environments differ vastly from the host. Host determinants (blood [269], serum [270], plasma [271]) or nutrients [110], [272] have been shown to alter activities of antimicrobials. Therefore, the screening process should be adapted to resemble a more physiological significant (host-mimicking) environment [273]. This could be achieved by using defined-media like artificial urine for uropathogens [274] or iron-depleted media mimicking wound or bloodstream infections [275]. Such biomimetic assays have the potential to yield more robust hit/lead compounds that are active in the host.

Third, some antimicrobial activity of AMPs is based on a peptide/lipid ratio. As highlighted in Table 1, a wide range of ratios was used between different assays. This was not taken into consideration for all applied assays in the workflow. Future iterations of the pipeline workflow should synchronize the overall compound concentration. Those adjustments should improve the comparability and significance of the results.

Fourth, as highlighted in **paper II** microscopy offers a strong tool to elucidate MOAs. The cell morphology is a good indicator of potential antibacterial effects. A new tool — bacterial cytological profiling [276], [277] — has been shown to be a fast approach to analysing potential MOAs. Compounds with similar MOA can be grouped by staining major cellular components and analysing them in a principal component analysis. This technique can offer an additional angle to generate an MOA profile.

Furthermore, as peptides are relatively easy synthesized, they offer the potential for further modification. Regular dyes introduce a bulky extension to the molecule, this might interfere with the activity. Currently, a pilot study aiming for label-free peptide visualization using fluorescent amino acids is in progress. This would allow us to visualize the direct spatial target of the peptides, circumventing possible sterically hindrances.

## 6 Conclusion

This chapter will conclude the study by summarising the key research findings in relation to the research objectives and aims and the value and contribution thereof.

The thesis aimed to investigate small antibacterial molecules effective against clinically relevant bacteria. The results indicate that each compound was membrane-active. Further findings showed that each selected molecule had a different MOA, highlighting multiple attack angles for antimicrobial treatment. Additionally, AMPs were investigated for a potential application as an anti-colonising surface coating.

Within four publications, several molecules were screened for their antimicrobial effect. Multiple hit compounds with activity against clinically relevant bacteria were identified:

- Lulworthinone, a dimeric naphthopyrone isolated from a marine fungus, showed activity against many Gram-positive bacteria – including MRSA.
- Multiple amphipathic barbiturates, based on the scaffold of eusyntyelamides, demonstrated antimicrobial properties against a panel of ESKAPE bacteria. The barbiturate **7e**, containing guanidine, was further investigated due to its good antibacterial activity and low toxicity.
- The library of small cationic peptides displayed a mixture of antimicrobial activity related to changes in the bulkiness of the cationic groups, attachment of chemical linkers and cyclisation

*In vitro* test systems elucidated the potential MOAs of two selected molecules as membrane-active. Those MOAs are currently a research focus in drug development.

- Lulworthinone displayed an MOA that is potentially based on the dissipation of the membrane potential. This caused a delocalisation of the cell division apparatus and led to improper cell division.
- The barbiturates showed a primary membranolytic MOA. Hit compound **7e** indicated a secondary MOA in Gram-negatives as cells were slowly lysed but rapidly killed.

The membrane-targeting MOAs offer potential use they are known to interfere more with the physical properties than biological targets on the surface

- Lulworthinone showed promising bactericidal activity. Unfortunately, the MOA is based on self-aggregation. Currently, this behaviour is undesirable for drug molecules due to challenging ADMET properties. Nonetheless, the colloidal aggregation process itself is under investigation as a potential drug delivery system.
- The barbiturate **7e** has shown a broad-spectrum activity *in vitro* and bacterial clearing in the first *in vivo* pilot. In combination with its easy to modify scaffold, it offers the potential to be moved to the Hit-to-Lead phase for further investigation as a potential antimicrobial.
- All short cationic peptides could be uniformly attached to the model surface at a high density. This lays the foundation for a potential application as a surface coating. Furthermore, the cyclic versions of the peptides showed a strong anti-colonisation effect which offers the opportunity for AMPs as a surface coating on medical devices.

The current study demonstrates how the interdisciplinary approach of the DigiBiotics project can lay the foundation for efficient drug discovery in the academic setting. In the future, our **paper I-IV** findings should help provide a mechanistic knowledge of molecules targeting the bacterial membrane.



## References

- [1] C. J. Murray *et al.*, ‘Global burden of bacterial antimicrobial resistance in 2019: a systematic analysis’, *The Lancet*, vol. 0, no. 0, Jan. 2022, doi: 10.1016/S0140-6736(21)02724-0.
- [2] U. Theuretzbacher, K. Outterson, A. Engel, and A. Karlén, ‘The global preclinical antibacterial pipeline’, *Nat. Rev. Microbiol.*, vol. 18, no. 5, pp. 275–285, May 2020, doi: 10.1038/s41579-019-0288-0.
- [3] K. Lewis, ‘The Science of Antibiotic Discovery’, *Cell*, vol. 181, no. 1, pp. 29–45, Apr. 2020, doi: 10.1016/j.cell.2020.02.056.
- [4] S. A. Fleming, ‘Nobel Lecture’, *NobelPrize.org*, 1945. <https://www.nobelprize.org/prizes/medicine/1945/fleming/lecture/> (accessed Apr. 12, 2022).
- [5] World Health Organization, *Antimicrobial resistance: global report on surveillance*. Geneva: World Health Organization, 2014. Accessed: Apr. 12, 2022. [Online]. Available: <https://apps.who.int/iris/handle/10665/112642>
- [6] J. O’Neil, ‘Tackling drug-resistant infections globally: final report and recommendations.’, United Kingdom, May 2016. [Online]. Available: [https://amr-review.org/sites/default/files/160518\\_Final%20paper\\_with%20cover.pdf](https://amr-review.org/sites/default/files/160518_Final%20paper_with%20cover.pdf)
- [7] E. Tacconelli *et al.*, ‘Discovery, research, and development of new antibiotics: the WHO priority list of antibiotic-resistant bacteria and tuberculosis’, *Lancet Infect. Dis.*, vol. 18, no. 3, pp. 318–327, Mar. 2018, doi: 10.1016/S1473-3099(17)30753-3.
- [8] L. B. Rice, ‘Federal Funding for the Study of Antimicrobial Resistance in Nosocomial Pathogens: No ESKAPE’, *J. Infect. Dis.*, vol. 197, no. 8, pp. 1079–1081, Apr. 2008, doi: 10.1086/533452.
- [9] M. I. Hutchings, A. W. Truman, and B. Wilkinson, ‘Antibiotics: past, present and future’, *Curr. Opin. Microbiol.*, vol. 51, pp. 72–80, Oct. 2019, doi: 10.1016/j.mib.2019.10.008.
- [10] K. Lewis, ‘Antibiotics: Recover the lost art of drug discovery’, *Nature*, vol. 485, no. 7399, pp. 439–440, May 2012, doi: 10.1038/485439a.
- [11] S. A. Cochrane and J. C. Vederas, ‘Lipopeptides from *Bacillus* and *Paenibacillus* spp.: A Gold Mine of Antibiotic Candidates’, *Med. Res. Rev.*, vol. 36, no. 1, pp. 4–31, 2016, doi: 10.1002/med.21321.
- [12] R. Shukla *et al.*, ‘Mode of action of teixobactins in cellular membranes’, *Nat. Commun.*, vol. 11, no. 1, Art. no. 1, Jun. 2020, doi: 10.1038/s41467-020-16600-2.
- [13] J. M. Stokes *et al.*, ‘A Deep Learning Approach to Antibiotic Discovery’, *Cell*, vol. 180, no. 4, pp. 688–702.e13, Feb. 2020, doi: 10.1016/j.cell.2020.01.021.
- [14] T. F. Durand-Reville *et al.*, ‘Rational design of a new antibiotic class for drug-resistant infections’, *Nature*, vol. 597, no. 7878, Art. no. 7878, Sep. 2021, doi: 10.1038/s41586-021-03899-0.
- [15] C. Årdal *et al.*, ‘Insights into early stage of antibiotic development in small- and medium-sized enterprises: a survey of targets, costs, and durations’, *J. Pharm. Policy Pract.*, vol. 11, p. 8, Apr. 2018, doi: 10.1186/s40545-018-0135-0.
- [16] J. A. DiMasi, H. G. Grabowski, and R. W. Hansen, ‘Innovation in the pharmaceutical industry: New estimates of R&D costs’, *J. Health Econ.*, vol. 47, pp. 20–33, May 2016, doi: 10.1016/j.jhealeco.2016.01.012.
- [17] O. J. Wouters, M. McKee, and J. Luyten, ‘Estimated Research and Development Investment Needed to Bring a New Medicine to Market, 2009–2018’, *JAMA*, vol. 323, no. 9, pp. 844–853, Mar. 2020, doi: 10.1001/jama.2020.1166.

- [18] J. Rex, ‘What does an antibiotic cost to develop? What is it worth? How to afford it?’, *AMR.Solutions*, Mar. 06, 2020. <https://amr.solutions/2020/03/06/what-does-an-antibiotic-cost-to-develop-what-is-it-worth-how-to-afford-it/> (accessed Apr. 13, 2022).
- [19] J. Cama *et al.*, ‘To Push or To Pull? In a Post-COVID World, Supporting and Incentivizing Antimicrobial Drug Development Must Become a Governmental Priority’, *ACS Infect. Dis.*, vol. 7, no. 8, pp. 2029–2042, Aug. 2021, doi: 10.1021/acsinfecdis.0c00681.
- [20] C. Årdal *et al.*, ‘Antibiotic development — economic, regulatory and societal challenges’, *Nat. Rev. Microbiol.*, vol. 18, no. 5, pp. 267–274, May 2020, doi: 10.1038/s41579-019-0293-3.
- [21] E. Petrova, ‘Innovation in the Pharmaceutical Industry: The Process of Drug Discovery and Development’, in *Innovation and Marketing in the Pharmaceutical Industry: Emerging Practices, Research, and Policies*, M. Ding, J. Eliashberg, and S. Stremersch, Eds. New York, NY: Springer, 2014, pp. 19–81. doi: 10.1007/978-1-4614-7801-0\_2.
- [22] E. D. Zanders, ‘Drug Discovery Pipeline Overview’, in *The Science and Business of Drug Discovery*, Cham: Springer International Publishing, 2020, pp. 95–98. doi: 10.1007/978-3-030-57814-5\_5.
- [23] J. Hughes, S. Rees, S. Kalindjian, and K. Philpott, ‘Principles of early drug discovery’, *Br. J. Pharmacol.*, vol. 162, no. 6, pp. 1239–1249, Mar. 2011, doi: 10.1111/j.1476-5381.2010.01127.x.
- [24] M. Schenone, V. Dančik, B. K. Wagner, and P. A. Clemons, ‘Target identification and mechanism of action in chemical biology and drug discovery’, *Nat. Chem. Biol.*, vol. 9, no. 4, pp. 232–240, Apr. 2013, doi: 10.1038/nchembio.1199.
- [25] B. R. da Cunha, P. Zoio, L. P. Fonseca, and C. R. C. Calado, ‘Technologies for High-Throughput Identification of Antibiotic Mechanism of Action’, *Antibiotics*, vol. 10, no. 5, Art. no. 5, May 2021, doi: 10.3390/antibiotics10050565.
- [26] K. Lewis, ‘Platforms for antibiotic discovery’, *Nat. Rev. Drug Discov.*, vol. 12, no. 5, Art. no. 5, May 2013, doi: 10.1038/nrd3975.
- [27] G. E. Croston, ‘The utility of target-based discovery’, *Expert Opin. Drug Discov.*, vol. 12, no. 5, pp. 427–429, May 2017, doi: 10.1080/17460441.2017.1308351.
- [28] D. J. Payne, L. F. Miller, D. Findlay, J. Anderson, and L. Marks, ‘Time for a change: addressing R&D and commercialization challenges for antibacterials’, *Philos. Trans. R. Soc. B Biol. Sci.*, vol. 370, no. 1670, p. 20140086, Jun. 2015, doi: 10.1098/rstb.2014.0086.
- [29] R. Tommasi, D. G. Brown, G. K. Walkup, J. I. Manchester, and A. A. Miller, ‘ESKAPEing the labyrinth of antibacterial discovery’, *Nat. Rev. Drug Discov.*, vol. 14, no. 8, Art. no. 8, Aug. 2015, doi: 10.1038/nrd4572.
- [30] J. G. Moffat, F. Vincent, J. A. Lee, J. Eder, and M. Prunotto, ‘Opportunities and challenges in phenotypic drug discovery: an industry perspective’, *Nat. Rev. Drug Discov.*, vol. 16, no. 8, Art. no. 8, Aug. 2017, doi: 10.1038/nrd.2017.111.
- [31] G. C. Terstappen, C. Schlüpen, R. Raggiaschi, and G. Gaviraghi, ‘Target deconvolution strategies in drug discovery’, *Nat. Rev. Drug Discov.*, vol. 6, no. 11, Art. no. 11, Nov. 2007, doi: 10.1038/nrd2410.
- [32] E. Purssell, ‘Antimicrobials’, *Underst. Pharmacol. Nurs. Pract.*, pp. 147–165, Sep. 2019, doi: 10.1007/978-3-030-32004-1\_6.
- [33] P. Cardoso *et al.*, ‘Molecular engineering of antimicrobial peptides: microbial targets, peptide motifs and translation opportunities’, *Biophys. Rev.*, vol. 13, no. 1, pp. 35–69, Feb. 2021, doi: 10.1007/s12551-021-00784-y.
- [34] N. G. Bush, I. Diez-Santos, L. R. Abbott, and A. Maxwell, ‘Quinolones: Mechanism, Lethality and Their Contributions to Antibiotic Resistance’, *Molecules*, vol. 25, no. 23, p. 5662, Dec. 2020, doi: 10.3390/molecules25235662.

- [35] H. Mosaei and N. Zenkin, ‘Inhibition of RNA Polymerase by Rifampicin and Rifamycin-Like Molecules’, *EcoSal Plus*, vol. 9, no. 1, Apr. 2020, doi: 10.1128/ecosalplus.ESP-0017-2019.
- [36] S. B. Vakulenko and S. Mobashery, ‘Versatility of Aminoglycosides and Prospects for Their Future’, *Clin. Microbiol. Rev.*, vol. 16, no. 3, pp. 430–450, Jul. 2003, doi: 10.1128/CMR.16.3.430-450.2003.
- [37] G. M. Eliopoulos and P. Huovinen, ‘Resistance to Trimethoprim-Sulfamethoxazole’, *Clin. Infect. Dis.*, vol. 32, no. 11, pp. 1608–1614, Jun. 2001, doi: 10.1086/320532.
- [38] R. M. Eband, C. Walker, R. F. Eband, and N. A. Magarvey, ‘Molecular mechanisms of membrane targeting antibiotics’, *Biochim. Biophys. Acta BBA - Biomembr.*, vol. 1858, no. 5, pp. 980–987, May 2016, doi: 10.1016/j.bbamem.2015.10.018.
- [39] M.-P. Mingeot-Leclercq and J.-L. Décout, ‘Bacterial lipid membranes as promising targets to fight antimicrobial resistance, molecular foundations and illustration through the renewal of aminoglycoside antibiotics and emergence of amphiphilic aminoglycosides’, *MedChemComm*, vol. 7, no. 4, pp. 586–611, Apr. 2016, doi: 10.1039/C5MD00503E.
- [40] R. D. Turner, W. Vollmer, and S. J. Foster, ‘Different walls for rods and balls: the diversity of peptidoglycan’, *Mol. Microbiol.*, vol. 91, no. 5, pp. 862–874, Mar. 2014, doi: 10.1111/mmi.12513.
- [41] A. R. Brown, R. A. Gordon, S. N. Hyland, M. S. Siegrist, and C. L. Grimes, ‘Chemical Biology Tools for Examining the Bacterial Cell Wall’, *Cell Chem. Biol.*, vol. 27, no. 8, pp. 1052–1062, Aug. 2020, doi: 10.1016/j.chembiol.2020.07.024.
- [42] L. Pasquina-Lemonche *et al.*, ‘The architecture of the Gram-positive bacterial cell wall’, *Nature*, vol. 582, no. 7811, Art. no. 7811, Jun. 2020, doi: 10.1038/s41586-020-2236-6.
- [43] A. Guiotto, M. Pozzobon, M. Canevari, R. Manganeli, M. Scarin, and F. M. Veronese, ‘PEGylation of the antimicrobial peptide nisin A: problems and perspectives’, *Il Farm.*, vol. 58, no. 1, pp. 45–50, Jan. 2003, doi: 10.1016/S0014-827X(02)01301-0.
- [44] M. Baptista, F. Depardieu, P. Courvalin, and M. Arthur, ‘Specificity of induction of glycopeptide resistance genes in *Enterococcus faecalis*’, *Antimicrob. Agents Chemother.*, vol. 40, no. 10, pp. 2291–2295, Oct. 1996, doi: 10.1128/AAC.40.10.2291.
- [45] R. R. Yocum, J. R. Rasmussen, and J. L. Strominger, ‘The mechanism of action of penicillin. Penicillin acylates the active site of *Bacillus stearothermophilus* D-alanine carboxypeptidase’, *J. Biol. Chem.*, vol. 255, no. 9, pp. 3977–3986, May 1980.
- [46] J. M. Munita, A. S. Bayer, and C. A. Arias, ‘Evolving resistance among Gram-positive pathogens’, *Clin. Infect. Dis. Off. Publ. Infect. Dis. Soc. Am.*, vol. 61 Suppl 2, pp. S48-57, Sep. 2015, doi: 10.1093/cid/civ523.
- [47] T. Dörr, ‘Understanding tolerance to cell wall-active antibiotics’, *Ann. N. Y. Acad. Sci.*, vol. 1496, no. 1, pp. 35–58, Jul. 2021, doi: 10.1111/nyas.14541.
- [48] P. Sarkar, V. Yarlagadda, C. Ghosh, and J. Haldar, ‘A review on cell wall synthesis inhibitors with an emphasis on glycopeptide antibiotics’, *MedChemComm*, vol. 8, no. 3, pp. 516–533, Mar. 2017, doi: 10.1039/C6MD00585C.
- [49] J. F. Coyle, F. A. Pagliai, D. Zhang, G. L. Lorca, and C. F. Gonzalez, ‘Purification and partial characterization of LdtP, a cell envelope modifying enzyme in *Liberibacter asiaticus*’, *BMC Microbiol.*, vol. 18, no. 1, p. 201, Nov. 2018, doi: 10.1186/s12866-018-1348-8.
- [50] W. Stillwell, ‘Membrane Transport’, *Introd. Biol. Membr.*, pp. 423–451, 2016, doi: 10.1016/B978-0-444-63772-7.00019-1.
- [51] M.-T. Nguyen, M. Matsuo, S. Niemann, M. Herrmann, and F. Götz, ‘Lipoproteins in Gram-Positive Bacteria: Abundance, Function, Fitness’, *Front. Microbiol.*, vol. 11, p. 582582, Sep. 2020, doi: 10.3389/fmicb.2020.582582.

- [52] J. M. A. Blair, M. A. Webber, A. J. Baylay, D. O. Ogbolu, and L. J. V. Piddock, ‘Molecular mechanisms of antibiotic resistance’, *Nat. Rev. Microbiol.*, vol. 13, no. 1, Art. no. 1, Jan. 2015, doi: 10.1038/nrmicro3380.
- [53] G. Kapoor, S. Saigal, and A. Elongavan, ‘Action and resistance mechanisms of antibiotics: A guide for clinicians’, *J. Anaesthesiol. Clin. Pharmacol.*, vol. 33, no. 3, pp. 300–305, 2017, doi: 10.4103/joacp.JOACP\_349\_15.
- [54] R. E. Impey, D. A. Hawkins, J. M. Sutton, and T. P. Soares da Costa, ‘Overcoming Intrinsic and Acquired Resistance Mechanisms Associated with the Cell Wall of Gram-Negative Bacteria’, *Antibiotics*, vol. 9, no. 9, p. 623, Sep. 2020, doi: 10.3390/antibiotics9090623.
- [55] L. F. Westblade, J. Errington, and T. Dörr, ‘Antibiotic tolerance’, *PLOS Pathog.*, vol. 16, no. 10, p. e1008892, Oct. 2020, doi: 10.1371/journal.ppat.1008892.
- [56] K. Lewis, ‘Persister Cells’, *Annu. Rev. Microbiol.*, vol. 64, no. 1, pp. 357–372, Oct. 2010, doi: 10.1146/annurev.micro.112408.134306.
- [57] H.-C. Flemming and J. Wingender, ‘The biofilm matrix’, *Nat. Rev. Microbiol.*, vol. 8, no. 9, Art. no. 9, Sep. 2010, doi: 10.1038/nrmicro2415.
- [58] M. Kostakioti, M. Hadjifrangiskou, and S. J. Hultgren, ‘Bacterial biofilms: development, dispersal, and therapeutic strategies in the dawn of the postantibiotic era’, *Cold Spring Harb. Perspect. Med.*, vol. 3, no. 4, p. a010306, Apr. 2013, doi: 10.1101/cshperspect.a010306.
- [59] M. Dostert, M. J. Trimble, and R. E. W. Hancock, ‘Antibiofilm peptides: overcoming biofilm-related treatment failure’, *RSC Adv.*, vol. 11, no. 5, pp. 2718–2728, Jan. 2021, doi: 10.1039/d0ra09739j.
- [60] S. R. Partridge, S. M. Kwong, N. Firth, and S. O. Jensen, ‘Mobile Genetic Elements Associated with Antimicrobial Resistance’, *Clin. Microbiol. Rev.*, vol. 31, no. 4, pp. e00088-17, Aug. 2018, doi: 10.1128/CMR.00088-17.
- [61] J. Davies and D. Davies, ‘Origins and Evolution of Antibiotic Resistance’, *Microbiol. Mol. Biol. Rev.*, vol. 74, no. 3, pp. 417–433, Sep. 2010, doi: 10.1128/MMBR.00016-10.
- [62] J. Vila, J. Moreno-Morales, and C. Ballesté-Delpierre, ‘Current landscape in the discovery of novel antibacterial agents’, *Clin. Microbiol. Infect.*, vol. 26, no. 5, pp. 596–603, May 2020, doi: 10.1016/j.cmi.2019.09.015.
- [63] U. Theuretzbacher and L. J. V. Piddock, ‘Non-traditional Antibacterial Therapeutic Options and Challenges’, *Cell Host Microbe*, vol. 26, no. 1, pp. 61–72, Jul. 2019, doi: 10.1016/j.chom.2019.06.004.
- [64] Y. M. Lee, F. Almqvist, and S. J. Hultgren, ‘Targeting virulence for antimicrobial chemotherapy’, *Curr. Opin. Pharmacol.*, vol. 3, no. 5, pp. 513–519, Oct. 2003, doi: 10.1016/j.coph.2003.04.001.
- [65] U. Theuretzbacher, K. Outtersson, A. Engel, and A. Karlén, ‘The global preclinical antibacterial pipeline’, *Nat. Rev. Microbiol.*, vol. 18, no. 5, pp. 275–285, May 2020, doi: 10.1038/s41579-019-0288-0.
- [66] D. M. P. De Oliveira *et al.*, ‘Antimicrobial Resistance in ESKAPE Pathogens’, *Clin. Microbiol. Rev.*, vol. 33, no. 3, pp. e00181-19, /cmr/33/3/CMR.00181-19.atom, May 2020, doi: 10.1128/CMR.00181-19.
- [67] B. C. Wilson, T. Vatanen, W. S. Cutfield, and J. M. O’Sullivan, ‘The Super-Donor Phenomenon in Fecal Microbiota Transplantation’, *Front. Cell. Infect. Microbiol.*, vol. 9, 2019, Accessed: Apr. 15, 2022. [Online]. Available: <https://www.frontiersin.org/article/10.3389/fcimb.2019.00002>
- [68] R. Peraman *et al.*, ‘Insights on recent approaches in drug discovery strategies and untapped drug targets against drug resistance’, *Future J. Pharm. Sci.*, vol. 7, no. 1, p. 56, Mar. 2021, doi: 10.1186/s43094-021-00196-5.

- [69] C. R. Chong and D. J. Sullivan, 'New uses for old drugs', *Nature*, vol. 448, no. 7154, Art. no. 7154, Aug. 2007, doi: 10.1038/448645a.
- [70] N. K. Boyd, C. Teng, and C. R. Frei, 'Brief Overview of Approaches and Challenges in New Antibiotic Development: A Focus On Drug Repurposing', *Front. Cell. Infect. Microbiol.*, vol. 11, 2021, Accessed: Mar. 18, 2022. [Online]. Available: <https://www.frontiersin.org/article/10.3389/fcimb.2021.684515>
- [71] W. Younis, S. Thangamani, and M. N. Seleem, 'Repurposing Non-Antimicrobial Drugs and Clinical Molecules to Treat Bacterial Infections', *Curr. Pharm. Des.*, vol. 21, no. 28, pp. 4106–4111.
- [72] W. Kim *et al.*, 'A new class of synthetic retinoid antibiotics effective against bacterial persisters', *Nature*, vol. 556, no. 7699, Art. no. 7699, Apr. 2018, doi: 10.1038/nature26157.
- [73] S. H. Christiansen *et al.*, 'The Immunomodulatory Drug Glatiramer Acetate is Also an Effective Antimicrobial Agent that Kills Gram-negative Bacteria', *Sci. Rep.*, vol. 7, no. 1, Art. no. 1, Nov. 2017, doi: 10.1038/s41598-017-15969-3.
- [74] K. U. Jansen and A. S. Anderson, 'The role of vaccines in fighting antimicrobial resistance (AMR)', *Hum. Vaccines Immunother.*, vol. 14, no. 9, pp. 2142–2149, Sep. 2018, doi: 10.1080/21645515.2018.1476814.
- [75] I. Bekeredjian-Ding, 'Challenges for Clinical Development of Vaccines for Prevention of Hospital-Acquired Bacterial Infections', *Front. Immunol.*, vol. 11, 2020, Accessed: Jun. 05, 2022. [Online]. Available: <https://www.frontiersin.org/article/10.3389/fimmu.2020.01755>
- [76] D. Thomas and C. Wessel, 'The State of Innovation in Antibacterial Therapeutics', p. 39, 2022.
- [77] U. Theuretzbacher *et al.*, 'Critical analysis of antibacterial agents in clinical development', *Nat. Rev. Microbiol.*, vol. 18, no. 5, pp. 286–298, May 2020, doi: 10.1038/s41579-020-0340-0.
- [78] B. D. Raynor, 'Penicillin and ampicillin', *Prim. Care Update OBGYNS*, vol. 4, no. 4, pp. 147–152, Jul. 1997, doi: 10.1016/S1068-607X(97)00012-7.
- [79] Erlend Standal/MARBIO AS, 'Marbio', *MARBIO AS*, 2022. <https://marbio.no/en/frontpage/> (accessed Jun. 02, 2022).
- [80] Marbank, 'Marbank-Front page', *Institute of Marine Research*, 2022. <https://www.hi.no/en/hi/forskning/research-groups-1/marbank> (accessed Jun. 02, 2022).
- [81] Marine Biodiscovery Centre, 'Marine Biodiscovery | The School of Natural and Computing Sciences | The University of Aberdeen', 2022. <https://www.abdn.ac.uk/ncs/departments/chemistry/marine-biodiscovery-1280.php> (accessed Jun. 05, 2022).
- [82] E. F. Haney, S. C. Mansour, and R. E. W. Hancock, 'Antimicrobial Peptides: An Introduction', *Methods Mol. Biol. Clifton NJ*, vol. 1548, pp. 3–22, 2017, doi: 10.1007/978-1-4939-6737-7\_1.
- [83] L. Czaplewski *et al.*, 'Alternatives to antibiotics—a pipeline portfolio review', *Lancet Infect. Dis.*, vol. 16, no. 2, pp. 239–251, Feb. 2016, doi: 10.1016/S1473-3099(15)00466-1.
- [84] S. Datta and A. Roy, 'Antimicrobial Peptides as Potential Therapeutic Agents: A Review', *Int. J. Pept. Res. Ther.*, vol. 27, no. 1, pp. 555–577, Mar. 2021, doi: 10.1007/s10989-020-10110-x.
- [85] Z. Y. Ong, N. Wiradharma, and Y. Y. Yang, 'Strategies employed in the design and optimization of synthetic antimicrobial peptide amphiphiles with enhanced therapeutic potentials', *Adv. Drug Deliv. Rev.*, vol. 78, pp. 28–45, Nov. 2014, doi: 10.1016/j.addr.2014.10.013.
- [86] N. Raheem and S. K. Straus, 'Mechanisms of Action for Antimicrobial Peptides With Antibacterial and Antibiofilm Functions', *Front. Microbiol.*, vol. 10, 2019, Accessed: Apr.

- 06, 2022. [Online]. Available: <https://www.frontiersin.org/article/10.3389/fmicb.2019.02866>
- [87] N. Molchanova, P. R. Hansen, and H. Franzyk, 'Advances in Development of Antimicrobial Peptidomimetics as Potential Drugs', *Mol. Basel Switz.*, vol. 22, no. 9, p. E1430, Aug. 2017, doi: 10.3390/molecules22091430.
- [88] M. Wu, E. Maier, R. Benz, and R. E. Hancock, 'Mechanism of interaction of different classes of cationic antimicrobial peptides with planar bilayers and with the cytoplasmic membrane of *Escherichia coli*', *Biochemistry*, vol. 38, no. 22, pp. 7235–7242, Jun. 1999, doi: 10.1021/bi9826299.
- [89] A. Pokorny, T. H. Birkbeck, and P. F. F. Almeida, 'Mechanism and Kinetics of  $\delta$ -Lysin Interaction with Phospholipid Vesicles', *Biochemistry*, vol. 41, no. 36, pp. 11044–11056, Sep. 2002, doi: 10.1021/bi020244r.
- [90] Y. Shai and Z. Oren, 'From "carpet" mechanism to de-novo designed diastereomeric cell-selective antimicrobial peptides', *Peptides*, vol. 22, no. 10, pp. 1629–1641, Oct. 2001, doi: 10.1016/S0196-9781(01)00498-3.
- [91] K. Matsuzaki, O. Murase, N. Fujii, and K. Miyajima, 'An antimicrobial peptide, magainin 2, induced rapid flip-flop of phospholipids coupled with pore formation and peptide translocation', *Biochemistry*, vol. 35, no. 35, pp. 11361–11368, Sep. 1996, doi: 10.1021/bi960016v.
- [92] R. L. Crass *et al.*, 'Pharmacokinetics of Polymyxin B in Hospitalized Adults with Cystic Fibrosis', *Antimicrob. Agents Chemother.*, vol. 65, no. 10, pp. e00792-21, Sep. 2021, doi: 10.1128/AAC.00792-21.
- [93] B. T. Tsuji *et al.*, 'International Consensus Guidelines for the Optimal Use of the Polymyxins: Endorsed by the American College of Clinical Pharmacy (ACCP), European Society of Clinical Microbiology and Infectious Diseases (ESCMID), Infectious Diseases Society of America (IDSA), International Society for Anti-infective Pharmacology (ISAP), Society of Critical Care Medicine (SCCM), and Society of Infectious Diseases Pharmacists (SIDP)', *Pharmacotherapy*, vol. 39, no. 1, pp. 10–39, Jan. 2019, doi: 10.1002/phar.2209.
- [94] R. Wesgate, C. Evangelista, R. Atkinson, A. Shepard, O. Adegoke, and J.-Y. Maillard, 'Understanding the risk of emerging bacterial resistance to over the counter antibiotics in topical sore throat medicines', *J. Appl. Microbiol.*, vol. 129, no. 4, pp. 916–925, Oct. 2020, doi: 10.1111/jam.14682.
- [95] Q. Guan, S. Huang, Y. Jin, R. Campagne, V. Alezra, and Y. Wan, 'Recent Advances in the Exploration of Therapeutic Analogues of Gramicidin S, an Old but Still Potent Antimicrobial Peptide', *J. Med. Chem.*, vol. 62, no. 17, pp. 7603–7617, Sep. 2019, doi: 10.1021/acs.jmedchem.9b00156.
- [96] M. N. Neely *et al.*, 'Prospective Trial on the Use of Trough Concentration versus Area under the Curve To Determine Therapeutic Vancomycin Dosing', *Antimicrob. Agents Chemother.*, vol. 62, no. 2, pp. e02042-17, Feb. 2018, doi: 10.1128/AAC.02042-17.
- [97] J. I. Lachowicz *et al.*, 'The Best Peptidomimetic Strategies to Undercover Antibacterial Peptides', *Int. J. Mol. Sci.*, vol. 21, no. 19, Art. no. 19, Jan. 2020, doi: 10.3390/ijms21197349.
- [98] 'Antibiotics biotech firms are struggling', *The Economist*, May 02, 2019. Accessed: Oct. 04, 2021. [Online]. Available: <https://www.economist.com/business/2019/05/02/antibiotics-biotech-firms-are-struggling>
- [99] D. Hughes and A. Karlén, 'Discovery and preclinical development of new antibiotics', *Ups. J. Med. Sci.*, vol. 119, no. 2, Art. no. 2, Mar. 2014, doi: 10.3109/03009734.2014.896437.
- [100] H. X. Ngo and S. Garneau-Tsodikova, 'What are the drugs of the future?', *MedChemComm*, vol. 9, no. 5, pp. 757–758, Apr. 2018, doi: 10.1039/c8md90019a.

- [101] T. Prueksaritanont and C. Tang, ‘ADME of biologics-what have we learned from small molecules?’, *AAPS J.*, vol. 14, no. 3, pp. 410–419, Sep. 2012, doi: 10.1208/s12248-012-9353-6.
- [102] University of California Museum of Paleontology, “‘Basic assumptions of science.’ Understanding Science.’, 2022. [https://undsci.berkeley.edu/article/basic\\_assumptions](https://undsci.berkeley.edu/article/basic_assumptions) (accessed May 05, 2022).
- [103] A. Comte, J. H. Bridges, and A. Comte, *A general view of positivism: or, summary exposition of the system of thought and life, adapted to the great western republic, formed of the five advanced nations, the French, Italian, Spanish, British, and German, which, since the time of Charlemagne, have always constituted a political whole*, Reissued, Truebner and Co, 1865. Cambridge: Cambridge Univ. Press, 2009.
- [104] K. Moon and D. Blackman, ‘A Guide to Understanding Social Science Research for Natural Scientists: Social Science for Natural Scientists’, *Conserv. Biol.*, vol. 28, no. 5, pp. 1167–1177, Oct. 2014, doi: 10.1111/cobi.12326.
- [105] T. R. Vetter, ‘Fundamentals of Research Data and Variables: The Devil Is in the Details’, *Anesth. Analg.*, vol. 125, no. 4, pp. 1375–1380, Oct. 2017, doi: 10.1213/ANE.0000000000002370.
- [106] J. Neumann, ‘FAIR Data Infrastructure’, *Adv. Biochem. Eng. Biotechnol.*, Jan. 2022, doi: 10.1007/10\_2021\_193.
- [107] A. Yasgar *et al.*, ‘Compound Management for Quantitative High-Throughput Screening’, *JALA Charlottesville, Va*, vol. 13, no. 2, pp. 79–89, Apr. 2008, doi: 10.1016/j.jala.2007.12.004.
- [108] W. Sun *et al.*, ‘Rapid antimicrobial susceptibility test for identification of new therapeutics and drug combinations against multidrug-resistant bacteria’, *Emerg. Microbes Infect.*, vol. 5, no. 11, p. e116, Nov. 2016, doi: 10.1038/emi.2016.123.
- [109] Clinical and Laboratory Standards Institute, ‘M7-A7: Methods for Dilution Antimicrobial Susceptibility Tests for Bacteria That Grow Aerobically; Approved Standard—Seventh Edition’. Clinical and Laboratory Standards Institute, 2006.
- [110] C. R. Belanger and R. E. W. Hancock, ‘Testing physiologically relevant conditions in minimal inhibitory concentration assays’, *Nat. Protoc.*, vol. 16, no. 8, pp. 3761–3774, Aug. 2021, doi: 10.1038/s41596-021-00572-8.
- [111] F. Baquero and B. R. Levin, ‘Proximate and ultimate causes of the bactericidal action of antibiotics’, *Nat. Rev. Microbiol.*, vol. 19, no. 2, Art. no. 2, Feb. 2021, doi: 10.1038/s41579-020-00443-1.
- [112] W. R. Shoemaker, S. E. Jones, M. E. Muscarella, M. G. Behringer, B. K. Lehmkuhl, and J. T. Lennon, ‘Microbial population dynamics and evolutionary outcomes under extreme energy limitation’, *Proc. Natl. Acad. Sci.*, vol. 118, no. 33, p. e2101691118, Aug. 2021, doi: 10.1073/pnas.2101691118.
- [113] L. B. Reller, M. Weinstein, J. H. Jorgensen, and M. J. Ferraro, ‘Antimicrobial Susceptibility Testing: A Review of General Principles and Contemporary Practices’, *Clin. Infect. Dis.*, vol. 49, no. 11, pp. 1749–1755, Dec. 2009, doi: 10.1086/647952.
- [114] K. Lewis, ‘Riddle of Biofilm Resistance’, *Antimicrob. Agents Chemother.*, vol. 45, no. 4, pp. 999–1007, Apr. 2001, doi: 10.1128/AAC.45.4.999-1007.2001.
- [115] K. Qvortrup *et al.*, ‘Small Molecule Anti-biofilm Agents Developed on the Basis of Mechanistic Understanding of Biofilm Formation’, *Front. Chem.*, vol. 7, p. 742, Nov. 2019, doi: 10.3389/fchem.2019.00742.
- [116] E. F. Haney, M. J. Trimble, and R. E. W. Hancock, ‘Microtiter plate assays to assess antibiofilm activity against bacteria’, *Nat. Protoc.*, vol. 16, no. 5, pp. 2615–2632, May 2021, doi: 10.1038/s41596-021-00515-3.

- [117] L. Friedman and R. Kolter, ‘Genes involved in matrix formation in *Pseudomonas aeruginosa* PA14 biofilms’, *Mol. Microbiol.*, vol. 51, no. 3, pp. 675–690, 2004, doi: 10.1046/j.1365-2958.2003.03877.x.
- [118] J. J. Harrison, C. A. Stremick, R. J. Turner, N. D. Allan, M. E. Olson, and H. Ceri, ‘Microtiter susceptibility testing of microbes growing on peg lids: a miniaturized biofilm model for high-throughput screening’, *Nat. Protoc.*, vol. 5, no. 7, pp. 1236–1254, Jul. 2010, doi: 10.1038/nprot.2010.71.
- [119] B. Pitts, M. A. Hamilton, N. Zelver, and P. S. Stewart, ‘A microtiter-plate screening method for biofilm disinfection and removal’, *J. Microbiol. Methods*, vol. 54, no. 2, pp. 269–276, Aug. 2003, doi: 10.1016/S0167-7012(03)00034-4.
- [120] Y. Sun, S. E. Dowd, E. Smith, D. D. Rhoads, and R. D. Wolcott, ‘In vitro multispecies Lubbock chronic wound biofilm model’, *Wound Repair Regen. Off. Publ. Wound Heal. Soc. Eur. Tissue Repair Soc.*, vol. 16, no. 6, pp. 805–813, Dec. 2008, doi: 10.1111/j.1524-475X.2008.00434.x.
- [121] A. J. McBain, ‘Chapter 4: In vitro biofilm models: an overview’, *Adv. Appl. Microbiol.*, vol. 69, pp. 99–132, 2009, doi: 10.1016/S0065-2164(09)69004-3.
- [122] T. F. Bahamondez-Canas, L. A. Heersema, and H. D. C. Smyth, ‘Current Status of In Vitro Models and Assays for Susceptibility Testing for Wound Biofilm Infections’, *Biomedicines*, vol. 7, no. 2, p. 34, Apr. 2019, doi: 10.3390/biomedicines7020034.
- [123] A. Urban *et al.*, ‘Novel whole-cell antibiotic biosensors for compound discovery’, *Appl. Environ. Microbiol.*, vol. 73, no. 20, pp. 6436–6443, Oct. 2007, doi: 10.1128/AEM.00586-07.
- [124] T. Elad, H. B. Seo, S. Belkin, and M. B. Gu, ‘High-throughput prescreening of pharmaceuticals using a genome-wide bacterial bioreporter array’, *Biosens. Bioelectron.*, vol. 68, pp. 699–704, Jun. 2015, doi: 10.1016/j.bios.2015.01.067.
- [125] S. French, M. J. Ellis, B. E. Coutts, and E. D. Brown, ‘Chemical genomics reveals mechanistic hypotheses for uncharacterized bioactive molecules in bacteria’, *Curr. Opin. Microbiol.*, vol. 39, pp. 42–47, Oct. 2017, doi: 10.1016/j.mib.2017.09.005.
- [126] B. Hutter, C. Fischer, A. Jacobi, C. Schaab, and H. Loferer, ‘Panel of *Bacillus subtilis* reporter strains indicative of various modes of action’, *Antimicrob. Agents Chemother.*, vol. 48, no. 7, pp. 2588–2594, Jul. 2004, doi: 10.1128/AAC.48.7.2588-2594.2004.
- [127] A. Zaslaver *et al.*, ‘A comprehensive library of fluorescent transcriptional reporters for *Escherichia coli*’, *Nat. Methods*, vol. 3, no. 8, pp. 623–628, Aug. 2006, doi: 10.1038/nmeth895.
- [128] G. Baptist *et al.*, ‘A genome-wide screen for identifying all regulators of a target gene’, *Nucleic Acids Res.*, vol. 41, no. 17, p. e164, Sep. 2013, doi: 10.1093/nar/gkt655.
- [129] K. R. Mariner, N. Ooi, D. Roebuck, A. J. O’Neill, and I. Chopra, ‘Further characterization of *Bacillus subtilis* antibiotic biosensors and their use for antibacterial mode-of-action studies’, *Antimicrob. Agents Chemother.*, vol. 55, no. 4, pp. 1784–1786, Apr. 2011, doi: 10.1128/AAC.01710-10.
- [130] A. O’Rourke *et al.*, ‘Mechanism-of-Action Classification of Antibiotics by Global Transcriptome Profiling’, *Antimicrob. Agents Chemother.*, vol. 64, no. 3, pp. e01207-19, Feb. 2020, doi: 10.1128/AAC.01207-19.
- [131] C. H. R. Senges *et al.*, ‘Comparison of Proteomic Responses as Global Approach to Antibiotic Mechanism of Action Elucidation’, *Antimicrob. Agents Chemother.*, vol. 65, no. 1, pp. e01373-20, 2020, doi: 10.1128/AAC.01373-20.
- [132] P. Nonejuie, M. Burkart, K. Pogliano, and J. Pogliano, ‘Bacterial cytological profiling rapidly identifies the cellular pathways targeted by antibacterial molecules’, *Proc. Natl. Acad. Sci. U. S. A.*, vol. 110, no. 40, pp. 16169–16174, Oct. 2013, doi: 10.1073/pnas.1311066110.



- [133] J. G. Hurdle, A. J. O'Neill, I. Chopra, and R. E. Lee, 'Targeting bacterial membrane function: an underexploited mechanism for treating persistent infections', *Nat. Rev. Microbiol.*, vol. 9, no. 1, pp. 62–75, Jan. 2011, doi: 10.1038/nrmicro2474.
- [134] A. Viljoen, S. J. Foster, G. E. Fantner, J. K. Hobbs, and Y. F. Dufrêne, 'Scratching the Surface: Bacterial Cell Envelopes at the Nanoscale', *mBio*, vol. 11, no. 1, pp. e03020-19, /mbio/11/1/mBio.03020-19.atom, Feb. 2020, doi: 10.1128/mBio.03020-19.
- [135] M. Virta, K. E. O. Åkerman, P. Saviranta, C. Oker-Blom, and M. T. Karp, 'Real-time measurement of cell permeabilization with low-molecular-weight membranolytic agents', *J. Antimicrob. Chemother.*, vol. 36, no. 2, pp. 303–315, 1995, doi: 10.1093/jac/36.2.303.
- [136] A. H. Benfield and S. T. Henriques, 'Mode-of-Action of Antimicrobial Peptides: Membrane Disruption vs. Intracellular Mechanisms', *Front. Med. Technol.*, vol. 2, p. 610997, Dec. 2020, doi: 10.3389/fmedt.2020.610997.
- [137] J. Knobloch, D. K. Suhendro, J. L. Zieleniecki, J. G. Shapter, and I. Köper, 'Membrane-drug interactions studied using model membrane systems', *Saudi J. Biol. Sci.*, vol. 22, no. 6, pp. 714–718, Nov. 2015, doi: 10.1016/j.sjbs.2015.03.007.
- [138] M. Jakubec *et al.*, 'Cholesterol-containing lipid nanodiscs promote an  $\alpha$ -synuclein binding mode that accelerates oligomerization', *FEBS J.*, vol. 288, no. 6, pp. 1887–1905, 2021, doi: 10.1111/febs.15551.
- [139] A. Hollmann, M. Martinez, P. Maturana, L. C. Semorile, and P. C. Maffia, 'Antimicrobial Peptides: Interaction With Model and Biological Membranes and Synergism With Chemical Antibiotics', *Front. Chem.*, vol. 6, 2018, Accessed: Apr. 06, 2022. [Online]. Available: <https://www.frontiersin.org/article/10.3389/fchem.2018.00204>
- [140] V. Ambriz-Aviña, J. A. Contreras-Garduño, and M. Pedraza-Reyes, 'Applications of flow cytometry to characterize bacterial physiological responses', *BioMed Res. Int.*, vol. 2014, p. 461941, 2014, doi: 10.1155/2014/461941.
- [141] P. J. Hare, T. J. LaGree, B. A. Byrd, A. M. DeMarco, and W. W. K. Mok, 'Single-Cell Technologies to Study Phenotypic Heterogeneity and Bacterial Persisters', *Microorganisms*, vol. 9, no. 11, p. 2277, Nov. 2021, doi: 10.3390/microorganisms9112277.
- [142] S.-R. Wang *et al.*, 'OMIP 071: A 31-Parameter Flow Cytometry Panel for In-Depth Immunophenotyping of Human T-Cell Subsets Using Surface Markers', *Cytometry A*, vol. 99, no. 3, pp. 273–277, 2021, doi: 10.1002/cyto.a.24272.
- [143] D. Novo, N. G. Perlmutter, R. H. Hunt, and H. M. Shapiro, 'Accurate flow cytometric membrane potential measurement in bacteria using diethyloxycarbocyanine and a ratiometric technique', *Cytometry*, vol. 35, no. 1, pp. 55–63, 1999, doi: 10.1002/(SICI)1097-0320(19990101)35:1<55::AID-CYTO8>3.0.CO;2-2.
- [144] R. Njemini, O. O. Onyema, W. Renmans, I. Bautmans, M. De Waele, and T. Mets, 'Shortcomings in the Application of Multicolour Flow Cytometry in Lymphocyte Subsets Enumeration', *Scand. J. Immunol.*, vol. 79, no. 2, pp. 75–89, 2014, doi: 10.1111/sji.12142.
- [145] L. Zhang, H. Xie, Y. Wang, H. Wang, J. Hu, and G. Zhang, 'Pharmacodynamic Parameters of Pharmacokinetic/Pharmacodynamic (PK/PD) Integration Models', *Front. Vet. Sci.*, vol. 9, 2022, Accessed: May 06, 2022. [Online]. Available: <https://www.frontiersin.org/article/10.3389/fvets.2022.860472>
- [146] M. Mueller, A. de la Peña, and H. Derendorf, 'Issues in Pharmacokinetics and Pharmacodynamics of Anti-Infective Agents: Kill Curves versus MIC', *Antimicrob. Agents Chemother.*, vol. 48, no. 2, pp. 369–377, Feb. 2004, doi: 10.1128/AAC.48.2.369-377.2004.
- [147] M. Balouiri, M. Sadiki, and S. K. Ibsouda, 'Methods for in vitro evaluating antimicrobial activity: A review', *J. Pharm. Anal.*, vol. 6, no. 2, pp. 71–79, Apr. 2016, doi: 10.1016/j.jpha.2015.11.005.
- [148] Clinical and Laboratory Standards Institute, 'M26-A - Methods for Determining Bactericidal Activity of Antimicrobial Agents; Approved Guideline'. Clinical and

- Laboratory Standards Institute, 1999. Accessed: Mar. 09, 2022. [Online]. Available: [https://webstore.ansi.org/standards/cls/clsim26?gclid=CjwKCAiAvaGRBhBIEiwAiY-yMNU0my0BfOMcJRvnbN0DccYib80LCm849I21IYyL5u7iOI34gi6oRoCtmoQAvD\\_BwE](https://webstore.ansi.org/standards/cls/clsim26?gclid=CjwKCAiAvaGRBhBIEiwAiY-yMNU0my0BfOMcJRvnbN0DccYib80LCm849I21IYyL5u7iOI34gi6oRoCtmoQAvD_BwE)
- [149] J. Davies, G. B. Spiegelman, and G. Yim, ‘The world of subinhibitory antibiotic concentrations’, *Curr. Opin. Microbiol.*, vol. 9, no. 5, pp. 445–453, Oct. 2006, doi: 10.1016/j.mib.2006.08.006.
- [150] J. F. Linares, I. Gustafsson, F. Baquero, and J. L. Martinez, ‘Antibiotics as intermicrobial signaling agents instead of weapons’, *Proc. Natl. Acad. Sci. U. S. A.*, vol. 103, no. 51, pp. 19484–19489, Dec. 2006, doi: 10.1073/pnas.0608949103.
- [151] R. Hazan, Y.-A. Que, D. Maura, and L. G. Rahme, ‘A method for high throughput determination of viable bacteria cell counts in 96-well plates’, *BMC Microbiol.*, vol. 12, p. 259, Nov. 2012, doi: 10.1186/1471-2180-12-259.
- [152] D. C. Broussou, P.-L. Toutain, F. Woehrlé, F. E. Garch, A. Bousquet-Melou, and A. A. Ferran, ‘Comparison of in vitro static and dynamic assays to evaluate the efficacy of an antimicrobial drug combination against *Staphylococcus aureus*’, *PLOS ONE*, vol. 14, no. 1, p. e0211214, Jan. 2019, doi: 10.1371/journal.pone.0211214.
- [153] Z. Sadouki *et al.*, ‘Application of the hollow fibre infection model (HFIM) in antimicrobial development: a systematic review and recommendations of reporting’, *J. Antimicrob. Chemother.*, vol. 76, no. 9, pp. 2252–2259, Jun. 2021, doi: 10.1093/jac/dkab160.
- [154] F. S. Aliabadi, M. F. Landoni, and P. Lees, ‘Pharmacokinetics (PK), Pharmacodynamics (PD), and PK-PD Integration of Danofloxacin in Sheep Biological Fluids’, *Antimicrob. Agents Chemother.*, vol. 47, no. 2, pp. 626–635, Feb. 2003, doi: 10.1128/AAC.47.2.626-635.2003.
- [155] R. J. Grant *et al.*, ‘Achieving Accurate Compound Concentration in Cell-Based Screening: Validation of Acoustic Droplet Ejection Technology’, *SLAS Discov.*, vol. 14, no. 5, pp. 452–459, May 2009, doi: 10.1177/1087057109336588.
- [156] I. Wiegand, K. Hilpert, and R. E. W. Hancock, ‘Agar and broth dilution methods to determine the minimal inhibitory concentration (MIC) of antimicrobial substances’, *Nat. Protoc.*, vol. 3, no. 2, pp. 163–175, Feb. 2008, doi: 10.1038/nprot.2007.521.
- [157] A. Gough *et al.*, ‘Biologically Relevant Heterogeneity: Metrics and Practical Insights’, *SLAS Discov. Adv. Sci. Drug Discov.*, vol. 22, no. 3, pp. 213–237, Mar. 2017, doi: 10.1177/2472555216682725.
- [158] S. J. Altschuler and L. F. Wu, ‘Cellular heterogeneity: when do differences make a difference?’, *Cell*, vol. 141, no. 4, pp. 559–563, May 2010, doi: 10.1016/j.cell.2010.04.033.
- [159] M. Tadesse *et al.*, ‘The antibacterial ent-eusynstyelamide B and eusynstyelamides D, E, and F from the Arctic bryozoan *Tegella cf. spitzbergensis*’, *J. Nat. Prod.*, vol. 74, no. 4, pp. 837–841, Apr. 2011, doi: 10.1021/np100499c.
- [160] World Health Organization, *2019 antibacterial agents in clinical development: an analysis of the antibacterial clinical development pipeline*. Geneva: World Health Organization, 2019. Accessed: Apr. 03, 2022. [Online]. Available: <https://apps.who.int/iris/handle/10665/330420>
- [161] M. Jenssen, ‘Bioprospecting of marine microorganisms for the discovery of antibacterial compounds - Isolation, structure elucidation and bioactivity assessment of marine microbial natural products’, 2022.
- [162] J. Wang *et al.*, ‘Discovery of a Small Molecule That Inhibits Cell Division by Blocking FtsZ, a Novel Therapeutic Target of Antibiotics \*’, *J. Biol. Chem.*, vol. 278, no. 45, pp. 44424–44428, Nov. 2003, doi: 10.1074/jbc.M307625200.

- [163] C. J. Zheng, M.-J. Sohn, S. Lee, Y.-S. Hong, J.-H. Kwak, and W.-G. Kim, ‘Cephalochromin, a FabI-directed antibacterial of microbial origin’, *Biochem. Biophys. Res. Commun.*, vol. 362, no. 4, pp. 1107–1112, Nov. 2007, doi: 10.1016/j.bbrc.2007.08.144.
- [164] L. Boudesocque-Delaye *et al.*, ‘Antibacterial Polyketide Heterodimers from *Pyrenacantha kaurabassana* Tubers’, *J. Nat. Prod.*, vol. 78, no. 4, pp. 597–603, Apr. 2015, doi: 10.1021/np5003252.
- [165] J. Rivera-Chávez *et al.*, ‘Mycopyranone: a 8,8’-binaphthopyranone with potent anti-MRSA activity from the fungus *Phialemoniopsis* sp’, *Tetrahedron Lett.*, vol. 60, no. 8, pp. 594–597, Feb. 2019, doi: 10.1016/j.tetlet.2019.01.029.
- [166] S. Lu *et al.*, ‘Bis-naphtho- $\gamma$ -pyrones from Fungi and Their Bioactivities’, *Molecules*, vol. 19, no. 6, pp. 7169–7188, May 2014, doi: 10.3390/molecules19067169.
- [167] L. Yet, *Privileged Structures in Drug Discovery: Medicinal Chemistry and Synthesis*. 2018.
- [168] A. J. Jervis, P. D. Thackray, C. W. Houston, M. J. Horsburgh, and A. Moir, ‘SigM-responsive genes of *Bacillus subtilis* and their promoters’, *J. Bacteriol.*, vol. 189, no. 12, pp. 4534–4538, Jun. 2007, doi: 10.1128/JB.00130-07.
- [169] A. Urban *et al.*, ‘Novel Whole-Cell Antibiotic Biosensors for Compound Discovery’, *Appl. Environ. Microbiol.*, vol. 73, no. 20, pp. 6436–6443, Oct. 2007, doi: 10.1128/AEM.00586-07.
- [170] T. Mascher, S. L. Zimmer, T.-A. Smith, and J. D. Helmann, ‘Antibiotic-inducible promoter regulated by the cell envelope stress-sensing two-component system LiaRS of *Bacillus subtilis*’, *Antimicrob. Agents Chemother.*, vol. 48, no. 8, pp. 2888–2896, Aug. 2004, doi: 10.1128/AAC.48.8.2888-2896.2004.
- [171] M. Wenzel *et al.*, ‘Small cationic antimicrobial peptides delocalize peripheral membrane proteins’, *Proc. Natl. Acad. Sci. U. S. A.*, vol. 111, no. 14, pp. E1409–E1418, Apr. 2014, doi: 10.1073/pnas.1319900111.
- [172] P. Rainsford *et al.*, ‘WIND-PVPA: Water/Ion NMR Detected PVPA to assess lipid barrier integrity in vitro through quantification of passive water- and ion transport’, *BBA - Biomembranes*, 2022.
- [173] S. D. Taylor and M. Palmer, ‘The action mechanism of daptomycin’, *Bioorg. Med. Chem.*, vol. 24, no. 24, pp. 6253–6268, Dec. 2016, doi: 10.1016/j.bmc.2016.05.052.
- [174] G. Upert, A. Luther, D. Obrecht, and P. Ermert, ‘Emerging peptide antibiotics with therapeutic potential’, *Med. Drug Discov.*, vol. 9, p. 100078, Mar. 2021, doi: 10.1016/j.medidd.2020.100078.
- [175] R. M. Losick, ‘*Bacillus subtilis*: a bacterium for all seasons’, *Curr. Biol.*, vol. 30, no. 19, pp. R1146–R1150, Oct. 2020, doi: 10.1016/j.cub.2020.06.083.
- [176] Q. O. Ababneh and J. K. Herman, ‘RelA Inhibits *Bacillus subtilis* Motility and Chaining’, *J. Bacteriol.*, vol. 197, no. 1, pp. 128–137, Jan. 2015, doi: 10.1128/JB.02063-14.
- [177] Y. Chai, R. Kolter, and R. Losick, ‘Reversal of an Epigenetic Switch Governing Cell Chaining in *Bacillus subtilis* by Protein Instability’, *Mol. Microbiol.*, vol. 78, no. 1, pp. 218–229, Oct. 2010, doi: 10.1111/j.1365-2958.2010.07335.x.
- [178] D. W. Adams and J. Errington, ‘Bacterial cell division: assembly, maintenance and disassembly of the Z ring’, *Nat. Rev. Microbiol.*, vol. 7, no. 9, pp. 642–653, Sep. 2009, doi: 10.1038/nrmicro2198.
- [179] T. M. Privalsky *et al.*, ‘Prospects for Antibacterial Discovery and Development’, *J. Am. Chem. Soc.*, vol. 143, no. 50, pp. 21127–21142, Dec. 2021, doi: 10.1021/jacs.1c10200.
- [180] H. Feddersen, L. Würthner, E. Frey, and M. Bramkamp, ‘Dynamics of the *Bacillus subtilis* Min System’, *mBio*, Apr. 2021, doi: 10.1128/mBio.00296-21.

- [181] C. L. White and J. W. Gober, ‘MreB: pilot or passenger of cell wall synthesis?’, *Trends Microbiol.*, vol. 20, no. 2, pp. 74–79, Feb. 2012, doi: 10.1016/j.tim.2011.11.004.
- [182] S. Pichoff and J. Lutkenhaus, ‘Tethering the Z ring to the membrane through a conserved membrane targeting sequence in FtsA’, *Mol. Microbiol.*, vol. 55, no. 6, pp. 1722–1734, 2005, doi: 10.1111/j.1365-2958.2005.04522.x.
- [183] T. H. Szeto, S. L. Rowland, C. L. Habrukowich, and G. F. King, ‘The MinD membrane targeting sequence is a transplantable lipid-binding helix’, *J. Biol. Chem.*, vol. 278, no. 41, pp. 40050–40056, Oct. 2003, doi: 10.1074/jbc.M306876200.
- [184] H. Strahl and L. W. Hamoen, ‘Membrane potential is important for bacterial cell division’, *Proc. Natl. Acad. Sci.*, vol. 107, no. 27, pp. 12281–12286, Jul. 2010, doi: 10.1073/pnas.1005485107.
- [185] S. G. Addinall and J. Lutkenhaus, ‘FtsA is localized to the septum in an FtsZ-dependent manner’, *J. Bacteriol.*, vol. 178, no. 24, pp. 7167–7172, Dec. 1996, doi: 10.1128/jb.178.24.7167-7172.1996.
- [186] R.-L. Du *et al.*, ‘Discovery of FtsZ inhibitors by virtual screening as antibacterial agents and study of the inhibition mechanism’, *RSC Med. Chem.*, vol. 13, no. 1, pp. 79–89, Jan. 2022, doi: 10.1039/D1MD00249J.
- [187] K. E. D. Coan and B. K. Shoichet, ‘Stoichiometry and Physical Chemistry of Promiscuous Aggregate-Based Inhibitors’, *J. Am. Chem. Soc.*, vol. 130, no. 29, pp. 9606–9612, Jul. 2008, doi: 10.1021/ja802977h.
- [188] A. N. Ganesh, E. N. Donders, B. K. Shoichet, and M. S. Shoichet, ‘Colloidal aggregation: From screening nuisance to formulation nuance’, *Nano Today*, vol. 19, pp. 188–200, Apr. 2018, doi: 10.1016/j.nantod.2018.02.011.
- [189] J. B. Baell and J. W. M. Nissink, ‘Seven Year Itch: Pan-Assay Interference Compounds (PAIS) in 2017—Utility and Limitations’, *ACS Chem. Biol.*, vol. 13, no. 1, pp. 36–44, Jan. 2018, doi: 10.1021/acscchembio.7b00903.
- [190] D. Duan, A. K. Doak, L. Nedyalkova, and B. K. Shoichet, ‘Colloidal Aggregation and the in Vitro Activity of Traditional Chinese Medicines’, *ACS Chem. Biol.*, vol. 10, no. 4, pp. 978–988, Apr. 2015, doi: 10.1021/cb5009487.
- [191] C. K. McLaughlin, D. Duan, A. N. Ganesh, H. Torosyan, B. K. Shoichet, and M. S. Shoichet, ‘Stable Colloidal Drug Aggregates Catch and Release Active Enzymes’, *ACS Chem. Biol.*, vol. 11, no. 4, pp. 992–1000, Apr. 2016, doi: 10.1021/acscchembio.5b00806.
- [192] A. N. Ganesh *et al.*, ‘Colloidal Drug Aggregate Stability in High Serum Conditions and Pharmacokinetic Consequence’, *ACS Chem. Biol.*, vol. 14, no. 4, pp. 751–757, Apr. 2019, doi: 10.1021/acscchembio.9b00032.
- [193] D. Duan *et al.*, ‘Internal Structure and Preferential Protein Binding of Colloidal Aggregates’, *ACS Chem. Biol.*, vol. 12, no. 1, pp. 282–290, Jan. 2017, doi: 10.1021/acscchembio.6b00791.
- [194] D. M. Tapiolas *et al.*, ‘Eusynstyelamides A, B, and C, nNOS Inhibitors, from the Ascidian *Eusynstyela latericius*’, *J. Nat. Prod.*, vol. 72, no. 6, pp. 1115–1120, Jun. 2009, doi: 10.1021/np900099j.
- [195] O. V. Barykina and B. B. Snider, ‘Synthesis of (+/-)-eusynstyelamide A’, *Org. Lett.*, vol. 12, no. 11, pp. 2664–2667, Jun. 2010, doi: 10.1021/ol100896n.
- [196] M.-C. Gagnon *et al.*, ‘Influence of the Length and Charge on the Activity of  $\alpha$ -Helical Amphipathic Antimicrobial Peptides’, *Biochemistry*, vol. 56, no. 11, pp. 1680–1695, Mar. 2017, doi: 10.1021/acs.biochem.6b01071.
- [197] M. Dathe, H. Nikolenko, J. Meyer, M. Beyermann, and M. Bienert, ‘Optimization of the antimicrobial activity of magainin peptides by modification of charge’, *FEBS Lett.*, vol. 501, no. 2–3, pp. 146–150, Jul. 2001, doi: 10.1016/s0014-5793(01)02648-5.

- [198] Z. Jiang, A. I. Vasil, J. D. Hale, R. E. W. Hancock, M. L. Vasil, and R. S. Hodges, ‘Effects of net charge and the number of positively charged residues on the biological activity of amphipathic alpha-helical cationic antimicrobial peptides’, *Biopolymers*, vol. 90, no. 3, pp. 369–383, 2008, doi: 10.1002/bip.20911.
- [199] E. P. Gillis, K. J. Eastman, M. D. Hill, D. J. Donnelly, and N. A. Meanwell, ‘Applications of Fluorine in Medicinal Chemistry’, *J. Med. Chem.*, vol. 58, no. 21, pp. 8315–8359, Nov. 2015, doi: 10.1021/acs.jmedchem.5b00258.
- [200] N. Frimodt-Møller, J. D. Knudsen, and F. Espersen, ‘Chapter 14 - The Mouse Peritonitis/Sepsis Model’, in *Handbook of Animal Models of Infection*, O. Zak and M. A. Sande, Eds. London: Academic Press, 1999, pp. 127–136. doi: 10.1016/B978-012775390-4/50153-6.
- [201] A. Giuliani, G. Pirri, and S. Nicoletto, ‘Antimicrobial peptides: an overview of a promising class of therapeutics’, *Open Life Sci.*, vol. 2, no. 1, pp. 1–33, Mar. 2007, doi: 10.2478/s11535-007-0010-5.
- [202] J.-P. S. Powers and R. E. W. Hancock, ‘The relationship between peptide structure and antibacterial activity’, *Peptides*, vol. 24, no. 11, pp. 1681–1691, Nov. 2003, doi: 10.1016/j.peptides.2003.08.023.
- [203] A. H. Delcour, ‘Outer Membrane Permeability and Antibiotic Resistance’, *Biochim. Biophys. Acta*, vol. 1794, no. 5, pp. 808–816, May 2009, doi: 10.1016/j.bbapap.2008.11.005.
- [204] ‘Parker et al\_2020\_Implementation of permeation rules leads to a FabI inhibitor with activity.pdf’. Accessed: May 17, 2022. [Online]. Available: <https://europepmc.org/articles/pmc6953607?pdf=render>
- [205] M. F. Richter *et al.*, ‘Predictive compound accumulation rules yield a broad-spectrum antibiotic’, *Nature*, vol. 545, no. 7654, pp. 299–304, May 2017, doi: 10.1038/nature22308.
- [206] R. O’Shea and H. E. Moser, ‘Physicochemical Properties of Antibacterial Compounds: Implications for Drug Discovery’, *J. Med. Chem.*, vol. 51, no. 10, pp. 2871–2878, May 2008, doi: 10.1021/jm700967e.
- [207] K. A. Brogden, ‘Antimicrobial peptides: pore formers or metabolic inhibitors in bacteria?’, *Nat. Rev. Microbiol.*, vol. 3, no. 3, Art. no. 3, Mar. 2005, doi: 10.1038/nrmicro1098.
- [208] Q.-Y. Zhang *et al.*, ‘Antimicrobial peptides: mechanism of action, activity and clinical potential’, *Mil. Med. Res.*, vol. 8, no. 1, p. 48, Sep. 2021, doi: 10.1186/s40779-021-00343-2.
- [209] C. A. Lipinski, F. Lombardo, B. W. Dominy, and P. J. Feeney, ‘Experimental and computational approaches to estimate solubility and permeability in drug discovery and development settings’, *Adv. Drug Deliv. Rev.*, vol. 46, no. 1–3, pp. 3–26, Mar. 2001, doi: 10.1016/s0169-409x(00)00129-0.
- [210] E. N. Parker *et al.*, ‘Implementation of permeation rules leads to a FabI inhibitor with activity against Gram-negative pathogens’, *Nat. Microbiol.*, vol. 5, no. 1, pp. 67–75, Jan. 2020, doi: 10.1038/s41564-019-0604-5.
- [211] M. B. Strøm, B. E. Haug, M. L. Skar, W. Stensen, T. Stiberg, and J. S. Svendsen, ‘The Pharmacophore of Short Cationic Antibacterial Peptides’, *J. Med. Chem.*, vol. 46, no. 9, pp. 1567–1570, Apr. 2003, doi: 10.1021/jm0340039.
- [212] B. E. Haug and J. S. Svendsen, ‘The role of tryptophan in the antibacterial activity of a 15-residue bovine lactoferricin peptide’, *J. Pept. Sci. Off. Publ. Eur. Pept. Soc.*, vol. 7, no. 4, pp. 190–196, Apr. 2001, doi: 10.1002/psc.318.
- [213] B. E. Haug, M. L. Skar, and J. S. Svendsen, ‘Bulky aromatic amino acids increase the antibacterial activity of 15-residue bovine lactoferricin derivatives’, *J. Pept. Sci.*, vol. 7, no. 8, pp. 425–432, 2001, doi: 10.1002/psc.338.

- [214] F. Zhang, M. Liu, and H. Wan, ‘Discussion about Several Potential Drawbacks of PEGylated Therapeutic Proteins’, *Biol. Pharm. Bull.*, vol. 37, no. 3, pp. 335–339, 2014, doi: 10.1248/bpb.b13-00661.
- [215] M. Dathe, H. Nikolenko, J. Klose, and M. Bienert, ‘Cyclization Increases the Antimicrobial Activity and Selectivity of Arginine- and Tryptophan-Containing Hexapeptides’, *Biochemistry*, vol. 43, no. 28, pp. 9140–9150, Jul. 2004, doi: 10.1021/bi035948v.
- [216] Á. Roxin and G. Zheng, ‘Flexible or fixed: a comparative review of linear and cyclic cancer-targeting peptides’, *Future Med. Chem.*, vol. 4, no. 12, pp. 1601–1618, Aug. 2012, doi: 10.4155/fmc.12.75.
- [217] J. P. Tam, Y. A. Lu, and J. L. Yang, ‘Design of salt-insensitive glycine-rich antimicrobial peptides with cyclic tricyclic structures’, *Biochemistry*, vol. 39, no. 24, pp. 7159–7169, Jun. 2000, doi: 10.1021/bi0003487.
- [218] F. Costa, I. F. Carvalho, R. C. Montelaro, P. Gomes, and M. C. L. Martins, ‘Covalent immobilization of antimicrobial peptides (AMPs) onto biomaterial surfaces’, *Acta Biomater.*, vol. 7, no. 4, pp. 1431–1440, Apr. 2011, doi: 10.1016/j.actbio.2010.11.005.
- [219] R. Chen *et al.*, ‘Synthesis, characterization and in vitro activity of a surface-attached antimicrobial cationic peptide’, *Biofouling*, vol. 25, no. 6, pp. 517–524, Apr. 2009, doi: 10.1080/08927010902954207.
- [220] J. Ye, J. He, C. Wang, K. Yao, and Z. Gou, ‘Copper-containing mesoporous bioactive glass coatings on orbital implants for improving drug delivery capacity and antibacterial activity’, *Biotechnol. Lett.*, vol. 36, no. 5, pp. 961–968, May 2014, doi: 10.1007/s10529-014-1465-x.
- [221] M. Gabriel, K. Nazmi, E. C. Veerman, A. V. Nieuw Amerongen, and A. Zentner, ‘Preparation of LL-37-grafted titanium surfaces with bactericidal activity’, *Bioconjug. Chem.*, vol. 17, no. 2, pp. 548–550, Apr. 2006, doi: 10.1021/bc050091v.
- [222] M. Godoy-Gallardo *et al.*, ‘Covalent immobilization of hLf1-11 peptide on a titanium surface reduces bacterial adhesion and biofilm formation’, *Acta Biomater.*, vol. 10, no. 8, pp. 3522–3534, Aug. 2014, doi: 10.1016/j.actbio.2014.03.026.
- [223] K. Hilpert *et al.*, ‘Screening and characterization of surface-tethered cationic peptides for antimicrobial activity’, *Chem. Biol.*, vol. 16, no. 1, pp. 58–69, Jan. 2009, doi: 10.1016/j.chembiol.2008.11.006.
- [224] Y. R. Corrales-Ureña *et al.*, ‘Functionalization of hydrophobic surfaces with antimicrobial peptides immobilized on a bio-interfacial layer’, *RSC Adv.*, vol. 10, no. 1, pp. 376–386, Dec. 2019, doi: 10.1039/c9ra07380a.
- [225] S. Acosta, L. Quintanilla, M. Alonso, C. Aparicio, and J. C. Rodríguez-Cabello, ‘Recombinant AMP/Polypeptide Self-Assembled Monolayers with Synergistic Antimicrobial Properties for Bacterial Strains of Medical Relevance’, *ACS Biomater. Sci. Eng.*, vol. 5, no. 9, pp. 4708–4716, Sep. 2019, doi: 10.1021/acsbomaterials.9b00247.
- [226] Y. J. Gordon, E. G. Romanowski, and A. M. McDermott, ‘A review of antimicrobial peptides and their therapeutic potential as anti-infective drugs’, *Curr. Eye Res.*, vol. 30, no. 7, pp. 505–515, Jul. 2005, doi: 10.1080/02713680590968637.
- [227] E. Guaní-Guerra, T. Santos-Mendoza, S. O. Lugo-Reyes, and L. M. Terán, ‘Antimicrobial peptides: general overview and clinical implications in human health and disease’, *Clin. Immunol. Orlando Fla*, vol. 135, no. 1, pp. 1–11, Apr. 2010, doi: 10.1016/j.clim.2009.12.004.
- [228] N. Z. Fantoni, A. H. El-Sagheer, and T. Brown, ‘A Hitchhiker’s Guide to Click-Chemistry with Nucleic Acids’, *Chem. Rev.*, vol. 121, no. 12, pp. 7122–7154, Jun. 2021, doi: 10.1021/acs.chemrev.0c00928.

- [229] T. Pauloehrl *et al.*, ‘Spatially controlled surface immobilization of nonmodified peptides’, *Angew. Chem. Int. Ed Engl.*, vol. 52, no. 37, pp. 9714–9718, Sep. 2013, doi: 10.1002/anie.201302040.
- [230] S. L. Haynie, G. A. Crum, and B. A. Doele, ‘Antimicrobial activities of amphiphilic peptides covalently bonded to a water-insoluble resin’, *Antimicrob. Agents Chemother.*, vol. 39, no. 2, pp. 301–307, Feb. 1995, doi: 10.1128/AAC.39.2.301.
- [231] W.-M. Cho, B. P. Joshi, H. Cho, and K.-H. Lee, ‘Design and synthesis of novel antibacterial peptide-resin conjugates’, *Bioorg. Med. Chem. Lett.*, vol. 17, no. 21, pp. 5772–5776, Nov. 2007, doi: 10.1016/j.bmcl.2007.08.056.
- [232] M. Bagheri, M. Beyermann, and M. Dathe, ‘Immobilization reduces the activity of surface-bound cationic antimicrobial peptides with no influence upon the activity spectrum’, *Antimicrob. Agents Chemother.*, vol. 53, no. 3, pp. 1132–1141, Mar. 2009, doi: 10.1128/AAC.01254-08.
- [233] B. Yang, J. P. Lowe, R. Schweins, and K. J. Edler, ‘Small Angle Neutron Scattering Studies on the Internal Structure of Poly(lactide-co-glycolide)-block-poly(ethylene glycol) Nanoparticles as Drug Delivery Vehicles’, *Biomacromolecules*, vol. 16, no. 2, pp. 457–464, Feb. 2015, doi: 10.1021/bm501519u.
- [234] I. Banerjee, R. C. Pangule, and R. S. Kane, ‘Antifouling Coatings: Recent Developments in the Design of Surfaces That Prevent Fouling by Proteins, Bacteria, and Marine Organisms’, *Adv. Mater.*, vol. 23, no. 6, pp. 690–718, 2011, doi: 10.1002/adma.201001215.
- [235] S. I. Jeon, J. H. Lee, J. D. Andrade, and P. G. De Gennes, ‘Protein—surface interactions in the presence of polyethylene oxide: I. Simplified theory’, *J. Colloid Interface Sci.*, vol. 142, no. 1, pp. 149–158, Mar. 1991, doi: 10.1016/0021-9797(91)90043-8.
- [236] J. Bruenke, I. Roschke, S. Agarwal, T. Riemann, and A. Greiner, ‘Quantitative Comparison of the Antimicrobial Efficiency of Leaching versus Nonleaching Polymer Materials’, *Macromol. Biosci.*, vol. 16, no. 5, pp. 647–654, 2016, doi: 10.1002/mabi.201500266.
- [237] Y. Imura, M. Nishida, and K. Matsuzaki, ‘Action mechanism of PEGylated magainin 2 analogue peptide’, *Biochim. Biophys. Acta*, vol. 1768, no. 10, pp. 2578–2585, Oct. 2007, doi: 10.1016/j.bbamem.2007.06.013.
- [238] Y. Imura, M. Nishida, Y. Ogawa, Y. Takakura, and K. Matsuzaki, ‘Action mechanism of tachyplesin I and effects of PEGylation’, *Biochim. Biophys. Acta*, vol. 1768, no. 5, pp. 1160–1169, May 2007, doi: 10.1016/j.bbamem.2007.01.005.
- [239] K. Yu *et al.*, ‘Anti-adhesive antimicrobial peptide coating prevents catheter associated infection in a mouse urinary infection model’, *Biomaterials*, vol. 116, pp. 69–81, Feb. 2017, doi: 10.1016/j.biomaterials.2016.11.047.
- [240] G. H. De Zoysa and V. Sarojini, ‘Feasibility Study Exploring the Potential of Novel Battacin Lipopeptides as Antimicrobial Coatings’, *ACS Appl. Mater. Interfaces*, vol. 9, no. 2, pp. 1373–1383, Jan. 2017, doi: 10.1021/acsami.6b15859.
- [241] D. Dutta, N. Kumar, and M. D. P. Willcox, ‘Antimicrobial activity of four cationic peptides immobilised to poly-hydroxyethylmethacrylate’, *Biofouling*, vol. 32, no. 4, pp. 429–438, Apr. 2016, doi: 10.1080/08927014.2015.1129533.
- [242] C. Pinese *et al.*, ‘Simple and Specific Grafting of Antibacterial Peptides on Silicone Catheters’, *Adv. Healthc. Mater.*, vol. 5, no. 23, pp. 3067–3073, 2016, doi: 10.1002/adhm.201600757.
- [243] World Health Organization, *Global action plan on antimicrobial resistance*. Geneva: World Health Organization, 2015. Accessed: May 20, 2022. [Online]. Available: <https://apps.who.int/iris/handle/10665/193736>

- [244] European Commission, ‘A European One Health Action Plan against Antimicrobial Resistance. (AMR).’, 2017.
- [245] ‘JPIAMR – Joint Programming Initiative on Antimicrobial Resistance’. <https://www.jpiamr.eu/> (accessed May 24, 2022).
- [246] Digital Life Norway, ‘Research - Centre for Digital Life Norway’, 2022. <https://www.digitallifenorway.org/research/index.html> (accessed May 27, 2022).
- [247] Research Council of Norway, ‘DL: Digital discovery of antimicrobial molecules from marine Arctic resources with reduced risk of triggering resistance - Prosjektbanken’, *Prosjektbanken* - *Forskningsrådet*. <https://prosjektbanken.forskningsradet.no/project/FORISS/269425> (accessed May 27, 2022).
- [248] M. Miethke *et al.*, ‘Towards the sustainable discovery and development of new antibiotics’, *Nat. Rev. Chem.*, vol. 5, no. 10, pp. 726–749, 2021, doi: 10.1038/s41570-021-00313-1.
- [249] Helmholtz Centre for Infection Research, ‘Helmholtz Centre for Infections Research’, *Helmholtz Centre for Infection Research*, 2022. <https://www.helmholtz-hzi.de/en/> (accessed Jun. 09, 2022).
- [250] Translational Research Institute Australia, ‘Translational Research Institute Australia | Translational Research Institute’, 2022. <https://www.tri.edu.au/translational-research-institute-australia> (accessed Jun. 09, 2022).
- [251] REPAIR impact fund, ‘Home’, *REPAIR Impact Fund*, 2022. <https://www.repair-impact-fund.com/> (accessed May 24, 2022).
- [252] AMR action fund, ‘Antimicrobial Resistance Research & Development - AMR Action Fund’, 2022. <https://www.amractionfund.com> (accessed May 24, 2022).
- [253] D. K. Davis, ‘Text - H.R.4100 - 116th Congress (2019-2020): DISARM Act of 2019’, Jul. 31, 2019. <http://www.congress.gov/> (accessed May 24, 2022).
- [254] M. F. Doyle, ‘Text - H.R.3932 - 117th Congress (2021-2022): PASTEUR Act of 2021’, Feb. 08, 2021. <http://www.congress.gov/> (accessed May 24, 2022).
- [255] INCATE, ‘INCATE - Supporting innovators to fight drug-resistant infections’, *INCATE*, 2022. <https://www.incate.net/> (accessed May 24, 2022).
- [256] AiCuris, ‘AiCuris Anti-infective Cures AG - AiCubator’. <https://www.aicuris.com/57/AiCubator.htm> (accessed May 24, 2022).
- [257] GARDP, ‘Global Antibiotic Research and Development Partnership’, *GARDP*, 2022. <https://www.gardp.org/> (accessed May 24, 2022).
- [258] CARB-X, ‘Homepage’, *Carb-X*, 2022. <https://carb-x.org/> (accessed May 24, 2022).
- [259] BEAM Alliance, ‘BEAM Alliance’, *BEAM Alliance*, 2022. <https://beam-alliance.eu/> (accessed May 24, 2022).
- [260] A. A. Seyhan, ‘Lost in translation: the valley of death across preclinical and clinical divide – identification of problems and overcoming obstacles’, *Transl. Med. Commun.*, vol. 4, no. 1, p. 18, Nov. 2019, doi: 10.1186/s41231-019-0050-7.
- [261] R. L. Davis, ‘Mechanism matters’, *Nat. Med.*, vol. 16, no. 4, Art. no. 4, Apr. 2010, doi: 10.1038/nm0410-347.
- [262] E. Gregori-Puigjané *et al.*, ‘Identifying mechanism-of-action targets for drugs and probes’, *Proc. Natl. Acad. Sci.*, vol. 109, no. 28, pp. 11178–11183, Jul. 2012, doi: 10.1073/pnas.1204524109.
- [263] F. on N. and N. S. Disorders, B. on H. S. Policy, and I. of Medicine, *Drug Development Challenges*. National Academies Press (US), 2014. Accessed: May 26, 2022. [Online]. Available: <https://www.ncbi.nlm.nih.gov/books/NBK195047/>
- [264] D. C. Swinney and J. Anthony, ‘How were new medicines discovered?’, *Nat. Rev. Drug Discov.*, vol. 10, no. 7, Art. no. 7, Jul. 2011, doi: 10.1038/nrd3480.



- [265] Lederman, ‘The Evolving Role Of Drug Mechanism Of Action In Drug Discovery And Development’. <https://www.lifescienceleader.com/doc/the-evolving-role-of-drug-mechanism-of-action-in-drug-discovery-and-development-0001> (accessed May 24, 2022).
- [266] A. McPherson and J. A. Gavira, ‘Introduction to protein crystallization’, *Acta Crystallogr. Sect. F Struct. Biol. Commun.*, vol. 70, no. Pt 1, pp. 2–20, Dec. 2013, doi: 10.1107/S2053230X13033141.
- [267] L. Orellana, ‘Large-Scale Conformational Changes and Protein Function: Breaking the in silico Barrier’, *Front. Mol. Biosci.*, vol. 6, 2019, Accessed: Jun. 09, 2022. [Online]. Available: <https://www.frontiersin.org/article/10.3389/fmolb.2019.00117>
- [268] S. A. Hollingsworth and R. O. Dror, ‘Molecular dynamics simulation for all’, *Neuron*, vol. 99, no. 6, pp. 1129–1143, Sep. 2018, doi: 10.1016/j.neuron.2018.08.011.
- [269] N. Malachowa *et al.*, ‘Global Changes in Staphylococcus aureus Gene Expression in Human Blood’, *PLOS ONE*, vol. 6, no. 4, p. e18617, Apr. 2011, doi: 10.1371/journal.pone.0018617.
- [270] B. Quinn *et al.*, ‘Human serum albumin alters specific genes that can play a role in survival and persistence in Acinetobacter baumannii’, *Sci. Rep.*, vol. 8, no. 1, Art. no. 1, Oct. 2018, doi: 10.1038/s41598-018-33072-z.
- [271] U. Mäder *et al.*, ‘Staphylococcus aureus Transcriptome Architecture: From Laboratory to Infection-Mimicking Conditions’, *PLOS Genet.*, vol. 12, no. 4, p. e1005962, Apr. 2016, doi: 10.1371/journal.pgen.1005962.
- [272] M. A. Farha, S. French, J. M. Stokes, and E. D. Brown, ‘Bicarbonate Alters Bacterial Susceptibility to Antibiotics by Targeting the Proton Motive Force’, *ACS Infect. Dis.*, vol. 4, no. 3, pp. 382–390, Mar. 2018, doi: 10.1021/acsinfecdis.7b00194.
- [273] M. Lakemeyer, W. Zhao, F. A. Mandl, P. Hammann, and S. A. Sieber, ‘Thinking Outside the Box—Novel Antibacterials To Tackle the Resistance Crisis’, *Angew. Chem. Int. Ed.*, vol. 57, no. 44, pp. 14440–14475, 2018, doi: 10.1002/anie.201804971.
- [274] N. Sarigul, F. Korkmaz, and İ. Kurultak, ‘A New Artificial Urine Protocol to Better Imitate Human Urine’, *Sci. Rep.*, vol. 9, no. 1, p. 20159, Dec. 2019, doi: 10.1038/s41598-019-56693-4.
- [275] T. Ganz and E. Nemeth, ‘Iron homeostasis in host defence and inflammation’, *Nat. Rev. Immunol.*, vol. 15, no. 8, Art. no. 8, Aug. 2015, doi: 10.1038/nri3863.
- [276] P. Nonejuie, M. Burkart, K. Pogliano, and J. Pogliano, ‘Bacterial cytological profiling rapidly identifies the cellular pathways targeted by antibacterial molecules’, *Proc. Natl. Acad. Sci.*, vol. 110, no. 40, pp. 16169–16174, Oct. 2013, doi: 10.1073/pnas.1311066110.
- [277] A. Lamsa, J. Lopez-Garrido, D. Quach, E. P. Riley, J. Pogliano, and K. Pogliano, ‘Rapid Inhibition Profiling in Bacillus subtilis to Identify the Mechanism of Action of New Antimicrobials’, *ACS Chem. Biol.*, vol. 11, no. 8, pp. 2222–2231, Aug. 2016, doi: 10.1021/acscchembio.5b01050.



# Paper I



# Lulworthinone, a New Dimeric Naphthopyrone From a Marine Fungus in the Family Lulworthiaceae With Antibacterial Activity Against Clinical Methicillin-Resistant *Staphylococcus aureus* Isolates

Marte Jenssen<sup>1\*</sup>, Philip Rainsford<sup>2</sup>, Eric Juskewitz<sup>3</sup>, Jeanette H. Andersen<sup>1</sup>, Espen H. Hansen<sup>1</sup>, Johan Isaksson<sup>2</sup>, Teppo Rämä<sup>1</sup> and Kine Ø. Hansen<sup>1</sup>

## OPEN ACCESS

### Edited by:

Carolina Elena Girometta,  
University of Pavia, Italy

### Reviewed by:

Susan Semple,  
University of South Australia, Australia  
Adelaide Almeida,  
University of Aveiro, Portugal

### \*Correspondence:

Marte Jenssen  
mart.jenssen@uit.no

### Specialty section:

This article was submitted to  
Microbiotechnology,  
a section of the journal  
Frontiers in Microbiology

Received: 25 June 2021

Accepted: 06 September 2021

Published: 01 October 2021

### Citation:

Jenssen M, Rainsford P,  
Juskewitz E, Andersen JH,  
Hansen EH, Isaksson J, Rämä T and  
Hansen KØ (2021) Lulworthinone,  
a New Dimeric Naphthopyrone From  
a Marine Fungus in the Family  
Lulworthiaceae With Antibacterial  
Activity Against Clinical  
Methicillin-Resistant *Staphylococcus  
aureus* Isolates.  
Front. Microbiol. 12:730740.  
doi: 10.3389/fmicb.2021.730740

<sup>1</sup> Marbio, The Norwegian College of Fishery Science, Faculty of Biosciences, Fisheries and Economics, UiT the Arctic University of Norway, Tromsø, Norway, <sup>2</sup> Department of Chemistry, Faculty of Science and Technology, UiT the Arctic University of Norway, Tromsø, Norway, <sup>3</sup> Research Group for Host Microbe Interactions, Department of Medical Biology, Faculty of Health Sciences, UiT the Arctic University of Norway, Tromsø, Norway

The emergence of drug-resistant bacteria is increasing rapidly in all parts of the world, and the need for new antibiotics is urgent. In our continuous search for new antimicrobial molecules from under-investigated Arctic marine microorganisms, a marine fungus belonging to the family Lulworthiaceae (Lulworthiales, Sordariomycetes, and Ascomycota) was studied. The fungus was isolated from driftwood, cultivated in liquid medium, and studied for its potential for producing antibacterial compounds. Through bioactivity-guided isolation, a novel sulfated biaryl naphtho- $\alpha$ -pyrone dimer was isolated, and its structure was elucidated by spectroscopic methods, including 1D and 2D NMR and HRMS. The compound, named lulworthinone (**1**), showed antibacterial activity against reference strains of *Staphylococcus aureus* and *Streptococcus agalactiae*, as well as several clinical MRSA isolates with MICs in the 1.56–6.25  $\mu\text{g/ml}$  range. The compound also had antiproliferative activity against human melanoma, hepatocellular carcinoma, and non-malignant lung fibroblast cell lines, with IC<sub>50</sub> values of 15.5, 27, and 32  $\mu\text{g/ml}$ , respectively. Inhibition of bacterial biofilm formation was observed, but no eradication of established biofilm could be detected. No antifungal activity was observed against *Candida albicans*. During the isolation of **1**, the compound was observed to convert into a structural isomer, **2**, under acidic conditions. As **1** and **2** have high structural similarity, NMR data acquired for **2** were used to aid in the structure elucidation of **1**. To the best of our knowledge, lulworthinone (**1**) represents the first new bioactive secondary metabolite isolated from the marine fungal order Lulworthiales.

**Keywords:** antibacterial, marine fungi *sensu stricto*, Lulworthiales, lulworthinone, MRSA, natural product, mycology, natural product artifact

## INTRODUCTION

Antimicrobial resistance is quickly developing as a worldwide threat, causing problems not only in the general community but also in healthcare facilities. Infections caused by methicillin-resistant *Staphylococcus aureus* (MRSA) has become a worldwide health menace (WHO, 2014). There is an urgent need to develop new antibiotics to fight these resistant microbes. The fungal kingdom has historically played an important role in the discovery and development of antibiotics and other drugs against non-infective diseases (Demain, 2014). The penicillins and cephalosporins are examples of important antibiotics isolated from fungi (Demain, 2014), from the genera *Penicillium* and *Sarocladium* (one syn. *Cephalosporium*), respectively. In marine natural product discovery, the genera *Aspergillus* and *Penicillium* have proven to be the most prolific producers of new compounds with biological activities (Imhoff, 2016). As the focus of marine natural product discovery has been on mold fungi belonging to the few genera mentioned above, the strictly marine clades of fungi remain understudied (Overy et al., 2014).

One of the understudied marine clades include the fungal order Lulworthiales from which no secondary metabolites have been reported since the discovery of the type genus and species, *Lulworthia fucicola*, in the beginning of the twentieth century (Sutherland, 1915). The order Lulworthiales was established in 2000 to accommodate the new family Lulworthiaceae in the class Sordariomycetes (Kohlmeyer et al., 2000). More recently, a new subclass, Lulworthiomycetidae, was described containing the orders Lulworthiales and Koraliastetales (Maharachchikumbura et al., 2015). Lulworthiaceae is the sole family in the Lulworthiales order, and Lulworthiaceae spp. are regarded as strictly marine species, which include the following genera: *Cumulospora*, *Halazon*, *Hydea*, *Kohlmeyerella*, *Lulwoana*, *Lulworthia*, *Lindra*, *Matsusporium*, and *Moleospora* (Poli et al., 2020). Recently, a novel genus was introduced to the Lulworthiaceae, *Paralulworthia*, with two new species described, *Paralulworthia gigaspora* and *Paralulworthia posidoniae* (Poli et al., 2020). Hyde et al. (2020) also included the following genera in the family: *Haloguignardia*, *Lolwoidea*, *Moromyces*, *Orbimyces*, *Rostrupiella*, and *Sammeyersia*.

Fungi in the family Lulworthiaceae have been isolated from a variety of substrates and environments. Some examples include corals (Góes-Neto et al., 2020), plants located in salt marches (Calado et al., 2019), seagrass (Poli et al., 2020), Portuguese marinas (Azevedo et al., 2017), sandy beaches of the Cozumel island in Mexico (Velez et al., 2015), brown seaweed (Zuccaro et al., 2008), and driftwood (Rämä et al., 2014). The distribution of Lulworthiales fungi in marine habitats has been studied throughout the history of marine mycology (Johnson, 1958; Kohlmeyer et al., 2000; Koch et al., 2007; Rämä et al., 2014; Azevedo et al., 2017; Góes-Neto et al., 2020), but the biosynthetic potential of these fungi has not been investigated, most likely due to the special knowledge required for their isolation (Overy et al., 2019) and low growth rates.

In this paper, we report the isolation of a new antibacterial compound, lulworthinone (**1**), from a liquid culture of a marine fungus belonging to Lulworthiaceae (isolate 067bN1.2). We

elucidate the structure of **1** and study its bioactivity against prokaryotic and eukaryotic cells with focus on antibacterial activity against clinical MRSA isolates. Compound **1** represents the first secondary metabolite reported from this order of fungi, and to the best of our knowledge, the first biarylic dimeric naphtho- $\alpha$ -pyrone substituted with a sulfate group. Initially, the compound was isolated using preparative HPLC under acidic conditions. As this procedure caused significant wear and tear to the equipment, the isolation was switched to flash chromatography under neutral conditions. When comparing spectroscopic data from the two samples, one isolated at neutral and one at acidic conditions, structural differences were observed. It was later determined that **1** converts into the artifact **2** under acidic conditions.

## MATERIALS AND METHODS

### Biological Material and Phylogenetic Analysis of Isolate 067bN1.2

The marine fungus 067bN1.2 was isolated from a dead pine (*Pinus* sp.) collected in the splash zone in Kongsfjord, Berlevåg Norway in 2010. The isolate grew from a small wooden cube plated onto agar medium (specified below) during a campaign to study wood-inhabiting fungi of 50 intertidal and sea-floor logs along the Northern Norwegian coast, where Lulworthiales was one of the five most frequent orders isolated (Rämä et al., 2014). The fungus was subcultured and DNA sequenced, and the fungus was phylogenetically placed in the Lulworthiales order (isolate TR498 represents 067bN1.2 in Rämä et al., 2014). At the time of the publication (2014), the closest match from Blast, based on a 5.8S/large ribosomal subunit (LSU) dataset, was *Lulworthia medusa* (LSU sequence: AF195637). The following primer pairs were used for the internal transcribed spacer (ITS), LSU and small ribosomal subunit (SSU) sequencing, respectively: ITS5-ITS4 (White et al., 1990), LR0R-LR5 (Vilgalys and Hester, 1990; Rehner and Samuels, 1994), and NS1-NS4 (White et al., 1990). The ITS, LSU, and SSU sequences are deposited in GenBank under the following accessions: MW377595, MW375591, and MW375590. The mycelium of the fungus was preserved on pieces of agar in 20% glycerol solution at  $-80^{\circ}\text{C}$ .

To identify the isolate 067bN1.2 growing as an asexual morph in culture and determine its systematic position within the order Lulworthiales, a phylogenetic analysis was run using a dataset consisting of nrSSU, nrITS, and nrLSU sequences. The reference sequences included in the analyses were sampled based on recent phylogenetic studies focusing on Lulworthiales (Azevedo et al., 2017; Poli et al., 2020) and retrieved from Genbank (**Supplementary Table 1**). Sequences for each gene were aligned individually using the E-INS-I and G-INS-I algorithms of MAFFT v7.388 (Katoh et al., 2002; Katoh and Standley, 2013) in Geneious Prime v.11.0.4 followed by manual adjustment. The concatenated dataset consisting of SSU, 5.8S, and LSU sequences and having a length of 2,270 nt was run through PartitionFinder v2.1.1 (Lanfear et al., 2017) to test for best-fit partitioning schemes and evolutionary models with the following settings: models MrBayes, linked branch lengths, greedy search, and AIC

and BIC model selection (Lanfear et al., 2012). This suggested three partitions with varying models: symmetrical model with equal base frequencies and gamma distributed rate variation among sites without (SYM+G) and with (SYM+I+G) invariable sites and general time reversible model with variable base frequencies and gamma distributed rate variation among sites (GTR+G). A phylogenetic analysis was set up applying suggested models using Parallel-MPI MrBayes v3.2.7a with beagle, and was run for 5,000,000 generations or until average standard deviation of split frequencies was below 0.0009 with sampling each of the 2,500 generations (Ronquist et al., 2012). In addition, RAxML in Geneious v10.2.3 was run with the same partitions under GTRCAT and GTRGAMMA using rapid-bootstrapping algorithm with 2,000 replicates with search for best scoring ML tree (Stamatakis, 2006). The resulting MrBayes tree was similar to the RAxML tree, excluding some of the basal nodes within Lulworthiaceae shown as polytomies in the MrBayes tree.

## Fungal Cultivation and Extraction

For the purpose of this study, the fungal isolate was plated from glycerol stock and grown on nutrient-poor malt agar with sea salts [4 g/L malt extract (Moss Malt Extrakt, Jensen & Co AS), 40 g/L sea salts (S9883, Sigma-Aldrich), 15 g/L agar (A1296, Sigma-Aldrich) and Milli-Q<sup>®</sup> H<sub>2</sub>O] until the growth covered the entire agar plate (approximately 40 days). Milli-Q<sup>®</sup> H<sub>2</sub>O was produced with the in-house Milli-Q<sup>®</sup> system. One-half of the agar plate covered in mycelium was used to inoculate each liquid culture, in malt medium with added sea salts (4 g/L malt extract, 40 g/L sea salts). Two cultures of 200 ml were inoculated and incubated for 107 days at static conditions and 13°C. Before the addition of resin for extraction, mycelium was taken from the culture for inoculation of another round of cultures. The second cultivation contained four cultures with 250 ml of malt extract medium supplemented with sea salts and cultivated under the same conditions for 83 days. The total culture volume used for the extraction of **1** was 1.4 L. The cultures were extracted using Diaion HP-20 resin (13607, Supelco) and methanol (20864, HPLC grade, VWR) as described previously (Kristoffersen et al., 2018; Schneider et al., 2020). The extract was dried in a rotary evaporator at 40°C under reduced pressure and stored at -20°C.

## Dereplication

As part of our ongoing search for antimicrobial compounds, extracts of marine microorganisms are fractionated into six fractions using flash chromatography, as previously described (Schneider et al., 2020). When we investigated the antibacterial potential of fractions produced from several understudied marine fungi, one fraction from isolate 067bN1.2 piqued our interest due to its antibacterial activity. In the active fraction, **1** was the dominating peak. The monoisotopic mass, calculated elemental composition and fragmentation pattern of **1** was determined using UHPLC-ESI-HRMS. UHPLC-ESI-HRMS was performed with positive ionization mode, using an Acquity I-class UPLC with an Acquity UPLC C18 column (1.7 μm, 2.1 mm × 100 mm), coupled to a PDA detector and a Vion IMS QToF (all from Waters). Compounds were eluted with a gradient over 12 min, from 10 to 90% acetonitrile (LiChrosolv, 1.00029, Supelco) with

0.1% formic acid (Sigma-Aldrich) in Milli-Q H<sub>2</sub>O and a flow rate of 0.45 ml/min. Waters UNIFI 1.9.4 Scientific Information System was used to process and analyze the data. Elemental compositions of compounds in the samples were used to search relevant databases, such as Chemspider, in order to identify known compounds. Since the calculated elemental composition gave no hits in database searches, **1** was nominated for isolation.

## Isolation of 1

Initial attempts to isolate **1** was performed using mass guided preparative HPLC. This strategy proved difficult due to extensive binding of the compound to an Atlantis Prep C18 (10 μM, 10 × 250 mm) (Waters) column, leading to inefficient isolation and column contamination. The preparative system and mobile phases used were as previously described (Schneider et al., 2020). The resulting sample (referred to as compound **2**) was later used to assist in structure elucidation of compound **1**.

To avoid wear and tear of the preparative HPLC system, attempts were made to isolate **1** using flash chromatography. The dried extract was dissolved in 90% methanol, and 2 g of Diaion HP-20SS (13615, Supelco) was added before removing the solvent under reduced pressure. Flash columns were prepared as previously described (Kristoffersen et al., 2018). The column was equilibrated using 5% methanol, before the dried extract-Diaion HP-20SS mixture was applied to the top of the column (maximum 2 g of extract per round). The fractionation was performed on a Biotage SP4<sup>TM</sup> system (Biotage) with a flow rate of 12 ml/min and a stepwise gradient from 5 to 100% methanol over 32 min. The following stepwise elution method was used: methanol:water (5:95, 25:75, 50:50, 75:25, 6 min per step, resulting in 12 fractions) followed by methanol (100% over 12 min, resulting in six fractions). The MeOH fractions were analyzed using UHPLC-ESI-HRMS. In the second fraction eluting at 100% MeOH, **1** was the dominating peak and was submitted for NMR and bioactivity analysis. The sample of **1** was therefore produced by pooling the second fraction eluting at 100% MeOH from multiple rounds of flash fractionation and drying the resulting volume under reduced pressure.

## Structure Elucidation of 1

The structure of **1** was established by 1D and 2D NMR experiments. NMR spectra were acquired in DMSO-*d*<sub>6</sub> and methanol-*d*<sub>3</sub> on a Bruker Avance III HD spectrometer operating at 600 MHz for protons, equipped with an inverse TCI probe cryogenically enhanced for <sup>1</sup>H, <sup>13</sup>C, and <sup>2</sup>H. All NMR spectra were acquired at 298 K, in 3-mm solvent matched Shigemi tubes using standard pulse programs for proton, carbon, HSQC, HMBC, HMQC (*J* = 4–5 Hz), COSY, NOESY, ROESY and 1,1-ADEQUATE experiments with gradient selection and adiabatic versions where applicable. <sup>1</sup>H/<sup>13</sup>C chemical shifts were referenced to the residual solvent peak (δ<sub>H</sub> = 2.50 PPM, δ<sub>C</sub> = 39.52 PPM for DMSO). All data were acquired and processed using Topspin 3.5pl7 (Bruker Biospin) including the structure elucidation module CMC-se v. 2.5.1. <sup>13</sup>C prediction was done using Mestrelabs MestReNova software version 14.2.0-26256 with the Modgraph NMRPredict Desktop. Optical rotation

data were obtained using an AA-10R automatic polarimeter (Optical Activity LTD).

Lulworthinone (**1**): green colored film.  $[\alpha]^{20}_D -120 \pm 0.02$  (*c* 0.2 DMSO).  $^1\text{H}$  and  $^{13}\text{C}$  NMR spectroscopic data, **Supplementary Table 3**. HRESIMS *m/z* 741.2204  $[\text{M}+\text{H}]^+$  (calculated for  $\text{C}_{37}\text{H}_{41}\text{O}_{14}\text{S}$ , 741.2217).

## Minimal Inhibitory Concentration Determination Against Reference Bacteria

The Minimal Inhibitory Concentration (MIC) of **1** against a panel of Gram-positive and Gram-negative reference bacteria was determined by broth microdilution, at final concentrations 0.2–100  $\mu\text{g/ml}$  (twofold dilution series). The experiments were performed with three technical replicates. The panel of reference bacteria consisted of the following strains: *S. aureus* (ATCC 25923), MRSA (ATCC 33591), *Escherichia coli* (ATCC 25922), *Pseudomonas aeruginosa* (ATCC 27853), *Enterococcus faecalis* (ATCC 29212), and *Streptococcus agalactiae* (ATCC 12386), all strains from LGC Standards (Teddington). Briefly, the bacteria were inoculated from freeze stock onto blood agar plates (University Hospital of North Norway) and transferred to liquid medium for overnight incubation at 37°C. *S. aureus*, *E. coli*, and *P. aeruginosa* were grown in Brain Heart Infusion medium (BHI, 53286, Sigma-Aldrich), and *E. faecalis* and *S. agalactiae* were grown in Difco™ Mueller Hinton medium (MH, 275730, BD Biosciences). After overnight incubation in the respective media, the bacteria were brought to exponential growth by addition of fresh media, and incubated to reach a turbidity of 0.5 McFarland standard. The bacteria were diluted in their respective media 1:1,000 prior to addition. Subsequently, the bacteria were added to 96-well microtiter plates at 50  $\mu\text{l/well}$ . A mixture of 50  $\mu\text{l}$  of autoclaved Milli-Q® H<sub>2</sub>O and 50  $\mu\text{l}$  fresh autoclaved media was used as negative control, and 50  $\mu\text{l}$  of autoclaved Milli-Q® H<sub>2</sub>O was added to 50  $\mu\text{l}$  of bacteria suspension as growth control. The compound was diluted in DMSO and autoclaved Milli-Q® H<sub>2</sub>O (highest concentration of DMSO in the assay was 0.5%), and 50  $\mu\text{l}$  was added to the bacterial suspension. Final volume in the wells was 100  $\mu\text{l}$ . The plates were incubated overnight at 37°C. After incubation, growth was measured by absorbance at 600 nm with 1420 Multilabel Counter VICTOR<sup>3</sup>™ (Perkin Elmer). Assay controls with gentamicin in a dilution series are routinely run, as well as routine counting of CFUs for each bacterium. For the strains where the compound displayed activity, the MIC was determined with three biological replicates each containing three technical replicates (*n* = 9). The lowest concentration of **1** that completely inhibited the growth of the bacteria was determined as the MIC.

To investigate if **1** had a bacteriocidal or bacteriostatic effect on *S. aureus* and *S. agalactiae*, the compound was inoculated together with the bacteria, as described above, and after overnight incubation, the inoculum was plated onto agar and incubated overnight at 37°C. The experiment was done with 12.5 and 25  $\mu\text{g/ml}$  concentrations of **1** in triplicate, with two biological replicates (*n* = 6). Inspired by Zheng et al. (2007), we tested **1**, together with reserpine (broad spectrum efflux pump

inhibitor) against the Gram-negative reference strains *E. coli* and *P. aeruginosa*. The assay was conducted as described above, with reserpine (L03506, Thermo Fisher Scientific) added to a final concentration of 20  $\mu\text{g/ml}$ .

## Minimal Inhibitory Concentration Determination Against Clinical Bacterial Isolates

Initial testing of **1** was conducted against a panel containing clinically relevant antibiotic-resistant bacteria: Gram-positive MRSA, vancomycin-resistant *Enterococcus faecium* (VRE), and Gram-negative bacteria resistant to extended-spectrum beta-lactamases as well as carbapenemases (ESBL-Carba) (detailed information about the clinical isolates can be found in **Supplementary Table 2**). The initial testing was conducted at one concentration, 100  $\mu\text{g/ml}$ .

The final antibacterial testing of **1** was executed using the five clinical MRSA isolates and the VRE isolates (**Supplementary Table 2**). The isolates were tested by broth microdilution according to the Clinical Laboratory Standard Institute (CLSI) (2012) method MO7-A9. In brief, **1** was solubilized with 100% DMSO and diluted with autoclaved Milli-Q® H<sub>2</sub>O to prepare a 200  $\mu\text{g/ml}$  working solution. The final DMSO concentration did not exceed 1% to exclude any artificial influence on the assay. The bacterial inoculum was prepared to contain  $1 \times 10^6$  CFU/ml in cationic-adjusted BBL™ Mueller-Hinton II broth (BD). The inoculum was mixed in a 1:1 ratio with the working solution of **1** (twofold dilutions, ranging from 0.2 to 100  $\mu\text{g/ml}$ ) for a final amount of  $5 \times 10^5$  CFU/ml in each well of a 96-well round-bottom polypropylene plate (Greiner Bio-One GmbH). Growth control (without compound) and sterility control (without bacteria) were included for each strain. Each strain was tested in three independent biological replicates with four technical replicates on consecutive days. As quality assurance for the assay, the protocol was also performed with *E. coli* ATCC 25922 using Gentamicin (Merck Life Science) as a reference antibiotic. The 96-well plates were incubated at 37°C for 24 h without shaking. The MIC values were defined as the lowest concentration of **1** resulting in no visual bacterial growth, determined by visual inspection and 600 nm absorbance measurements with CLARIOstar plate reader (BMG LABTECH).

## Inhibition of Biofilm Production and Eradication of Established Biofilm

Inhibition of biofilm production by **1** of *Staphylococcus epidermidis* (ATCC 35984, LGC Standards) was determined at final concentrations 0.2–100  $\mu\text{g/ml}$  (twofold dilution series). Briefly, the bacteria were inoculated from freeze stock onto blood agar plates (University Hospital of North Norway) and transferred to tryptic soy broth (TSB, 22092, Sigma-Aldrich) for overnight incubation at 37°C. The overnight cultures were subsequently diluted 1:100 in fresh TSB with 1% glucose and added to 96-well microtiter plates, 50  $\mu\text{l/well}$ . Positive control was *S. epidermidis* in fresh media with glucose, and negative control was a non-biofilm producing *Staphylococcus haemolyticus* (clinical isolate 8-7A, University Hospital of North Norway) in

fresh media with glucose. The compound was diluted in DMSO and autoclaved Milli-Q® H<sub>2</sub>O (highest concentration of DMSO in the assay was 0.5%), and 50 µl was added to the bacterial suspension. Final volume in the wells was 100 µl. The plates were incubated at 37°C overnight. Growth inhibition of the bacterium was determined by visual inspection of the plates prior to further treatment. The bacterial suspension was poured out and the biofilm was fixated by heat, before adding 70 µl of 0.1% crystal violet solution (V5265, Sigma-Aldrich) and staining for 5 min. The crystal violet solution was removed and the wells were washed with water before the plates were dried by heat. The bound crystal violet was dissolved in 70 µl of 70% ethanol, and the presence of violet color, indicating biofilm formation, was measured at 600 nm absorbance using a 1420 Multilabel Counter VICTOR<sup>3</sup>™ reader. Percent biofilm formation was calculated using the equation below. The data were visualized using GraphPad Prism 8.4.2, and the built-in ROUT method was used to detect and remove outliers from the dataset ( $Q = 1\%$ ).

Percent (%) biofilm formation

$$= \frac{(\text{absorbance treated wells} - \text{absorbance negative control})}{(\text{absorbance positive control} - \text{absorbance negative control})} \times 100 \quad (1)$$

To determine whether **1** could eradicate biofilm established by *S. epidermidis*, a modified biofilm inhibition assay protocol was performed. Here, the bacteria were grown overnight in a microtiter plate to allow the biofilm to be established prior to the addition of **1**. After addition of **1**, the plates are incubated overnight. Following this, the biofilm was fixated and colored and results were read as stated above. The experiment was conducted once with three technical replicates with concentrations of 0.2–100 µg/ml (twofold dilution series).

### Determination of Antiproliferative Activity Toward Human Cell Lines

The antiproliferative activities of **1** was evaluated against the melanoma cell line A2058 (ATCC, CRL-11147<sup>TM</sup>), the hepatocellular carcinoma cell line HepG2 (ATCC, HB-8065<sup>TM</sup>), and the non-malignant lung fibroblast cell line MRC5 (ATCC, CCL-171<sup>TM</sup>) in a MTS *in vitro* cell proliferation assay. The compound was tested in concentrations from 6.3 to 100 µg/ml against all cell lines, with three biological replicates each containing three technical replicates ( $n = 9$ ). A2058 was cultured and assayed in Dulbecco's Modified Eagle's Medium (D-MEM, D6171, Sigma-Aldrich). HepG2 was cultured and assayed in MEM Earle's (F0325, Biochrom) supplemented with 5 ml of non-essential amino acids (K0293, Biochrom) and 1 mM sodium pyruvate (L0473, Biochrom). MRC5 was cultured and assayed in MEM Eagle (M7278, Sigma-Aldrich) supplemented with 5 ml of non-essential amino acids, 1 mM sodium pyruvate, and 0.15% (w/v) sodium bicarbonate (L1713, Biochrom). In addition, all media were supplemented with 10% fetal bovine serum (FBS, S1810, Biowest), 10 µg/ml gentamicin (A2712, Biochrom), and 5 ml of glutamine stable (200 mM per 500 ml medium, X0551, Biowest). Briefly, the cells were seeded in 96-well microtiter plates

(Nunclon Delta Surface, VWR) at 2,000 cells/well for A2058, 4,000 cells/well for MRC5, and 20,000 cells/well for HepG2. After incubation for 24 h in 5% CO<sub>2</sub> at 37°C, the media was replaced and compound was added, generating a total volume of 100 µl/well. A2058 and MRC5 were incubated for 72 h before assaying, and HepG2 for 24 h. Subsequently, 10 µl of CellTiter 96 AQueous One Solution Reagent (G358B, Promega) was added to each well and the plates were incubated for 1 h at 37°C. Following this, the absorbance was measured at 485 nm with a DTX 880 multimode detector (Beckman Coulter). Negative controls were cells assayed with their respective cell media, and positive controls were cells treated with 10% DMSO (D4540, Sigma-Aldrich). Percent cell survival was calculated using the equation below. The data were visualized using GraphPad Prism 8.4.2 and IC<sub>50</sub> was calculated. The built-in ROUT method was used to detect and remove outliers from the dataset ( $Q = 1\%$ ).

Percent (%) cell survival :

$$\frac{(\text{absorbance treated wells} - \text{absorbance positive control})}{(\text{absorbance negative control} - \text{absorbance positive control})} \times 100 \quad (2)$$

### Minimal Inhibitory Concentration Determination Against *Candida albicans*

The MIC of **1** was determined by broth microdilution against *C. albicans* (ATCC 90028, LGC Standards), at final concentrations of 0.2–100 µg/ml (twofold dilution series). The experiment was performed as one biological replicate, with three technical replicates ( $n = 3$ ). Briefly, the fungus was inoculated from freeze stock onto potato dextrose agar [24 g/L potato dextrose broth (P6685, Sigma-Aldrich), 15 g/L agar (A1296, Sigma-Aldrich)] and incubated overnight at 37°C. From the overnight culture, five to eight colonies were transferred to 5 ml of sterile 0.9% NaCl, before the cell density was adjusted to 1–5 × 10<sup>6</sup> cells/ml by adding 0.9% NaCl. The cell density was evaluated with 0.5 McFarland standard (Remel 0.5 McFarland Equivalence Turbidity Standard, 10026732, Thermo Fisher Scientific). The fungal suspension was further diluted 1:50, and then 1:20 (1–5 × 10<sup>3</sup> CFU/ml) in RPMI medium (R7755, Sigma-Aldrich) with 0.165 mol/L MOPS (M3183, Sigma-Aldrich) and 10.25 ml of L-glutamine. The compound was added to the microtiter plate together with the fungal suspension (1:1), to a final volume of 200 µl. The final concentration of fungal cells was 0.5–2.5 × 10<sup>3</sup> CFU/ml. Absorbance in the wells was measured with 1420 Multilabel Counter VICTOR<sup>3</sup>™ right after addition of compound, after 24 h and after 48 h. The plates were incubated at 37°C. Amphotericin B was used as negative control at final concentration 8 µg/ml. Growth control contained fungal suspension and autoclaved Milli-Q® H<sub>2</sub>O.

## RESULTS

### Systematic Placement of the Fungal Isolate 067bN1.2

Due to lack of distinct morphological characters of the cultured asexual morph and closely related reference sequences



in GenBank, the fungus is identified to family level, as Lulworthiaceae sp., for the purpose of this study. A phylogenetic study was carried out with 28 taxa (including outgroups and isolate 067bN1.2), all representing different species, as shown in **Figure 1**. The combined dataset of 5.8S, SSU, and LSU had an aligned length of 2,270 characters, and phylogenetic inference was estimated using both Maximum Likelihood and Bayesian Inference criteria. The isolate producing **1**, 067bN1.2, was placed on its own branch within the Lulworthiaceae, forming a sister clade to the clade including *Halazoon fuscus*, *Lulworthia medusa*, *Lulworthia cf. purpurea* and *Halazoon melhae*. Sequences of *Koralionastes ellipticus* were included to exclude the possibility that the isolate 067bN1.2 is part of the family Koralionastetaceae. *Koralionastes ellipticus* was placed outside of Lulworthiaceae.

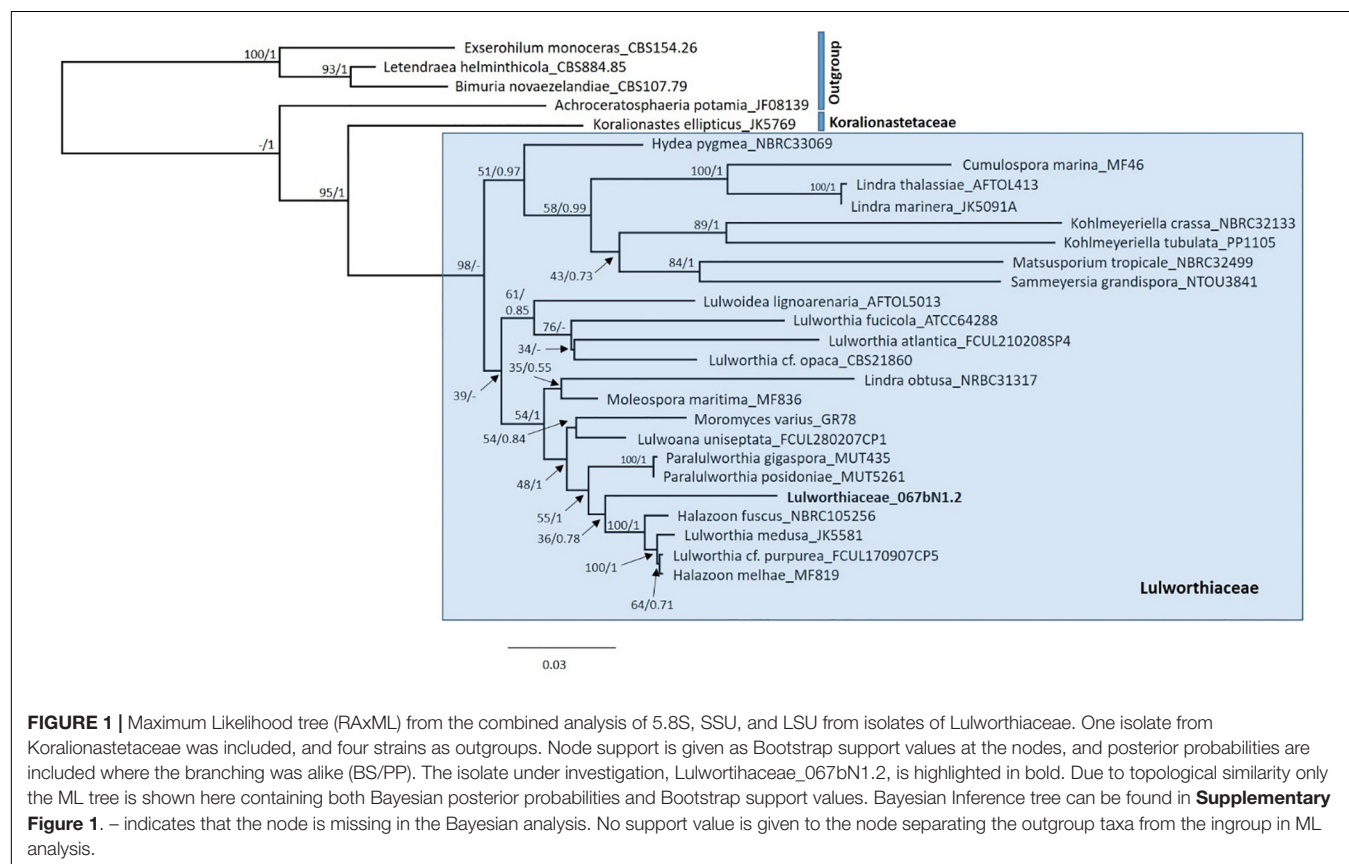
## Isolation and Structure Elucidation

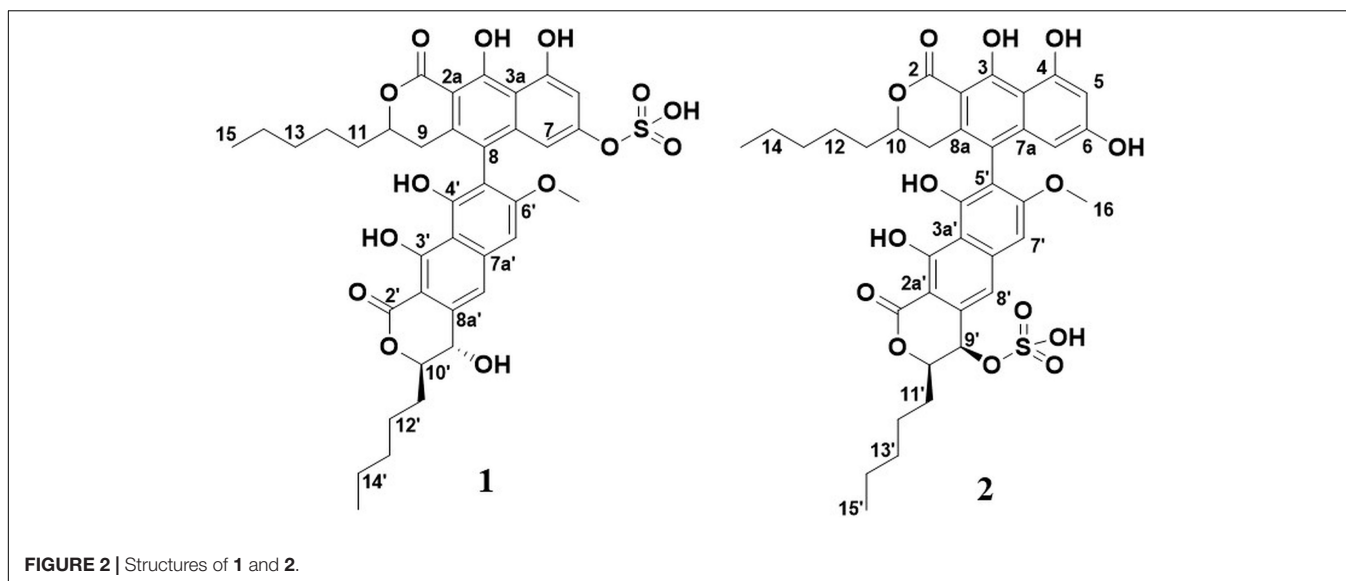
Compound **1** was selected for isolation due to its antibacterial activity in an initial screen of fractions from several understudied marine fungi. Compound **1** was the dominating peak in the active fraction from fungal isolate 067bN1.2 Lulworthiaceae sp., and subsequently the fungus was re-cultivated, cultures were extracted, and the compound was isolated using RP flash chromatography. The extraction of 1.4 L of fungal culture yielded 1,017.2 mg of extract.

Initially, attempts were made to isolate the compound using preparative HPLC. This strategy had several drawbacks, including unfavorable behavior of the compound in the

preparative column. This resulted in the compound eluting over several minutes (band broadening) and carryover. A batch of the compound was, however, retrieved using this strategy, resulting in a compound later determined to be a structural isomer and artifact of compound **1** (referred to as **2** throughout this article), produced due to the acidic conditions in the mobile phase. The structures of **1** and **2** can be seen in **Figure 2**.

Flash chromatography was better suited for the isolation of **1**. This isolation strategy yielded 63.8 mg of **1**, corresponding to a yield of ~45 mg/L culture medium. Compound **1** was obtained as a green colored substance. The molecular formula was calculated to be C<sub>37</sub>H<sub>40</sub>O<sub>14</sub>S by UHPLC-ESI-HRMS (*m/z* 741.2204 [M+H]<sup>+</sup>) (calculated as C<sub>37</sub>H<sub>41</sub>O<sub>14</sub>S, 741.2217), suggesting 18 degrees of unsaturation. The low-energy collision mass spectrum of **1** can be seen in **Supplementary Figure 2**. MS signals of a neutral loss of 80 Da (ESI<sup>+</sup>) was observed, indicating the presence of a sulfate group in the structure. The UV absorption maxima were 224, 260, and 373 nm, which corresponded well with the previously published dinapinones (Kawaguchi et al., 2013). The UV-vis spectrum for **1** can be seen in **Supplementary Figure 3**. The IR spectrum of **1** displayed absorption bands for sulfoxide (S=O, 1,002 cm<sup>-1</sup>), aromatic alkene (C=C, 1542 and 1,618 cm<sup>-1</sup>), carbonyl (C=O, 1,645 cm<sup>-1</sup>), alkane (C-H, 2,857 cm<sup>-1</sup>), aromatic alkene (C-H, 2926 cm<sup>-1</sup>), and hydroxyl (C-OH, 3455 cm<sup>-1</sup>) bonds. After isolation, the structure of **1** (**Figure 2**) was elucidated by 1D and 2D NMR experiments (**Supplementary Figures 4–16**).





Initial structure elucidation was made on the sample isolated by preparative HPLC with formic acid present in the mobile phases (compound **2**). The established molecular formula suggested a highly conjugated system. The purity of **2** was estimated to be ~80% from a quantitative proton spectrum with respect to non-solvent impurities (**Supplementary Figure 4**). Four singlet protons were identified in the aromatic region, along with three O-CH signals at ~4.5 ppm with complex couplings along with a methoxy singlet at 3.77 ppm. Furthermore, five hydroxyl protons were identified; three between 9.5 and 10.0 ppm, and two between 13.5 and 14.0 ppm. The deshielded nature of the latter sets them apart from the other hydroxyls and suggests they may be involved in an angled intramolecular hydrogen bond, which is commonly seen for keto-enol pair configurations such as this. All 37 carbons could be identified by 1D  $^{13}\text{C}$  NMR (**Supplementary Figure 5**), which showed **2** to contain a large number of aromatic quaternary carbons, two ester-like carbonyls, along with 10 peaks in the aliphatic region (**Table 1**).

HSQC, HMBC, and 1,1-ADEQUATE spectra (**Supplementary Figures 6, 7**) allowed the identification of two substituted naphthopyrone-like moieties, as well as two five-membered aliphatic chains (denoted  $C15$ - $C11$  and  $C15'$ - $C11'$ , respectively), which were fully assigned using a combination of HSQC-TOCSY, TOCSY, COSY, and HMBC (**Figure 3i**). The aliphatic chains were determined to be attached at the  $C10$  position of the naphthopyrone-like moieties by tracing the spin system into  $H9$  and  $H9'$ , respectively, and supported by multiple long-range  $^1\text{H}$ - $^{13}\text{C}$  correlations. The  $C2$  and  $C2'$  carbonyls could be directly assigned from long-range couplings from the  $10/10'$  position, but the hydroxyl carrying carbons in positions  $3/3'$  and  $4/4'$  could only be assigned through weak  $^4J_{\text{CH}}$  correlations from the aromatic protons (**Figure 3iii**).

The  $\text{OH-4}$  and  $\text{OH-6}$  could be assigned based on NOE correlations between  $\text{OH-6}$  and both  $H5$  and  $H7$ , while  $\text{OH-4}$  only displayed correlations with  $H5$ . The  $\text{OH-3}$  and  $\text{OH-3'}$  are predicted to have more deshielded chemical shifts due

to their proximity to the carbonyl moiety and a probable intramolecular hydrogen bond—however, it was not possible to individually distinguish  $\text{OH3}$  and  $\text{OH-3'}$  due to the absence of any correlations in NOESY, ROESY, and HMBC spectra. Thus, four fragments could initially be elucidated (**Figure 3i**). A weak  $^4J_{\text{C8H7'}}$  correlation could be detected, linking fragment **A** to fragment **B** (**Figure 3i**) at the  $C8$  and  $C5'$  positions, respectively, and thus the only remaining ambiguity is the position of the  $-\text{SO}_3^-$  group vis-à-vis the remaining  $-\text{OH}$  in the  $9'$  or  $4'$  positions. The absence of NOEs and COSY correlations between  $\text{OH-4'}$  and  $H9'$  suggests that it is positioned at  $C4'$  with the sulfate positioned at  $C9'$  (**Figure 3ii**). The  $^3J_{\text{HH}}$  coupling constant between  $H9'$  and  $H10'$  was measured to be 2.0 Hz from line shape fitting the splitting of  $H9'$ , indicating that these protons are at a significantly offset dihedral angle to one another—thus suggesting a relative R/S or S/R configuration of  $9'$  and  $10'$ .  $^{13}\text{C}$  prediction was consistent with the structure of **2** (**Supplementary Figure 9**), with a mean error of 2.79 ppm between the observed and predicted  $^{13}\text{C}$  shifts.

A second isolation where no acidic conditions were used, yielding **1**, was also examined.  $^1\text{H}$  NMR revealed significantly perturbed chemical shifts as well as line broadening and heterogeneity throughout the spectra (**Supplementary Figure 11**). Multiple resonances in the carbon spectrum (**Supplementary Figures 12, 13**), especially for two resonances in the carbonyl area (presumably  $C3$  and  $C3'$ ), are heterogeneous, reflecting the nuclei existing in several stable, but slightly different micro environments. The same observation is made in the proton spectrum (**Supplementary Figure 11**) for  $H9'$ ,  $\text{OMe-6}$ ,  $H5$ ,  $H7$ ,  $4'$ -OH, and  $4$ -OH. A major difference was observed in the non-acidic preparation (**1**), compared to **2**, the presence of a  $9'$ -OH. At ~15 ppm, two heterogeneous OH protons were observed, deshielded by approximately 1 ppm compared to the  $\text{OH-3}$ 's in the original sample preparation, while the three hydroxyls at ~10 ppm could no longer be detected (**Supplementary Figures 8–13**). Thus, the detectable aromatic hydroxyl groups, identified as  $\text{OH-4'}$  and  $\text{OH-4}$ ,

**TABLE 1** | Summary of chemical shift and correlations for **2** (DMSO-*d*<sub>6</sub>).

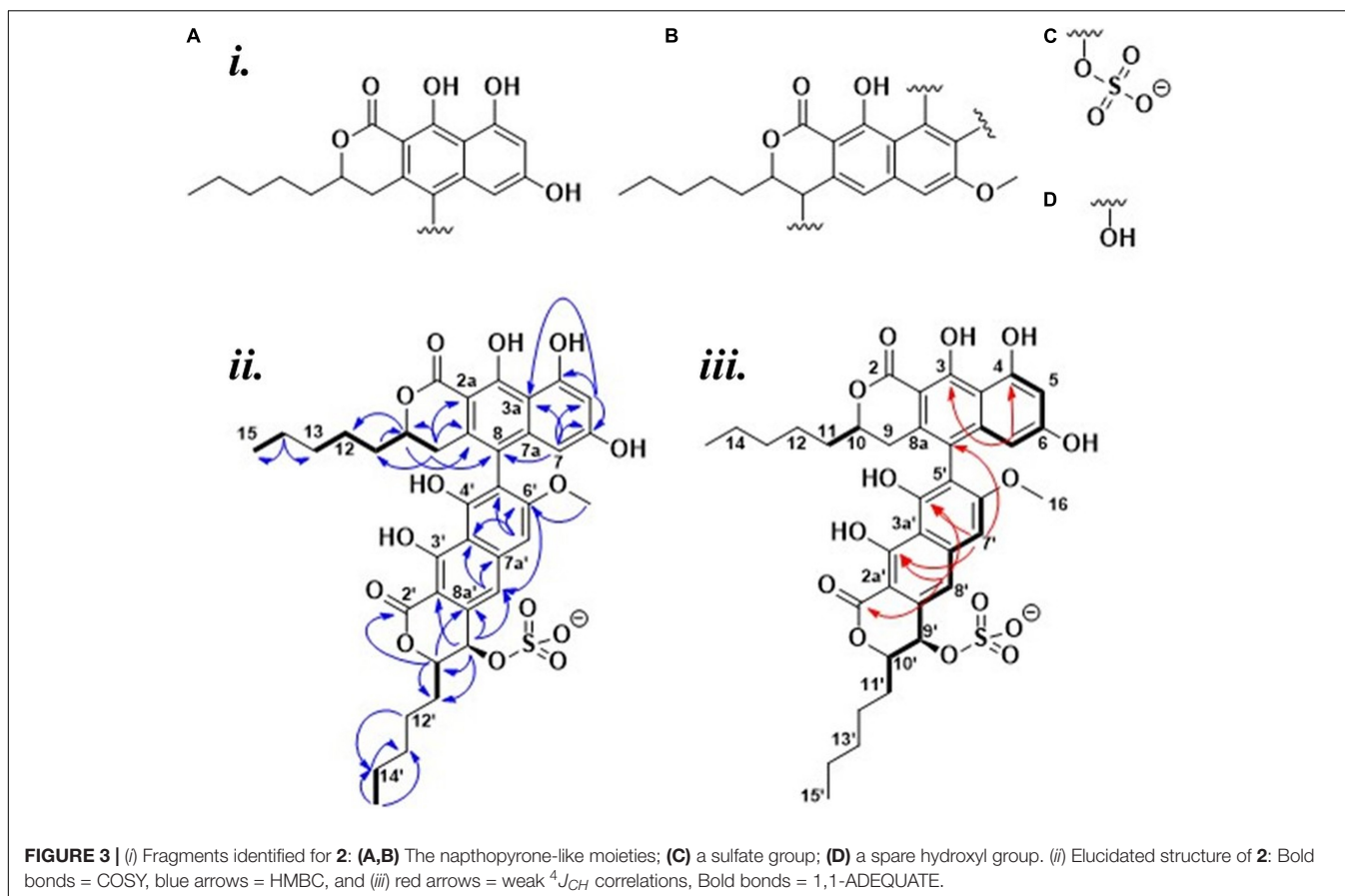
Position	$\delta^{13}\text{C}$ , type	$\delta^1\text{H}$ , splitting (Hz)	COSY	HMBC ( $^1\text{H} \rightarrow ^{13}\text{C}$ )
2	171.6, C	–	–	–
2'	171.0, C	–	–	–
2a'	99.4, C	–	–	–
2a	99.2, C	–	–	–
3	162.5, C	–	–	–
3'	161.5, C	–	–	–
3a'	108.6, C	–	–	–
3a	107.5, C	–	–	–
4	159.0, C	–	–	–
4'	154.9, C	–	–	–
5'	111.7, C	–	–	–
5	102.1, CH	6.35, s	–	3, 3a, 4, 6, 7
6	161.2, C	–	–	–
6'	160.7, C	–	–	–
7a	140.6, C	–	–	–
7a'	140.1, C	–	–	–
7	100.7, CH	6.04, s	–	3, 3a, 5, 6, 8
7'	99.7, CH	7.14, s	–	3', 3a', 4', 5', 6', 8, 8'
8a'	137.4, C	–	–	–
8a	132.9, C	–	–	–
8	118.7, C	–	–	–
8'	117.5, CH	7.36, s	–	2', 3a', 4', 6', 7'a, 7', 9'
9'	65.3, CH	4.69, d ( $J = 2.0$ )	–	2a', 8', 8a', 10', 11'
9	31.0, CH <sub>2</sub>	2.59, m	10	2a, 7a, 8, 8a, 10, 11
10'	83.2, CH	4.62, ddd ( $J = 7.9, 6.0, 2.0$ )	11'	2', 8a', 9', 11', 12'
10	79.4, CH	4.56, dddd ( $J = 9.6, 7.4, 5.5, 4.1$ )	9, 11	2, 8a, 12
11	34.2, CH <sub>2</sub>	1.59, dd ( $J = 16.7, 9.5$ ) 1.68, dd ( $J = 16.5, 4.0$ )	10, 12	10, 12
11'	30.0, CH <sub>2</sub>	1.85, m	10', 12'	9', 10', 12', 13'
12'	24.7, CH <sub>2</sub>	1.48, 1.52, m	11', 13'	11', 13', 14'
12	24.5, CH <sub>2</sub>	1.27, 1.36, m	11, 13	11, 13, 14
13'	31.3, CH <sub>2</sub>	1.23, m	12', 14'	11', 12', 14', 15'
13	31.6, CH <sub>2</sub>	1.36, m	12, 14	11, 12, 14, 15
14'	22.5, CH <sub>2</sub>	1.36, m	13', 15'	12', 13', 15'
14	22.4, CH <sub>2</sub>	1.24, m	15	12, 13, 15
15'	14.4, CH <sub>3</sub>	0.92, m	14'	13', 14'
15	14.3, CH <sub>3</sub>	0.82, m	14	13, 14
16	56.5, O-CH <sub>3</sub>	3.77, s	–	6'
OH3*	–	13.71, s	–	–
OH3*	–	13.62, s	–	–
OH4	–	9.80, s	–	–
OH4'	–	9.51, s	–	–
OH6	–	9.94, s	–	–

\*Ambiguous assignment.

appeared to be involved in (stronger) hydrogen bonding, while three aromatic hydroxyls, the remaining OH-6, OH-3' and OH-3, were unaccounted for. At the same time, the majority of all other nuclei in the molecule are shielded by approximately 0.5 ppm. Together, these observations suggest that the neutral pH preparation resulted in a different molecule, **1**, that formed loose aggregates in DMSO and methanol, stabilized by both hydrogen bonding (deshielding) and stacking (shielding) interactions. Overall, worse spectral quality resulted in that the C2 and C3 from **2** could not be individually assigned in **1**, although they

must correspond to the two chemical shifts of 169.4 and 173 ppm by the logic of elimination. A number of the carbons show heterogenic peaks (notably the presumed C3 and C3'), most likely as the result of through space proximity to the sulfate group and sensitivity to its different possible conformation (details in section "Discussion").

The identity of **1** was established to be identical to **2** with the only difference being that the sulfate group was attached to C6 instead of C9', supported by the loss of the OH correlating with H5 and H7, and the appearance of an OH



correlating with H9' through a  $^3J_{HH}$ . There is furthermore a heterogeneity and chemical shift perturbation hotspot (vis-à-vis 2) around the C6 position to support the assignment of a C6 sulfate. All chemical shifts and correlations are summarized in **Supplementary Table 3**. The data do not unambiguously prove whether the 3-OH's are deprotonated or if the signal is lost due to rapid exchange, but the fact that the OH-9' is observable under the same conditions is an indicium for the OH-3's to be deprotonated in **1**. No plausible resonance structures to explain the deprotonation and deshielding that does not involve the oxidation, and thus change in mass, have been found.

The non-aggregated **2** could be scavenged by lowering the pH of **1** with the addition of hydrochloric acid, upon which  $^1\text{H}$  and HSQC spectra of the two samples of **2** show a great resemblance (**Supplementary Figure 10**). The molecular formula of **2** and **1** as well as the scavenged **2** were identical in the two preparations, as no change in mass was observed by high-resolution mass spectrometry.

## Antibacterial Activity Against Reference and Clinical Strains

Compound **1** was tested against six reference bacteria (four Gram-positive and two Gram-negative strains). The compound was active against two of the Gram-positive reference strains, *S. aureus* and *S. agalactiae*, with MIC values of 6.25 and

12.5  $\mu\text{g/ml}$ , respectively. No activity was observed against the Gram-negative strains, *E. coli* and *P. aeruginosa*, or the Gram-positive *E. faecalis* or MRSA strain (**Supplementary Table 4**). As bacterial resistance toward available antibiotics is the main challenge in future treatment of pathogenic diseases, **1** was tested against a panel of drug-resistant clinical strains (**Supplementary Table 2**). The panel included five MRSA and six VRE strains. Compound **1** was also tested in a pre-screen against four Gram-negative clinical bacterial strains: *E. coli*, *Klebsiella pneumoniae*, *Acinetobacter baumannii*, and *P. aeruginosa* (all ESBL-Carba). No activity was detected against the Gram-negative bacteria (**Supplementary Table 4**). Compound **1** showed activity against the MRSA strains with MICs in the 1.56–6.25  $\mu\text{g/ml}$  (2.12–8.44  $\mu\text{M}$ ) range, see **Table 2**. The activity of the compound was significantly less profound against the VRE strains (MIC = 50  $\mu\text{g/ml}$  or higher) (**Supplementary Table 4**).

To investigate if **1** has bacteriostatic or bacteriocidal effects on the two reference strains *S. aureus* and *S. agalactiae*, both were incubated with the compound at 12.5 and 25  $\mu\text{g/ml}$  overnight and subsequently plated onto agar. For *S. aureus*, there was no growth on the plates after overnight incubation, indicating a bacteriocidal effect of **1**. For *S. agalactiae*, one of the parallels at 12.5  $\mu\text{g/ml}$  (MIC of **1** against this bacterium) displayed growth on the agar plate, which was expected as visual growth could also be seen in the microtiter plate for this parallel. The remaining five parallels at this concentration, and the concentration above,

had no growth in the microtiter plates, or on agar after overnight incubation. This strongly indicates that **1** also has bacteriocidal effect on *S. agalactiae*. Compound **1** was also tested together with the efflux pump inhibitor reserpine to see if the lack of activity toward Gram-negative strains was caused by efflux of **1**, but no activity was obtained.

## Inhibition of Biofilm Production and Eradication of Established Biofilm

The ability of **1** to inhibit biofilm production by *S. epidermidis* and to remove established *S. epidermidis* biofilm was assessed. In the biofilm inhibition assay, the biofilm production was completely inhibited (below 5% biofilm formation) down to 12.5  $\mu\text{g/ml}$  (Figure 4). Clear inhibition of the bacterial growth could also be observed to 25  $\mu\text{g/ml}$  by visual inspection of plates before fixation of biofilm, raising the question if the biofilm inhibition is mainly caused by growth inhibition of the bacterium. To further evaluate the potential biofilm activity, removal of established biofilm was assessed. There was no activity of **1** at concentrations up to 100  $\mu\text{g/ml}$  against the established biofilm, further supporting the hypothesis that the biofilm inhibition is mainly due to growth inhibition of the bacterium.

**TABLE 2** | Minimal inhibitory concentrations (MICs) of **1** against reference strains and clinical isolates.

Strain type	Strain	MIC in $\mu\text{g/ml}$
Clinical strains	<i>S. aureus</i> N315	1.56
	<i>S. aureus</i> 85/2082	3.13
	<i>S. aureus</i> NCTC 10442	3.13
	<i>S. aureus</i> WIS [WBG8318]	6.25
	<i>S. aureus</i> IHT 99040	3.13
Reference strains	<i>S. aureus</i> ATCC <sup>®</sup> 25923	6.25
	<i>S. agalactiae</i> ATCC <sup>®</sup> 12386	12.5

The median MIC values are reported ( $n = 12$  for clinical isolates,  $n = 9$  for reference strains).

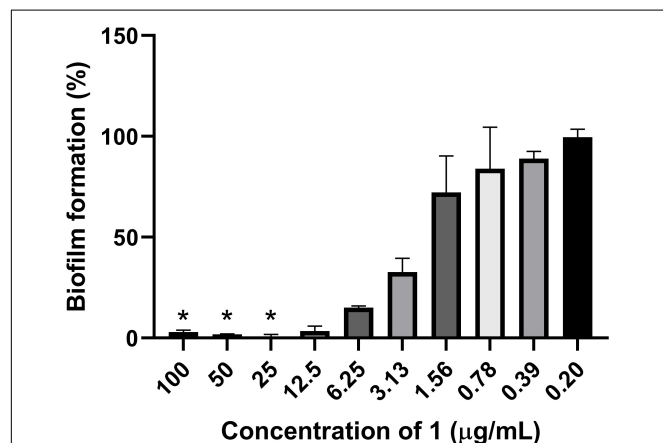


**FIGURE 4** | Inhibition of bacterial biofilm formation by **1** against the biofilm producing *S. epidermidis*. \*The bacterial growth was completely inhibited at compound concentrations down to 25  $\mu\text{g/ml}$ .

## Antiproliferative Activity Against Human Cells and Antifungal Activity

The antiproliferative activities of **1** was assessed against human melanoma cells (A2058), human non-malignant lung fibroblasts (MRC5), and human hepatocellular carcinoma cells (HepG2), in a concentration range of 6.25–100  $\mu\text{g/ml}$ . The non-malignant cell line was included as a test for general toxicity, while the other cell line was included to assess possible anti-cancer activities. Antiproliferative activity was observed against all cell lines, with  $\text{IC}_{50}$  values of 15.5, 32, and 27  $\mu\text{g/ml}$  against A2058, MRC5, and HepG2, respectively (Table 3). Compound **1** was also assayed for antifungal activity against *C. albicans* at concentrations up to 100  $\mu\text{g/ml}$ , and no activity was seen.

## DISCUSSION

In this study, we describe the discovery, isolation, and characterization of the new secondary metabolite lulworthinone (**1**). This novel antibacterial compound was isolated from an extract of a slow-growing marine fungus of the family Lulworthiaceae. To the best of our knowledge, this is the first reported secondary metabolite isolated from this fungal family and the order Lulworthiales. Since the isolate did not branch close to the *Lulworthia* type species, *L. fucicola* (in the *Lulworthia sensu stricto* clade) and there was a lack of support at many nodes of the phylogenetic tree, we restrained from identifying the isolate 067bN1.2 to genus and determine its identity to family level only.

A fraction of the Lulworthiaceae sp. extract was nominated for chemical investigation as it was active in an initial antibacterial screen. The content of the active Lulworthiaceae sp. fraction was dominated by **1**, whose calculated elemental composition gave no hits in database searches, indicating that the compound suspected to be responsible for the observed antibacterial activity, was novel. In the attempt to utilize preparative HPLC to isolate this compound, **2** was generated during the procedure (acidic mobile phase). As compounds **1** and **2** have the same mass, HRMS analysis did not detect the change in the positioning of the sulfate group, and the sample from the preparative HPLC isolation was characterized using NMR, believing it was **1**. As preparative HPLC was deemed inconvenient for compound isolation, flash chromatography (neutral mobile phase) was utilized to isolate sufficient amounts of **1** to conduct a thorough characterization of the compound's bioactivity. This method allows larger amounts of sample to be processed per run, but generally is less effective in separating compounds of interest from sample impurities, compared to preparative HPLC isolation. However, due to the high concentration of **1** in the extract, **1** was successfully isolated using this method. The resulting sample was submitted

**TABLE 3** | Antiproliferative activity ( $\text{IC}_{50}$ ) of **1** against human cell lines ( $n = 9$ ).

Cell type	$\text{IC}_{50}$ in $\mu\text{g/ml}$
A2058, melanoma	15.5 $\pm$ 0.6
MRC5, normal lung fibroblasts	32 $\pm$ 1
HepG2, hepatocellular carcinoma	27 $\pm$ 1

to NMR analysis to confirm its structure. The samples from both isolations were confirmed to be novel biarylic dimeric naphtho- $\alpha$ -pyrones substituted with a sulfate group. However, NMR analysis revealed that the sulfate group was located on different positions in the two compounds. The rearrangement was hypothesized to be catalyzed by the acidic nature of the HPLC mobile phase. This hypothesis was confirmed by subjecting **1** to acidic conditions (**Supplementary Figure 10**). The resulting sample was analyzed using NMR, confirming that **1** had indeed converted into **2**. As **2** was proven to be an artifact of **1**, all bioactivity testing was conducted using **1** isolated under neutral conditions.

The propensity of **1** to interact with itself to form higher-ordered structures, while **2** did not, offered some insight into their structural behavior in solution. In particular, the sulfate in the 6-position appeared to facilitate oligomeric aggregation, and a simple 3D model allows some speculation as to why this could be (**Figure 5**). The ground state of the naphthopyrone does not have the ability to form complementary “base pairs” with itself through hydrogen bonds between the carbonyls and hydroxyls. However, when the sulfate is in the 6-position, it can reach the C3 double OH “mismatch” in the three-dimensional structure and potentially stabilize the hydroxyls either by 4-coordinating a water molecule or a Na<sup>+</sup> ion together with deprotonated 3'-hydroxyls, or by directly hydrogen bonding to the protonated hydroxyls.

This would provide a feasible rationale for the propensity for aggregation of **1** but not of **2**. The structural dimer model also provides a plausible explanation as to why the sulfate group would specifically and irreversibly migrate to C9' under acidic conditions even though the C9' is expected to be a less likely position for the sulfate than any other phenol position. The sulfate is in an oligomeric state involving this kind of “base pairing” positioned to be intermolecularly attacked by the OH-9' of the paired molecule, which is not possible in the monomeric state. Lowered pH is expected to ensure protonated sulfate, which would make it more susceptible for an electrophilic attack from OH-9'. If oligomeric states are indeed stabilized by the coordination of water or sodium, then lowered pH and the protonation of the 3- and 3'-oxygens would further destabilize the oligomer, which together with the lack of stabilization from the position 6 sulfate would make both the association and the reaction irreversible and trap the sulfate in the 9' position of monomeric **2** with lowered ability to self-aggregate.

*Lulworthia* spp. fungi have spores with end chambers containing mucus, which helps in spore attachment to surfaces (Jones, 1994). It has been observed that in liquid culture of the isolate 067bN1.2, the fungus forms a gel-like mucus, having the ability to adhere to the bottom of the culture flasks. No spores are formed in culture, and it remains unclear whether the mucus formed under cultivation of 067bN1.2 has chemical resemblance

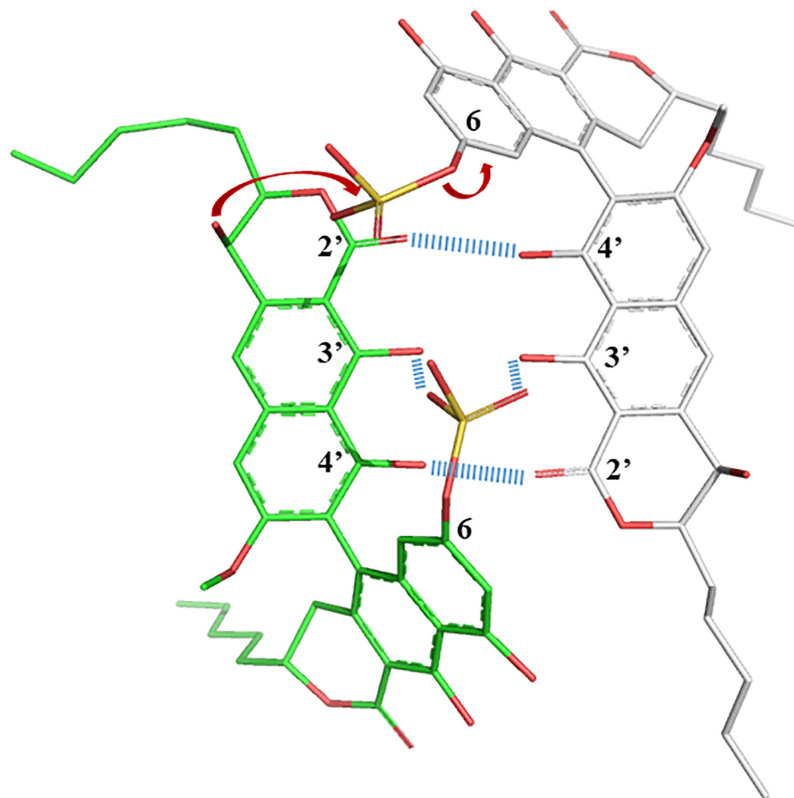


**FIGURE 5** | Crude sculpted and minimized structural model of **1** displaying the sulfate potential role in stabilizing oligomerization, as well as the possibility to intermolecularly react specifically at the C-9' position to form **2** under acidic conditions.

to the mucus in end chambers of *Lulworthia* spp. spores, as it has not yet been characterized. The sheathing of mucoid by *L. medusa* has been reported in a publication from 1973, where the fungus was found and isolated from a piece of submerged pine and cultivated in bottles in media supplemented with artificial seawater (Davidson, 1973). Also in the current study, the fungus was found to adhere to the culture flask during cultivation in artificial seawater media. Davidson hypothesizes around the physiological and ecological implications of the mucoid, important in cation binding and transport, for the adhesion of other microorganisms, avoiding desiccation in intertidal regions or for the production of a matrix to concentrate exoenzymes (Davidson, 1973). Compound **1** is isolated in high yields from the fungal culture, but the ecological role of naphthopyrone-type compounds is largely unclear. The antibacterial activity of **1**, however, could indicate a protective role against pathogenic attacks, but the compound may have other types of bioactivities as well. It has been speculated that similar compounds (bis-naphthopyrones) from filamentous ascomycetes were produced to protect the fungus from predators (Xu et al., 2019). The study found that several animal predators, like woodlice, preferred feeding on fungi that had disrupted aurofusarin synthesis, and also that predation stimulated the production of aurofusarin in several *Fusarium* species (Xu et al., 2019). We have also observed marine mites feeding on fruitbody contents of Lulworthiales fungi. It is thus possible that in the natural habitat of these fungi, the naphthopyrones are produced as a means of protection.

Compound **1** was found to be a dimeric biaryl naphtho- $\alpha$ -pyrone substituted with a sulfate group. The naphthopyrone moiety is recurring in nature, as monomers, dimers, and trimers, and has been found from several natural sources, like plants and filamentous fungi. Naphthopyrones have also previously been isolated from organisms from the marine environment (Li et al., 2016). Compounds from this class have shown different bioactivities, among these the inhibition of triacylglycerol synthesis (Kawaguchi et al., 2013), inhibition of enzymatic activity (Zheng et al., 2007), protection against animal predators (Xu et al., 2019), antimalarial activities (Isaka et al., 2010), and antiproliferative activities (Isaka et al., 2010; Li et al., 2016). Several of these compounds have displayed antibacterial activities against Gram-positive bacteria (Suzuki et al., 1992; Wang et al., 2003; Zheng et al., 2007; Boudesocque-Delaye et al., 2015; Rivera-Chavez et al., 2019). Lu et al. (2014) defined three groups of bis-naphtho- $\gamma$ -pyrones based on the diaryl bond connection between the monomers, the chaetochromin-, asperpyrone-, and nigerone-type bis-naphtho- $\gamma$ -pyrones. Based on this categorization, **1** would be categorized as an asperpyrone-type bis-naphtho- $\alpha$ -pyrone, due to the relative placement of the oxygen atoms in the pyrone moieties. Compound **1** is substituted with a sulfate group. One of the most abundant elements in seawater is sulfur, and many sulfated compounds have been isolated from marine organisms, mostly from marine invertebrates, but also from microorganisms (Kornprobst et al., 1998; Francisca et al., 2018). Compound **1** represents, however, the first report of a dimeric naphtho- $\alpha$ -pyrone substituted with a sulfate group.

In the current study, **1** was broadly assessed for potential bioactivities: antibacterial activities against bacterial reference strains and clinical strains, antiproliferative activities toward a selection of human cell lines, both malignant and non-malignant, anti-fungal activity, inhibition of bacterial biofilm formation, and the eradication of established bacterial biofilm. Intriguingly, **1** showed activity against multidrug-resistant MRSA strains with MICs between 1.56 and 6.25  $\mu\text{g/ml}$  (2.12–8.44  $\mu\text{M}$ ). In comparison, a natural product originally isolated from *Clitophilus scyphoides* (organism name at time of isolation: *Pleurotus mutilus*, Basidiomycota) pleuromutilin showed MICs in a similar range against selected reference strains (e.g., MIC = 0.66  $\mu\text{M}$  against *S. aureus*, MIC = 2.64  $\mu\text{M}$  against *K. pneumoniae*, and MIC = 21.13  $\mu\text{M}$  against *B. subtilis*) while having significantly higher MIC values against other reference strains (e.g., MIC  $\geq$  100  $\mu\text{M}$  against *P. aeruginosa*) (Kavanagh et al., 1951). An optimized analog of pleuromutilin, lefamulin (Xenleta<sup>®</sup>), was approved as an antibiotic drug by the US Food and Drug Administration in 2019. The herein reported MIC values thus place **1** in an activity segment, which makes it an interesting candidate for further development toward becoming a marketed antibiotic drug. In comparison to other antibacterial naphthopyrones, **1** falls within the same MIC range with regard to activity toward Gram-positive bacteria. Two heterodimers, isolated from the tubers of *Pyrenacantha kaurabassana*, showed antibacterial activity against different strains of *S. aureus* with MICs in the range of 2.7–89.9  $\mu\text{M}$  (Boudesocque-Delaye et al., 2015). In a recent paper from 2019, mycopyranone, a new binaphthopyranone, was isolated from the fermentation broth of *Phialemoniopsis*. The compound showed antibacterial activity against both *S. aureus* and a MRSA strain, with MICs of  $\leq$  8.7  $\mu\text{M}$  against both strains (Rivera-Chavez et al., 2019). Possibly the most known naphthopyrone, viriditoxin showed MICs in the 4–8  $\mu\text{g/ml}$  range against different *Staphylococcus* isolates (Wang et al., 2003).

Furthermore, the lack of activity against the Gram-negative reference and clinical strains shows the selectivity of **1** against Gram-positive bacteria. Yet, no activity or weak activity was observed against the clinical VRE isolates and the reference strain of *E. faecalis*, indicating that the activity is selective toward groups of Gram-positives, in this case *S. aureus* and *S. agalactiae*. Surprisingly, no activity was observed against the reference MRSA strain, and the reason behind this is not clear. No activity was observed for the combination of **1** and the efflux pump inhibitor reserpine, indicating that the lack of susceptibility by Gram-negatives is caused by another mechanism. In the antiproliferative activity assay, the most potent activity of **1** was observed against the melanoma cells (IC<sub>50</sub> = 15.5  $\mu\text{g/ml}$ ). Against the non-malignant lung fibroblasts, which were included as a test for general toxicity, the compound had an IC<sub>50</sub> of 32  $\mu\text{g/ml}$ , which is more than five times higher than the highest MIC value against the multidrug-resistant MRSA. The concentrations where **1** did not display any toxic effect on the cells ( $\sim$ 100% cell survival) were 20, 12.5, and 15  $\mu\text{g/ml}$  for MRC5, A2058, and HepG2, respectively. This indicates that there is little overlap between the concentration where **1** has antibacterial activity and the concentration where toxicity occurs against the human cells.

This observed difference is a good starting point when entering structure optimization, as it indicates that production of non-toxic variants of **1** can be obtained.

We isolated 45 mg/L of **1** when the Lulworthiaceae sp. fungus was grown in liquid media supplemented with sea salts. This shows that slow-growing marine fungi *sensu stricto* can produce high yields of novel compounds for chemical characterization and screening for biological activities. Compound **1** was found to be a novel sulfated dimeric naphthopyrone, and showed potent growth inhibition of multidrug-resistant MRSA with MICs down to 1.56 µg/ml, which is much lower than the IC<sub>50</sub> detected against the non-malignant cell line (32 µg/ml). This study demonstrates that the family Lulworthiaceae and order Lulworthiales have biosynthetic potential to produce bioactive secondary metabolites and supports the view of Overy et al. (2014) that marine fungi *sensu stricto* should be studied for natural product discovery, despite their slow growth (Overy et al., 2014). Our study highlights the potential role of marine fungi *sensu stricto* in tackling the worldwide AMR crisis.

## DATA AVAILABILITY STATEMENT

The datasets presented in this study can be found in online repositories. The names of the repository/repositories and accession number(s) can be found in the article/**Supplementary Material**.

## AUTHOR CONTRIBUTIONS

MJ was responsible for conducting experiments, data analysis, and writing and revising the draft manuscript. PR and JI were responsible for the NMR analysis of the compound and the writing related to this. EJ conducted the antibacterial testing against the clinical bacterial isolates and wrote this section in the “Materials and Methods,” and contributed to the writing of the MIC results. KH assisted in writing and revision of the manuscript and contributed to the experiment design. TR did

the initial isolation of the fungus and the phylogenetic analysis, contributed to the experiment design by selecting this fungus for the study, and revised the manuscript. JA and EH contributed to the conceptualization of the work, supervised the work, and revised the manuscript. All authors reviewed and approved the final manuscript.

## FUNDING

This project received funding from the DigiBiotics project of the Research Council of Norway (project ID 269425), the AntiBioSpec project of UiT the Arctic University of Norway (Cristin ID 20161326), and the Centre for New Antibacterial Strategies at UiT the Arctic University of Norway (TR). The publication charges for this article have been funded by the publication fund of UiT the Arctic University of Norway.

## ACKNOWLEDGMENTS

We would like to acknowledge the technical support by Kirsti Helland and Marte Albrigtsen by execution of the bioactivity assays, the contribution of Chun Li in the work with the sequencing of the genetic elements of the isolate, and Ole Christian Hagestad with his assistance in the phylogenetic analysis. We thank the Advanced Microscopy Core Facility (AMCF) of the UiT the Arctic University of Norway for the access to their devices. We would also like to acknowledge the Norwegian National Advisory Unit on Detection of Antimicrobial Resistance (K-res), University Hospital of North Norway for the VREs.

## SUPPLEMENTARY MATERIAL

The Supplementary Material for this article can be found online at: <https://www.frontiersin.org/articles/10.3389/fmicb.2021.730740/full#supplementary-material>

## REFERENCES

- Azevedo, E., Barata, M., Marques, M. I., and Caeiro, M. F. (2017). Lulworthia atlantica: a new species supported by molecular phylogeny and morphological analysis. *Mycologia* 109, 287–295. doi: 10.1080/00275514.2017.1302255
- Boudesocque-Delaye, L., Agostinho, D., Bodet, C., Thery-Kone, I., Allouchi, H., Gueffier, A., et al. (2015). Antibacterial polyketide heterodimers from *Pyrenacantha kaurabassana* Tubers. *J. Nat. Prod.* 78, 597–603. doi: 10.1021/np5003252
- Calado, M. D. L., Carvalho, L., Barata, M., and Pang, K.-L. (2019). Potential roles of marine fungi in the decomposition process of standing stems and leaves of *Spartina maritima*. *Mycologia* 111, 371–383. doi: 10.1080/00275514.2019.1571380
- Clinical Laboratory Standard Institute (CLSI) (2012). Clinical and laboratory standards institute methods for dilution antimicrobial susceptibility tests for bacteria that grow aerobically approved standard. *J. Infect. Chemother.* 18, 816–826.
- Davidson, D. E. (1973). Mucoïd sheath of *Lulworthia medusa*. *Trans. Brit. Mycol. Soc.* 60, 577–579. doi: 10.1016/S0007-1536(73)80042-7
- Demain, A. L. (2014). “Valuable secondary metabolites from fungi,” in *Biosynthesis and Molecular Genetics of Fungal Secondary Metabolites*, eds J. F. Martin, S. Zeilinger, and C. García-Estrada (Springer).
- Francisca, C., Marta, C.-D.-S., Emília, S., Madalena, P., and Anake, K. (2018). Sulfation pathways: sources and biological activities of marine sulfated steroids. *J. Mol. Endocrinol.* 61, T211–T231. doi: 10.1530/JME-17-0252
- Góes-Neto, A., Marcelino, V. R., Verbruggen, H., da Silva, F. F., and Badotti, F. (2020). Biodiversity of endolithic fungi in coral skeletons and other reef substrates revealed with 18S rDNA metabarcoding. *Coral. Reefs* 39, 229–238. doi: 10.1007/s00338-019-01880-y
- Hyde, K. D., Norphanphoun, C., Maharachchikumbura, S. S. N., Bhat, D. J., Jones, E. B. G., Bundhun, D., et al. (2020). Refined families of sordariomycetes. *Mycosphere* 11:1059. doi: 10.5943/mycosphere/11/1/7
- Imhoff, J. F. (2016). Natural products from marine fungistill an underrepresented resource. *Mar. Drugs* 14, 1–19. doi: 10.3390/md14010019
- Isaka, M., Yangchum, A., Rachtawee, P., Komwijit, S., and Lutthisungneon, A. (2010). Hopane-type triterpenes and binaphthopyrones from the scale insect pathogenic fungus *Aschersonia paraphysata* BCC 11964. *J. Nat. Prod.* 73, 688–692. doi: 10.1021/np1000363



- Johnson, T. W. (1958). Marine fungi. IV. *Lulworthia* and *Ceriosporopsis*. *Mycologia* 50, 151–163. doi: 10.2307/3756191
- Jones, E. B. G. (1994). Fungal adhesion. *Mycol. Res.* 98, 961–981. doi: 10.1016/S0953-7562(09)80421-8
- Katoh, K., and Standley, D. M. (2013). MAFFT multiple sequence alignment software version 7: improvements in performance and usability. *Mol. Biol. Evol.* 30, 772–780. doi: 10.1093/molbev/mst010
- Katoh, K., Misawa, K., Kuma, K., and Miyata, T. (2002). MAFFT: a novel method for rapid multiple sequence alignment based on fast Fourier transform. *Nucleic Acids Res.* 30, 3059–3066. doi: 10.1093/nar/gkf436
- Kavanagh, F., Hervey, A., and Robbins, W. J. (1951). Antibiotic substances from *Basidiomycetes*: VIII. *Pleurotus Multilus* (Fr.) Sacc. and *Pleurotus Passeckerianus* Pilat. *Proc. Natl. Acad. Sci. U.S.A.* 37, 570–574. doi: 10.1073/pnas.37.9.570
- Kawaguchi, M., Uchida, R., Ohte, S., Miyachi, N., Kobayashi, K., Sato, N., et al. (2013). New dinapinone derivatives, potent inhibitors of triacylglycerol synthesis in mammalian cells, produced by *Talaromyces pinophilus* FKI-3864. *J. Antibiot.* 66, 179–189. doi: 10.1038/ja.2012.127
- Koch, J., Pang, K.-L., and Jones, E. B. G. (2007). *Rostrupiella danica* gen. et sp. nov., a *Lulworthia*-like marine lignicolous species from Denmark and the USA. *Bot. Mar.* 50, 294–301. doi: 10.1515/BOT.2007.034
- Kohlmeier, J., Spatafora, J. W., and Volkmann-Kohlmeier, B. (2000). *Lulworthiales*, a new order of marine Ascomycota. *Mycologia* 92, 453–458. doi: 10.2307/3761504
- Kornprobst, J.-M., Sallenave, C., and Barnathan, G. (1998). Sulfated compounds from marine organisms. *Comput. Biochem. Physiol.* 119, 1–51. doi: 10.1016/S0305-0491(97)00168-5
- Kristoffersen, V., Rämä, T., Isaksson, J., Andersen, J. H., Gerwick, W. H., Hansen, E., et al. (2018). Characterization of rhamnolipids produced by an Arctic marine bacterium from the *Pseudomonas* fluorescence Group. *Mar. Drugs* 16:163. doi: 10.3390/md16050163
- Lanfear, R., Calcott, B., Ho, S. Y. W., and Guindon, S. (2012). PartitionFinder: combined selection of partitioning schemes and substitution models for phylogenetic analyses. *Mol. Biol. Evol.* 29, 1695–1701. doi: 10.1093/molbev/mss020
- Lanfear, R., Frandsen, P. B., Wright, A. M., Senfeld, T., and Calcott, B. (2017). PartitionFinder 2: new methods for selecting partitioned models of evolution for molecular and morphological phylogenetic analyses. *Mol. Biol. Evol.* 34, 772–773. doi: 10.1093/molbev/msw260
- Li, D.-H., Han, T., Guan, L.-P., Bai, J., Zhao, N., Li, Z.-L., et al. (2016). New naphthopyrones from marine-derived fungus *Aspergillus niger* 2HL-M-8 and their in vitro antiproliferative activity. *Nat. Prod. Res.* 30, 1116–1122. doi: 10.1080/14786419.2015.1043553
- Lu, S., Tian, J., Sun, W., Meng, J., Wang, X., Fu, X., et al. (2014). Bis-naphtho- $\gamma$ -pyrones from fungi and their bioactivities. *Molecules* 19, 7169–7188. doi: 10.3390/molecules19067169
- Maharachchikumbura, S. S. N., Hyde, K. D., Jones, E. B. G., McKenzie, E. H. C., Huang, S.-K., Abdel-Wahab, M. A., et al. (2015). Towards a natural classification and backbone tree for Sordariomycetes. *Fungal Divers.* 72:301. doi: 10.1007/s13225-015-0331-z
- Overy, D. P., Bayman, P., Kerr, R. G., and Bills, G. F. (2014). An assessment of natural product discovery from marine (*sensu strictu*) and marine-derived fungi. *Mycology* 5, 145–167. doi: 10.1080/21501203.2014.931308
- Overy, D. P., Rämä, T., Oosterhuis, R., Walker, A. K., and Pang, K.-L. (2019). The neglected marine fungi, *sensu stricto*, and their isolation for natural products' discovery. *Mar. Drugs* 17, 1–20. doi: 10.3390/md17010042
- Poli, A., Bovio, E., Ranieri, L., Varese, G. C., and Prigione, V. (2020). Fungal diversity in the Neptune forest: Comparison of the mycobiota of *Posidonia oceanica*, *Flabellia petiolata*, and *Padina pavonica*. *Front. Microbiol.* 11:933. doi: 10.3389/fmicb.2020.00933
- Rämä, T., Nordén, J., Davey, M. L., Mathiassen, G. H., Spatafora, J. W., and Kausserud, H. (2014). Fungi ahoy! Diversity on marine wooden substrata in the high North. *Fungal Ecol.* 8, 46–58. doi: 10.1016/j.funeco.2013.12.002
- Rehner, S. A., and Samuels, G. J. (1994). Taxonomy and phylogeny of *Gliocladium* analysed from nuclear large subunit ribosomal DNA sequences. *Mycol. Res.* 98, 625–634. doi: 10.1016/S0953-7562(09)80409-7
- Rivera-Chavez, J., Caesar, L., Garcia-Salazar, J. J., Raja, H. A., Cech, N. B., Pearce, C. J., et al. (2019). Mycopyranone: a 8,8'-binaphthopyranone with potent anti-MRSA activity from the fungus *Phialemoniopsis* sp. *Tetrahedron Lett.* 60, 594–597. doi: 10.1016/j.tetlet.2019.01.029
- Ronquist, F., Teslenko, M., van der Mark, P., Ayres, D. L., Darling, A., Höhna, S., et al. (2012). MrBayes 3.2: efficient Bayesian phylogenetic inference and model choice across a large model space. *Syst. Biol.* 61, 539–542. doi: 10.1093/sysbio/sys029
- Schneider, Y., Jenssen, M., Isaksson, J., Hansen, K. Ø., Andersen, J. H., and Hansen, E. H. (2020). Bioactivity of serratiochelin A, a siderophore isolated from a co-culture of *Serratia* sp. and *Shewanella* sp. *Microorganisms* 8, 1–17. doi: 10.3390/microorganisms8071042
- Stamatakis, A. (2006). RAXML-VI-HPG: maximum likelihood-based phylogenetic analyses with thousands of taxa and mixed models. *Bioinformatics* 22, 2688–2690. doi: 10.1093/bioinformatics/btl446
- Sutherland, G. K. (1915). Additional notes on marine Pyrenomycetes. *New Phytol.* 14, 183–193. doi: 10.1111/j.1469-8137.1915.tb07185.x
- Suzuki, K., Nozawa, K., Nakajima, S., Udagawa, S., and Kawai, K. (1992). Isolation and structures of antibacterial binaphtho- $\alpha$ -pyrones, talaroderxines A and B, from *Talaromyces derxii*. *Chem. Pharm. Bull.* 40, 1116–1119. doi: 10.1248/cpb.40.1116
- Velez, P., González, M. C., Cifuentes, J., Rosique-Gil, E., and Hanlin, R. T. (2015). Diversity of sand inhabiting marine ascomycetes in some tourist beaches on Cozumel Island, Mexico. *Mycoscience* 56, 136–140. doi: 10.1016/j.myc.2014.04.007
- Vilgalys, R., and Hester, M. (1990). Rapid genetic identification and mapping of enzymatically amplified ribosomal DNA from several *Cryptococcus* species. *J. Bacteriol.* 172, 4238–4246. doi: 10.1128/jb.172.8.4238-4246.1990
- Wang, J., Galgocsi, A., Kodali, S., Herath, K. B., Jayasuriya, H., Dorso, K., et al. (2003). Discovery of a small molecule that inhibits cell division by blocking FtsZ, a novel therapeutic target of antibiotics. *J. Biol. Chem.* 278, 44424–44428. doi: 10.1074/jbc.M307625200
- White, T. J., Bruns, T., Lee, S., and Taylor, J. (1990). “Amplification and direct sequencing of fungal ribosomal RNA genes for phylogenetics,” in *PCR Protocols A Guide to Methods and Applications*, eds M. A. Innis, D. H. Gelfand, J. J. Sninsky, and T. J. White (San Diego: Academic Press).
- WHO (2014). *Antimicrobial Resistance Global Report on Surveillance*. Available online at: <http://www.who.int/drugresistance/documents/surveillance-report/en/>. (accessed February 26, 2018).
- Xu, Y., Vinas, M., Alsarrag, A., Su, L., Pfohl, K., Rohlf, M., et al. (2019). Bis-naphthopyrone pigments protect filamentous ascomycetes from a wide range of predators. *Nat. Commun.* 10, 1–12. doi: 10.1038/s41467-019-11377-5
- Zheng, C. J., Sohn, M.-J., Lee, S., Hong, Y.-S., Kwak, J.-H., and Kim, W.-G. (2007). Cephalochromin, a FabI-directed antibacterial of microbial origin. *Biochem. Biophys. Res. Commun.* 362, 1107–1112. doi: 10.1016/j.bbrc.2007.08.144
- Zuccaro, A., Schoch, C. L., Spatafora, J. W., Kohlmeier, J., Draeger, S., and Mitchell, J. I. (2008). Detection and identification of fungi intimately associated with the brown seaweed *Fucus serratus*. *Appl. Environ. Microbiol.* 74, 931–941. doi: 10.1128/AEM.01158-07

**Conflict of Interest:** The authors declare that the research was conducted in the absence of any commercial or financial relationships that could be construed as a potential conflict of interest.

**Publisher's Note:** All claims expressed in this article are solely those of the authors and do not necessarily represent those of their affiliated organizations, or those of the publisher, the editors and the reviewers. Any product that may be evaluated in this article, or claim that may be made by its manufacturer, is not guaranteed or endorsed by the publisher.

Copyright © 2021 Jenssen, Rainsford, Juskewitz, Andersen, Hansen, Isaksson, Rämä and Hansen. This is an open-access article distributed under the terms of the Creative Commons Attribution License (CC BY). The use, distribution or reproduction in other forums is permitted, provided the original author(s) and the copyright owner(s) are credited and that the original publication in this journal is cited, in accordance with accepted academic practice. No use, distribution or reproduction is permitted which does not comply with these terms.



## Paper II

## Article

# Lulworthinone: In Vitro Mode of Action Investigation of an Antibacterial Dimeric Naphthopyrone Isolated from a Marine Fungus

Eric Juskewitz <sup>1,\*</sup>, Ekaterina Mishchenko <sup>1</sup>, Vishesh K. Dubey <sup>1</sup>, Marte Jenssen <sup>2</sup>, Martin Jakubec <sup>3</sup>, Philip Rainsford <sup>3</sup>, Johan Isaksson <sup>3</sup>, Jeanette H. Andersen <sup>2</sup> and Johanna U. Ericson <sup>1,\*</sup>

<sup>1</sup> Research Group for Host Microbe Interactions, Department of Medical Biology, Faculty of Health Sciences, UiT the Arctic University of Norway, 9019 Tromsø, Norway; ekaterina.mishchenko@uit.no (E.M.); vishesh.k.dubey@uit.no (V.K.D.)

<sup>2</sup> Marbio, The Norwegian College of Fishery Science, Faculty of Biosciences, Fisheries and Economics, UiT the Arctic University of Norway, 9019 Tromsø, Norway; marte.jenssen@uit.no (M.J.); jeanette.andersen@uit.no (J.H.A.)

<sup>3</sup> Department of Chemistry, Faculty of Science and Technology, UiT the Arctic University of Norway, 9019 Tromsø, Norway; martin.jakubec@uit.no (M.J.); philip.rainsford@uit.no (P.R.); johan.isaksson@uit.no (J.I.)

\* Correspondence: eric.juskewitz@uit.no (E.J.); johanna.e.sollid@uit.no (J.U.E.)

**Abstract:** Treatment options for infections caused by antimicrobial-resistant bacteria are rendered ineffective, and drug alternatives are needed—either from new chemical classes or drugs with new modes of action. Historically, natural products have been important contributors to drug discovery. In a recent study, the dimeric naphthopyrone lulworthinone produced by an obligate marine fungus in the family *Lulworthiaceae* was discovered. The observed potent antibacterial activity against Gram-positive bacteria, including several clinical methicillin-resistant *Staphylococcus aureus* (MRSA) isolates, prompted this follow-up mode of action investigation. This paper aimed to characterize the antibacterial mode of action (MOA) of lulworthinone by combining in vitro assays, NMR experiments and microscopy. The results point to a MOA targeting the bacterial membrane, leading to improper cell division. Treatment with lulworthinone induced an upregulation of genes responding to cell envelope stress in *Bacillus subtilis*. Analysis of the membrane integrity and membrane potential indicated that lulworthinone targets the bacterial membrane without destroying it. This was supported by NMR experiments using artificial lipid bilayers. Fluorescence microscopy revealed that lulworthinone affects cell morphology and impedes the localization of the cell division protein FtsZ. Surface plasmon resonance and dynamic light scattering assays showed that this activity is linked with the compound's ability to form colloidal aggregates. Antibacterial agents acting at cell membranes are of special interest, as the development of bacterial resistance to such compounds is deemed more difficult to occur.

**Keywords:** marine natural product; antimicrobial agents; mode of action; *B. subtilis*; MRSA; FtsZ; colloidal aggregate



**Citation:** Juskewitz, E.; Mishchenko, E.; Dubey, V.K.; Jenssen, M.; Jakubec, M.; Rainsford, P.; Isaksson, J.; Andersen, J.H.; Ericson, J.U. Lulworthinone: In Vitro Mode of Action Investigation of an Antibacterial Dimeric Naphthopyrone Isolated from a Marine Fungus. *Mar. Drugs* **2022**, *20*, 277. <https://doi.org/10.3390/md20050277>

Academic Editor: Hyukjae Choi

Received: 15 March 2022

Accepted: 16 April 2022

Published: 21 April 2022

**Publisher's Note:** MDPI stays neutral with regard to jurisdictional claims in published maps and institutional affiliations.



**Copyright:** © 2022 by the authors. Licensee MDPI, Basel, Switzerland. This article is an open access article distributed under the terms and conditions of the Creative Commons Attribution (CC BY) license (<https://creativecommons.org/licenses/by/4.0/>).

## 1. Introduction

Antimicrobial-resistant bacterial pathogens have emerged as a serious threat to public health, and there is an urgent need for new antibiotics. In 2019, infections caused by antimicrobial-resistant (AMR) bacteria were the third leading cause of death. Patients infected by *Staphylococcus aureus* were 64% more likely to die if the strain was methicillin-resistant than if it was susceptible. As a result, methicillin-resistant *S. aureus* (MRSA) alone killed over 100,000 patients globally in 2019 [1]. Thus, the World Health Organisation (WHO) has declared MRSA as one of their priority pathogens to develop treatments against. Since AMR mechanisms are known to evolve and protect against related drug iterations,

there is an urgent need for compounds with either a new mode of action (MOA) or from new chemical classes. Currently, 32 antibiotics targeting the WHO priority pathogens are under development. However, only six of them fulfil typical criteria for innovation (absence of cross-resistance, new chemical class, new target or new mode of action) [2,3]. The last truly new antibiotic class discovered were acid lipopeptides in 1987 [4].

Still, unexplored parts of nature can provide new molecules with novel antibacterial properties. Bioprospecting has the potential to supply the drug development pipeline with new compounds. Through history, natural products have contributed the most to the development of drugs in clinical use [5]. Either they contain the antibacterial activity themselves (e.g., aminoglycosides,  $\beta$ -lactams, macrolides, tetracyclines) [6] or their molecule scaffolds have been adapted for drug development [7]. The focus on marine bioprospecting has increased in the last decades. Due to the dilution processes occurring in seawater, the antimicrobial compounds produced by marine organisms should be highly potent in order to be effective against their targets.

The strictly marine clades of fungi are less explored in natural product discovery [8,9]. Lulworthinone was the first bioactive compound to be published from the strictly marine fungal family *Lulworthiaceae* [10]. The compound was shown to have potent activity against several clinical MRSA isolates and displayed antiproliferative activity against three human cell lines (melanoma, hepatocellular carcinoma and non-malignant lung fibroblasts) at higher concentrations. During purification, acid-induced degradation was observed, forming a structural isomer [10]. This structural isomer was identical to lulworthinone, differing only in the position of the sulphate group (Figure 1). Lulworthinone appeared to form aggregates in DMSO and methanol, which was not observed for its isomer. The compound fits structurally in the class of naphthopyrones, which have been previously isolated from different sources, including filamentous fungi. Antibacterial activity against Gram-positive bacteria has been reported for several naphthopyrones [11–14]. The well-studied naphthopyrone viriditoxin has minimal inhibitory concentrations (MICs) in the range of 4–8  $\mu\text{g}/\text{mL}$  against different *Staphylococcus* isolates, by inhibiting cell division through blocking of FtsZ polymerization [15]. Another antibacterial fungal naphthopyrone, cephalochromin, inhibits the bacterial enoyl-acyl carrier protein reductase FabI, involved in fatty acid synthesis [12].

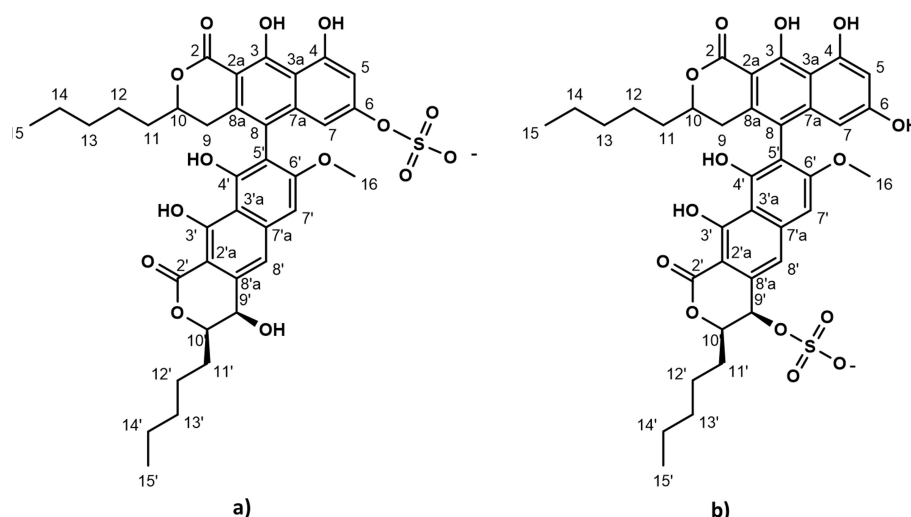


**Figure 1.** Chemical structure of lulworthinone (a) and acidified lulworthinone (b); under acidic conditions the sulphate group migrates from C6 to C9'.

Target identification and mode of action studies are essential steps in natural product drug discovery and development to facilitate further optimization by medicinal chemistry efforts. In this paper, the MOA of the published antibacterial natural product lulworthinone and its acidified form was investigated. The MOA was characterized using biosynthetic

pathway markers, quantifying membrane permeability with a water/ion NMR detected-phospholipid vesicle permeability assay (WIND-PVPA), in vitro membrane integrity assays and membrane potential assays, time-kill curves, pharmacodynamic calculations, surface plasmon resonance (SPR), fluorescence microscopy and quantitative phase microscopy. The combined results suggest that lulworthinone is a membrane-active antibacterial compound effective against MRSA; meanwhile, its acidified form loses this ability.

## 2. Results

### 2.1. Lulworthinone Induces Transcription from Promoters Known to Respond to Cell Envelope Stress

Induction of gene expression from selected cellular pathways (i.e., DNA replication, transcription, translation, fatty acid, folic acid, cell wall and membrane) was assayed after the addition of increasing concentrations of lulworthinone. Strains of *B. subtilis* 168 containing reporter-gene constructs of relevant promoters fused to the luciferase gene are listed in Table 1. The relative luminescence activity was measured for concentrations ranging from 0 to  $8 \times \text{MIC}$  for either reference antibiotics or lulworthinone (Table 1) (Figure 2). *B. subtilis* 168 EM13 harboring the *yupA* promoter-fusion (responding to cell wall biosynthesis inhibitor or general cell envelope stress) and *B. subtilis* 168 HMB67, carrying the *lial* promoter-fusion (responding to general cell envelope stress) produced an increasing amount of luminescence in response to lulworthinone between 0.5 and  $2 \times \text{MIC}$  (Figure 2a,c). At  $4 \times$  and  $8 \times \text{MIC}$ , the luminescence was almost completely abolished, which indicates cell death. The control antibiotic, bacitracin, induced luciferase production at  $0.125\text{--}2 \times \text{MIC}$  from the *yupA* promoter and from the *lial* promoter at all concentrations tested. This suggests that lulworthinone generates a general stress response in bacteria and is likely targeting the cell envelope.

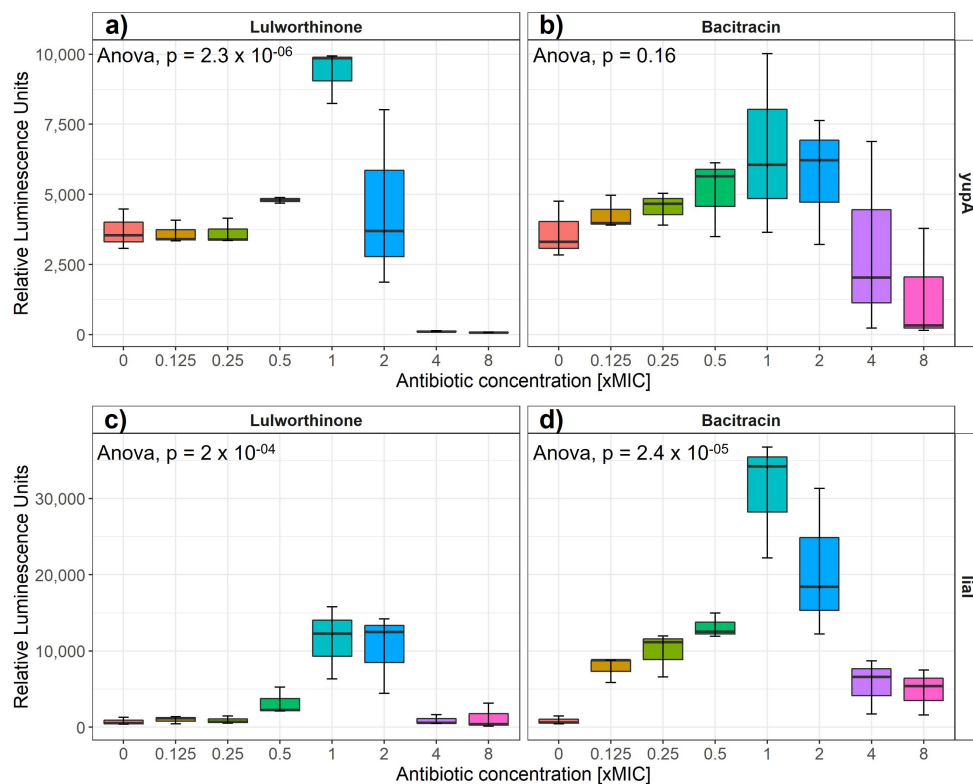


**Figure 2.** Luminescence units induced by either lulworthinone (a,c) or bacitracin (b,d) per tested concentration from 0 to  $8 \times \text{MIC}$  for *yupA* (a,b) and *lial* (c,d) promoter fusions. Statistics performed by two-sided ANOVA comparing data of each drug concentration and biological replicates ( $n = 3$ ).

**Table 1.** Bacterial strains sensing stress on key molecular pathways.

Bacteria	Strain Number	Target Pathway	Promotor	Control Antibiotic	MIC in µg/mL	
					Control Antibiotic	Lulworthinone
<i>Bacillus subtilis</i> 168	EM10	DNA replication	<i>yorB</i>	Ciprofloxacin	0.031	8
<i>B. subtilis</i> 168	EM11	Transcription	<i>belD</i>	Rifampicin	0.5	8
<i>B. subtilis</i> 168	EM12	Translation	<i>yheI</i>	Erythromycin	0.125	8
<i>B. subtilis</i> 168	EM13	Cell wall and membrane	<i>yupA</i>	Bacitracin	16	8
<i>B. subtilis</i> 168	HMB62	Viability control	<i>laiG</i>	All antibiotics	*	8
<i>B. subtilis</i> 168	HMB67	Cell wall and membrane	<i>liaI</i>	Bacitracin	16	8
<i>B. subtilis</i> 168	HMB69	Fatty acid synthesis	<i>fabJB</i>	Triclosan	4	8
<i>B. subtilis</i> 168	HMB70	Folic acid synthesis	<i>panB</i>	Trimethoprim	1	8

Abbreviations: MIC—minimal inhibitory concentration; \* MICs are equivalent to the other strains.

## 2.2. Lulworthinone Alters Membrane Permeability without Influencing Membrane Integrity

### 2.2.1. Lulworthinone Interacts with Membrane Lipids

SPR was used to determine the affinity of lulworthinone and its isomer towards an inert lipid bilayer composed of 1,2-dimyristoyl-sn-glycero-phosphocholine (DMPC) vesicles and its subsequent rate of dissociation (Table 2). A high partitioning of lulworthinone into lipid layers was observed with a  $K_P$  reaching up to  $44.81 \pm 2.47 \times 10^3$  with a dissociation rate of  $4.2 \pm 0.5 \times 10^{-2} \text{ s}^{-1}$ . Such values are typically encountered by very good lipid interactors (like AMC-109 [16]; see Table 2). However, there was no observable decrease in the signal (RU) after lulworthinone dissociation from the bilayer. This suggests that the lipid layer stayed intact, and that lulworthinone was able to self-aggregate on top of the lipid bilayer without disturbing it. In addition, there was no observable binding of lulworthinone to the lipid layer in concentrations  $< 30 \mu\text{M}$  ( $3 \times \text{MIC}$ ) (Figure S1). Only in higher concentrations of lulworthinone a measurable increase in resonance units was observed. Thus, the measured  $K_P$  for lulworthinone seems to represent both partitioning into the lipid layer and self-aggregation on top of the membrane. On the other hand, acidified lulworthinone partitioning into the lipid layer is much smaller with  $K_P = 0.76 \pm 0.04$  and with a much faster dissociation rate  $k_{\text{off}} = 5.185 \pm 1.594 \text{ s}^{-1}$ . This suggests that the isomer lost its ability to bind to the lipid layer.

**Table 2.** Lulworthinone and acidified lulworthinone's affinity towards and subsequent dissociation rate from an inert lipid bilayer. Positive and negative [17] controls are included.

Treatment	$K_P \times 10^3$	$k_{\text{off}} \text{ s}^{-1}$
Lulworthinone	$44.81 \pm 2.47$	$0.042 \pm 0.005$
acid. Lulworthinone	$0.76 \pm 0.04$	$5.185 \pm 1.594$
pos. control—AMC 109	$14.97 \pm 0.99$	$0.174 \pm 0.007$
neg. control—LWwNkr	$0.40 \pm 0.02$	$1.746 \pm 0.162$

$K_P$ —partitioning constant,  $k_{\text{off}}$ —dissociation rate.

### 2.2.2. Lipid Bilayer Permeability Is Not Affected by Lulworthinone

The ability of lulworthinone and its isomer to disrupt the lipid bilayer was explored using WIND-PVPA to determine the  $P_{\text{app}}$  of water and  $\text{Mg}^{2+}$  and  $\text{Ca}^{2+}$  ions across packed lipid vesicles [18]. The PVPA barriers were exposed to  $100 \mu\text{M}$  of lulworthinone, acidified lulworthinone, and Triton X-100, with the latter as positive control. Figure 3 shows that neither water (Figure 3a) nor ion (Figure 3b) permeability was affected by lulworthinone. The  $P_{\text{app}}$  of  $\text{Mg}^{2+}$  in the presence of lulworthinone and the isomer were slightly lower relative to the blank (blank:  $0.42 \times 10^{-6} \text{ cm/s}$ ; lulworthinone:  $0.37 \times 10^{-6} \text{ cm/s}$ ; acidified lulworthinone:  $0.37 \times 10^{-6} \text{ cm/s}$ ), but these differences were not statistically relevant ( $t$ -test,  $p > 0.05$ ). In comparison, the detergent Triton X-100's higher permeability was observed for both water and ions (water:  $69 \times 10^{-6} \text{ cm/s}$ ;  $\text{Ca}^{2+}$ :  $0.41 \times 10^{-6} \text{ cm/s}$ ;

$Mg^{2+}$ :  $0.49 \times 10^{-6}$  cm/s). Thus, concentrations of 100  $\mu$ M lulworthinone or acidified lulworthinone did not disrupt the lipid layer of membranes.

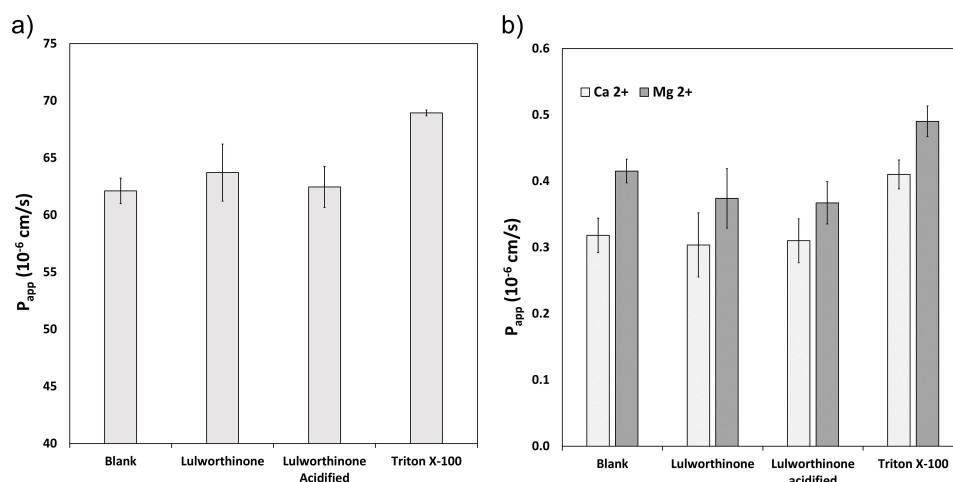


**Figure 3.** Permeability  $P_{app}$  of water (a) and  $Ca^{2+}$  and  $Mg^{2+}$  (b) measured under the influence of lulworthinone, acidified lulworthinone, and Triton X-100.

### 2.2.3. Lulworthinone Increases the Permeability of Biological Membranes While Membrane Integrity Is Not Affected

The effect of lulworthinone on membrane integrity was investigated on bacterial cells, *B. subtilis* 168, carrying the pCSS962 plasmid from which luciferase is constitutively expressed. From this strain, bioluminescence is emitted once the bacterial cell membrane is affected, and D-luciferin from the growth medium is allowed to enter the cell. A change in membrane permeability is detected by a rise in luminescence due to substrate influx. A strong drop of luminescence is detected either after cell death or complete membrane disruption due to a fast consumption of cellular ATP needed for the enzymatic process. Bioluminescence was recorded in the presence of  $0.5\text{--}4 \times$  MIC of lulworthinone or ciprofloxacin (CIP, negative control).

After 270 s, cells that survived the first treatment were lysed by injecting a membranolytic dosage of chlorhexidine (CHX, positive control). The relative luminescence was recorded for 300 s, including the CHX injection at 270 s (Figure 4). Each concentration of lulworthinone increased the luminescence production in comparison to the basal water values (Figure 4a). The decrease in luminescence at  $4 \times$  MIC after 30 s suggests ATP depletion or cell death, as to the fast drop after CHX injection.

In contrast, CIP did not influence the membrane integrity, and the luminescence stayed at basal values of the water control until CHX injection (Figure 4b). This implies that the membrane permeability is increasingly affected by rising lulworthinone concentrations, which seemingly destroys the membrane at  $4 \times$  MIC.

### 2.3. Lulworthinone Affects the Membrane Potential

Changes in the membrane potential after exposure to concentrations of  $0.25\text{--}4 \times$  MIC of lulworthinone was measured by a DiOC<sub>2</sub>(3) membrane depolarisation assay. *S. aureus* ATCC 29213 cells were stained with the membrane potential-sensitive dye 3,3'-diethyloxycarbocyanine iodide (DiOC<sub>2</sub>(3)) and analysed by flow cytometry. The dye fluorescence shifts from green to red by self-aggregation if the membrane potential is maintained [19]. A decrease in the ratio of red by green signals indicates a change in membrane potential. Water (positive control) and carbonylcyanide 3-chlorophenylhydrazone (CCCP, negative control) were included in each assay. At  $0.25 \times$  MIC, the membrane potential decreased by half, whereas concentrations of  $0.5\text{--}4 \times$  MIC depleted the potential close to levels of the potential inhibitor CCCP (Figure 5); an overview of all measured samples is provided in Supplementary Figure S2. This suggests that lulworthinone has a strong influence on the membrane potential.



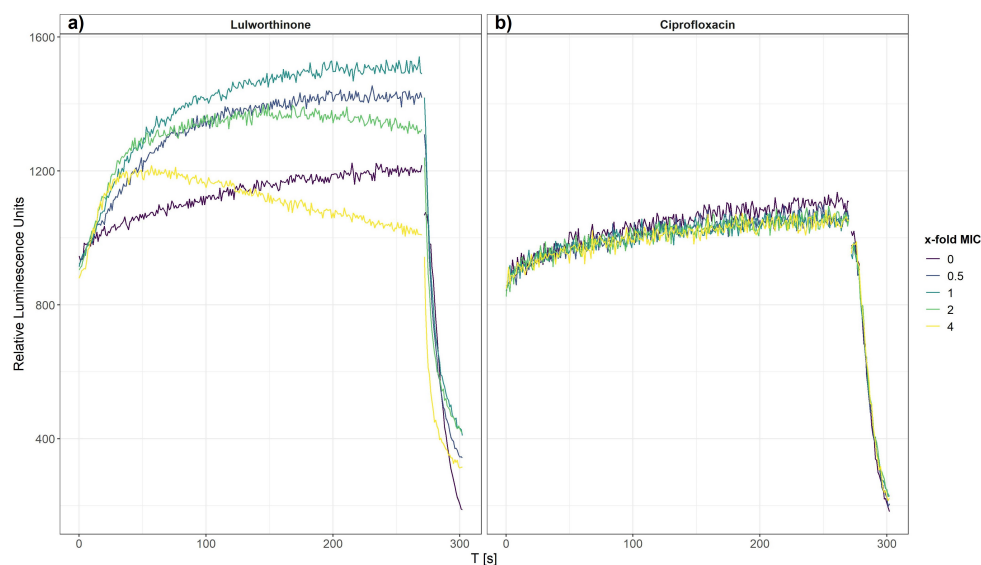


**Figure 4.** Membrane integrity of *B. subtilis* 168 carrying the pCSS962 plasmid, monitored as relative luminescence units, in the presence of different concentrations of lulworthinone (a) or ciprofloxacin (b). In both experiments, membranolytic chlorhexidine was injected at 270 s. Data presented are the means of 3 biological replicates.

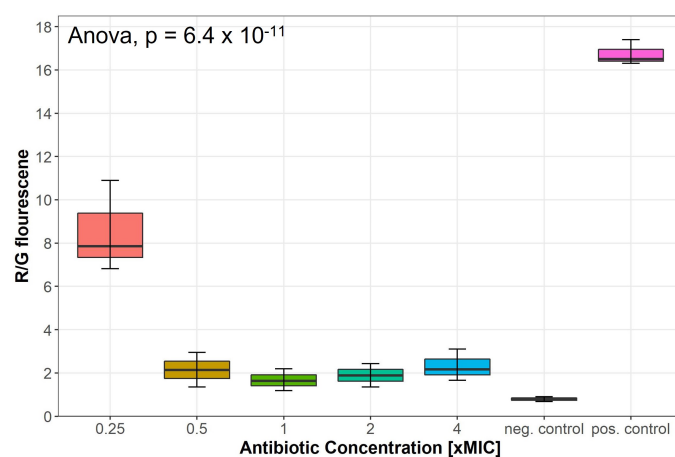


**Figure 5.** Membrane potential after exposure to increasing concentrations of lulworthinone measured by 3,3'-diethyloxa-carbocyanine iodide (DiOC<sub>2</sub>(3)) membrane depolarisation assay. Water (pos. control) and carbonylcyanide 3-chlorophenylhydrazon (CCCP, neg. control) were included in each assay. Statistics performed by two-sided ANOVA comparing data of each drug concentrations and biological replicates ( $n = 3$ ).

#### 2.4. Lulworthinone Influences Cell Morphology and Localization of the Cell Division Protein FtsZ

Bacterial cell morphology in the presence of either lulworthinone or the membrane-acting antibiotic daptomycin (DAP) was analysed using fluorescence microscopy. Cells were stained with membrane dye FM4-64 and DNA dye DAPI. A concentration of  $1 \times$  MIC lulworthinone affected the morphology as shown in Figure 6. When comparing the lulworthinone-treated cells (Figure 6e) to the control (Figure 6a), an increased number of bacterial filaments was observed, indicating an effect on the division process. Additionally, the altered FM4-64 distribution shown as patches of strong signal and regions of nearly no staining at all (as seen in Figure 6g) points to membrane perturbations. Changes in cell size after lulworthinone treatment were further analysed by quantitative phase microscopy (QPM). Figure 7 shows an example of a quantitative phase map (a), and the measured cell length (c), width (d) and volume (e). Data based on a total of 6700 cells from each sample, untreated or treated with  $1 \times$  MIC lulworthinone (Figure 7c–e), showed that the

average cell length was extended from 4.974 to 6.763  $\mu\text{m}$ , while the average width was increased from 1.898 to 2.048  $\mu\text{m}$ . Accordingly, the mean volume increased from 4.788  $\mu\text{m}^3$  to 6.649  $\mu\text{m}^3$ . Cell localisation of the cell division protein FtsZ is known to be influenced by membrane potential [20]. Thus, a reporter strain *B. subtilis* 2020 (expressing FtsZ::GFP fusion protein) was used to study the influence of lulworthinone on the membrane structure. Normally, FtsZ forms the Z-ring that defines the next septum formation and cell division site in the bacteria. The fluorescence micrographs (Figure 8) show FtsZ localisation without treatment (a,b) in the presence of lulworthinone (c,d) and with the positive control DAP (e,f). In the control (a,b), FtsZ was localized in the middle of bacteria, forming the Z-ring preceding cell division. Treatment with lulworthinone led to the elongated cells or filaments and appearance of multiple Z-rings or FtsZ patches along the cells (c,d). Daptomycin treatment (e,f) had a severe effect on FtsZ localisation and resulted in some bacteria with additional “spots” and “rings” of FtsZ. Few elongated cells and very few chains were observed. This suggests that lulworthinone has an influence on cell division, supposedly via its effect on membrane structure.

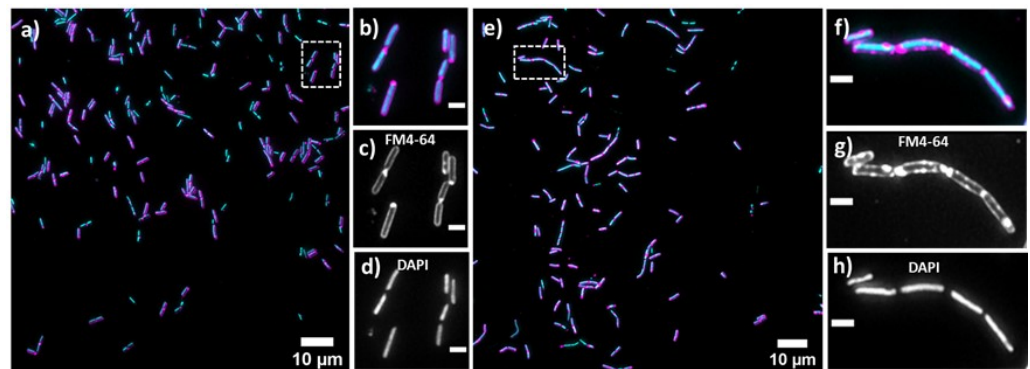


**Figure 6.** Cell morphology of *Bacillus subtilis* 168, membrane staining (FM4-64; magenta; (c,d)) and DNA staining (DAPI; blue; (d,h)) without treatment (a–d) or in the presence of  $1 \times \text{MIC}$  lulworthinone (e–h);  $60\times$  magnification in (b–d) and (f–h), respectively.

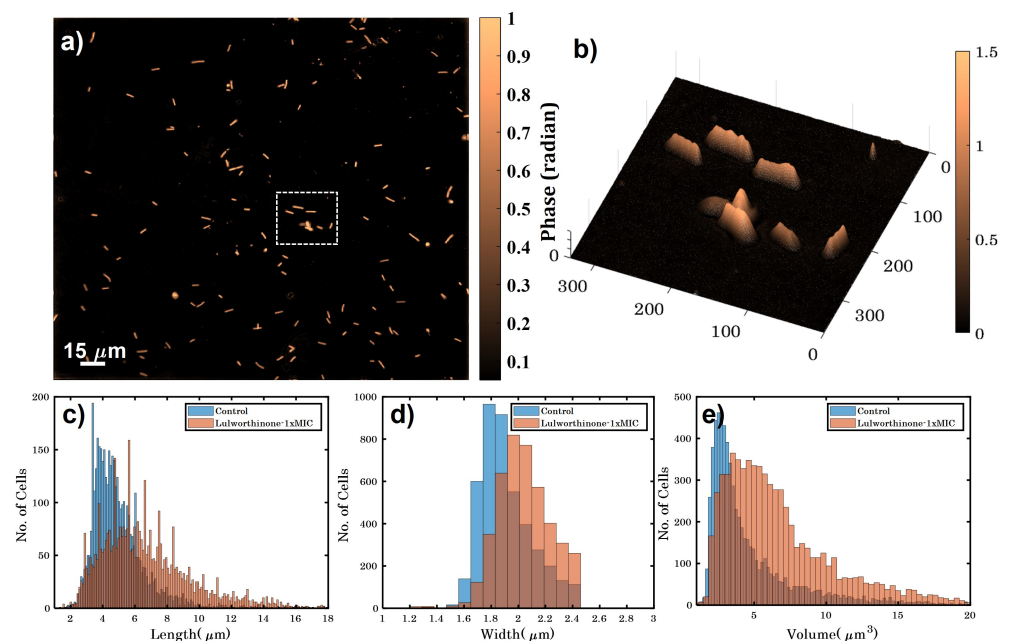


**Figure 7.** (a) Quantitative phase map of *B. subtilis* 168 cells (scale bar is 15  $\mu\text{m}$  and color bar is in radians). (b) A 3D phase map of the zoomed area enclosed by white dotted box shown in (a). (c–e) show the variation in height, width and volume for untreated and bacteria treated with  $1 \times \text{MIC}$  lulworthinone.

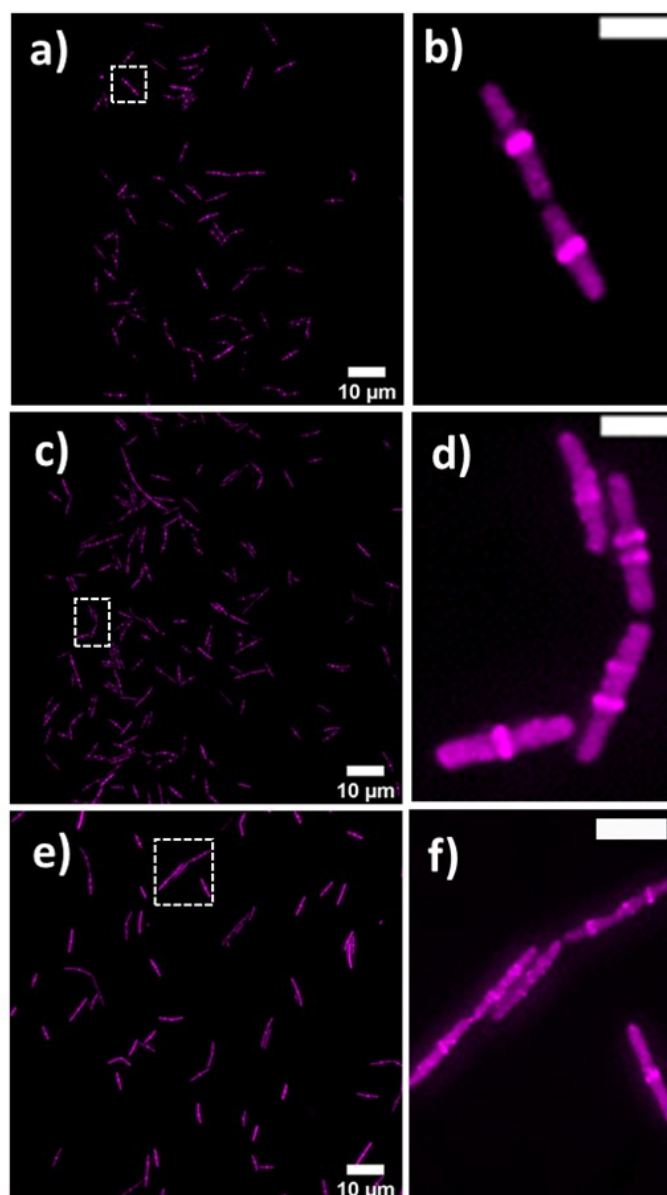


**Figure 8.** FtsZ localisation in *B. subtilis* 2020 with GFP-labeled FtsZ (a) without treatment, (c) with  $1 \times \text{MIC}$  lulworthinone or (e)  $1 \times \text{MIC}$  daptomycin, at  $60 \times$  magnification in (b,d,f), respectively.

## 2.5. Lulworthinone Has a Strong Bactericidal Effect on *B. subtilis*

### 2.5.1. Time-Kill Curves Reveal a Fast Bacterial Killing

The kill kinetics of lulworthinone was determined by measuring bacterial survival over time at multiple concentrations ranging from 0 to  $64 \mu\text{g}/\text{mL}$  ( $0\text{--}4 \times \text{MIC}$ ) (Figure 9). Using *B. subtilis* 168, it is shown that lulworthinone (Figure 9a) was bactericidal at concentrations  $\geq 1 \times \text{MIC}$ . Higher concentrations ( $2\text{--}4 \times \text{MIC}$ ) led to rapid killing, and cell counts fell below the detection limit ( $50 \text{ CFU}/\text{mL}$ ). At  $4 \times \text{MIC}$ , this was observed within 30 min. Sub-MIC concentrations induced a lag-phase of 30 and 120 min at  $0.25$  and  $0.5 \times \text{MIC}$ , respectively, before growth was restored to rates comparable to the control. This suggests that some kind of adaption is required before growth continues. Time-kill curves for CHX were prepared in parallel (Figure 9b). Like lulworthinone, CHX was bactericidal above the MIC and at the highest concentration ( $4 \times \text{MIC}$ ), cell counts dropped below the detection limit. These data suggest that lulworthinone has a strong and fast bactericidal mode of action.

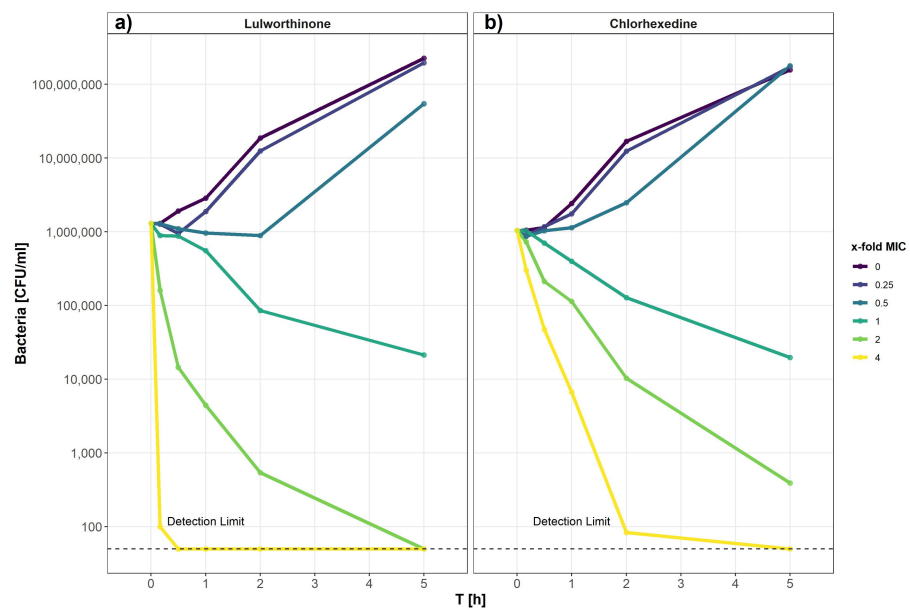


**Figure 9.** Time-kill curve of *B. subtilis* 168 of lulworthinone (a) and chlorhexidine (b).

### 2.5.2. Pharmacodynamic Calculations Reveal an Unusual Dose-Response Curve

Using the data from the time-kill curves, the pharmacodynamic parameters of lulworthinone were calculated using the *pharmacodynamic function* according to Regoes et al. (2004) [21]. The bacterial growth rates ( $\psi$ ) were estimated by calculating linear regressions to the logarithm of the colony count for each concentration, respectively.

The pharmacodynamic function was then fitted to the estimated  $\psi$  per concentration (Figure 10). The maximal growth rate  $\psi_{\max}$ , at  $0 \times \text{MIC}$ , was  $0.6492 \text{ h}^{-1}$ . Compound lulworthinone induced a strong bactericidal effect with a minimal growth rate, at  $4 \times \text{MIC}$ , of  $\psi_{\min} -7.88 \text{ h}^{-1}$ . This led to a steep hill coefficient ( $\kappa$ ) of 3.72. The estimated zMIC of  $9.59 \mu\text{g/mL}$  agreed with the experimentally acquired MIC of  $8 \mu\text{g/mL}$ . It was not possible to generate the typical sigmoidal “S”-shape for the drug response curve. This suggests that lulworthinone forms colloidal aggregates [22].

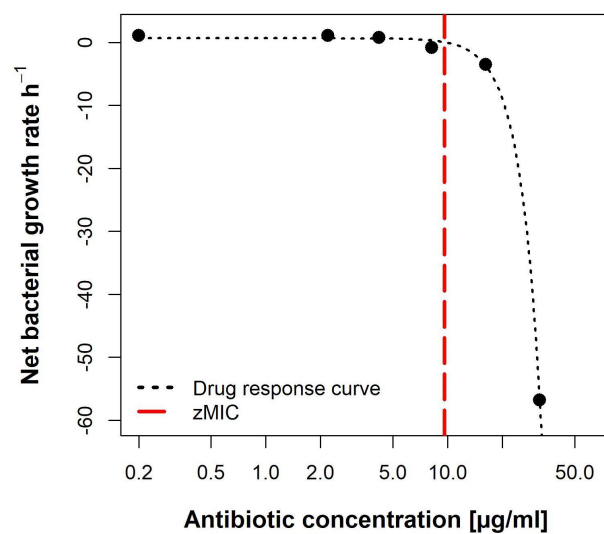


**Figure 10.** Pharmacodynamic model of lulworthinone against *B. subtilis* 168 with predicted MIC (zMIC).

## 2.6. Lulworthinone Is a Self-Aggregating Molecule

### 2.6.1. Confirmation of Aggregation

To monitor the aggregation of lulworthinone and its isomer, the molecules were assayed using dynamic light scattering (DLS). DLS is a common technique to determine particle sizes in solute by using a coherent and monochromatic source of light—a laser beam. The Brownian motion of particles causes the time-dependent fluctuation of the local concentration, which corresponds to fluctuations in the intensity of the scattering light. These fluctuations in intensity can be transformed into an autocorrelation function, from which a hydrodynamic radius can be determined using the Stokes–Einstein equation (1)

$$R_h = kT/6\pi\eta D \quad (1)$$

where  $R_h$  is the hydrodynamic radius,  $k$  is Boltzmann’s constant,  $T$  is the absolute temperature,  $\eta$  is the shear viscosity of solvent and  $D$  is the translational diffusion coefficient. It has been previously shown that DLS can be used to estimate critical micellar concentrations [23]. We have used changes in intensity counts of particles > 10 nm in diameter to estimate the critical colloidal concentration, as shown in Table 3. Compound lulworthinone showed a variety of aggregates at two major diameter ranges of  $192.7 \pm 70.80$  and  $1319 \pm 611.7$  nm (Figure 11). To investigate if lulworthinone is a self-aggregating colloidal aggregate, we included a non-ionic detergent (Tween 80) as proposed by Ganesh et al. (2018) [24] to reverse this kind of interaction. In the presence of detergent, the aggregates vanished, and we could detect only the typical Tween 80 micelles at 10 nm, as shown in Figure 11b. This suggests that lulworthinone forms colloidal aggregates.

**Table 3.** Aggregate sizes determined by DLS.

Treatment	Environment	Critical Aggregation Concentration (CAC)	Prevalent Size of Aggregates at CAC
Lulworthinone	37 °C	53.71 $\mu$ M	117.4 $\pm$ 25.9 d.nm
Lulworthinone with 0.025% Tween 80	37 °C	No aggregation	No aggregation

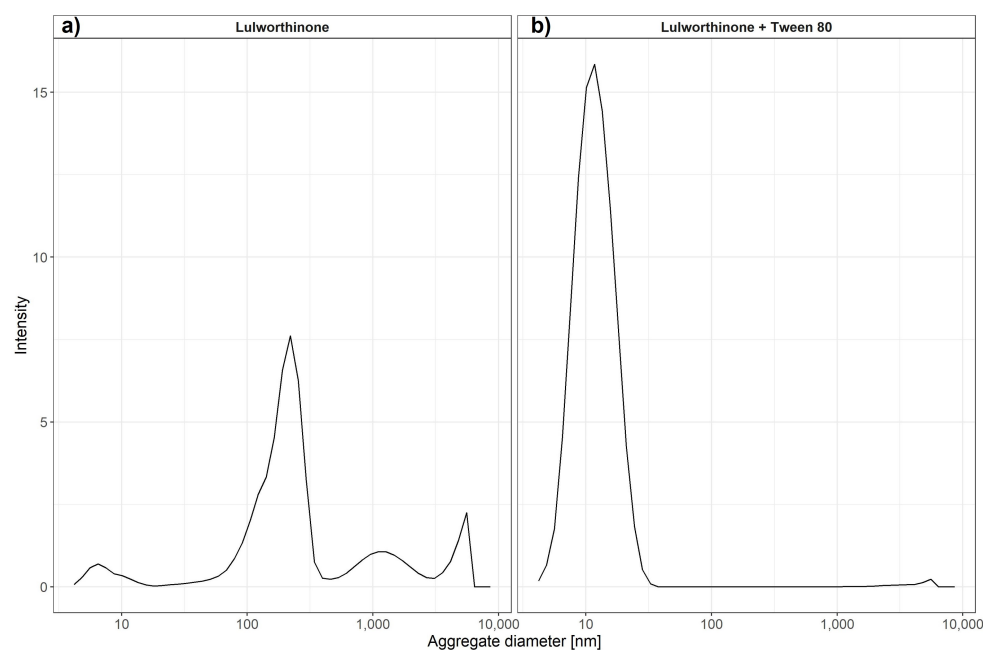


**Figure 11.** Average aggregate sizes of lulworthinone in the concentration range 0.625–320  $\mu$ M in MiliQ water with 1% DMSO and without (a) or with 0.025% Tween 80 (b) measured by dynamic light scattering.

### 2.6.2. The Antibacterial Activity Is Dependent on Aggregation

To determine if the antibacterial activity of lulworthinone is altered by the presence of detergent (indicating that the compound is a colloidal aggregator), Tween 80 was included in our MIC assays as proposed by Ganesh et al. (2018) [24].

The addition of detergent resulted in a strong attenuation of the antibacterial activity from 6.15 µg/mL to >128 µg/mL against *S. aureus* ATCC 25923 (Table 4). This indicates that lulworthinone antibacterial activity is based on aggregation, as the compound also lost its antimicrobial activity after acidification.

**Table 4.** Antibacterial activity of lulworthinone.

Bacterial Strain	Treatment	MIC
<i>Staphylococcus aureus</i> ATCC 25923	Lulworthinone	6.15 µg/mL
<i>S. aureus</i> ATCC 25923	Lulworthinone + Tween 80	>128 µg/mL
<i>S. aureus</i> ATCC 25923	Acidified lulworthinone	>128 µg/mL

### 3. Discussion

Antibiotic resistance is making the treatment of bacterial infections difficult, and new drugs with new modes of action are needed to tackle this increasing problem. The cell membrane is a promising target for new antibiotics, as resistance is coupled to a high fitness cost for the bacterium [25]. Identifying the bacterial target and establishing the mode of action are essential steps in natural product drug discovery. This information is essential to identify promising hit compounds that can be further altered by medicinal chemistry on the road to becoming marketed drugs.

In the current study, an antibacterial compound, lulworthinone, isolated from an obligate marine fungus was studied for its MOA. The compound's MOA includes the following key elements: (1) stress or influence on the bacterial envelope, (2) membrane permeabilization and membrane potential dissipation without destroying the membrane integrity, (3) changes in cell morphology, including increased length and width, leading to extended cells or filament formation, (4) FtsZ, a key protein for cell division, is delocalized within the bacterial cells, and (5) the antibacterial activity is based on aggregation.

As several naphthopyrones have antibacterial activity against *S. aureus* and other Gram-positive bacteria [11–14], it was not surprising to find that lulworthinone also has similar activity. This indicated that the naphthopyrone backbone might be a so-called privileged structure [26,27], with the ability to interact with a bacterial target common for some Gram-positive bacteria. The lack of activity against Gram-negative species might also be caused by the outer membrane barrier. Lulworthinone generates a general stress response in bacteria by targeting the cell envelope. The cell envelope is rather conserved among many bacterial species, and the potential for resistance development towards membrane active compounds is low as they are known to have multiple MOA targets. Taken together, this makes the cell envelope an interesting target for new antibacterial drugs (e.g., lipopeptides (daptomycin [28]), lipoglycopeptides (teicoplanin [29]) and cyclopeptides (polymyxin B [30]). Most membrane-active molecules interact with lipophilic targets in the membrane (disrupting the lipid composition or the functional architecture), change the conformation or localisation of membrane-embedded proteins, or cause alterations in the proton motif force (PMF) [25].

However, lulworthinone does not seem to alter the structural integrity of the membrane bilayers or change the permeability of the lipid barrier. SPR indicated that lulworthinone has a high affinity towards lipids, but it also showed that there is no observable retention of lulworthinone in the lipid bilayer, as the lipid bilayer was completely recovered after the experiment. This was not expected, as good lipid associators either intercalate into the lipid bilayer and increase the overall measured signal or disrupt the layer and release vesicles and lipid matter from the surface of the chip [31]. In addition, there was no observable association of lulworthinone with DMPC vesicles at concentrations < 30 µM.

Indeed, SPR results suggested that rather than disrupting lipid layer, lulworthinone can use it as a scaffold for aggregation. This fact was further confirmed by permeability results from WIND-PVPA [18]. Neither lulworthinone nor its acidified form showed any changes in water or ion transmission in artificial lipid barriers. In contrast, an increase in permeability was detectable in bacterial membranes, albeit without the loss of envelope integrity marked by cell death (as a sharp drop in fluorescence was observed only at the highest MIC concentration). The combination of these results suggests that even though lulworthinone is able to bind to the lipid bilayer, it does not disrupt artificial models, but it is still able to increase permeability in live cells. Either the disruptive effect of lulworthinone is very mild and below detection limits used in artificial models or lulworthinone needs other membrane components present in live cells to be active.

Additionally, the dissipation of the membrane potential was detected. This can be an indication that lulworthinone interacts with surface proteins (e.g., transporters or ion channels) and inactivates them. Strahl and Hamoen (2010) [20] have shown that the membrane potential is a crucial factor for the localisation of proteins forming the cytoskeleton. Over 20 proteins involved in cell morphology, division and cell division regulation are delocalised shortly after the membrane potential is dissipated. Indeed, compound lulworthinone changed cell morphology and led to cell widening and elongation, filaments and membrane perturbation (Figures 6 and 7). Signs of incomplete cell division or separation were observed.

The changes in cell morphology were accompanied by the delocalisation of FtsZ (Figure 8), a key protein for cell division as it forms the Z-ring, a molecular structure that divides cells after DNA multiplication. FtsZ was found to be delocalised into patches all over the cell or multiple Z-rings at unusual sites in the cell. As a key element for cell division, FtsZ is a focus target for antibacterial treatments [32–36]. As an explanation for the delocalisation, Strahl and Hamoen (2010) showed that the FtsZ guiding proteins FtsA and MinD are inactivated after loss of the membrane potential. Both have a C-terminal alpha helix structure used for membrane binding. Thus, membrane potential depletion might prevent the FtsZ guiding proteins from binding and correctly directing Z-ring formation. Without a functional Z-ring formation, cell division is affected, and filaments are formed. At sub-MIC concentrations of lulworthinone, this effect could be compensated or overcome during the observed lag phase observed for 30 and 120 min at 0.25 and  $0.5 \times \text{MIC}$ , respectively, in the time-kill curves. The current study indicates that the antibacterial activity of lulworthinone is based on self-aggregation. Compound aggregation was initially observed in the NMR experiments conducted during the structure elucidation of the compound [10]. Follow-up studies (SPR, DLS, time-kill curves, pharmacodynamics) supported the notion of aggregation. MIC testing in the presence of detergent strongly suggested that the aggregation is necessary for antibacterial activity. The structural isomer did not aggregate and was also not active against *S. aureus* 29523 (Table 3). Thus, it was concluded that lulworthinone is a colloidal aggregate, and the aggregation is necessary for its antibacterial activity. The role of aggregation in antimicrobial compounds is currently an unexplored venue as most colloidal aggregators are viewed as undesirable new drug leads due to their non-specific protein adsorption and inhibition of enzymes [24,37]. To our knowledge, this is the first time that aggregation is mentioned for compounds in the naphthopyrone class. However, to what extent lulworthinone is representative for the chemical class or an individual actor remains to be investigated.

#### 4. Conclusions

In this study, we investigated the MOA of a dimeric naphthopyrone isolated in high yields from an obligate marine fungus. The naphthopyrone chemical class has previously been investigated for several types of bioactivities, among them antibacterial activity against Gram-positive isolates. The results from this study shows that lulworthinone exerts its activity towards the bacterial membrane without disrupting it. The membrane potential is influenced and changes in FtsZ localization, indicating an impaired cell division.

Several experiments (NMR, SPR and DLS) indicate that the compound has the ability to form aggregates with itself, a property which is usually regarded as undesirable for new drug leads. To investigate if the aggregation affected the antibacterial activity, the compound's MIC was tested in the presence of detergent. In the presence of detergent, all antibacterial activity was lost, indicating that the aggregation was necessary for the compound's bioactivity. The study provides extended information about the target and MOA of naphthopyrones towards Gram-positive bacteria. The study also describes the effect of aggregation, and to the best of our knowledge, this is the first study in which compound aggregation has been published for naphthopyrones.

## 5. Materials and Methods

### 5.1. Bacterial Strains and Material

All bacterial strains used are listed in Table 5. Overnight cultures were grown in cationic-adjusted BD BBL Mueller Hinton II Broth (MHB II, 212322, Becton, Dickson and Company, Sparks, MD, USA) if not indicated otherwise. Lulworthinone was isolated using FLASH chromatography [10].

**Table 5.** Bacterial strains.

Strain	Relevant Characteristics	MIC in µg/mL					References
		Lulworthinone	Acid. Lulworthinone	CHX	CIP	DAP	
<i>Bacillus subtilis</i> 168	-	8	-	0.5	-	-	ATCC 23857
<i>B. subtilis</i> 168	pCSS962	8	-	0.5	0.00195	-	[38]
<i>B. subtilis</i> 168 EM10	P <sub>yorB</sub> luxABCDE	8	-	-	-	-	[39–41]
<i>B. subtilis</i> 168 EM11	P <sub>belD</sub> luxABCDE	8	-	-	-	-	[39–41]
<i>B. subtilis</i> 168 EM12	P <sub>yheI</sub> luxABCDE	8	-	-	-	-	[39–41]
<i>B. subtilis</i> 168 EM13	P <sub>yupA</sub> luxABCDE	8	-	-	-	-	[39–41]
<i>B. subtilis</i> 168 HMB62	P <sub>liaG</sub> luxABCDE	8	-	-	-	-	[39–41]
<i>B. subtilis</i> 168 HMB67	P <sub>liaI</sub> luxABCDE	8	-	-	-	-	[39–41]
<i>B. subtilis</i> 168 HMB69	P <sub>fabHB</sub> luxABCDE	8	-	-	-	-	[39–41]
<i>B. subtilis</i> 168 HMB70	P <sub>panB</sub> luxABCDE	8	-	-	-	-	[39–41]
<i>B. subtilis</i> 2020	amyE::spc P <sub>xyl</sub> -gfp-ftsZ	-	-	-	-	2	[20]
<i>Echerichia coli</i> Top10	pBS3Clux	-	-	-	-	-	[39,40]
<i>Staphylococcus aureus</i> 29213	-	6.25	-	-	-	-	ATCC 29213
<i>S. aureus</i> 25923	-	6.25	>128	-	-	-	ATCC 25923

Abbreviations: MIC—minimal inhibitory concentration; CHX—chlorhexedine; CIP—ciprofloxacin; DAP—daptomycin.

### 5.2. Promoter-Based Biosensor Assay

A biosensor assay was used to correlate the activity of lulworthinone with previously known MOAs. Interaction of lulworthinone with DNA replication, transcription, and translation, the cell envelope, and fatty and folic acid synthesis was determined using *B. subtilis* 168 derivatives containing *luc*-genes fused to the *yorB*, *belD*, *yheI*, *yupA*, *liaI*, *fabHB*, *panB* or *liaG* promoters (Table 1). The biosensor constructs were cloned using building blocks directly from, or PCR products adapted to, the cloning enzymes used by the Bacillus BioBrick Box [40]. The plasmid pBS3Clux was used as a vector during cloning in *E. coli* Top10. The promoter regions used were either directly applied from the BioBrick Box as digestible plasmid constructs provided through the Bacillus Genetic Stock Center or adapted and amplified from Urban et al. (2007) [39] and patent US20020164602A1 by the respective primers. The promoter regions were digested with *EcoRI* and *PstI* and subsequently ligated into the vector cut with the same combination of restriction enzymes. *B. subtilis* 168 was finally transformed with the *ScaI*-linearized plasmids under 5 µg/mL chloramphenicol selection and verified by colony PCR of the disrupted *sacA* locus. Fresh colonies from agar plates were transferred to 5 mL MH medium containing 5 µg/mL chloramphenicol and incubated at 37 °C. Overnight cultures were diluted to an OD<sub>600</sub> = 0.1 and grown to an OD<sub>600</sub> = 0.2 before addition to the assay plates already containing the analytes. The analytes and control antibiotics were diluted in two-fold dilution series, with the highest concentration representing 8 × of the respective MIC. A total of 5 µL of each



dilution series and 45  $\mu\text{L}$  bacterial suspensions were added to the wells of the 386-well plates (6007490, PerkinElmer, Waltham, MA, USA) and covered by breatheasy sealing membrane (Z380059, Sigma-Aldrich, Darmstadt, Germany) to reduce evaporation. The plates were kept in the plate reader (EnVision<sup>®</sup>, PerkinElmer, Waltham, MA, USA) at 35 °C. The peak luminescence of the controls was compared to the luminescence of cells treated with lulworthinone. Luminescence and OD<sub>595</sub> were recorded every 30 min for a total of 10 hours. The experiment was conducted three times. Data analysis and code can be found at the data repository [42].

### 5.3. Lipid Interactions Using Surface Plasmon Resonance

The SPR experiments were performed at room temperature using the T200 Biacore instrument (GE Healthcare, Chicago, IL, USA) and L1 chip. Chip treatment, cleaning, regeneration and flowrate settings are the same as in Jakubec et al. (2021) [43]. Briefly, extruded DMPC liposomes (100 nm diameter, 1 mM in 10 mM HEPES buffer pH 7.4 with 150 mM NaCl) were immobilised on a clean surface using a flowrate of 2  $\mu\text{L}/\text{min}$  for 2400 s. Successful immobilisation and stabilisation was tested by an injection of 0.1 mg/mL of bovine serum albumin (BSA, A7030, Sigma-Aldrich, Saint Louis, MO, USA) for 1 min at 30  $\mu\text{L}/\text{min}$ ; a change of <400 RU indicated sufficient coverage. A dilution of lulworthinone and its isomer from 4 to 128  $\mu\text{M}$  in HEPES buffer was injected over immobilised vesicles. Due to the possibility of sample retention, injections were made from low to high concentration with 200 s contact time and a 400 s dissociation phase. Between runs, liposomes were regenerated by three subsequent injections of 10 mM NaOH at 30  $\mu\text{L}/\text{min}$  for 30 s each. The control flow cell was treated the same way as sample cells, except 1 injection was replaced by HEPES buffer. The results were processed using in-laboratory written MATLAB scripts (MATLAB R2020a; scripts are available at <https://github.com/MarJakubec>, accessed on 15 March 2022). We have obtained both partitioning constant ( $K_P$ ) and dissociation rate ( $k_{\text{off}}$ ) using the method developed by Figueira et al. (2017) [31].  $K_P$  was evaluated from the steady-state affinity at the 190-s time mark after injection and fitting the obtained curve into (Equation (2))

$$\frac{RU_S}{RU_L} = \frac{\gamma_L K_P \frac{M_S}{M_L} [S]_W}{1 + \sigma \gamma_L K_P \frac{M_S}{M_L} [S]_W} \quad (2)$$

where  $RU_S$  and  $RU_L$  are the relative response of the solute (lulworthinone) and the total lipid deposition response, respectively,  $\gamma_L$  is the molar volume of the lipids,  $M_S$  and  $M_L$  are the molecular mass of the solute and lipid, respectively, and  $[S]_W$  is the concentration of solute in water.  $K_P$  and  $\sigma$  are obtained from fit and are, respectively, the partitioning constant and the lipid-to-solute ratio. The  $k_{\text{off}}$  rate was obtained by fitting the first 200 s of the dissociation run. We have identified the contribution of two populations to the dissociation response, which led us to use adapted formalism from Figuera et al. [31] (Equation (3)) to obtain the average  $k_{\text{off}}$  response (Equation (4)).

$$S_L(t) = \alpha e^{-k_{\text{off},\alpha} t} + \beta e^{-k_{\text{off},\beta} t} + S_{L,r} \quad (3)$$

$$k_{\text{off}} = \frac{\alpha k_{\text{off},\alpha} + \beta k_{\text{off},\beta}}{\alpha + \beta} \quad (4)$$

where  $S_L$  is the linearised ratio of responses of the solute and lipid, which is plotted against the time of dissociation;  $\alpha$  and  $\beta$  are individual populations, and  $S_{L,r}$  is the retained solute fraction.

### 5.4. Cell Membrane Integrity as Determined by Bioluminescence

A bioluminescence-based assay developed by Virta et al. (1995) [38] was used to investigate the membrane disruptive properties of lulworthinone. Upon the disruption of the membrane, the intracellular produced luciferase would interact with its extracellular provided substrate—D-luciferin—and emit luminescence in real time. For this, a *Bacillus subtilis* 168 strain expressing luciferase encoded on the pCSS962 plasmid was used.

Concentrations ranging from 0 to  $4 \times \text{MIC}$ , including chlorhexidine as a membranolytic control (200  $\mu\text{g}/\text{mL}$ ) and ciprofloxacin as a non-membrane active negative control, were tested. Overnight cultures were grown in MHB II containing 5  $\mu\text{g}/\text{mL}$  chloramphenicol (220551, Calbiochem, San Diego, CA, USA). The bacteria were pelleted and resuspended in fresh MHB II to  $\text{OD}_{600}$  of 0.1 D-luciferin potassium salt (pH 7.4, SynChem Inc., Elk Grove Village, IL, USA), which was added to achieve a final concentration of 1 mM. Subsequently, 96-well plates (655209, Greiner Bio-One, Kresmmuenster, Austria) containing 20  $\mu\text{L}$  of compound dilutions were prepared and loaded into a plate reader (Synergy H1 Hybrid reader, BioTek, Winooski, VT, USA). For each test well, 180  $\mu\text{L}$  bacterial inoculums were injected by an automatic injector. The bioluminescence was measured for 270 s before 35  $\mu\text{L}$  chlorhexidine (vnr 007214, Fresenius Kabi Norge AS, Halden, Norway) was added at a membranolytic concentration (30  $\mu\text{g}/\text{mL}$ ). The luminescence was measured for an additional 30 s. The light emission with CHX indicates the lysis of bacterial cells that are still alive after the first treatment. The experiment was performed three times. Data, analysis and code at can be found in the data repository [42].

##### 5.5. $\text{DiOC}_2(3)$ Cytoplasmic Membrane Depolarization Assay

To characterize the influence of lulworthinone on the cytoplasmic membrane potential, the fluorescence of a membrane potential indicator dye was measured with flow cytometry. The BacLight Bacterial Membrane Potential Kit (B34950, Invitrogen, Carlsbad, CA, USA), which includes a fluorescent membrane potential indicator dye, 3,3'-Diethyloxacarbocyanine iodide ( $\text{DiOC}_2(3)$ ) and carbonyl cyanide m-chlorophenyl hydrazone (CCCP) as a membrane potential inhibitor [19], was used. In low abundance,  $\text{DiOC}_2(3)$  emits green fluorescence in bacterial cells. When cells maintain their membrane potential, they accumulate more dye, which self-associates, and the fluorescence shifts into the red spectrum. The assay was performed according to the manufacturer. *B. subtilis* 168 was replaced by *S. aureus* ATCC 29213, since it showed much clearer detectable differences in potential change. In short, an inoculum of  $1 \times 10^6$  CFU/mL was prepared in sterile filtered (0.22  $\mu\text{m}$  pore size) PBS (P4417, Sigma-Aldrich, Saint Louis, MO, USA). For each sample, 1 mL inoculum was transferred in flow cytometer tubes (352054, Corning Science, Reynosa, Mexico). Additional tubes for a depolarized control (CCCP, 10  $\mu\text{L}$  of 500  $\mu\text{M}$  stock) and unstained control were included. Lulworthinone was added for concentrations ranging from 0.25 to  $4 \times \text{MIC}$ . Samples were vortexed and added to 10  $\mu\text{L}$  of  $\text{DiOC}_2(3)$  (to each tube besides the unstained control), mixed and incubated for 30 min. Samples were exited at 480 nm, and fluorescence was collected with 530/30 nm and 616/23 nm emission filters using the BD LSRFortessa Cell Analyser (647794, BD Bioscience, Eysins, Switzerland). Samples were gated on the bacterial cell size with a set threshold at 1500 sideward scatter. A total of 10,000 events were collected. The data were analysed using the FlowJo software (v10.8.0, FlowJo, LLC, Ashland, OR, USA), and the gated population mean fluorescence intensity (MFI) was obtained in a red vs. green fluorescence dot plot. The ratio of red MFI divided by green MFI reflecting the membrane potential. The experiment was performed three times; data, analysis, and code can be found in the data repository [42].

##### 5.6. Cell Morphology and Biomarker Detection Using Microscopy

*B. subtilis* 168 was grown in MHB II at 37 °C under agitation. Reporter strain 2020 was grown in MHB II supplemented with 100  $\mu\text{g}/\text{mL}$  spectinomycin (S9007, Sigma-Aldrich, Saint Louis, MO, USA) and 0.5% xylose (PHR2102-500MG, Merck Ag, Darmstadt, Germany) at 30 °C under agitation. Additionally, MHB II was supplemented with 1.25 mM  $\text{CaCl}_2$  for all experiments with daptomycin (DAP, Cubicin, Novartis, London, UK) [44]. For *B. subtilis* 168, aliquots from the overnight cultures were diluted 1:50 in prewarmed MHB II and incubated at 37 °C under agitation until an  $\text{OD}_{600}$  of 0.3. The cultures were diluted 1:1 with the solutions of lulworthinone and the reference antibiotic DAP in the wells of a 96-well microtiter plate (249943 Nunc, Thermo scientific, Loughborough, UK). The final concentration of all compounds in the wells was  $1 \times \text{MIC}$ . In parallel, a 1:1 combination of

the cultures with sterile Milli-Q H<sub>2</sub>O or 1.25 mM CaCl<sub>2</sub> for DAP were used as untreated controls. Bacteria were incubated for 90 min at 37 °C with agitation and pelleted at 13.5 × g for 5 min and carefully suspended in prewarmed 0.9% NaCl. Subsequently, bacteria were stained with 12 µg/mL FM 4-64 (T13320, Invitrogen, Waltham, MA, USA) and 2 µg/mL DAPI (D9542, Sigma-Aldrich, Saint Louis, MO, USA) for 25 min at 37 °C with agitation. Cells were pelleted again and carefully resuspended in preheated 0.9% NaCl. Aliquots of the bacterial suspensions were applied to the bottom of 35 mm confocal dishes (75856-742, VWR, Radnor, PA, USA) and covered by 2.4% agarose pads prepared in 0.9% NaCl. For *B. subtilis* 2020, the sample preparation was like the one described above, with the following modifications. Aliquots from the overnight cultures were incubated in the presence of 0.5% xylose. Samples were treated for a total of 45 min prior to microscopy. No washing steps were included. Incubation at all steps was performed at 30 °C with agitation. Aliquots of the stained suspensions were applied to the round 1.5 coverslips (631-0161, VWR, Radnor, PA, USA). The fluorescence images of the bacteria were acquired via a DeltaVision Elite Deconvolution Microscope (GE Healthcare, Chicago, IL, USA). For the wide-field deconvolution imaging of bacteria, an oil immersion 60 × (1.42NA) objective lens was utilized. For DAPI, the excitation wavelength range was 381–401 nm, and the emission was in the 409–456 nm range. The excitation and emission wavelength range for FM 4-64 were 425–495 nm and 652–700 nm, respectively. For GFP, the excitation and emission wavelength range were 425–495 nm and 500–550 nm, respectively. To achieve a superior contrast and resolution in images, a volume stack of 12 planes over 3 µm depth were acquired and deconvolved. For each treatment, 10–20 imaging fields were viewed. Experiments were done in three biological replicates. Pictures can be found at the data repository [42].

#### 5.7. Cell Morphology Determination with Quantitative Phase Microscopy

Digital holography-based quantitative phase microscopy (QPM) has been developed to obtain quantitative information about the bacteria in a label-free manner. QPM improves the image contrast of transparent cells while quantifying parameters such as: optical thickness (sample thickness × refractive index (n)), refractive index variation, cell dry mass and other morphological parameters [45,46]. *B. subtilis* 168 were cultivated in MHB II at 37 °C until an OD<sub>600</sub> = 0.3 was reached. The cultures were diluted 1:1 with the solutions of lulworthinone for 90 min. Subsequently, 90 µL samples were pelleted at 13.5 × g for 5 min and carefully suspended in 200 µL PHEM (pH 7.3) buffer containing 2% paraformaldehyde (PFA) and 1% glutaraldehyde (GA). For QPM measurements, the bacterial cells were placed in a polydimethylsiloxane (PDMS) chamber on a reflective Si substrate and covered with a standard 1.5 thickness coverslip. Before sample preparation, the surface of the Si substrate was treated with 0.1% poly-L-lysine for 10 min to enhance cell attachment. The interferograms were acquired with a 60 × (1.2NA) objective lens and further post-processed in MATLAB to get the phase map of the bacteria. The individual bacteria were segmented for the quantitative assessment of length, width, volume and other morphological parameters of the bacteria.

#### 5.8. Kill Kinetics Using Time-Kill Curves

The kill kinetics of lulworthinone can be expressed as rate over time with a fixed drug concentration—so called time-kill curves [47]. Time-kill curve analyses were performed by culturing *B. subtilis* 168 in MHB II at antimicrobial concentrations ranging from 4 × MIC to 0.25 × MIC. The MICs were determined according to CLSI guidelines [48], presented in Table 5). The antimicrobials examined were lulworthinone and chlorhexidine (17850, Sigma-Adrich, Saint Louis, MO, USA). Cultures were inoculated from MH agar plates and grown in MHB II for 18–20 h at 37 °C, reinoculated and grown to mid-log phase for 3 h in MHB II, before diluting them to 1 × 10<sup>6</sup> CFU/mL in pre-warmed MHB II (37 °C). For the test setup, the two-fold drug concentrations were prepared in 750 µL MHB II each. An antibiotic-free growth control was included and prepared in a 24-well polypropylene

plate (SKU:1300-00312, Bellco Glass Inc., Vineland, NJ, USA). For each drug concentration, 750  $\mu$ L inoculum was added to each well. The plates were incubated for 5 h at 37 °C and sampled at 10, 30, 60, 120 and 300 min. Samples for the start time point ( $T_0$ ) were taken from the inoculum, diluted 1:1 with MHB II. Each sample was diluted seven times in PBS, and 20  $\mu$ L of each dilution was plated out in a run-streak on MH agar plates. Samples were plated in duplicates; each experiment was performed three times. Data, analysis and code can be found in the data repository [42].

### 5.9. Pharmacodynamic Parameters

The data of the time-kill curves were used to model the pharmacodynamic parameters of lulworthinone. The bacterial net growth rates ( $\psi$ ) were estimated from the surviving bacteria (CFU/mL) over time between 0 and 300 min, as described above. The pharmacodynamic function [21] was fitted to the  $\psi$  present at different drug concentrations. In this model, the top asymptote ( $\psi_{max}$ ) and the bottom asymptote ( $\psi_{min}$ ) indicate the maximal and minimal bacterial net growth rate in relation to the drug concentration. The slope of the curve ( $\kappa$  or the Hill coefficient) represents the relationship between bacterial growth and antimicrobial concentration. The antimicrobial concentration that results in a  $\psi$  of zero is the pharmacodynamic MIC (zMIC). Data analysis was done in R [49], and the *censReg* package [50] was used to calculate concentrations containing censored data points. Data and code are available at the data repository [42].

### 5.10. Aggregation Formation Detection with Dynamic Light Scattering

We have tested the ability of lulworthinone to form oligomers by Zetasizer Nano ZS (Malvern Ins., Malvern, UK). Lulworthinone was dissolved in 5% DMSO in MiliQ and then diluted to obtain a concentration range from 320  $\mu$ M to 0.625  $\mu$ M in 1% DMSO. We have tested its ability to form oligomers at 37 °C with or without the presence of 0.025% Tween 80.

### 5.11. Influence of Detergent on Antibacterial Activity

To determine if lulworthinone forms colloidal aggregates that affect its antimicrobial activity, an MIC assay including a non-ionic detergent was used. The antibacterial activity of a colloidal aggregate should be heavily attenuated in the presence of non-ionic detergents [24,51]. An MIC assay was performed according to CLSI guidelines [48] using *S. aureus* ATCC 25923. The MIC values used are from the previous study [10]. Overnight cultures were grown in MHB (275730, BD Difco, Le Pont de Claix, France) at 37 °C. Two-fold dilution series of lulworthinone ranging from 128  $\mu$ g/mL to 0.25  $\mu$ g/mL with or without 0.025% (*v/v*) Tween 80 (P8074, Sigma-Aldrich, Saint Louis, MO, USA) were tested.

Assay was conducted in 96-well plates (Nunclon  $\Delta$  734-2073, VWR, Radnor, PA, USA). OD<sub>600</sub> values were recorded by a plate reader (Victor multilabel counter, PerkinElmer, MA, USA) at 37 °C for 24 h. Each test run included a growth control (media and inoculum) and a sterility control (media and water), and for quality assurance, *S. aureus* ATCC 25923 was tested against gentamicin (A2712, VWR, Radnor, PA, USA). Tests were performed in triplicates with three technical replicates; median MIC values are displayed.

### 5.12. Data Analysis

Data handling, analysis, statistics and presentation were done using R 4.1.0 [49], the *tidyverse* package [52], the *ggplot2* package [53], the *ggpubr* package [54] and the *cowplot* package [55]. Data documentation was done using the *bookdown* package [56].

**Supplementary Materials:** The following are available online at <https://www.mdpi.com/article/10.3390/md20050277/s1>, Figure S1: SPR sensogram for (A) lulworthinone and (B) acidified lulworthinone; Figure S2: Membrane potential shift in the presence of lulworthinone.

**Author Contributions:** Conceptualization, E.J. and J.U.E.; data curation, E.J.; formal analysis, E.J., V.K.D., M.J. (Martin Jakubec); investigation, E.J., E.M., V.K.D., M.J. (Marte Jenssen) and P.R.; project

administration, E.J.; resources, M.J. (Marte Jenssen); software, E.J., V.K.D., M.J. (Martin Jakubec); supervision, E.M. and J.U.E.; visualization, E.J.; writing—original draft preparation, E.J.; writing review and editing, E.J., E.M., M.J. (Marte Jenssen), M.J. (Martin Jakubec), P.R., J.H.A., J.I. and J.U.E. All authors have read and agreed to the published version of the manuscript.

**Funding:** The project was funded by The Research Council of Norway (RCN) grant no. 269425. The APC was covered by the open access publishing fund, UiT.

**Data Availability Statement:** The data presented in this study are openly available in DataverseNO at <https://doi.org/10.18710/6Z0VJX>, accessed on 15 March 2022.

**Acknowledgments:** The authors would like to acknowledge the technical support by Mikal E. Fitsum, Marte Albrigsten and Theresa Wagner for in vivo experimental lab work. Antal Martinecz and Fabrizio Clarelli are acknowledged for advising on pharmacodynamic modelling. Roland Regoes is acknowledged for providing the pharmacodynamic workflow. We would also like to acknowledge Michaela Wenzel for providing the *B. subtilis* 2020 strain, Kine Østnes Hansen for providing the SMILES structure of lulworthinone, and Deanna Wolfson for suggestions to optimize the microscopy methods used. We thank the Advanced Microscopy Core Facility (AMCF) of the UiT, the Arctic University of Norway for the access to their devices. Furthermore, we are grateful for the formal education and training provided by the Digital Life Norway research school and National Graduate School in Infection Biology and Antimicrobials (IBA, project number: 249062).

**Conflicts of Interest:** The authors declare no potential conflict of interest with respect to the research, authorship, and/or publication of this article.

## References

1. Murray, C.J.; Ikuta, K.S.; Sharara, F.; Swetschinski, L.; Aguilar, G.R.; Gray, A.; Han, C.; Bisignano, C.; Rao, P.; Wool, E.; et al. Global Burden of Bacterial Antimicrobial Resistance in 2019: A Systematic Analysis. *Lancet* **2022**, *399*, 629–655. [CrossRef]
2. World Health Organization. *2019 Antibacterial Agents in Clinical Development: An Analysis of the Antibacterial Clinical Development Pipeline*; World Health Organization: Geneva, Switzerland, 2019; Chapter 4, 8p.
3. Theuretzbacher, U.; Bush, K.; Harbarth, S.; Paul, M.; Rex, J.H.; Tacconelli, E.; Thwaites, G.E. Critical Analysis of Antibacterial Agents in Clinical Development. *Nat. Rev. Microbiol.* **2020**, *18*, 286–298. [CrossRef] [PubMed]
4. Silver, L.L. Challenges of Antibacterial Discovery. *Clin. Microbiol. Rev.* **2011**, *24*, 71–109. [CrossRef] [PubMed]
5. Newman, D.J.; Cragg, G.M. Natural Products as Sources of New Drugs over the Nearly Four Decades from 01/1981 to 09/2019. *J. Nat. Prod.* **2020**, *83*, 770–803. [CrossRef] [PubMed]
6. Cushnie, T.P.T.; Cushnie, B.; Echeverría, J.; Fowsantear, W.; Thammawat, S.; Dodgson, J.L.; Law, S.; Clow, S.M. Bioprospecting for Antibacterial Drugs: A Multidisciplinary Perspective on Natural Product Source Material, Bioassay Selection and Avoidable Pitfalls. *Pharm. Res.* **2020**, *37*, 125. [CrossRef]
7. Davison, E.K.; Brimble, M.A. Natural Product Derived Privileged Scaffolds in Drug Discovery. *Curr. Opin. Chem. Biol.* **2019**, *52*, 1–8. [CrossRef]
8. Imhoff, J.F. Natural Products from Marine Fungi—Still an Underrepresented Resource. *Mar. Drugs* **2016**, *14*, 19. [CrossRef]
9. Overy, D.P.; Bayman, P.; Kerr, R.G.; Bills, G.F. An Assessment of Natural Product Discovery from Marine (*Sensu Strictu*) and Marine-Derived Fungi. *Mycology* **2014**, *5*, 145–167. [CrossRef]
10. Jenssen, M.; Rainsford, P.; Juskevit, E.; Andersen, J.H.; Hansen, E.H.; Isaksson, J.; Rämä, T.; Hansen, K.Ø. Lulworthinone, a New Dimeric Naphthopyrone From a Marine Fungus in the Family Lulworthiaceae With Antibacterial Activity Against Clinical Methicillin-Resistant *Staphylococcus Aureus* Isolates. *Front. Microbiol.* **2021**, *12*, 2862. [CrossRef]
11. Suzuki, K.; Nozawa, K.; Nakajima, S.; Udagawa, S.i.; Kawai, K.i. Isolation and Structures of Antibacterial Binaphtho- $\alpha$ -pyrones, Talaroderxines A and B, from *Talaromyces Deroxii*. *Chem. Pharm. Bull.* **1992**, *40*, 1116–1119. [CrossRef]
12. Zheng, C.J.; Sohn, M.J.; Lee, S.; Hong, Y.S.; Kwak, J.H.; Kim, W.G. Cephalochromin, a FabI-directed Antibacterial of Microbial Origin. *Biochem. Biophys. Res. Commun.* **2007**, *362*, 1107–1112. [CrossRef] [PubMed]
13. Boudesocque-Delaye, L.; Agostinho, D.; Bodet, C.; They-Kone, I.; Allouchi, H.; Gueiffier, A.; Nuzillard, J.M.; Enguehard-Gueiffier, C. Antibacterial Polyketide Heterodimers from *Pyrenacantha Kaurabassana* Tubers. *J. Nat. Prod.* **2015**, *78*, 597–603. [CrossRef] [PubMed]
14. Rivera-Chávez, J.; Caesar, L.; Garcia-Salazar, J.J.; Raja, H.A.; Cech, N.B.; Pearce, C.J.; Oberlies, N.H. Mycopyranone: A 8,8'-Binaphthopyranone with Potent Anti-MRSA Activity from the Fungus *Phialemoniopsis* sp. *Tetrahedron Lett.* **2019**, *60*, 594–597. [CrossRef] [PubMed]
15. Wang, J.; Galgoci, A.; Kodali, S.; Herath, K.B.; Jayasuriya, H.; Dorso, K.; Vicente, F.; González, A.; Cully, D.; Bramhill, D.; et al. Discovery of a Small Molecule That Inhibits Cell Division by Blocking FtsZ, a Novel Therapeutic Target of Antibiotics. *J. Biol. Chem.* **2003**, *278*, 44424–44428. [CrossRef] [PubMed]
16. Isaksson, J.; Brandsdal, B.O.; Engqvist, M.; Flaten, G.E.; Svendsen, J.S.M.; Stensen, W. A Synthetic Antimicrobial Peptidomimetic (LTX 109): Stereochemical Impact on Membrane Disruption. *J. Med. Chem.* **2011**, *54*, 5786–5795. [CrossRef] [PubMed]

17. Silk, M.R. (University of Tromsø, Tromsø, Norway). Personal communication, 2021.
18. Rainsford, P.; Sarre, R.B.; Brandsdal, B.O.; Falavigna, M.; Flaten, G.E.; Jakubec, M.; Isaksson, J. WIND-PVPA: Water/Ion NMR Detected PVPA to Assess Lipid Barrier Integrity in Vitro through Quantification of Passive Water- and Ion Transport. *Biochim. Biophys. Acta-(BBA)-Biomembr.* **2022**, *1864*, 183911. [[CrossRef](#)]
19. Novo, D.; Perlmutter, N.G.; Hunt, R.H.; Shapiro, H.M. Accurate Flow Cytometric Membrane Potential Measurement in Bacteria Using Diethyloxycarbocyanine and a Ratiometric Technique. *Cytometry* **1999**, *35*, 55–63. [[CrossRef](#)]
20. Strahl, H.; Hamoen, L.W. Membrane Potential Is Important for Bacterial Cell Division. *Proc. Natl. Acad. Sci. USA* **2010**, *107*, 12281–12286. [[CrossRef](#)]
21. Regoes, R.R.; Wiuff, C.; Zappala, R.M.; Garner, K.N.; Baquero, F.; Levin, B.R. Pharmacodynamic Functions: A Multiparameter Approach to the Design of Antibiotic Treatment Regimens. *Antimicrob. Agents Chemother.* **2004**, *48*, 3670–3676. [[CrossRef](#)]
22. Shoichet, B.K. Interpreting Steep Dose-Response Curves in Early Inhibitor Discovery. *J. Med. Chem.* **2006**, *49*, 7274–7277. [[CrossRef](#)]
23. Topel, Ö.; Çakır, B.A.; Budama, L.; Hoda, N. Determination of Critical Micelle Concentration of Polybutadiene-Block-Poly(Ethyleneoxide) Diblock Copolymer by Fluorescence Spectroscopy and Dynamic Light Scattering. *J. Mol. Liq.* **2013**, *177*, 40–43. [[CrossRef](#)]
24. Ganesh, A.N.; Donders, E.N.; Shoichet, B.K.; Shoichet, M.S. Colloidal Aggregation: From Screening Nuisance to Formulation Nuance. *Nano Today* **2018**, *19*, 188–200. [[CrossRef](#)] [[PubMed](#)]
25. Mingeot-Leclercq, M.P.; Décout, J.L. Bacterial Lipid Membranes as Promising Targets to Fight Antimicrobial Resistance, Molecular Foundations and Illustration through the Renewal of Aminoglycoside Antibiotics and Emergence of Amphiphilic Aminoglycosides. *MedChemComm* **2016**, *7*, 586–611. [[CrossRef](#)]
26. Yet, L. *Privileged Structures in Drug Discovery: Medicinal Chemistry and Synthesis*; John Wiley & Sons: Hoboken, NJ, USA, 2018.
27. Zhang, L.; Zhang, G.; Xu, S.; Song, Y. Recent Advances of Quinones as a Privileged Structure in Drug Discovery. *Eur. J. Med. Chem.* **2021**, *223*, 113632. [[CrossRef](#)] [[PubMed](#)]
28. Sauermann, R.; Rothenburger, M.; Graninger, W.; Joukhadar, C. Daptomycin: A Review 4 Years after First Approval. *Pharmacology* **2008**, *81*, 79–91. [[CrossRef](#)]
29. Bernareggi, A.; Borghi, A.; Borgonovi, M.; Cavenaghi, L.; Ferrari, P.; Vékey, K.; Zanol, M.; Zerilli, L.F. Teicoplanin Metabolism in Humans. *Antimicrob. Agents Chemother.* **1992**, *36*, 1744–1749. [[CrossRef](#)]
30. Cochrane, S.A.; Vederas, J.C. Lipopeptides from *Bacillus* and *Paenibacillus* Spp.: A Gold Mine of Antibiotic Candidates. *Med. Res. Rev.* **2016**, *36*, 4–31. [[CrossRef](#)]
31. Figueira, T.N.; Freire, J.M.; Cunha-Santos, C.; Heras, M.; Gonçalves, J.; Moscona, A.; Porotto, M.; Salomé Veiga, A.; Castanho, M.A.R.B. Quantitative Analysis of Molecular Partition towards Lipid Membranes Using Surface Plasmon Resonance. *Sci. Rep.* **2017**, *7*, 45647. [[CrossRef](#)]
32. Tripathy, S.; Sahu, S.K. FtsZ Inhibitors as a New Genera of Antibacterial Agents. *Bioorg. Chem.* **2019**, *91*, 103169. [[CrossRef](#)]
33. Kusuma, K.D.; Payne, M.; Ung, A.T.; Bottomley, A.L.; Harry, E.J. FtsZ as an Antibacterial Target: Status and Guidelines for Progressing This Avenue. *ACS Infect. Dis.* **2019**, *5*, 1279–1294. [[CrossRef](#)]
34. Silber, N.; de Opitz, C.L.M.; Mayer, C.; Sass, P. Cell Division Protein FtsZ: From Structure and Mechanism to Antibiotic Target. *Future Microbiol.* **2020**, *15*, 801–831. [[CrossRef](#)] [[PubMed](#)]
35. Chai, W.C.; Whittall, J.J.; Song, D.; Polyak, S.W.; Ogunniyi, A.D.; Wang, Y.; Bi, F.; Ma, S.; Semple, S.J.; Venter, H. Antimicrobial Action and Reversal of Resistance in MRSA by Difluorobenzamide Derivatives Targeted at FtsZ. *Antibiotics* **2020**, *9*, 873. [[CrossRef](#)] [[PubMed](#)]
36. Pradhan, P.; Margolin, W.; Beuria, T.K. Targeting the Achilles Heel of FtsZ: The Interdomain Cleft. *Front. Microbiol.* **2021**, *12*, 732796. [[CrossRef](#)] [[PubMed](#)]
37. McLaughlin, C.K.; Duan, D.; Ganesh, A.N.; Torosyan, H.; Shoichet, B.K.; Shoichet, M.S. Stable Colloidal Drug Aggregates Catch and Release Active Enzymes. *ACS Chem. Biol.* **2016**, *11*, 992–1000. [[CrossRef](#)]
38. Virta, M.; Åkerman, K.E.O.; Saviranta, P.; Oker-Blom, C.; Karp, M.T. Real-Time Measurement of Cell Permeabilization with Low-Molecular-Weight Membranolytic Agents. *J. Antimicrob. Chemother.* **1995**, *36*, 303–315. [[CrossRef](#)]
39. Urban, A.; Eckermann, S.; Fast, B.; Metzger, S.; Gehling, M.; Ziegelbauer, K.; Rübsamen-Waigmann, H.; Freiberg, C. Novel Whole-Cell Antibiotic Biosensors for Compound Discovery. *Appl. Environ. Microbiol.* **2007**, *73*, 6436–6443. [[CrossRef](#)]
40. Radeck, J.; Kraft, K.; Bartels, J.; Cikovic, T.; Dürr, F.; Emenegger, J.; Kelterborn, S.; Sauer, C.; Fritz, G.; Gebhard, S.; et al. The *Bacillus* BioBrick Box: Generation and Evaluation of Essential Genetic Building Blocks for Standardized Work with *Bacillus Subtilis*. *J. Biol. Eng.* **2013**, *7*, 29. [[CrossRef](#)]
41. Hansen, K.Ø.; Hansen, I.K.Ø.; Richard, C.S.; Jenssen, M.; Andersen, J.H.; Hansen, E.H. Antimicrobial Activity of Securamines From the Bryozoan *Securiflustra Securifrons*. *Nat. Prod. Commun.* **2021**, *16*, 1934578X21996180. [[CrossRef](#)]
42. Juskewitz, E. Replication Data for: Lulworthinone: In Vitro Mode of Action Investigation of an Antibacterial Dimeric Naphthopyrone Isolated from a Marine Fungus. 2022, *in submission*. [[CrossRef](#)]
43. Jakubec, M.; Bariãs, E.; Furse, S.; Govasli, M.L.; George, V.; Turcu, D.; Iashchishyn, I.A.; Morozova-Roche, L.A.; Halskau, Ø. Cholesterol-Containing Lipid Nanodiscs Promote an  $\alpha$ -Synuclein Binding Mode That Accelerates Oligomerization. *FEBS J.* **2021**, *288*, 1887–1905. [[CrossRef](#)]

44. Müller, A.; Wenzel, M.; Strahl, H.; Grein, F.; Saaki, T.N.V.; Kohl, B.; Siersma, T.; Bandow, J.E.; Sahl, H.G.; Schneider, T.; et al. Daptomycin Inhibits Cell Envelope Synthesis by Interfering with Fluid Membrane Microdomains. *Proc. Natl. Acad. Sci. USA* **2016**, *113*, E7077–E7086. [[CrossRef](#)]
45. Dubey, V.; Ahmad, A.; Singh, R.; Wolfson, D.L.; Basnet, P.; Acharya, G.; Mehta, D.S.; Ahluwalia, B.S. Multi-Modal Chip-Based Fluorescence and Quantitative Phase Microscopy for Studying Inflammation in Macrophages. *Opt. Express* **2018**, *26*, 19864–19876. [[CrossRef](#)] [[PubMed](#)]
46. Dubey, V.; Popova, D.; Ahmad, A.; Acharya, G.; Basnet, P.; Mehta, D.S.; Ahluwalia, B.S. Partially Spatially Coherent Digital Holographic Microscopy and Machine Learning for Quantitative Analysis of Human Spermatozoa under Oxidative Stress Condition. *Sci. Rep.* **2019**, *9*, 3564. [[CrossRef](#)] [[PubMed](#)]
47. Clinical and Laboratory Standards Institute. *M26-A—Methods for Determining Bactericidal Activity of Antimicrobial Agents; Approved Guideline*; Clinical and Laboratory Standards Institute: Wayne, PA, USA, 1999
48. Clinical and Laboratory Standards Institute. *M7-A7: Methods for Dilution Antimicrobial Susceptibility Tests for Bacteria That Grow Aerobically; Approved Standard*, 7th ed.; Clinical and Laboratory Standards Institute: Wayne, PA, USA, 2006.
49. R Core Team. *R: A Language and Environment for Statistical Computing*; R Foundation for Statistical Computing: Vienna, Austria, 2021.
50. Henningsen, A. *censReg: Censored Regression (Tobit) Models*; R Package Version 0.5-32. 2020. Available online: <https://CRAN.R-project.org/package=censReg> (accessed on 15 March 2022).
51. Shoichet, B.K. Screening in a Spirit Haunted World. *Drug Discov. Today* **2006**, *11*, 607–615. [[CrossRef](#)] [[PubMed](#)]
52. Wickham, H.; Averick, M.; Bryan, J.; Chang, W.; McGowan, L.D.; François, R.; Grolemund, G.; Hayes, A.; Henry, L.; Hester, J.; et al. Welcome to the tidyverse. *J. Open Source Softw.* **2019**, *4*, 1686. [[CrossRef](#)]
53. Wickham, H.; Chang, W.; Henry, L.; Pedersen, T.L.; Takahashi, K.; Wilke, C.; Woo, K.; Yutani, H.; Dunnington, D.; RStudio. *Ggplot2: Create Elegant Data Visualisations Using the Grammar of Graphics*; Springer: New York, NY, USA, 2021.
54. Kassambara, A. *ggpubr: 'ggplot2' Based Publication Ready Plots*; R Package Version 0.4.0. 2020. Available online: <https://CRAN.R-project.org/package=ggpubr> (accessed on 15 March 2022).
55. Wilke, C.O. *Cowplot: Streamlined Plot Theme and Plot Annotations for 'Ggplot2'*; R Package Version 1.1.1. 2020. Available online: <https://CRAN.R-project.org/package=cowplot> (accessed on 15 March 2022).
56. Xie, Y. *Bookdown: Authoring Books and Technical Documents with R Markdown*; R Package Version 0.26. 2021. Available online: <https://github.com/rstudio/bookdown> (accessed on 15 March 2022).

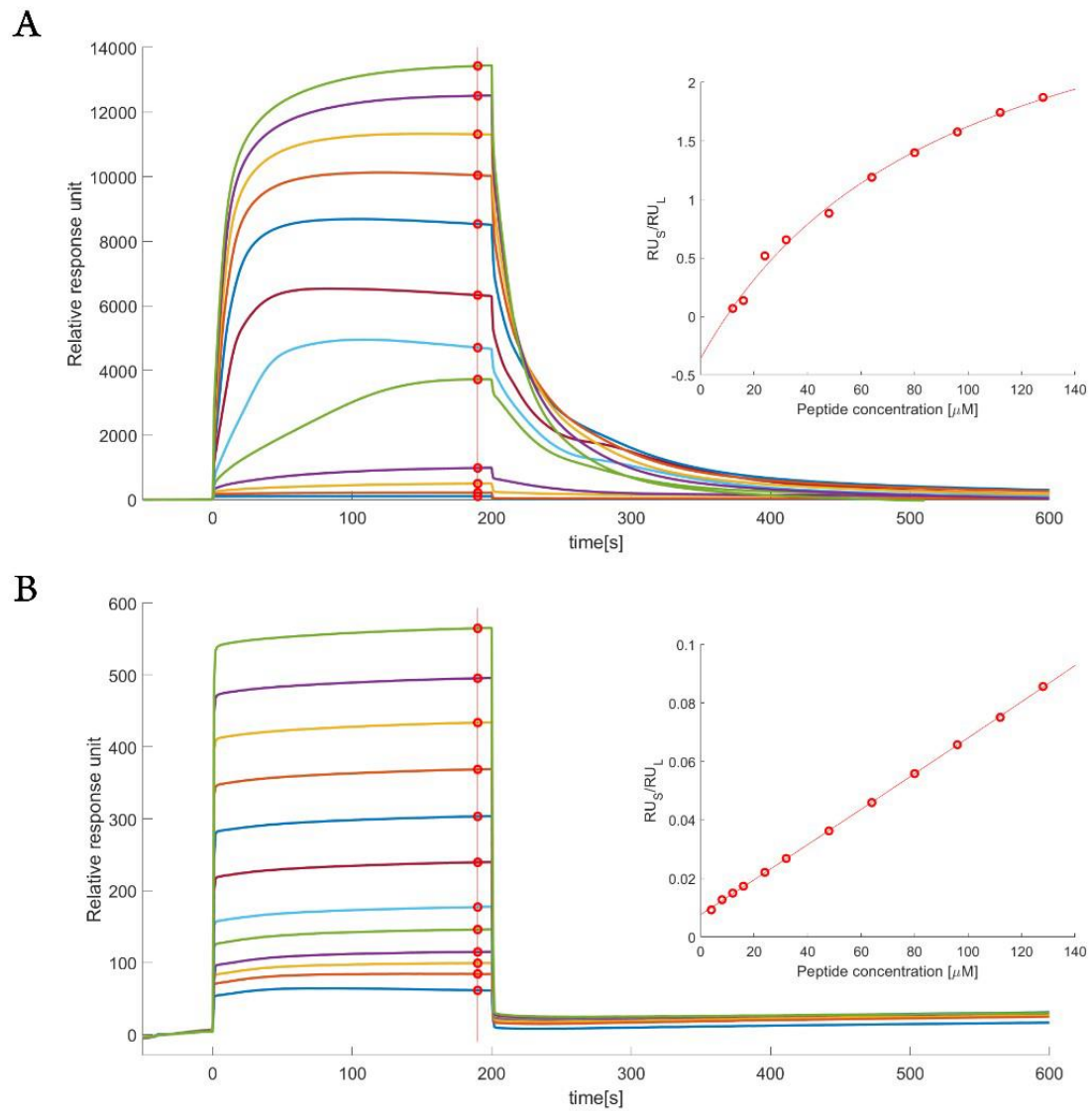


**Figure S1.** SPR sensogram for (A) lulworthinone and (B) acidified lulworthinone. Red line points to a steady state where relative response was read. Values were fitted (inset) to obtain KP. Please note the different range in relative response units for both compounds.



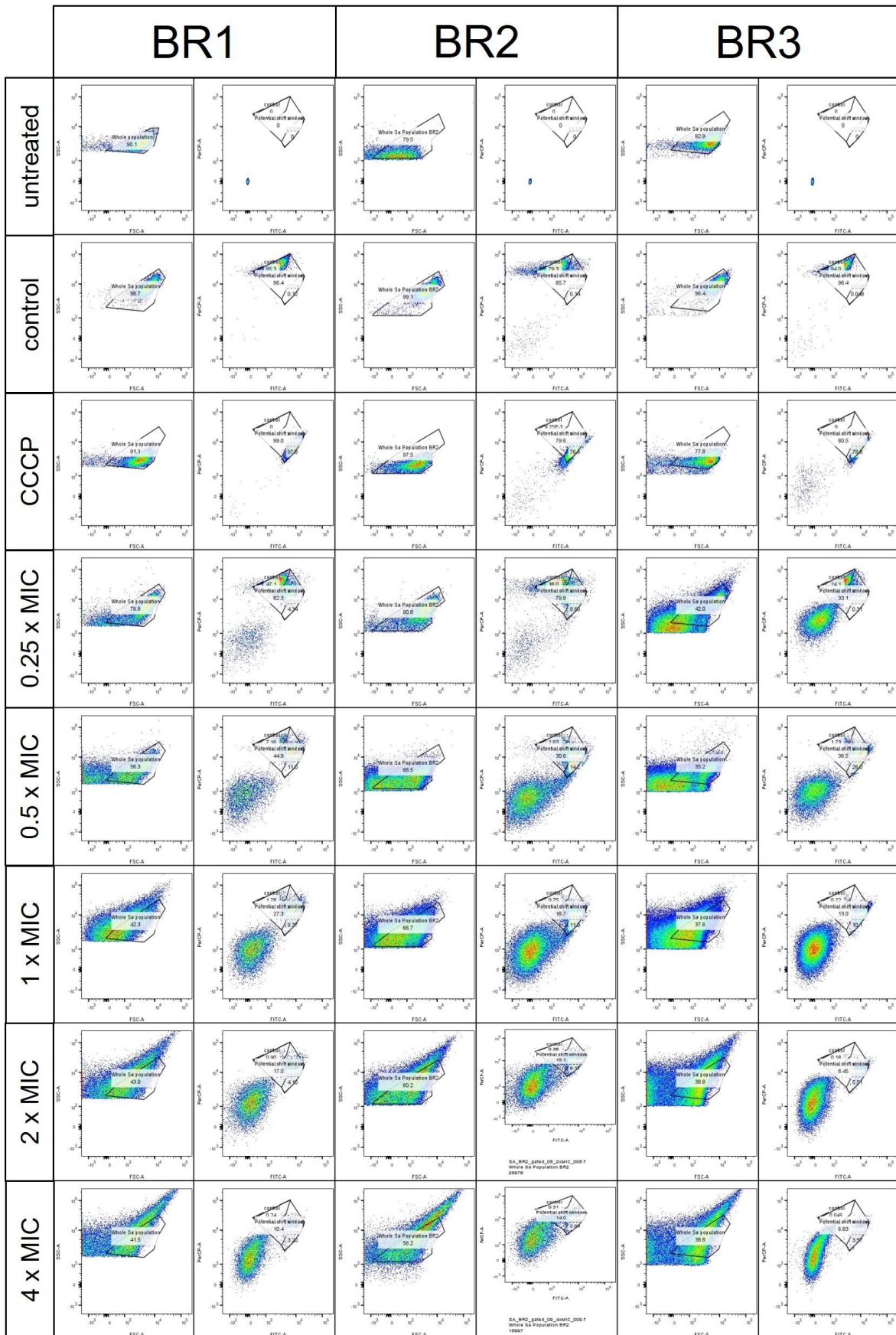


Figure S2. Membrane potential shift in the presence of lulworthinone. Red cultures have a membrane potential, while green cultures show a dissipation the membrane potential.



## Paper III

## Amphipathic Barbiturates as Mimics of Antimicrobial Peptides and the Marine Natural Products Eusynstyelamides with Activity against Multi-resistant Clinical Isolates

Marianne H. Paulsen, Magnus Engqvist, Dominik Ausbacher, Trude Anderssen, Manuel K. Langer, Tor Haug, Glenn R. Morello, Laura E. Liikanen, Hans-Matti Blencke, Johan Isaksson, Eric Juskewitz, Annette Bayer,\* and Morten B. Strøm\*

Cite This: *J. Med. Chem.* 2021, 64, 11395–11417

Read Online

ACCESS |



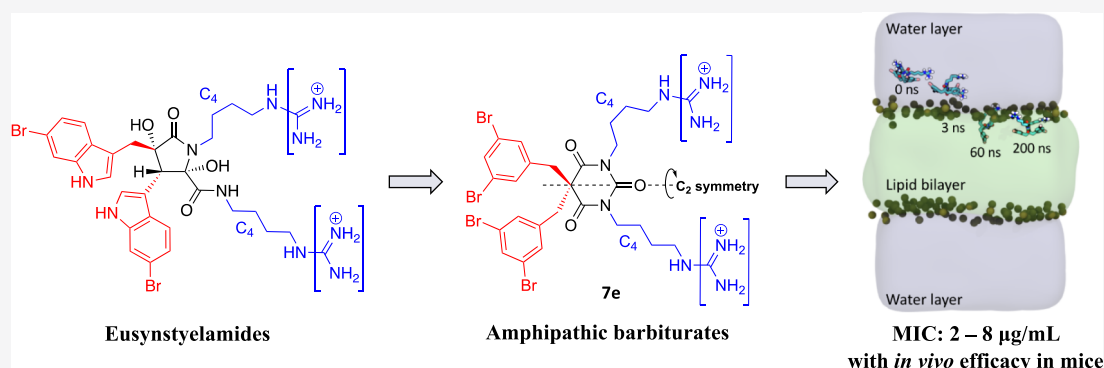
Metrics &amp; More



Article Recommendations



Supporting Information



**ABSTRACT:** We report a series of synthetic cationic amphipathic barbiturates inspired by the pharmacophore model of small antimicrobial peptides (AMPs) and the marine antimicrobials eusynstyelamides. These *N,N'*-dialkylated-5,5-disubstituted barbiturates consist of an achiral barbiturate scaffold with two cationic groups and two lipophilic side chains. Minimum inhibitory concentrations of 2–8 µg/mL were achieved against 30 multi-resistant clinical isolates of Gram-positive and Gram-negative bacteria, including isolates with extended spectrum  $\beta$ -lactamase–carbapenemase production. The guanidine barbiturate **7e** (3,5-di-Br) demonstrated promising *in vivo* antibiotic efficacy in mice infected with clinical isolates of *Escherichia coli* and *Klebsiella pneumoniae* using a neutropenic peritonitis model. Mode of action studies showed a strong membrane disrupting effect and was supported by nuclear magnetic resonance and molecular dynamics simulations. The results express how the pharmacophore model of small AMPs and the structure of the marine eusynstyelamides can be used to design highly potent lead peptidomimetics against multi-resistant bacteria.

## INTRODUCTION

There is a desperate need for developing new antimicrobial agents to meet the worldwide emergence and spread of resistant bacteria.<sup>1</sup> Resistant bacteria are currently causing deaths of 33,000 European patients annually, and the worst scenarios estimate 10 million deaths by 2050 per year if no measures are effectuated.<sup>2,3</sup> WHO announced in their Global action plan on antimicrobial resistance that access to and appropriate use of existing and new antimicrobial drugs are absolutely mandatory to maintain the ability to treat serious infections.<sup>4</sup> Increasing antimicrobial resistance has also dramatic consequences for common medical interventions in cancer treatment, caesarean sections, and organ transplantations. Large pharmaceutical companies show nevertheless little interest in antimicrobial drug development, mainly due to economic reasons. Academia and smaller research institutions are now conceivably the most important contributors for

discovery and synthesis of new lead compounds for antimicrobial drug development.

The eusynstyelamides are in this setting a fascinating class of antimicrobials isolated from the marine Arctic bryozoan *Tegella cf. spitzbergensis* and the Australian ascidian *Eusynstyela latericius*.<sup>5,6</sup> The eusynstyelamides display moderate antimicrobial activity, and a method for the synthesis of ( $\pm$ )-eusynstyelamide A is reported.<sup>5,7</sup> An intriguing structural feature of the eusynstyelamides is that they consist of two cationic groups

Received: April 23, 2021

Published: July 27, 2021



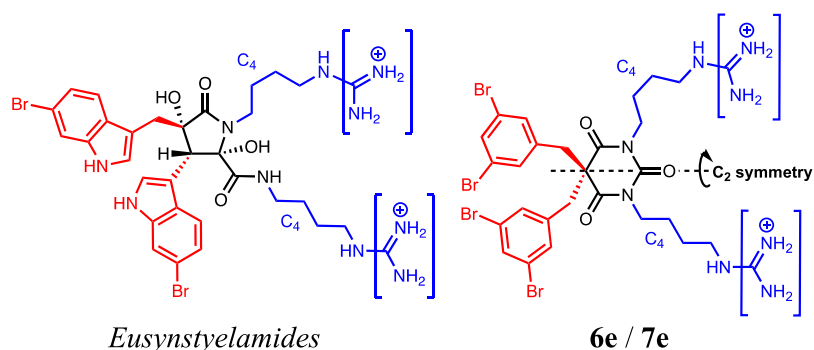
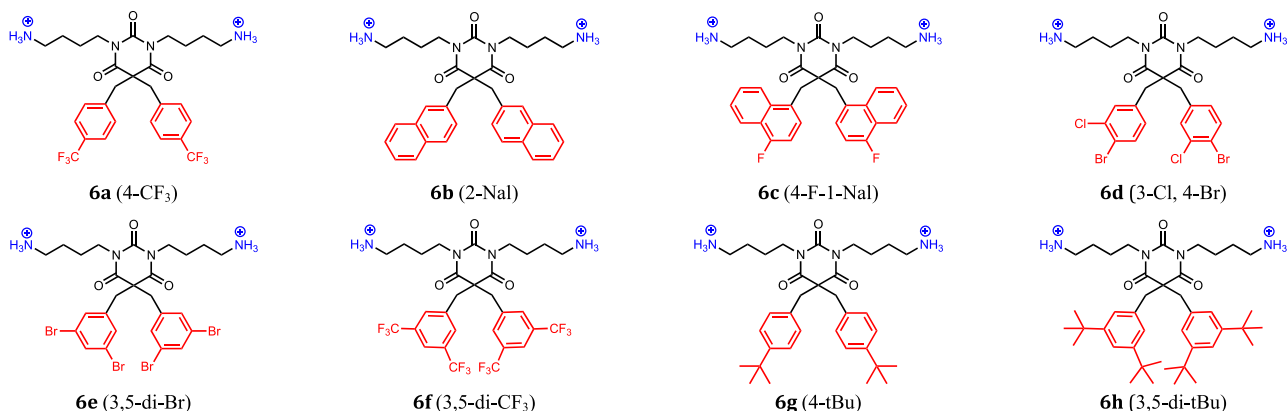
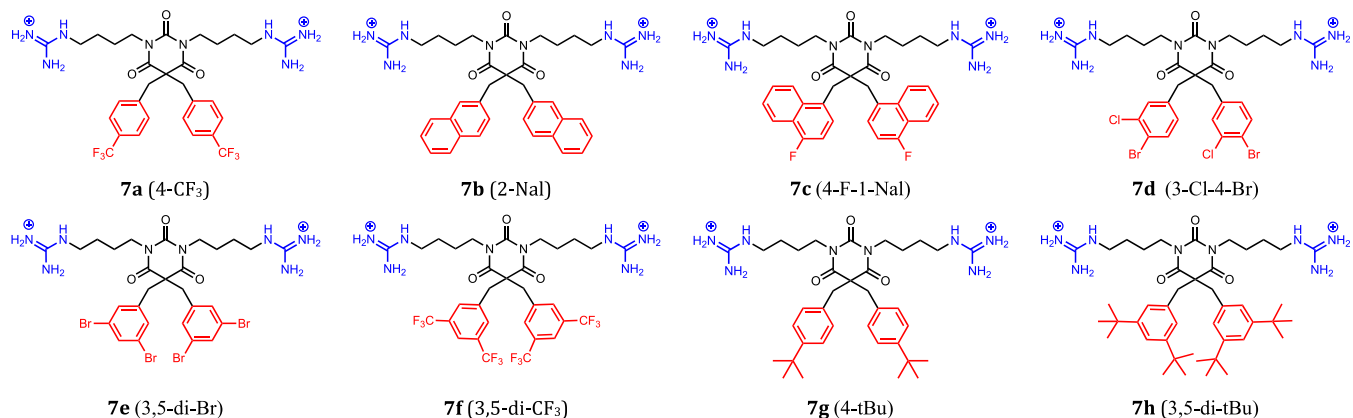


**Figure 1.** General structures of the marine antimicrobials eusynstyelamides (left) and the novel amphipathic barbiturates **6e** (3,5-di-Br) (amine) and **7e** (3,5-di-Br) (guanidine) (right). Brackets imply variations between cationic amine and guanidine groups. The eusynstyelamides can have different combinations of amine and guanidine groups,<sup>5</sup> but in the present study, both cationic groups were identical in the synthesized amphipathic barbiturates.

#### Series 6: Amine barbiturates



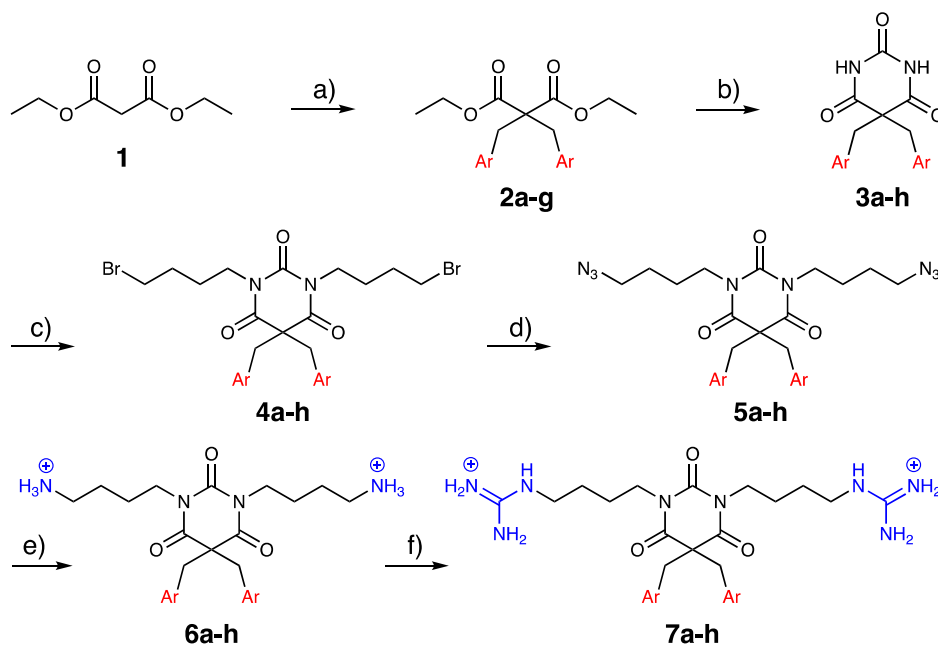
#### Series 7: Guanidine barbiturates



**Figure 2.** Structures of the synthesized amphipathic amine barbiturates (series 6) and guanidine barbiturates (series 7) investigated for antimicrobial activity. The cationic groups have TFA<sup>-</sup> as the counterion.

(amine or guanidine) and two lipophilic groups attached to a five-membered dihydroxybutyrolactam ring (Figure 1). This amphipathic structural arrangement of cationic and lipophilic groups satisfies the pharmacophore model of small antimicrobial peptides (AMPs) that we and others have studied extensively by design of peptidomimetics of AMPs [also named synthetic mimics of AMPs (SMAMPs)].<sup>8–11</sup> AMPs play a crucial part of innate immunity in virtually all species and constitute the first line of defense against infections by bacteria, virus, fungi, and parasites.<sup>12–14</sup> Natural AMPs are

however rather large cationic peptides (+2 to +9) consisting of 12–50 amino acid residues where 20–50% are lipophilic residues. They have an amphipathic characteristic that is essential for their membrane disruptive mode of action against bacteria.<sup>12,15</sup> The limitation of AMPs as drugs is related to their pharmacokinetic properties, such as low proteolytic stability, low oral bioavailability, and potential immunogenicity.<sup>16</sup> The design of SMAMPs can offer a solution to these limitations.

Scheme 1. Successful Strategy for the Synthesis of Target Amphipathic Barbiturates<sup>a</sup>

<sup>a</sup>Conditions: (a) ArCH<sub>2</sub>Br, base, and DMF; (b) urea, NaH, and DMF; (c) 1,4-dibromobutane, K<sub>2</sub>CO<sub>3</sub>, and DMF; (d) NaN<sub>3</sub> and DMF; (e) (i) NaBH<sub>4</sub>, 1,3-propanedithiol, and THF:isopropanol 1:1 and (ii) Boc<sub>2</sub>O; (iii) CH<sub>2</sub>Cl<sub>2</sub>/TFA; and (f) (i) *N*-Boc-1*H*-pyrazole-1-carboxamide and THF and (ii) CH<sub>2</sub>Cl<sub>2</sub>/TFA. Purified using C-18 flash chromatography. The Ar groups are depicted in Figure 2.

In the present study, we report a peptidomimetic amphipathic scaffold inspired by the marine antimicrobials eusynstyelamides and fulfilling the pharmacophore model of small AMPs (Figure 1). A barbiturate ring was used as a structurally simplified mimic of the more complex dihydroxybutyrolactam ring of the eusynstyelamides, providing a scaffold without stereogenic centers. Different lipophilic and cationic groups could then be introduced on the barbiturate scaffold and provide a variety of amphipathic barbiturates (Figure 2). Selection of lipophilic side chains was based on our previous work with SMAMPs.<sup>17,18</sup> The present amphipathic barbiturates were then investigated for their antimicrobial activity against bacterial reference strains and multi-resistant clinical isolates, and toxicity against human cell lines. One selected compound was investigated *in vivo* using a peritonitis model in mice to determine the efficacy against Gram-negative clinical isolates. The mode of action was studied *in vitro* using two luciferase-based membrane assays. To gain further insights into the membrane interaction of the amphipathic barbiturates, conformational analysis by nuclear magnetic resonance (NMR) in a membrane mimicking environment and molecular dynamics (MD) simulations of the interaction progression of compounds with an inner *Escherichia coli* cell membrane were performed.

## RESULTS AND DISCUSSION

**Synthesis.** Reported methods for the synthesis of substituted barbiturates include the condensation of alkylated malonate esters with urea,<sup>19–21</sup> cyclization with *N*-alkylated urea and diethyl malonate or malonic acid,<sup>22,23</sup> Knoevenagel condensation of barbituric acid and aldehydes or ketones,<sup>20,24,25</sup> and alkylation of barbituric acid.<sup>26</sup>

We first focused on a divergent synthetic strategy to gain quick access to tetrasubstituted, amphipathic barbiturates by cyclization of *N,N'*-dialkylated ureas and disubstituted diethyl

malonates. Unfortunately, no suitable reaction conditions for the cyclization of a number of malonate derivatives with *N,N'*-dialkylated urea with a short C<sub>2</sub> linker to the cationic groups were found (see the Supporting Information; Section 1 for details). Depending on the reaction conditions, the dialkylated urea proved to be either unreactive, decomposed, or led to undesired side products. As this strategy did not deliver the desired results, we turned our attention to a different approach.

The condensation of dialkylated malonate esters with urea followed by *N*-alkylation became a successful strategy for the synthesis of amphipathic barbiturates (Scheme 1). Symmetrically disubstituted malonates 2a–g were obtained from diethyl malonate 1 by dialkylation with the appropriate arylmethyl halides and were subsequently cyclized with urea by treatment with NaH in dimethylformamide (DMF) to provide the 5,5-disubstituted barbiturates 3a–h in yields of 70–92%. Dry conditions were imperative to the yield. Cyclization of malonate 2f (3,5-di-CF<sub>3</sub>) gave low yields (27%) due to decarboxylation under the reaction conditions. The 5,5-disubstituted barbiturates 3a–h were alkylated with an excess of 1,4-dibromobutane under basic conditions (K<sub>2</sub>CO<sub>3</sub> in DMF) to afford *N,N'*-dialkylated barbiturates 4a–h in 40–96% yield. These were converted to the corresponding azides 5a–h with NaN<sub>3</sub> (2–3 equiv) in DMF (68–100% yield). Reduction of the azides to amines with NaBH<sub>4</sub> and a catalytic amount of propane-1,3-dithiol,<sup>27</sup> and subsequent Boc-protection, provided Boc-protected diamines after purification by flash chromatography. Boc-protection was important to increase the yield and ease the purification.

Deprotection with 2,2,2-trifluoroacetic acid (TFA) provided the target amine barbiturates 6a–h [ $>95\%$  purity as determined by analytical C<sub>18</sub> reversed phase (RP) HPLC]. The amine barbiturates 6a–h were guanylated with *N*-Boc-1*H*-pyrazole-1-carboxamide in tetrahydrofuran (THF) and purified before the Boc-protecting groups were removed.

**Table 1.** Antimicrobial Activity (MIC in  $\mu\text{g/mL}$ ) of Synthesized Compounds against Antibiotic Susceptible Gram-Positive and Gram-Negative Reference Strains and Hemolytic Activity ( $\text{EC}_{50}$  in  $\mu\text{g/mL}$ ) against Human Erythrocytes (RBC)

Comp.	(side chain)	Clog $P^b$	$M_w^c$	Antimicrobial activity <sup>a</sup>				RBC
				S. a	C. g	E. c	P. a	tox.
6a	(4- $\text{CF}_3$ )	3.52	814.62	64	4	128	64	>398
6b	(2-Nal)	3.82	778.75	8	1	16	16	250
6c	(4-F-1-Nal)	3.96	814.73	4	1	16	8	160
6d	(3-Cl, 4-Br)	4.08	905.31	4	1	16	32	172
6e	(3,5-di-Br)	4.37	994.21	4	1	4	8	79
6f	(3,5-di- $\text{CF}_3$ )	4.41	950.62	16	4	16	16	177
6g	(4-tBu)	4.47	790.85	4	1	4	8	145
6h	(3,5-di-tBu)	6.29	903.06	1	0.25	2	4	<5
7a	(4- $\text{CF}_3$ )	3.52	898.71	2	0.25	8	64	>449
7b	(2-Nal)	3.82	862.83	1	0.25	1	8	133
7c	(4-F-1-Nal)	3.96	898.81	1	0.25	1	4	90
7d	(3-Cl, 4-Br)	4.08	989.39	0.5	0.25	2	8	77
7e	(3,5-di-Br)	4.37	1078.30	1	0.25	2	4	62
7f	(3,5-di- $\text{CF}_3$ )	4.41	1034.70	2	2	2	8	98
7g	(4-tBu)	4.47	874.93	1	<0.13	2	4	77
7h	(3,5-di-tBu)	6.29	987.14	1	0.25	4	4	<6
Oxytetracycline		460.43	0.65	0.65	2.5	20		

<sup>a</sup>Bacterial reference strains: S. a—*Staphylococcus aureus* ATCC 9144, C. g—*Corynebacterium glutamicum* ATCC 13032, E. c—*Escherichia coli* ATCC 25922, and P. a—*Pseudomonas aeruginosa* PA01, DSM 19880 (ATCC 15692). <sup>b</sup>Side chain Clog  $P$  was calculated for a substituted toluene, 1-methyl-Nal, or 2-methyl-Nal (ChemBioDraw Ultra v13.0.2.3020). <sup>c</sup>Molecular weight including 2 equiv of  $\text{CF}_3\text{COO}^-$  except for oxytetracycline.

Purification by  $\text{C}_{18}$  RP flash chromatography gave the TFA salts of the target guanylated barbiturates **7a–h** with >95% purity.

**Structure–Activity Relationship Study against Reference Strains and Human Erythrocytes.** Two series of amphipathic barbiturates were prepared, in which series **6** consisted of barbiturates with two cationic amino groups and series **7** encompassed barbiturates with two cationic guanidine groups (Figure 2). Note that an abbreviation for the lipophilic side chain substituents is included in parentheses to aid the discussion. The barbiturates were initially screened for antimicrobial activity against antibiotic susceptible Gram-positive and Gram-negative reference strains (Table 1). Hemolytic activity was tested against human red blood cells (RBCs) as a measurement of toxicity.

**Amine Barbiturates of Series 6 against Reference Strains.** For the amine barbiturates in series **6**, the minimum inhibitory concentration (MIC) values ranged from 0.25 to 64  $\mu\text{g/mL}$  against the Gram-positive strains *Staphylococcus aureus* and *Corynebacterium glutamicum* and MIC values from 2 to 128  $\mu\text{g/mL}$  against the Gram-negative bacteria *E. coli* and *Pseudomonas aeruginosa* (Table 1). Higher antimicrobial activity was thereby in general observed against Gram-positive bacteria than against Gram-negative bacteria, although the differences were marginal for the most potent amine barbiturates of series **6**. Considering a membrane-disruptive mode of action (see below), the outer cell wall of Gram-negative bacteria may provide additional protection and thereby result in higher MIC values compared to Gram-positive bacteria. For comparison, the four different eusyn-styelamides isolated from *Tegella cf. spitzbergensis* display MIC values of 6.25–12.5  $\mu\text{g/mL}$  against the Gram-positive bacteria *S. aureus* and *C. glutamicum* and 12.5–25  $\mu\text{g/mL}$  against the Gram-negative bacteria *E. coli* and *P. aeruginosa*.<sup>5</sup>

The most potent amine barbiturate was **6h** (3,5-di-tBu), which had two super-bulky lipophilic 3,5-di-tBu-benzylic side chains and displayed MIC values in the very low range of

0.25–4  $\mu\text{g/mL}$  against all Gram-positive and Gram-negative reference strains. The side chain Clog  $P$  of **6h** (3,5-di-tBu) (Clog  $P$ : 6.29) was the highest calculated for all the lipophilic side chains included in the study (Table 1). Derivative **6h** (3,5-di-tBu) showed, however, unacceptable high hemolytic toxicity ( $\text{EC}_{50}$ : <5  $\mu\text{g/mL}$ ).

The two barbiturates **6e** (3,5-di-Br) and **6g** (4-tBu) were the second most potent derivatives displaying MIC values of 1–8  $\mu\text{g/mL}$  against the bacterial reference strains and were both less hemolytic (**6e**  $\text{EC}_{50}$ : 79  $\mu\text{g/mL}$  and **6g**  $\text{EC}_{50}$ : 145  $\mu\text{g/mL}$ ). These had smaller lipophilic side chains and implied a correlation between side chain size or calculated side chain Clog  $P$  and antimicrobial activity.

The 3,5-di-substituted derivative **6f** (3,5-di- $\text{CF}_3$ ) was less potent and displayed MIC values of 16  $\mu\text{g/mL}$  against all strains except for the very susceptible strain *C. glutamicum* (MIC: 4  $\mu\text{g/mL}$ ). The *C. glutamicum* strain is a valuable strain for identifying antimicrobial agents in screenings since it is so susceptible but is otherwise not of any medical importance. Its high susceptibility resulted in that none of the barbiturates from series **6** (nor series **7**) displayed MIC values above 4  $\mu\text{g/mL}$  against *C. glutamicum*.

It is noteworthy that the calculated Clog  $P$  of **6e** (3,5-di-Br) was lower than the calculated Clog  $P$  of the less potent **6f** (3,5-di- $\text{CF}_3$ ), showing that not only the lipophilic effects of the side chains affected the antimicrobial potency but possibly also the size and electronic effects. With respect to electronic effects, a difference in electron distribution was observed both in  $^{13}\text{C}$  NMR and when calculating the electron density of the bromine and trifluoromethyl substituents of **6e** (3,5-di-Br) and **6f** (3,5-di- $\text{CF}_3$ ). The electron distribution in the side chains of **6e** (3,5-di-Br) and **6f** (3,5-di- $\text{CF}_3$ ) was different hosting an overall more negative partial charge on the  $\text{CF}_3$  groups compared to the bromine substituents (results not shown). This may affect the electron distribution of the aromatic side chains and possibly affect the lipophilic side chains in their interaction with the bacterial membrane and especially related to

**Table 2.** Antimicrobial Activity (MIC in  $\mu\text{g/mL}$ ) of Selected Amine (Series 6) and Guanidine (Series 7) Barbiturates against 30 Multi-resistant Clinical Isolates<sup>a</sup>

Toxicity	Amine barbiturates								Guanidine barbiturates								
	6a	6b	6c	6d	6e	6f	6g	6h	7a	7b	7c	7d	7e	7f	7g	7h	
RBC EC <sub>50</sub>	>398	250	160	172	79	177	145	<5	>449	133	90	77	62	98	77	<6	
HepG2 IC <sub>50</sub>	40	7	5	6	4	9	3	2	104	59	56	15	30	19	28	15	
MRC-5 IC <sub>50</sub>	16	2	2	10	2	17	1	1	74	30	23	36	11	29	14	17	
<b>Clinical isolates</b>	ESBL–CARBA <sup>b</sup>																
<i>S. aureus</i> N315	>32	8	8	8	4	16	8	2	4	8	2	2	2	2	2	4	
<i>S. aureus</i> NCTC 10442	>32	8	8	8	4	16	8	2	4	8	2	4	2	2	2	2	
<i>S. aureus</i> strain 85/2082	>32	8	4	4	4	16	8	2	4	8	2	2	2	2	2	2	
<i>S. aureus</i> strain WIS	>32	8	8	8	4	16	8	2	4	8	2	2	2	2	2	2	
<i>S. aureus</i> IHT 99040	>32	8	8	4	4	16	8	2	8	8	2	2	2	2	2	2	
<i>E. faecium</i> 50673722	>32	16	8	16	4	8	8	2	32	16	4	4	4	2	2	2	
<i>E. faecium</i> 50901530	>32	8	4	8	4	8	4	2	8	8	4	2	2	2	4	2	
<i>E. faecium</i> K36-18	>32	16	8	16	8	16	8	2	32	16	4	4	4	4	2	2	
<i>E. faecium</i> 50758899	>32	16	8	16	4	16	8	2	>32	16	4	4	4	4	2	2	
<i>E. faecium</i> TUHSO-22	>32	8	4	4	4	8	8	2	32	8	4	2	2	2	2	2	
<i>E. coli</i> 50579417	>32	16	16	16	8	16	8	4	32	16	8	4	4	8	4	16	OXA-48
<i>E. coli</i> 50639799	>32	16	16	16	8	16	8	4	16	8	4	4	4	4	4	8	VIM-29
<i>E. coli</i> 50676002	>32	16	16	16	8	16	4	8	32	8	4	4	4	4	4	16	NDM-1
<i>E. coli</i> 50739822	>32	16	16	16	8	16	8	4	32	8	8	4	4	8	4	8	NDM-1
<i>E. coli</i> 50857972	>32	16	16	16	8	8	4	4	16	8	4	4	4	4	4	8	IMP-26
<i>P. aeruginosa</i> K34-7	>32	32	32	32	16	32	>32	8	>32	32	16	16	8	16	16	16	VIM-2
<i>P. aeruginosa</i> K34-73	>32	32	32	32	16	32	>32	16	>32	32	8	8	8	16	8	8	VIM-4
<i>P. aeruginosa</i> K44-24	>32	>32	32	32	16	32	>32	8	>32	32	16	16	8	16	16	16	IMP-14
<i>P. aeruginosa</i> 50692172	>32	32	16	32	16	32	>32	8	>32	32	16	32	8	16	16	16	NDM-1
<i>P. aeruginosa</i> 50692520	>32	32	16	32	16	32	>32	8	>32	32	16	16	16	16	16	16	VIM
<i>K. pneumoniae</i> K47-25 <sup>c</sup>	>32	>32	>32	32	16	>32	>32	16	>32	16	8	4	4	16	4	16	KPC-2
<i>K. pneumoniae</i> K66-45	>32	>32	32	32	16	32	32	8	>32	16	4	8	4	16	4	8	NDM-1
<i>K. pneumoniae</i> 50531633 <sup>c</sup>	>32	32	16	16	8	32	16	8	>32	16	8	4	4	16	4	16	NDM-1+OXA-181
<i>K. pneumoniae</i> 50625602	>32	>32	32	32	16	32	16	8	>32	16	16	4	4	8	4	16	OXA-245
<i>K. pneumoniae</i> 50667959	>32	>32	32	32	16	32	32	8	>32	16	4	8	4	16	16	8	VIM-1
<i>A. baumannii</i> K12-21	>32	32	32	32	16	16	16	4	>32	32	8	8	4	16	4	4	OXA-58
<i>A. baumannii</i> K44-35	>32	32	32	32	16	32	32	4	>32	32	8	8	4	16	8	4	OXA-23
<i>A. baumannii</i> K47-42	>32	32	32	32	16	32	16	4	>32	32	8	8	4	16	8	4	OXA-23
<i>A. baumannii</i> K55-13	>32	32	32	32	16	32	16	4	>32	32	8	8	8	16	8	4	OXA-24
<i>A. baumannii</i> K63-58 <sup>c</sup>	>32	16	16	32	16	32	16	4	>32	32	8	8	4	16	4	4	OXA-23

<sup>a</sup>Toxicity is displayed as the hemolytic activity against human RBCs (EC<sub>50</sub> in  $\mu\text{g/mL}$  from Table 1) and cytotoxicity against HepG2 and MRC-5 cells (IC<sub>50</sub> in  $\mu\text{g/mL}$ ). <sup>b</sup>ESBL–CARBA: extended spectrum  $\beta$ -lactamase–carbapenemase producing isolates. OXA, oxacillinase; VIM, verona integron-encoded metallo- $\beta$ -lactamase; NDM, New Delhi metallo- $\beta$ -lactamase; IMP, imipenem-type carbapenemase; and KPC, *K. pneumoniae* carbapenemase. <sup>c</sup>Clinical isolates resistant to the antibiotic colistin.

localization in the water–lipid interface region of the membrane. This may also explain why **6f** (3,5-di-CF<sub>3</sub>) displayed much lower hemolytic activity (EC<sub>50</sub>: 177  $\mu\text{g/mL}$ ) than **6e** (3,5-di-Br) (EC<sub>50</sub>: 79  $\mu\text{g/mL}$ ).

The 3,4-disubstituted derivative **6d** (3-Cl, 4-Br) displayed high antimicrobial activity against the Gram-positive reference strains (MIC: 1–4  $\mu\text{g/mL}$ ) but was clearly less potent than the previous derivatives against the Gram-negative reference strains (MIC: 16–32  $\mu\text{g/mL}$ ). Derivative **6d** (3-Cl, 4-Br) also showed very low hemolytic activity (EC<sub>50</sub>: 172  $\mu\text{g/mL}$ ).

The Nal-derivatives **6b** (2-Nal) and **6c** (4-F-1-Nal) showed comparable antimicrobial activities, that is, MIC: 1–8  $\mu\text{g/mL}$

against the Gram-positive reference strains and MIC: 8–16  $\mu\text{g/mL}$  against the Gram-negative strains. These Nal derivatives differed slightly in calculated side chain lipophilicity [**6b** (2-Nal): Clog *P* 3.82, and **6c** (4-F-1-Nal): Clog *P* 3.96]. An important prospect with these Nal derivatives is possible tuning of pharmacokinetic properties related to phase I hepatic oxidations *in vivo*. Our previous studies on small  $\beta^{2,2}$ -amino acid-based AMP peptidomimetics have shown that 2-Nal side chains can be extensively oxidized by liver microsomes, which is a model system used to assess the potential hepatic phase I metabolism.<sup>17,28</sup> This oxidation is however reduced by having electron-withdrawing aromatic fluorine substituents such as in



**6c** (4-F-1-Nal). Aromatic fluorine substituents are often used as “metabolic blockers” in drugs to improve the pharmacokinetic properties.<sup>29</sup> Both Nal-derivatives **6b** (2-Nal) and **6c** (4-F-1-Nal) showed very low hemolytic activity. When comparing the hemolytic results in detail, the somewhat less lipophilic derivative **6b** (2-Nal) displayed lower hemolytic activity ( $EC_{50}$ : 250  $\mu\text{g}/\text{mL}$ ) than **6c** (4-F-1-Nal) ( $EC_{50}$ : 160  $\mu\text{g}/\text{mL}$ ). In this case, a small modification by having an aromatic fluorine-substituent seemingly had an impact on RBC toxicity.

A surprisingly low antimicrobial activity was observed for the least lipophilic derivative **6a** (4- $\text{CF}_3$ ), which only had acceptable antimicrobial activity against *C. glutamicum* but very low potency against the remaining reference strains (MIC: 64–128  $\mu\text{g}/\text{mL}$ ). Derivative **6a** (4- $\text{CF}_3$ ) was also all together non-hemolytic within the concentration range tested ( $EC_{50}$ : >398  $\mu\text{g}/\text{mL}$ ).

**Guanidine Barbiturates of Series 7 against the Reference Strains.** Guanylation of the amine barbiturates in series **6** resulted in a striking increase in the antimicrobial activity of the resulting guanidine barbiturates in series **7** (Table 1). The highly potent guanylated barbiturates of series **7** displayed a narrow range in the MIC values of <0.13–2  $\mu\text{g}/\text{mL}$  against the Gram-positive strains *S. aureus* and *C. glutamicum* and MIC 1–8  $\mu\text{g}/\text{mL}$  against the Gram-negative bacteria *E. coli* and *P. aeruginosa*. One exception lacking increased potency against *P. aeruginosa* was **7a** (4- $\text{CF}_3$ ) (MIC: 64  $\mu\text{g}/\text{mL}$ ), which was the smallest guanidine derivative (in volume) and least lipophilic derivative.

Overall, the results for the guanidine series **7** followed the structural considerations discussed for the antimicrobial activity of the amine barbiturates in series **6**. Highest broad-spectrum antimicrobial activity (MIC  $\leq 4$   $\mu\text{g}/\text{mL}$ ) was displayed by **7c** (4-F-1-Nal), **7e** (3,5-di-Br), **7g** (4-tBu), and **7h** (3,5-di-tBu). The guanylated barbiturates **7b** (2-Nal), **7d** (3-Cl, 4-Br), and **7f** (3,5-di- $\text{CF}_3$ ) showed the same high potency against the Gram-positive reference strains and *E. coli* but a little lower activity against *P. aeruginosa*. Altogether, the differences in MIC values were small. The largest improvements in the antimicrobial activity following guanylation was observed for **7a** (4- $\text{CF}_3$ ) and **7f** (3,5-di- $\text{CF}_3$ ) against the Gram-positive reference strains and *E. coli*.

The guanylated barbiturates of series **7** were in comparison more hemolytic than the amine barbiturates in series **6**, and only derivatives, **7a** (4- $\text{CF}_3$ ) and **7b** (2-Nal), displayed hemolytic toxicity with  $EC_{50}$  values above 100  $\mu\text{g}/\text{mL}$ . The guanylated barbiturates **7c** (4-F-1-Nal), **7d** (3-Cl, 4-Br), **7e** (3,5-di-Br), **7f** (3,5-di- $\text{CF}_3$ ), and **7g** (4-tBu) displayed hemolytic toxicity in the range  $EC_{50}$ : 62–98  $\mu\text{g}/\text{mL}$ , whereas the super-bulky barbiturate **7h** (3,5-di-tBu) was highly hemolytic ( $EC_{50}$ : <6  $\mu\text{g}/\text{mL}$ ).

The general increase in the hemolytic activity following guanylation can be a result of the larger guanidine group forming more intricate electrostatic and hydrogen-bonding interactions than a primary amine group and thereby interact with both anionic and zwitterionic phospholipids (PLs). As we and others have reported, there is little consistency, and both increase and reduction of RBC toxicity is observed when amine groups are interchanged by guanidine groups.<sup>17,30–34</sup>

**Antimicrobial Activity against 30 Multi-resistant Clinical Isolates.** The amine and guanidine barbiturates were screened against a panel of 30 multi-resistant clinical isolates of Gram-positive and Gram-negative bacteria (Table 2). These isolates represented different resistance mechanisms,

in which the Gram-positive isolates were methicillin-resistant *S. aureus* (MRSA) and vancomycin-resistant *Enterococcus faecium* (VRE), and the Gram-negative isolates included multi-resistant *E. coli*, *P. aeruginosa*, *Klebsiella pneumoniae*, and *Acinetobacter baumannii* with extended spectrum  $\beta$ -lactamase–carbapenemase (ESBL–CARBA) production. Three strains were also resistant to the last resort antibiotic colistin. Cytotoxicity was also determined against human hepatocyte carcinoma cells (HepG2) and human lung fibroblast cells (MRC-5).

Antimicrobial activity against the multi-resistant clinical isolates was high with MIC values as low as 2–4  $\mu\text{g}/\text{mL}$  for the most potent barbiturates, thereby following the same tendencies as against the antibiotic susceptible reference strains. As opposed to RBC toxicity, the guanidine barbiturates of series **7** were less cytotoxic against human HepG2 and MRC-5 cells compared to the amine barbiturates of series **6** (Table 2). The interplay between the two different cationic groups and the various lipophilic side chains thereby influenced the antimicrobial potency, hemolytic toxicity, and human cell cytotoxicity differently.

For the amine barbiturates of series **6**, highest antimicrobial potencies (MIC: 2–16  $\mu\text{g}/\text{mL}$ ) were achieved against the Gram-positive multi-resistant clinical isolates of *S. aureus* and *E. faecium* and the Gram-negative isolates of *E. coli*. The overall most potent amine barbiturate of series **6** was **6h** (3,5-di-tBu), closely followed by **6e** (3,5-di-Br). These amine derivatives showed high potency also against the clinical challenging isolates of *P. aeruginosa*, *K. pneumoniae*, and *A. baumannii*. The high cytotoxicity against human HepG2 and MRC-5 cells ( $IC_{50}$ : 1–17  $\mu\text{g}/\text{mL}$ ) displayed by the active amine barbiturates of series **6** was unsatisfactory.

The guanidine series **7** represented a major increase in the antimicrobial activity against the Gram-negative multi-resistant clinical isolates compared to the amine series **6**. The guanidine barbiturates of series **7** were also less cytotoxic against human HepG2 and MRC-5 cells compared to the amine barbiturates of series **6**. The most potent broad-spectrum guanidine barbiturates were **7c** (4-F-1-Nal), **7d** (3-Cl, 4-Br), **7e** (3,5-di-Br), **7f** (3,5-di- $\text{CF}_3$ ), **7g** (4-tBu), and **7h** (3,5-di-tBu) displaying MIC values of 2–16  $\mu\text{g}/\text{mL}$  (Table 2). The cytotoxicity of these guanidine barbiturates against human HepG2 and MRC-5 cells was in the range  $IC_{50}$ : 11–59  $\mu\text{g}/\text{mL}$  and thereby less cytotoxic than the amine barbiturates of series **6**. The broad-spectrum guanidine barbiturate **7e** (3,5-di-Br) showed overall highest antimicrobial potency against all multi-resistant clinical isolates tested and became the selected compound for the *in vivo* pilot study described below.

It should also be noted that the least lipophilic guanidine barbiturate **7a** (4- $\text{CF}_3$ ) may be a promising compound when considering specifically MRSA infections by its high potency (MIC: 4–8  $\mu\text{g}/\text{mL}$ ) against the clinical multi-resistant *S. aureus* isolates, low cytotoxicity against human HepG2 ( $IC_{50}$ : 104  $\mu\text{g}/\text{mL}$ ) and MRC-5 cells ( $IC_{50}$ : 74  $\mu\text{g}/\text{mL}$ ), and by being all together non-hemolytic ( $EC_{50}$ : >449  $\mu\text{g}/\text{mL}$ , Table 2).

All the investigated amphipathic barbiturates displayed antimicrobial activity against the three colistin-resistant clinical isolates *K. pneumoniae* K47-25, *K. pneumoniae* S0531633, and *A. baumannii* K63-58 in the same range as against the colistin-susceptible clinical isolates. The mechanism of resistance of these clinical isolates is thought to involve altered lipopolysaccharide (LPS) outer cell wall composition and charge, changes that affect the mechanism of action of the last-resort cationic antibiotic colistin (pers. commun. prof Ø. Samuelson).

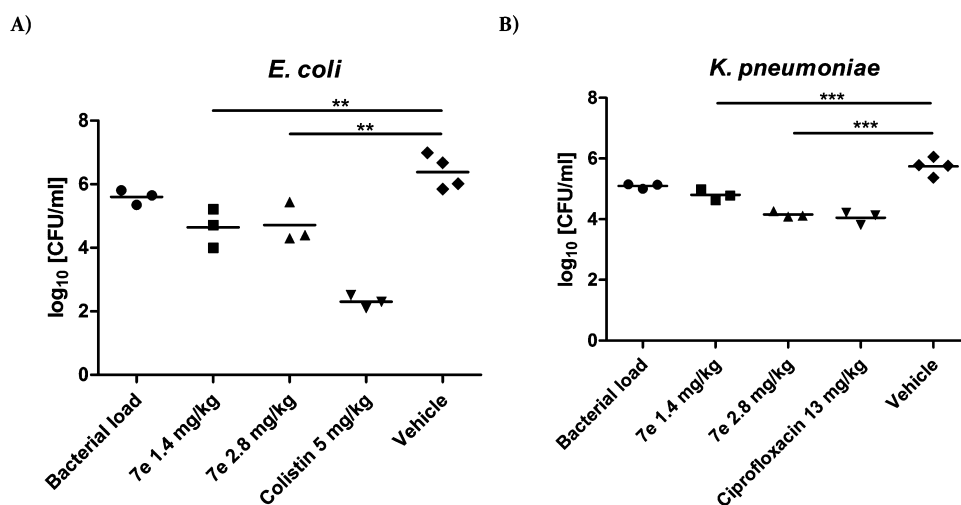


**Figure 3.** Reduction in the CFU of (A) *E. coli* (EC106-09) and (B) *K. pneumoniae* (KP3010) after i.p. treatment with 1.4 mg/kg (1 h post-infection) and 2.8 mg/kg (1.4 mg/kg 1 h + 3 h post-infection) of 7e (3,5-di-Br) compared to single i.p. treatment with (A) colistin (positive control, 5 mg/kg 1 h post-infection) and (B) ciprofloxacin (positive control, 13 mg/kg, 1 h post-infection) and vehicle (negative control, 1 h post-infection) was observed. The symbols ( $\blacktriangle$ ,  $\blacklozenge$ ,  $\bullet$ ,  $\blacktriangledown$ , and  $\blacksquare$ ) represent the individual mice in the experiment. The horizontal line represents the mean value of CFU counted for the parallels for the same experiment. Asterisks indicate the significant difference between vehicle control and treatment with 7e (Dunnet's test;  $**p < 0.01$  and  $***p < 0.001$ ).

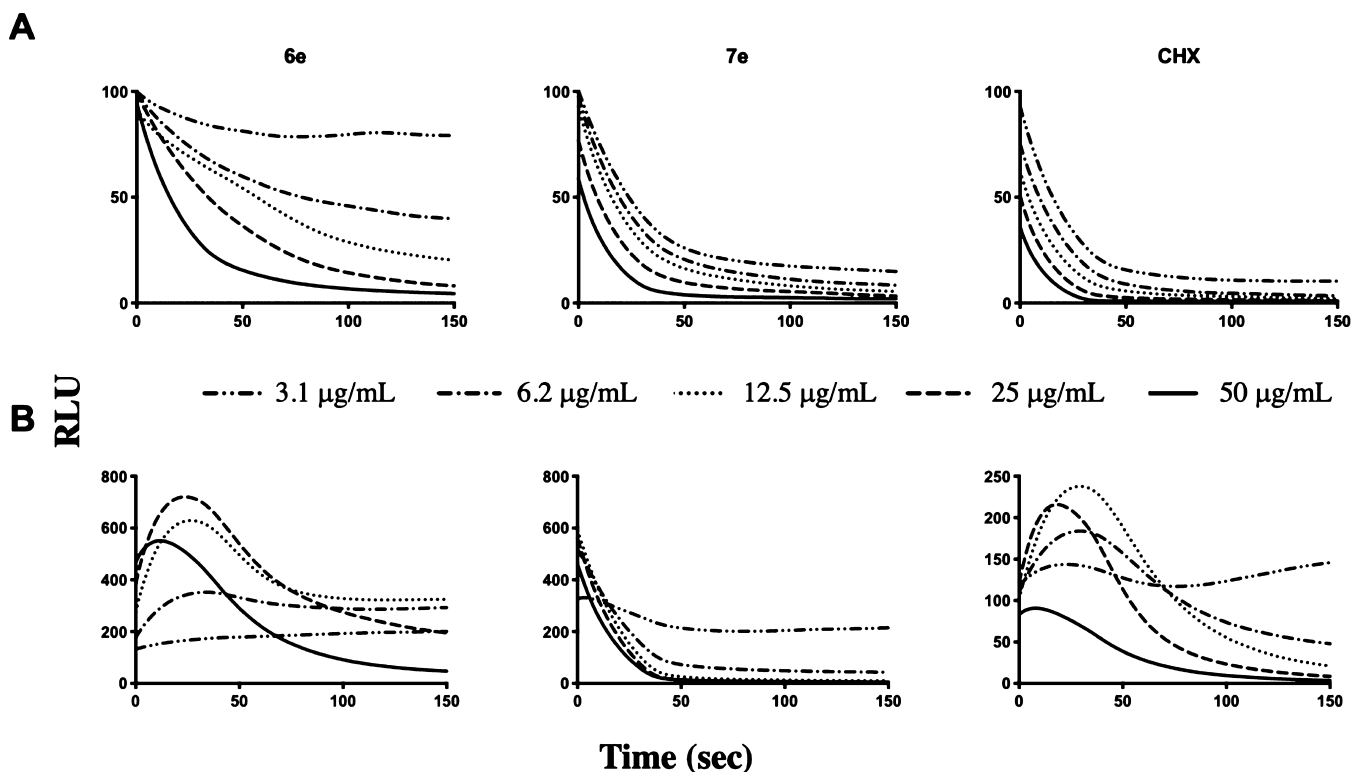


**Figure 4.** Comparison of the effects of 6e (3,5-di-Br), 7e (3,5-di-Br), and CHX on the kinetics of (A) viability and (B) membrane integrity in *B. subtilis*. Light emission normalized to an untreated water control (negative control) is plotted as relative light units (RLUs) over time (seconds) with untreated luminescence set to 100 RLU. After addition of the bacterial cell suspension (with 1 mM D-luciferin for the membrane integrity assay) to the analytes in each well, the light emission was measured each second for 150 s. Each line represents the kinetics of 150 subsequent data points of the analyte concentration. Each analysis was repeated at least three times independently. The figure shows a representative data set.

The altered LPS structure seemed not to have any major impact on the binding and activity of the most potent amphipathic barbiturates.

**In Vivo Efficacy of 7e (3,5-di-Br) in a Murine Neutropenic Peritonitis Model.** The overall most potent guanidine barbiturate 7e (3,5-di-Br) was investigated *in vivo*

using an established murine peritonitis model at Statens Serum Institut (SSI, Denmark).<sup>35</sup> Our aim was to determine the efficacy of 7e (3,5-di-Br) in mice infected with clinical isolates of *E. coli* (EC106-09) and *K. pneumoniae* (KP3010). Initially, the MIC of 7e (3,5-di-Br) was determined to be 4  $\mu\text{g}/\text{mL}$  against both strains, which was in coherence with our previous

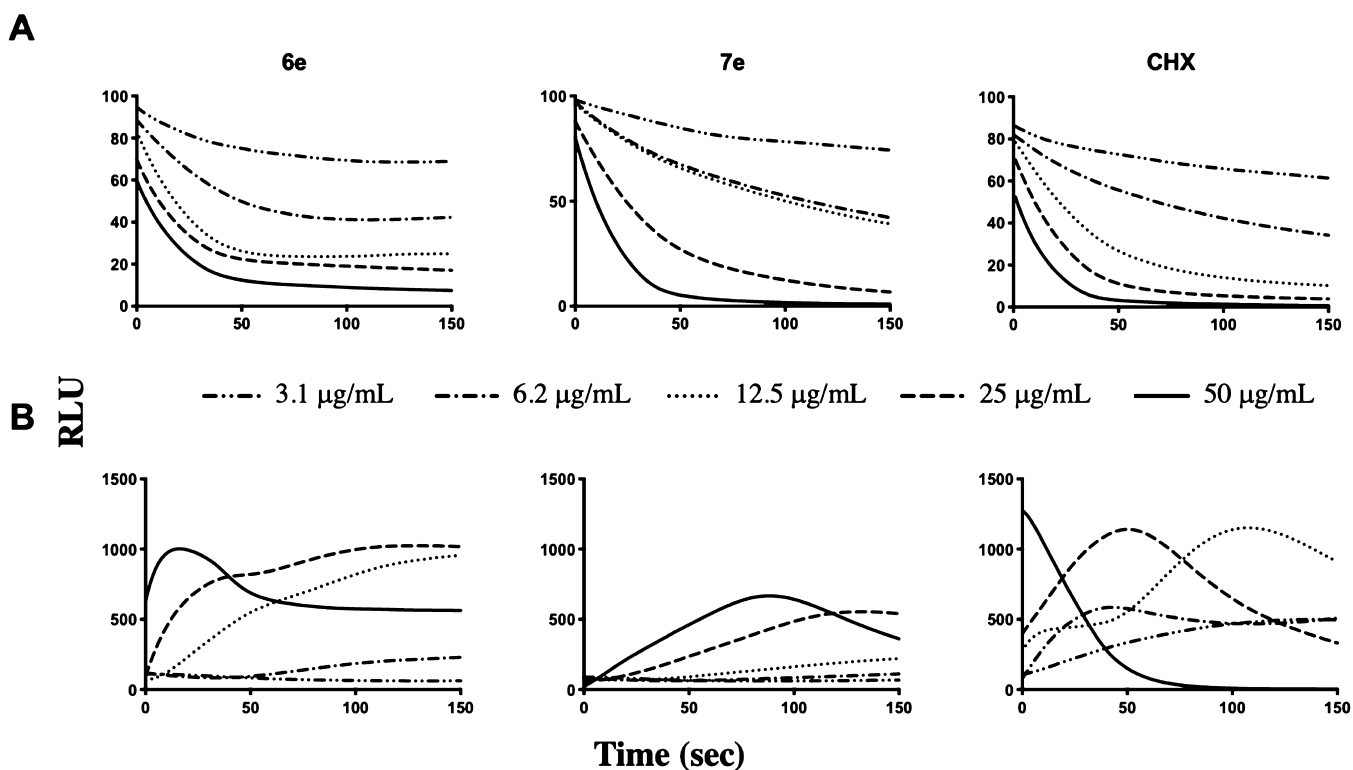


**Figure 5.** Comparison of the effects of **6e** (3,5-di-Br), **7e** (3,5-di-Br), and CHX on the kinetics of (A) viability and (B) membrane integrity in *E. coli*. Light emission normalized to the untreated water control (negative control) is plotted as RLU over time (seconds) with untreated luminescence set to 100 RLU. After addition of the bacterial cell suspension (with 1 mM D-luciferin for the membrane assay) to the analytes in each well, the light emission was measured each second for 150 s. Each line represents the kinetics of 150 subsequent data points of the analyte concentration. Each analysis was repeated at least three times independently. The figure shows a representative data set.

screening results. A maximal tolerated dose (MTD) was determined prior to evaluation of *in vivo* efficacy. In brief, the MTD was determined by intraperitoneal (i.p.) injection of escalating doses of derivative **7e** (3,5-di-Br). Derivative **7e** (3,5-di-Br) was well tolerated up to 2.8 mg/kg after i.p. injection with no or mild clinical signs of discomfort. At 3.6 mg/kg, moderate signs of discomfort were observed, but the mice recovered within a few hours. The MTD was determined to be 7 mg/kg.

In our vehicle controls, a log colony-forming unit per mL (CFU/mL) of 6.4 was determined for *E. coli*, indicating a 0.8 log CFU increase at the end of the experiment. A log CFU/mL of 5.7 was determined for *K. pneumoniae* corresponding to an approximately 0.6 CFU/mL increase at the end of the experiment. In contrast, treatment with **7e** (3,5-di-Br) caused a 1.7-log (98%) reduction of the bacterial loads of *E. coli* already at a concentration of 1.4 mg/mL (Figure 3A). Treatment with 1.4 mg/kg of **7e** (3,5-di-Br) against *K. pneumoniae* resulted in a 1 log CFU/mL reduction (90%) compared to treatment with vehicle (Figure 3B). A repeated injection after 3 h with **7e** (3,5-di-Br) resulted in a 1.6 log CFU/mL (97%) reduction of the bacterial load. Despite limitations regarding the MTD, our results demonstrated that **7e** (3,5-di-Br) could significantly reduce the number of viable bacterial cells in this *in vivo* model. We can conclude that the complex environment of the peritoneal cavity and the peritoneal fluid did not lead to a rapid inactivation of **7e** (3,5-di-Br). However, at this point, we can only speculate about the time range **7e** (3,5-di-Br) is present in sufficient concentrations for effective bacterial killing. Pharmacokinetic

studies as well as different routes of administration have to be undertaken in order to fully reveal the potential of this type of compound *in vivo*.

**Mode of Action Studies.** The amphipathic amine barbiturate **6e** (3,5-di-Br) and guanidine barbiturate **7e** (3,5-di-Br) were compared in a mode of action study using two luciferase-based biosensor assays in *Bacillus subtilis* 168 and *E. coli* HB101 (Figures 4 and 5).<sup>36,37</sup> The two different biosensor systems evaluate the effects on bacterial viability and membrane integrity, respectively, which are closely linked functionalities in bacterial cells (see the Supporting Information; Section S9 for detailed information regarding the assays). The bacteriolytic agent chlorhexidine (CHX), known for its membrane-disruptive properties, was analyzed for comparison.<sup>38</sup>

The overall results demonstrated a strong and immediate membrane disrupting activity for both compounds. A more rapid membranolytic effect was observed against the Gram-positive *B. subtilis* compared to Gram-negative *E. coli*. We also observed the differences in the rate of membrane lysis related to the test concentrations, in which concentrations higher than the MIC value led to a more rapid lysis, that is, a concentration-dependent killing effect.

The observed effects in the viability assay corresponded well with the respective MICs [**6e** (3,5-di-Br): 6.3 µg/mL and **7e** (3,5-di-Br): 3.1 µg/mL against both *B. subtilis* and *E. coli* biosensor strains], in spite of an initial 1000-fold higher concentration of bacteria in the inoculum compared to the MIC assay. The decrease in light emission was rapid, dose-dependent, and similar to the CHX control, suggesting a

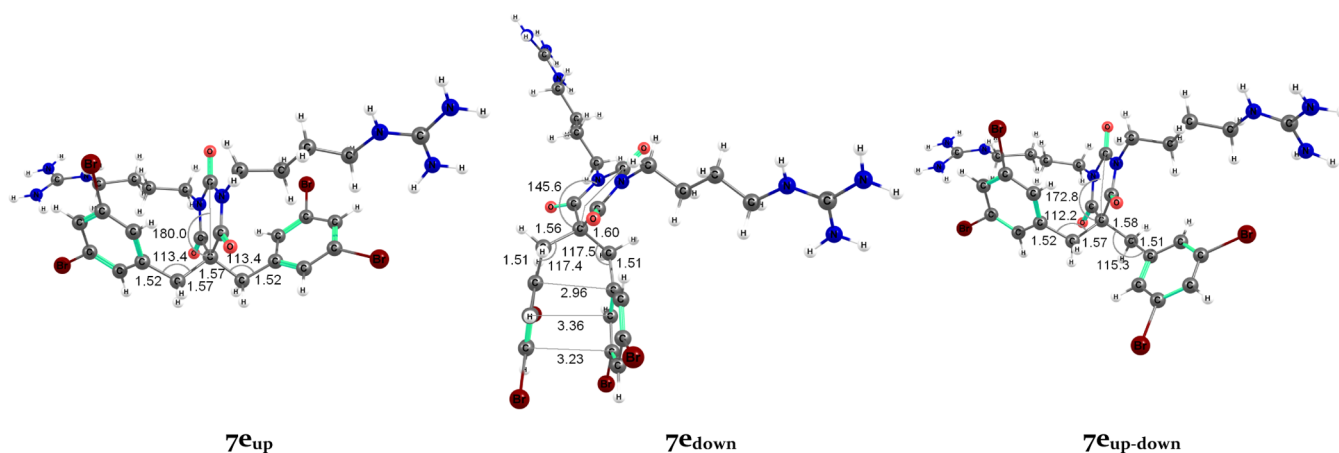


**Figure 6.** Optimized geometries from DFT calculations of  $7e_{up}$  (left, also described as the W-shaped conformation),  $7e_{down}$  (middle), and  $7e_{up-down}$  (right). The bond distances are reported in Å and the bond angles are given in degrees.

membrane-related mode of action against both strains (Figures 4A and 5A). In order to confirm that the rapid decrease in bacterial viability was due to membrane damage, the membrane integrity assay was performed. Also, in this assay, a dose-dependent effect was observed against both strains (Figures 4B and 5B). The effects (rapid peak emission due to the influx of D-luciferin into the cells) were for the most part coinciding with the respective MIC values, indicating that membrane damage was indeed a major effect. The well-by-well measurements allowed for catching the actual light peaks, apart from measurements with  $7e$  (3,5-di-Br) in *B. subtilis*, which seemed to act substantially faster than  $6e$  (3,5-di-Br) and CHX and therefore only showed a decrease in light emission from a level substantially higher than the control (Figure 4B).

When comparing the results obtained from the viability assay (Figure 4A) and the membrane integrity assay (Figure 4B) in *B. subtilis* for compounds  $6e$  (3,5-di-Br),  $7e$  (3,5-di-Br), and CHX, the patterns appeared somewhat similar, indicating a rapid membranolytic activity for all compounds. However, in the membrane integrity assay in *B. subtilis*, we were not able to determine a peak in light emission for any concentration above MIC for  $7e$  (3,5-di-Br) (Figure 4B). Light emission declined immediately, indicating that peak emission already had occurred before the first measurement, that is, within 2 s after analyte addition. At MIC (3.1  $\mu\text{g/mL}$ ), a small peak in light emission was observed after approximately 5 s, but the emission did neither decrease nor increase substantially within the measurement window. Altogether, the effect of  $7e$  (3,5-di-Br) on *B. subtilis* shown in the viability assay seemed to be immediate (Figure 4A) and corresponded to the membranolytic effect shown in the membrane integrity assay (Figure 4B).

In *E. coli*, the observed overall picture was somewhat different. A rise or peak of light emission in the membrane integrity assay for  $6e$  (3,5-di-Br) coincided with an immediate decrease of light emission in the viability assay (similar to the results in *B. subtilis*) (Figure 5). However, an emission peak was not reached for the lowest (1–4 $\times$  MIC) concentrations of  $7e$  (3,5-di-Br) within the 150 s test window in the membrane integrity assay (Figure 5B). On the other hand, the concentration-dependent reduction in viability observed with the guanidine barbiturate  $7e$  (3,5-di-Br) resembled the results of the guanidine-containing CHX (Figure 5A), but the decrease in viability was substantially slower than for similar concentrations in *B. subtilis* (Figure 4B). In general, the

membrane integrity effects of all tested compounds seemed to occur at a slightly slower rate in the Gram-negative *E. coli* compared to the Gram-positive *B. subtilis*. It is tempting to speculate that especially for  $7e$  (3,5-di-Br), the outer membrane of *E. coli* acted as a barrier, causing a delayed action in the membrane integrity assay. This would however not explain the presence of light production at a time point where the viability assay emits almost no light at all and accordingly indicates complete metabolic shutdown. This effect, even though less pronounced, was also observable for  $6e$  (3,5-di-Br) and the CHX control. Although ATP is necessary for replenishment of the fatty aldehyde pool, this might indicate that reduction equivalents were the limiting factor for light emission of the viability sensor assay and that ATP under these conditions was not a limiting factor after treatment with  $6e$  (3,5-di-Br), and especially,  $7e$  (3,5-di-Br) until after the measurement window ended. Alternatively, there were different subpopulations of bacterial cells present, with different susceptibility to the analytes, resulting in an average light emission, which does not represent any of the subpopulations.

While the main mode of action against *B. subtilis* for both  $6e$  (3,5-di-Br) and  $7e$  (3,5-di-Br) seemed to be disruption of membrane integrity, our results did not exclude the possibility that especially  $7e$  (3,5-di-Br) might have additional targets than the bacterial cytoplasmic membrane. Further work is needed to elucidate if  $7e$  (3,5-di-Br) possibly targets other components of the cell and if there is a dual mode of action.

**Conformational Analysis and Membrane Interaction Simulations.** To gain insights into the interactions of the amphipathic barbiturates with a PL membrane surface, we determined the most stable conformations of the barbiturates, followed by a membrane interaction simulation. Density functional theory (DFT)-based geometry optimizations of amine  $6e$  (3,5-di-Br) and guanidine  $7e$  (3,5-di-Br) gave similar distortions and energy differences and indicated three low-energy conformations mainly differing in the orientation of the benzylic side chains (Figure 6). In the up ( $7e_{up}$ ), down ( $7e_{down}$ ), and up-down ( $7e_{up-down}$ ) conformations, the benzylic side chains were either directed upward in a W-shape, downward, or having one side chain pointing up and the other pointing down. The  $7e_{up}$  conformation was lowest in energy, whereas  $7e_{up-down}$  and  $7e_{down}$  were 4.9 and 9.8 kcal/mol higher in energy, respectively (see Supporting Information

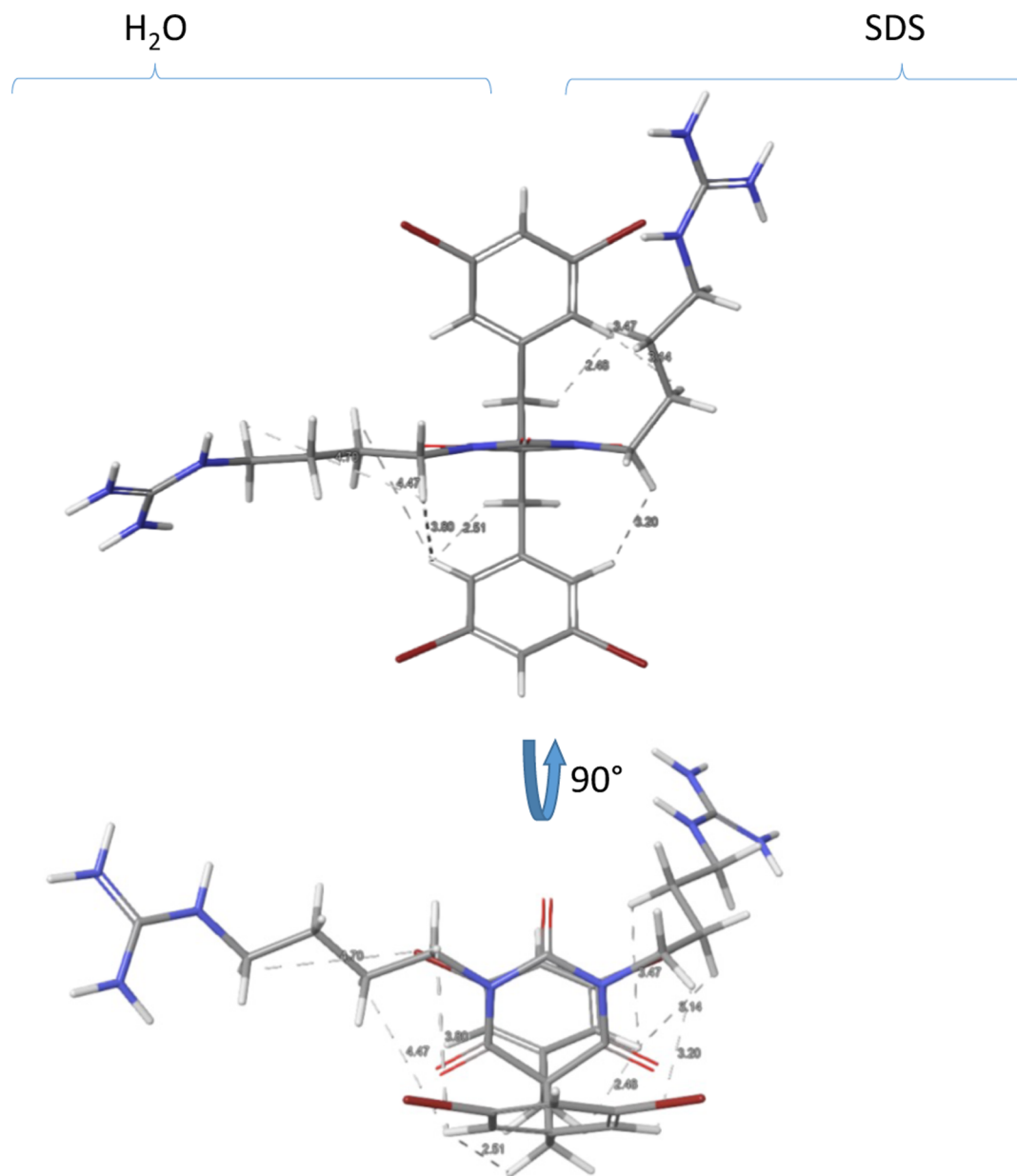


**Figure 7.** Schematic visualization of the observed ROESY correlations for **7e** (3,5-di-Br) in water (left side) and in SDS (right side) using sculpted structures.

Section S10 for more details of the conformational analysis). An X-ray structure of **7b** (2-Nal) supported the low energy conformation suggested by DFT calculations (see [Supporting Information](#) Section S11 for details).

The ROESY spectra acquired in water and micelle [sodium dodecyl sulfate (SDS)] solutions of the guanidine barbiturate **7e** (3,5-di-Br) were used to qualitatively assess the conformation experimentally (see [Supporting Information](#) Section 12 for details of the NMR conformational analysis). The structural NMR data in water ([Figure 7](#), left side) supported the orientations of the benzylic side chains described by the DFT calculations. It was evident from the ROESY detectable correlations between H7 and H10–H12 (5–10% of the reference volume) that the benzylic side chains and the barbiturate ring adopted the W-shape (similar to the **7e<sub>up</sub>** conformation in [Figure 6](#)). There were no dramatic conformational changes in SDS, but there was a shift of

populations that made the guanidine side chains spend more time closer to the 3,5-dibromophenyl rings ([Figure 7](#), right side). This was reflected in the volumes of the H7/H11,12 cross-peaks that increased from ~10 to ~40% of the reference volume.

MD simulations were used to elucidate details on the membrane interactions of **7e** (3,5-di-Br) with an *E. coli* inner membrane model ([Figure 8](#)).<sup>39</sup> Similar MD simulations of **6a** (4-CF<sub>3</sub>), **6e** (3,5-di-Br), **6g** (4-tBu), and **7g** (4-tBu) are included in the [Supporting Information](#) (Table S3 and Figures S6–S10), and a possible explanation to the low potency of **6a** (4-CF<sub>3</sub>) is included below. For each compound, three parallel simulations were performed.

The course of the membrane insertion was tracked by following the location of the sp<sup>3</sup> carbon opposite from the carbonyl carbon (C<sub>5</sub>), as noted by the *z*-coordinate position in the simulation box ([Figure 8B](#)). The lipid bilayer surface (black

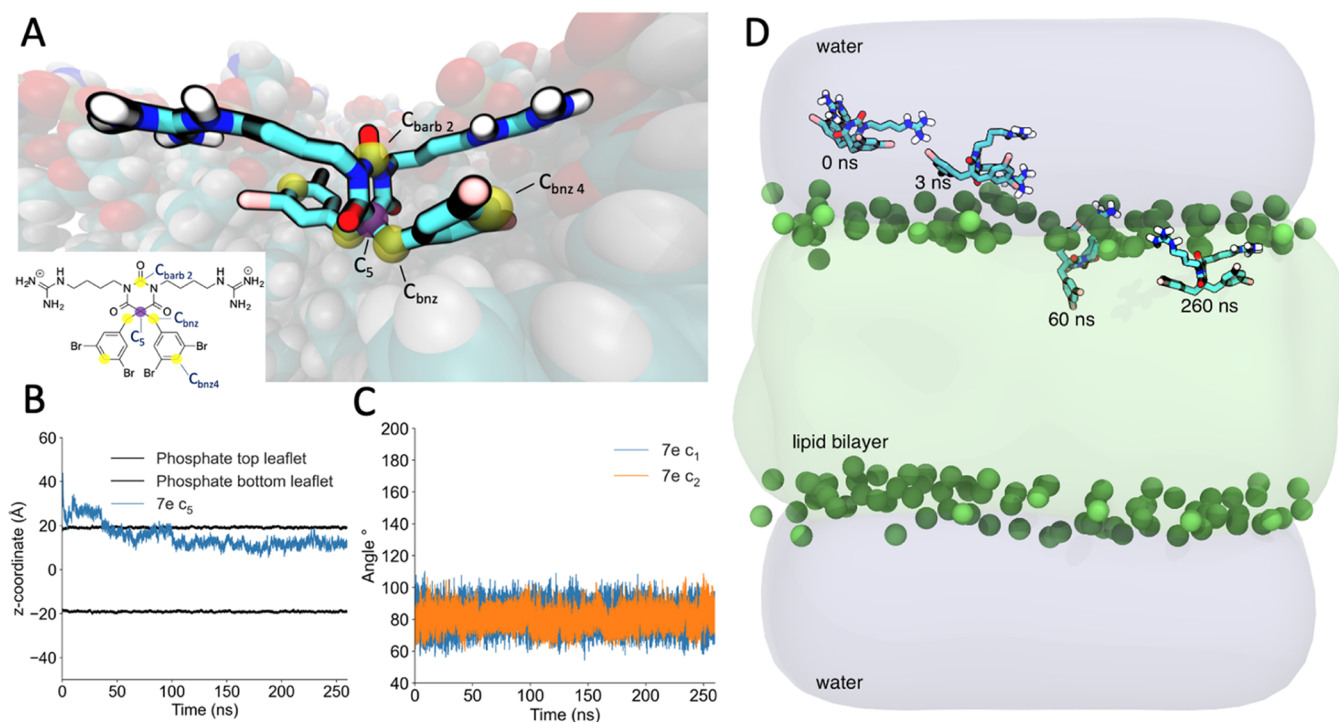


**Figure 8.** MD simulations of the interactions and conformations of **7e** (3,5-di-Br) in an *E. coli* inner membrane model. (A) **7e** (3,5-di-Br) in the membrane environment after 260 ns and the naming of atoms used for tracking of the compound. The purple sphere highlights carbon  $C_5$ , which was the atom used for tracking the position of **7e** (3,5-di-Br) with respect to the PL headgroups ( $z$ -coordinate). The yellow spheres highlight atoms  $C_{\text{barb}2}$ ,  $C_{\text{bnz}}$ , and  $C_{\text{bnz}4}$ , which formed the tracked angles  $c_1$  or  $c_2$  representing the conformation of two benzylic side chains. (B) Time evolution for location of the  $C_5$  carbon (blue line) of **7e** (3,5-di-Br) in the simulation box. The lipid bilayer surface (black line) is shown as the average position of the phosphorous atoms ( $z$ -coordinate,  $-20$  and  $20$  Å) of the PL headgroups. (C) Tracking of the two angles  $c_1$  (in blue) and  $c_2$  (in orange), which revealed if the compound remained in the up conformation or changed to the up–down conformation. Since both the blue and orange lines in the shown parallel oscillated around  $80^\circ$ , the compound was in the up conformation. When one of the lines also oscillated around  $140^\circ$  (not shown), the compound adopted the up–down conformation. (D) Simplified side view of the MD simulation system. Light gray pads represent water, light green pad in the middle is the PL bilayer, green spheres at the upper and lower borders of the PL bilayer are phosphorous atoms of the lipid headgroups, and the repeated copies of a small molecule in the upper half of the image is the **7e** (3,5-di-Br) compound. The time evolution of **7e** (3,5-di-Br) is shown as snapshots from the simulation and spanning from left to right; 0, 3, 60, and 260 ns. Explicit water molecules, PL tails and headgroups, ions, and non-polar hydrogen atoms in **7e** (3,5-di-Br) are omitted for clarity.

lines) is shown as the average position of the phosphorous atoms of the PL headgroups ( $z$ -coordinate,  $-20$  and  $20$  Å). The blue line shows the time evolution for location of the  $C_5$  carbon of **7e** (3,5-di-Br). The MD simulations for compounds **6e** (3,5-di-Br), **6g** (4-tBu), **7e** (3,5-di-Br), and **7g** (4-tBu) revealed a rapid membrane insertion between 7 and 35 ns, which was as expected due to the electrostatic interaction between the negatively charged membrane surface and the positively charged compounds.

The starting conformation of **7e** (3,5-di-Br) in the MD simulations was up. In the shown simulation parallel in Figure 8C, tracking of the two angles  $c_1$  (blue) and  $c_2$  (orange), representing the two benzylic side chains, revealed that **7e** (3,5-di-Br) remained in the up conformation throughout this simulation. This is shown by the blue and orange lines both oscillating around  $80^\circ$ , as opposed to if one of the lines was also oscillating around  $140^\circ$ , indicating an up–down conformation (Figure 8C). As shown in the Supporting Information, however, the conformations of all modeled compounds varied between the up and up–down conformations in at least one of the three parallels, and the changes from up to the up–down conformation occurred sometime between 60 and 255 ns (Table S3 and Figures S6–S10). In most parallels of the MD simulation, the compounds remained incorporated in the membrane throughout the duration of the

simulation. Except for **6a** (4-CF<sub>3</sub>) as described below, if a molecule left the membrane, it was only for a few nanoseconds before it returned to the membrane environment, as can be seen from the time evolution of the  $C_5$   $z$ -coordinate for the other modeled compounds.

A simplified side view of the MD simulation system is presented in Figure 8D, which shows the interaction of **7e** (3,5-di-Br) with an *E. coli* inner membrane model. This includes a water pad over and under the PL bilayer, a PL bilayer in the middle, the phosphorous atoms of the lipid headgroups, and the location and time evolution of **7e** (3,5-di-Br) when interacting with the model membrane.

A reference set of simulations were also run with **6a** (4-CF<sub>3</sub>) to investigate the selectivity of the membrane model. As described above, compound **6a** (4-CF<sub>3</sub>) was much less potent against *E. coli* (MIC:  $128$  μg/mL) compared to the other modeled compounds. The simulations also showed that **6a** (4-CF<sub>3</sub>) had less affinity to remain in the model membrane environment compared to the other compounds (Table S3 and Figure S6). In all the three parallels of MD simulations of **6a** (4-CF<sub>3</sub>), it entered and left the membrane environment several times. This contrasted with the behavior seen in the simulations of **6e** (3,5-di-Br), **6g** (4-tBu), **7e** (3,5-di-Br), and **7g** (4-tBu) where once incorporated, the compounds remained in the membrane environment. The conformation of **6a** (4-

CF<sub>3</sub>) varied between up and up–down, but there was an increase in events where **6a** (4-CF<sub>3</sub>) returned from up–down to the up conformation (Figure S6). This behavior was not observed for other compounds in the MD simulations where only the shift from up to up–down was observed. As can be seen from Figure S6, **6a** (4-CF<sub>3</sub>) also traveled out from the top of the simulation box and appeared at the bottom side of the simulation box and did this several times during the 260 ns simulation (Table S3). The periodic boundary conditions in the MD simulations allowed the free flow of molecules in and out of the simulation box. The behavior of **6a** (4-CF<sub>3</sub>) compared to the other modeled compounds suggested that **6a** (4-CF<sub>3</sub>) did not find favorable interactions in the membrane environment, and this may in part explain its low antimicrobial potency against *E. coli*.

## CONCLUSIONS

In order to succeed transforming AMPs with non-optimal pharmacokinetic properties into clinical useful antimicrobials, an innovative strategy is to develop SMAMPs with imperative functional side chains embodied on a peptidomimetic scaffold. We have in the present study developed a novel peptidomimetic scaffold that fulfills the pharmacophore model of small AMPs and that was inspired by the marine antimicrobials eusynstyelamides. Compared to the structure of the eusynstyelamides, this novel series of cationic amphipathic barbiturates is achiral and easy to modify synthetically with respect to variation in cationic and lipophilic groups for optimization studies. The relative ease of synthesis has important implications for reducing future production costs and enabling large-scale production, which is an argument often raised against several classes of AMPs. We achieved improved antimicrobial activity compared with the eusynstyelamides, and several of the barbiturates displayed high antimicrobial activity against a panel of 30 multi-resistant clinical isolates of Gram-positive and Gram-negative bacteria. This included high activity against Gram-negative ESBL–CARBA isolates and strains resistant to the last resort antibiotic colistin. A pilot *in vivo* study using a murine neutropenic peritonitis model demonstrated that the overall most potent lead peptidomimetic **7e** (3,5-di-Br) significantly reduced the number of viable bacterial cells of clinical isolates of *E. coli* and *K. pneumoniae*. Although further structural optimizations are required to improve the MTD in mice, as well as pharmacokinetic studies including exploration of different routes of administration, demonstration of *in vivo* efficacy gives hope to the drug potential of this class of SMAMPs for treatment of serious infections.

## EXPERIMENTAL SECTION

**Chemicals and Equipment.** All reagents and solvents were purchased from commercial sources and used as supplied with the exception of the starting material 1-(bromomethyl)-4-fluoronaphthalene, which was synthesized from the 4-fluoro-1-naphthoic acid according to the literature procedures.<sup>40</sup> Anhydrous DMF was prepared by storage over 4 Å molecular sieves. The reactions were monitored by thin-layer chromatography (TLC) with Merck pre-coated silica gel plates (60 F<sub>254</sub>). Visualization was accomplished with either UV light or by immersion in potassium permanganate or phosphomolybdic acid (PMA), followed by light heating with a heating gun. Purifications using normal phase flash chromatography were either done by normal column chromatography using Normal Sil 60, 40–63 mm silica gel, or by automated normal phase flash chromatography (heptane/EtOAc) with the sample preloaded on a

Samplet cartridge belonging to a Biotage SP-1. Purification of reactions by RP C<sub>18</sub> column chromatography (water with 0.1% TFA/ acetonitrile with 0.1% TFA) was also executed on an automated purification module with the sample preloaded on a Samplet cartridge. All samples used for biological testing were determined to be of >95% purity. The analyses were carried out on a Waters ACQUITY UPC<sup>2</sup> system equipped with a Torus DEA 130 Å, 1.7 μm, 2.1 mm × 50 mm column coupled to a Waters ACQUITY PDA detector spanning from wavelengths 190–650 nm. The derivatives were eluted with a mobile phase consisting of supercritical CO<sub>2</sub> and MeOH containing 0.1% NH<sub>3</sub> and a linear gradient of 2–40% MeOH over 2 or 4 min, followed by isocratic 0.5 min of 40% MeOH. The flow rate was 1.5 mL/min. NMR spectra were obtained on a 400 MHz Bruker Avance III HD equipped with a 5 mm SmartProbe BB<sup>+</sup>H (BB = <sup>19</sup>F, <sup>31</sup>P–<sup>15</sup>N). Data are represented as follows: chemical shift, multiplicity (s = singlet, d = doublet, t = triplet, q = quartet, p = pentet, h = heptet, and m = multiplet), coupling constant (J, Hz), and integration. Chemical shifts (δ) are reported in ppm relative to the residual solvent peak (CDCl<sub>3</sub>: δ<sub>H</sub> 7.26 and δ<sub>C</sub> 77.16; CD<sub>3</sub>OD: δ<sub>H</sub> 3.31 and δ<sub>C</sub> 49.00). Positive and negative ion electrospray ionization mass spectrometry (ESI-MS) was conducted on a Thermo electron LTQ Orbitrap XL spectrometer.

**Synthesis. Dialkylated Malonate Ester (2a–g). General Procedure.** To a stirred solution of diethyl malonate in DMF (≈100 mg/mL) and base was added arylmethyl halide (≈2 equiv). The reaction was continuously stirred at room temperature overnight. The reaction mixture was diluted with EtOAc (30 mL) and washed with water (25 mL), aqueous 5% LiCl solution (3 × 25 mL), and brine (25 mL). The organic phase was dried over Na<sub>2</sub>SO<sub>4</sub>, filtered, and concentrated. The crude product was dissolved in CH<sub>2</sub>Cl<sub>2</sub> (20 mL) and adsorbed on Celite. The product was purified on a silica column using 1–5% EtOAc in pentane as the mobile phase.

**Diethyl 2,2-Bis(4-(trifluoromethyl)benzyl)malonate (2a).** According to the general procedure, to a stirred solution of diethyl malonate (3.26 g, 20.4 mmol) in DMF (25 mL) over K<sub>2</sub>CO<sub>3</sub> (8.5 g, 61.2 mmol) was added 1-(bromomethyl)-4-(trifluoromethyl)benzene (10 g, 41.8 mmol). The reaction was stirred at room temperature overnight. The reaction mixture was diluted with EtOAc (75 mL) and washed with water (5 × 50 mL), aqueous 5% LiCl solution (30 mL), and brine (40 mL). The organic phase was dried over Na<sub>2</sub>SO<sub>4</sub>, filtered, and concentrated. The crude product (9.97 g) was dissolved in CH<sub>2</sub>Cl<sub>2</sub> (50 mL) and adsorbed on Celite. The product was purified on a silica column using 1–5% EtOAc in pentane as the mobile phase to afford **2a** (8.64 g, 89%) as a white solid. <sup>1</sup>H NMR (400 MHz, CDCl<sub>3</sub>): δ 7.54 (d, J = 8.1 Hz, 4H), 7.28 (d, J = 8.1 Hz, 4H), 4.10 (q, J = 7.2 Hz, 4H), 3.27 (s, 4H), 1.13 (t, J = 7.1 Hz, 6H). <sup>13</sup>C NMR (101 MHz, CDCl<sub>3</sub>): δ 170.5, 140.4 (d, <sup>4</sup>J<sub>C,F</sub> = 1.8 Hz), 130.6, 129.6 (q, <sup>2</sup>J<sub>C,F</sub> = 32.5 Hz), 125.3 (q, <sup>3</sup>J<sub>C,F</sub> = 3.8 Hz), 124.3 (q, <sup>1</sup>J<sub>C,F</sub> = 271.9 Hz), 61.7, 60.1, 39.8, 13.9. HRMS-ESI: C<sub>23</sub>H<sub>22</sub>F<sub>6</sub>NaO<sub>4</sub><sup>+</sup> [M + Na]<sup>+</sup> calcd, 499.1315; found, 499.1298.

**Diethyl 2,2-Bis(naphthalen-2-yl-methyl)malonate (2b).** To a stirred solution of diethyl malonate (3.44 g, 21.5 mmol) in 15 mL of CH<sub>2</sub>Cl<sub>2</sub> at 0 °C was added DBU (3.3 mL, 22.6 mmol). The reaction mixture was stirred for 5 min before adding 2-(bromomethyl)naphthalene (5.0 g, 22.6 mmol). The reaction was allowed to reach room temperature and stirred overnight. The reaction was concentrated, and the crude product isolated as a brown oil. The oil was dissolved in EtOAc (30 mL) and washed with water (2 × 30 mL), 10% citric acid (30 mL), 10% NaHCO<sub>3</sub> soln (30 mL), and brine (30 mL). The organic phase was dried over Na<sub>2</sub>SO<sub>4</sub>, filtered, and concentrated affording 4.83 g of almost pure monoalkylated diethyl malonate. To a suspension of NaH (774 mg, 32.2 mmol) in dry THF (15 mL) at 0 °C was added diethyl 2-(naphthalen-2-ylmethyl)malonate (4.8 g) dropwise as a solution in THF (15 mL). The resulting mixture was stirred for 10 min before adding 2-naphthyl methyl bromide (5 g, 22.6 mmol). The reaction was allowed to reach room temperature and stirred overnight. The reaction mixture was cooled in an ice bath, unreacted NaH was quenched with 10% citric acid solution, and the reaction mixture was concentrated. The crude product was then dissolved in EtOAc and washed with 10% citric acid soln (3 × 30 mL), 10% NaHCO<sub>3</sub> soln (2

× 30 mL), and brine (30 mL). The organic phase was dried over Na<sub>2</sub>SO<sub>4</sub>, filtered, and concentrated to afford crude **2b** (7.35 g, 78%). <sup>1</sup>H NMR (400 MHz, CDCl<sub>3</sub>): δ 7.85–7.80 (m, 2H), 7.77 (d, *J* = 8.1 Hz, 4H), 7.65 (d, *J* = 1.7 Hz, 2H), 7.49–7.43 (m, 4H), 7.32 (dd, *J* = 8.5, 1.7 Hz, 2H), 4.14 (q, *J* = 7.1 Hz, 4H), 3.45 (s, 4H), 1.14 (t, *J* = 7.1 Hz, 6H). <sup>13</sup>C NMR not determined. HRMS-ESI: C<sub>29</sub>H<sub>29</sub>O<sub>4</sub><sup>+</sup> [M + H]<sup>+</sup> calcd, 441.2060; found, 441.2059.

**Diethyl 2,2-Bis(4-fluoronaphthalene-1-yl)methylmalonate (2c).** According to the general procedure, to a stirred solution of diethyl malonate (1.3 g, 8.16 mmol) in DMF (10 mL) over K<sub>2</sub>CO<sub>3</sub> (3.36 g, 24.3 mmol) was added 1-(bromomethyl)-4-fluoronaphthalene (4 g, 16.7 mmol). The reaction was continuously stirred at room temperature overnight. The reaction mixture was diluted with EtOAc (30 mL) and washed with water (3 × 20 mL), aqueous 5% LiCl solution (20 mL), and brine (20 mL). The organic phase was dried over Na<sub>2</sub>SO<sub>4</sub>, filtered, and concentrated. In a round-bottomed flask, the brown solid crude product was dissolved in warm EtOH, capped with alumina foil, and left for 4 days at room temperature. Upon standing for an hour, the product **2c** crashed out of the brown solution as a white solid (1.6 g, 41%). <sup>1</sup>H NMR (400 MHz, CDCl<sub>3</sub>): δ 8.18–8.08 (m, 2H), 8.05–7.95 (m, 2H), 7.57–7.46 (m, 4H), 7.36 (dd, *J* = 8.0, 5.5 Hz, 2H), 7.04 (dd, *J* = 10.2, 8.0 Hz, 2H), 3.81 (s, 4H), 3.75 (q, *J* = 7.2 Hz, 4H), 0.85 (t, *J* = 7.1 Hz, 6H). <sup>13</sup>C NMR (101 MHz, CDCl<sub>3</sub>): δ 171.3, 158.1 (d, *J*<sub>C,F</sub> = 251.4 Hz), 134.2 (d, *J*<sub>C,F</sub> = 4.2 Hz), 128.9 (d, *J*<sub>C,F</sub> = 4.6 Hz), 127.6 (d, *J*<sub>C,F</sub> = 8.2 Hz), 126.8, 125.9 (d, *J*<sub>C,F</sub> = 2.1 Hz), 124.1–123.9 (m), 121.2 (d, *J*<sub>C,F</sub> = 6.0 Hz), 108.9 (d, *J*<sub>C,F</sub> = 19.7 Hz), 61.5, 59.8, 35.5, 13.6. HRMS-ESI: C<sub>29</sub>H<sub>26</sub>F<sub>2</sub>NaO<sub>4</sub><sup>+</sup> [M + Na]<sup>+</sup> calcd, 499.1691; found, 499.1689.

**Diethyl 2,2-Bis(4-bromo-3-chlorobenzyl)malonate (2d).** According to the general procedure, to a stirred solution of diethyl malonate (313 mg, 1.95 mmol) in DMF (6 mL) over Cs<sub>2</sub>CO<sub>3</sub> (1.91 g, 5.86 mmol) was added 1-bromo-4-(bromomethyl)-2-chlorobenzene (1.14 g, 4.01 mmol). The reaction was continuously stirred at 40 °C for 22 h. The reaction mixture was diluted with EtOAc (20 mL) and washed with aqueous 5% LiCl solution (3 × 20 mL). The organic phase was dried over MgSO<sub>4</sub>, filtered, and concentrated. The crude product was dissolved in CH<sub>2</sub>Cl<sub>2</sub> (20 mL) and adsorbed on Celite. The product was purified on a silica column using 5% EtOAc in heptane as the mobile phase to afford **2d** (1.04 g, 94%) as a white solid. <sup>1</sup>H NMR (400 MHz, CDCl<sub>3</sub>): δ 7.50 (d, *J* = 8.3 Hz, 2H), 7.24 (d, *J* = 2.1 Hz, 2H), 6.91 (dd, *J* = 8.3, 2.1 Hz, 2H), 4.13 (q, *J* = 7.1 Hz, 4H), 3.12 (s, 4H), 1.18 (t, *J* = 7.1 Hz, 6H). <sup>13</sup>C NMR (101 MHz, CDCl<sub>3</sub>): δ 170.3, 137.1, 134.4, 133.6, 132.1, 129.8, 121.2, 61.9, 59.9, 39.1, 14.0. HRMS-ESI: C<sub>21</sub>H<sub>20</sub>Br<sub>2</sub>Cl<sub>2</sub>O<sub>4</sub><sup>+</sup> [M + Na]<sup>+</sup> calcd, 586.8998; found, 586.9005.

**Diethyl 2,2-Bis(3,5-dibromobenzyl)malonate (2e).** According to the general procedure, to a stirred solution of diethyl malonate (460 mg, 2.9 mmol) in DMF (5 mL) over Cs<sub>2</sub>CO<sub>3</sub> (2.0 g, 6.37 mmol) was added 1,3-dibromo-5-(bromomethyl)benzene (2.0 g, 6.0 mmol). The reaction was continuously stirred at room temperature overnight. The reaction mixture was diluted with EtOAc (30 mL) and washed with water (25 mL), aqueous 5% LiCl solution (3 × 25 mL), and brine (25 mL). The organic phase was dried over Na<sub>2</sub>SO<sub>4</sub>, filtered, and concentrated. The crude product was dissolved in CH<sub>2</sub>Cl<sub>2</sub> (20 mL) and adsorbed on Celite. The product was purified on a silica column using 1–5% EtOAc in pentane as the mobile phase to afford **2e** (1.17 g, 61%) as a white solid. <sup>1</sup>H NMR (400 MHz, CDCl<sub>3</sub>): δ 7.56 (t, *J* = 1.8 Hz, 2H), 7.24 (d, *J* = 1.8 Hz, 4H), 4.15 (q, *J* = 7.1 Hz, 4H), 3.11 (s, 4H), 1.20 (t, *J* = 7.2 Hz, 6H). <sup>13</sup>C NMR (101 MHz, CDCl<sub>3</sub>): δ 170.0, 139.9, 132.8, 132.0, 122.7, 61.9, 60.0, 39.3, 13.9. HRMS-ESI: C<sub>21</sub>H<sub>20</sub>Br<sub>4</sub>NaO<sub>4</sub><sup>+</sup> [M + Na]<sup>+</sup> calcd, 674.7987; found, 674.7961.

**Diethyl 2,2-Bis(3,5-bis(trifluoromethyl)benzyl)malonate (2f).** According to the general procedure, to a stirred solution of diethyl malonate (490 mg, 3.1 mmol) in DMF (5 mL) over Cs<sub>2</sub>CO<sub>3</sub> (2.2 g, 6.83 mmol) was added 1-(bromomethyl)-3,5-bis(trifluoromethyl)benzene (2 g, 6.51 mmol). The reaction was continuously stirred at room temperature overnight. The reaction mixture was diluted with EtOAc (30 mL) and washed with water (25 mL), aqueous 5% LiCl solution (3 × 25 mL), and brine (25 mL). The organic phase was dried over Na<sub>2</sub>SO<sub>4</sub>, filtered, and concentrated. The crude product was dissolved in CH<sub>2</sub>Cl<sub>2</sub> (20 mL) and adsorbed on Celite. The product

was purified on a silica column using 1–5% EtOAc in pentane as the mobile phase to afford **2f** (0.89 g, 63%) as a white solid. <sup>1</sup>H NMR (400 MHz, CDCl<sub>3</sub>): δ 7.79 (s, 2H), 7.71–7.54 (m, 4H), 4.10 (q, *J* = 7.1 Hz, 4H), 3.32 (s, 4H), 1.13 (t, *J* = 7.1 Hz, 6H). <sup>13</sup>C NMR (101 MHz, CDCl<sub>3</sub>): δ 169.8, 138.5, 131.8 (q, <sup>2</sup>*J*<sub>C,F</sub> = 33.3 Hz), 130.9–130.2 (m), 123.3 (q, <sup>1</sup>*J*<sub>C,F</sub> = 272.7 Hz), 121.5 (p, <sup>3</sup>*J*<sub>C,F</sub> = 3.9 Hz), 62.2, 60.3, 40.3, 13.8. HRMS-ESI: C<sub>25</sub>H<sub>19</sub>F<sub>12</sub>O<sub>4</sub><sup>−</sup> [M − H]<sup>−</sup> calcd, 611.1098; found, 611.1097.

**Diethyl 2,2-Bis(4-tert-butylbenzyl)malonate (2g).** According to the general procedure, to a stirred solution of diethyl malonate (3.43 g, 21.4 mmol) in DMF (25 mL) over K<sub>2</sub>CO<sub>3</sub> (8.8 g, 64.2 mmol) was added 1-(bromomethyl)-4-tert-butylbenzene (10 g, 44 mmol). The reaction was continuously stirred at room temperature overnight. The reaction mixture was diluted with EtOAc (80 mL) and washed with water (3 × 50 mL), aqueous 5% LiCl solution (50 mL), and brine (50 mL). The organic phase was dried over Na<sub>2</sub>SO<sub>4</sub>, filtered, and concentrated. The crude product was dissolved in CH<sub>2</sub>Cl<sub>2</sub> (20 mL) and adsorbed on Celite. The product was purified on a silica column using 1–5% EtOAc in pentane as the mobile phase to afford **2g** (8.80 g, 90%) as a white solid. <sup>1</sup>H NMR (400 MHz, CDCl<sub>3</sub>): δ 7.28 (d, *J* = 8.3 Hz, 4H), 7.11 (d, *J* = 8.4 Hz, 4H), 4.10 (q, *J* = 7.1 Hz, 4H), 3.19 (s, 4H), 1.30 (s, 18H), 1.14 (t, *J* = 7.1 Hz, 6H). <sup>13</sup>C NMR (101 MHz, CDCl<sub>3</sub>): δ 171.2, 149.7, 133.4, 129.9, 125.2, 61.2, 60.4, 38.6, 34.5, 31.5, 14.0. HRMS-ESI: C<sub>29</sub>H<sub>40</sub>NaO<sub>4</sub><sup>+</sup> [M + Na]<sup>+</sup> calcd, 475.2818; found, 475.2795.

**Condensation of Malonates (2) with Urea to Barbiturates (3).**  
**5,5-Bis(4-trifluoromethylbenzyl)pyrimidine-2,4,6-(1H,3H,5H)-trione (3a).** To a solution of urea (3.15 g, 52.5 mmol) in anhydrous DMF (15 mL) was added NaH (315 mg, 13.1 mmol). The reaction mixture was stirred 5 min before adding a solution of **2a** (2.5 g, 5.22 mmol) in anhydrous DMF (10 mL) dropwise. The reaction mixture was left under stirring overnight until TLC showed full conversion using 5% EtOAc in CHCl<sub>3</sub> as the mobile phase [*R*<sub>f</sub> (product) 0.38, *R*<sub>f</sub> (starting material) 0.89]. The reaction was diluted with 100 mL of EtOAc and washed with 10% citric acid soln (3 × 50 mL), 10% NaHCO<sub>3</sub> soln (2 × 50 mL), and brine (2 × 50 mL). The organic phase was dried over Na<sub>2</sub>SO<sub>4</sub>, filtered, and concentrated, yielding the crude product (2.39 g). The crude was dissolved in CH<sub>2</sub>Cl<sub>2</sub> and adsorbed onto Celite before being purified on a silica column using 5% EtOAc in CHCl<sub>3</sub> as the mobile phase to afford **3a** (1.63 g, 70%) as a white solid. <sup>1</sup>H NMR (400 MHz, CDCl<sub>3</sub>): δ 7.53 (d, *J* = 8.1 Hz, 4H), 7.26\* (d, 4H), 3.50 (s, 4H). <sup>13</sup>C NMR (101 MHz, CDCl<sub>3</sub>): δ 170.4, 146.4, 138.1, 130.6 (q, <sup>2</sup>*J*<sub>C,F</sub> = 32.7 Hz), 130.2, 126.0 (q, <sup>3</sup>*J*<sub>C,F</sub> = 3.7 Hz), 124.0 (q, <sup>1</sup>*J*<sub>C,F</sub> = 272.2 Hz), 60.3, 44.3. \*Overlap with solvent. HRMS-ESI: C<sub>20</sub>H<sub>13</sub>F<sub>6</sub>N<sub>2</sub>O<sub>3</sub><sup>−</sup> [M − H]<sup>−</sup> calcd, 443.0836; found, 443.0826.

**5,5-Bis(naphthalen-2-yl)methylpyrimidine-2,4,6-(1H,3H,5H)-trione (3b).** NaH (9 mg, 0.37 mmol) was added to a stirred solution of urea (91 mg, 1.49 mmol) in anhydrous DMF (3 mL) at room temperature. The reaction mixture was left to stir for 10 min before adding **2b** (66 mg, 0.15 mmol) slowly, and the reaction was left to stir overnight. The reaction mixture was diluted with EtOAc (20 mL) and washed with water (4 × 20 mL), followed by brine (20 mL). The organic phase was dried over Na<sub>2</sub>SO<sub>4</sub>, filtered, and concentrated. The crude product was dissolved in CHCl<sub>3</sub> and adsorbed onto Celite before purification on a silica column using 0–5% EtOAc in CHCl<sub>3</sub> as the mobile phase to afford **3b** (50 mg, 82%). <sup>1</sup>H NMR (400 MHz, CD<sub>3</sub>OD): δ 7.76–7.70 (m, 4H), 7.69 (d, *J* = 8.6 Hz, 2H), 7.62 (s, 2H), 7.44–7.36 (m, 4H), 7.26 (dd, *J* = 8.4, 1.7 Hz, 2H), 3.60 (s, 4H). <sup>13</sup>C NMR (101 MHz, CD<sub>3</sub>OD): δ 173.2, 149.5, 133.8, 133.1, 132.8, 129.1, 128.7, 128.1, 127.9, 127.8, 126.6, 126.4, 60.8, 45.1. HRMS-ESI: C<sub>26</sub>H<sub>19</sub>N<sub>2</sub>O<sub>3</sub><sup>−</sup> [M − H]<sup>−</sup> calcd, 407.1417; found, 407.1416.

**5,5-Bis(4-fluoronaphthalene-1-yl)methylpyrimidine-2,4,6-(1H,3H,5H)-trione (3c).** To a stirred solution of urea (630 mg, 10.49 mmol) in anhydrous DMF (4 mL) was added NaH (76 mg, 3.16 mmol), and the resulting solution was stirred for 10 min before adding **2c** (500 mg, 1.05 mmol) slowly. The resulting mixture was stirred overnight. The reaction mixture was diluted with 25 mL of EtOAc and washed with 4 × 50 mL of water, followed by 20 mL of brine. The organic phase was dried over Na<sub>2</sub>SO<sub>4</sub>, filtered, and concentrated. The crude product was dissolved in CHCl<sub>3</sub> and



adsorbed onto Celite before purification on a silica column using 0–5% EtOAc in CHCl<sub>3</sub> as the mobile phase to afford **3c** (430 mg, 92%). <sup>1</sup>H NMR (400 MHz, CDCl<sub>3</sub>): δ 8.23 (d, *J* = 8.5 Hz, 2H), 8.14–8.04 (m, 2H), 7.64–7.49 (m, 4H), 7.46 (s, 2H), 7.29–7.26\* (m, 2H), 7.00 (dd, *J* = 9.9, 8.1 Hz, 2H), 4.05 (s, 4H). <sup>13</sup>C NMR (101 MHz, CDCl<sub>3</sub>): δ 171.4, 158.7 (d, *J*<sub>C,F</sub> = 253.3 Hz), 146.8, 133.3 (d, *J*<sub>C,F</sub> = 4.5 Hz), 128.0 (d, *J*<sub>C,F</sub> = 8.7 Hz), 127.4, 126.7 (d, *J* = 4.7 Hz), 126.5 (d, *J* = 1.9 Hz), 124.4–124.1 (m), 121.3 (d, *J* = 6.2 Hz), 109.1 (d, *J* = 20.1 Hz), 59.8, 40.0. \*Overlap with solvent. HRMS-ESI: C<sub>26</sub>H<sub>31</sub>F<sub>2</sub>N<sub>2</sub>O<sub>3</sub><sup>−</sup> [M − H]<sup>−</sup> calcd, 443.1213; found, 443.1181.

**5,5-Bis(4-bromo-3-chlorobenzyl)pyrimidine-2,4,6-(1H,3H,5H)-trione (3d)**. To a stirred solution of urea (621 mg, 10.3 mmol) in anhydrous DMF (8 mL) was added NaH (124 mg, 3.1 mmol, 60% in mineral oil), and the resulting solution was stirred for 20 min before slowly adding **2d** (586 mg, 1.03 mmol), dissolved in 2 mL of anhydrous DMF. The resulting mixture was stirred for 20 h. The reaction mixture was diluted with 20 mL of EtOAc and washed with 4 × 20 mL of aq 5% LiCl. The organic phase was dried over MgSO<sub>4</sub>, filtered, and concentrated. The crude product was adsorbed onto Celite before purification on a silica column using 20% EtOAc in heptane as the mobile phase to afford **3d** (364 mg, 66%). <sup>1</sup>H NMR (400 MHz, DMSO-*d*<sub>6</sub>): δ 11.51 (NH, s, 2H), 7.71 (d, *J* = 8.2 Hz, 2H), 7.24 (d, *J* = 2.1 Hz, 2H), 6.93 (dd, *J* = 8.3, 2.1 Hz, 2H), 3.26 (s, 4H). <sup>13</sup>C NMR (101 MHz, DMSO-*d*<sub>6</sub>): δ 171.4, 148.8, 136.7, 134.0, 133.0, 131.3, 129.8, 120.6, 58.2, 41.9. HRMS-ESI: C<sub>18</sub>H<sub>11</sub>Br<sub>2</sub>Cl<sub>2</sub>N<sub>2</sub>O<sub>3</sub><sup>−</sup> [M − H]<sup>−</sup> calcd, 530.8519; found, 530.8520.

**5,5-Bis(3,5-dibromobenzyl)pyrimidine-2,4,6-(1H,3H,5H)-trione (3e)**. To a stirred solution of urea (1.83 g, 2.79 mmol) in anhydrous DMF (15 mL) was added NaH (183 mg, 7.6 mmol), and the resulting solution was stirred for 10 min before adding **2e** (2.0 g, 3.05 mmol). The resulting mixture was stirred overnight. The reaction was diluted with EtOAc (50 mL) and washed with 10% citric acid soln (3 × 25 mL), 10% NaHCO<sub>3</sub> soln (2 × 30 mL), and brine (30 mL). The organic phase was dried over Na<sub>2</sub>SO<sub>4</sub>, filtered, and concentrated. The white solid was dissolved in CHCl<sub>3</sub> (25 mL), concentrated again, and purified by flash chromatography to afford **3e** (1.52 g, 88%). <sup>1</sup>H NMR (400 MHz, CDCl<sub>3</sub>): δ 7.82 (NH, s, 2H), 7.58 (t, *J* = 1.8 Hz, 2H), 7.21 (d, *J* = 1.5 Hz, 4H), 3.32 (s, 4H). <sup>13</sup>C NMR (101 MHz, CDCl<sub>3</sub>): δ 170.0, 146.4, 137.7, 134.2, 131.5, 123.6, 59.9, 43.4. HRMS-ESI: C<sub>18</sub>H<sub>11</sub><sup>79</sup>Br<sub>4</sub>N<sub>2</sub>O<sub>3</sub><sup>−</sup> [M − H]<sup>−</sup> calcd, 618.7509; found, 618.7501.

**5,5-Bis(3,5-bis(trifluoromethyl)benzyl)pyrimidine-2,4,6-(1H,3H,5H)-trione (3f)**. To a solution of urea (1.3 g, 21.6 mmol) in 20 mL of anhydrous DMF was added NaH (128 mg, 5.3 mmol), and the resulting solution was stirred for 10 min before adding **2f** (1.0 g, 1.7 mmol). The resulting mixture was stirred overnight. The reaction was diluted with EtOAc (50 mL) and washed with 10% citric acid soln (3 × 30 mL), 10% NaHCO<sub>3</sub> soln (2 × 20 mL), and brine (30 mL). The organic phase was dried over Na<sub>2</sub>SO<sub>4</sub>, filtered, and concentrated. The crude was purified by automated flash chromatography to afford **3f** (0.27 g, 27%) as a white powder. <sup>1</sup>H NMR (400 MHz, CDCl<sub>3</sub>): δ 7.82 (NH, s, 2H), 7.73 (s, 2H), 7.62–7.57 (m, 4H), 3.57 (s, 4H). <sup>13</sup>C NMR (101 MHz, CDCl<sub>3</sub>): δ 169.8, 146.1, 136.3, 132.6 (q, <sup>2</sup>*J*<sub>C,F</sub> = 33.6 Hz), 130.4–129.7 (m), 122.0 (q, <sup>1</sup>*J*<sub>C,F</sub> = 272.8 Hz), 122.9–122.2 (m), 59.9, 43.5. HRMS-ESI: C<sub>22</sub>H<sub>11</sub>F<sub>12</sub>N<sub>2</sub>O<sub>3</sub><sup>−</sup> [M − H]<sup>−</sup> calcd, 579.0584; found, 579.0583.

**5,5-Bis(4-tert-butylbenzyl)pyrimidin-2,4,6-(1H,3H,5H)-trione (3g)**. To a stirred solution of urea (6.63 g, 110 mmol) at room temperature in anhydrous DMF (20 mL) was added NaH (660 mg, 27.5 mmol), and the reaction was stirred for 5 min. A solution of **2g** (5 g, 11 mmol) in anhydrous DMF (20 mL) was added dropwise to the reaction mixture, and the reaction was stirred overnight. The reaction mixture was diluted with EtOAc (20 mL) and washed with 10% citric acid (100 mL), 10% NaHCO<sub>3</sub> soln (50 mL), brine (50 mL), water (20 mL), and brine (2 × 50 mL). The organic phase was dried over Na<sub>2</sub>SO<sub>4</sub>, filtered, and concentrated. The crude product was purified by automated flash chromatography (heptane/EtOAc) affording 4.09 g (88%) of **3g** as a white powder. <sup>1</sup>H NMR (400 MHz, CD<sub>3</sub>OD): δ 7.26 (d, *J* = 7.7 Hz, 2H), 7.05 (d, *J* = 7.6 Hz, 2H), 3.31 (s, 4H, overlap CD<sub>3</sub>OD), 1.24 (s, 18H). <sup>13</sup>C NMR (101 MHz, CD<sub>3</sub>OD): δ 174.2, 151.5\*, 133.5, 130.4, 126.4, 61.4, 45.0, 35.3, 31.7. \*Assumed overlap

of two signals. HRMS-ESI: C<sub>26</sub>H<sub>31</sub>N<sub>2</sub>O<sub>3</sub><sup>−</sup> [M − H]<sup>−</sup> calcd, 419.2340; found, 419.2335.

**5,5-Bis(3,5-di-tert-butylbenzyl)pyrimidine-2,4,6-(1H,3H,5H)-trione (3h)**. Compound **3h** was provided to us by Elizaveta M. Igumnova. <sup>1</sup>H NMR (400 MHz, CDCl<sub>3</sub>): δ 7.25–7.24 (m, 2H), 6.96 (d, *J* = 1.8 Hz, 4H), 3.45 (s, 4H), 1.26 (s, 36H). <sup>13</sup>C NMR (101 MHz, CDCl<sub>3</sub>): δ 171.5, 151.3, 133.7, 123.9, 121.3, 61.7, 45.4, 34.9, 31.5. HRMS-ESI: C<sub>34</sub>H<sub>47</sub>N<sub>2</sub>O<sub>3</sub><sup>−</sup> [M − H]<sup>−</sup> calcd, 531.3592; found, 531.3592.

**N-Alkylation of Barbiturates (3) with 1,4-Dibromobutane. 1,3-Bis(4-bromobutyl)-5,5-bis(4-trifluoromethylbenzyl)pyrimidine-2,4,6-(1H,3H,5H)-trione (4a)**. To a stirred solution of **3a** (1.59 g, 3.58 mmol) at room temperature in DMF (15 mL) were added K<sub>2</sub>CO<sub>3</sub> (2.00 g, 14.47 mmol) and 1,4-dibromobutane (4.24 mL, 35.8 mmol). The reaction mixture was stirred for 48 h, diluted with EtOAc (50 mL), and washed with 10% citric acid soln (3 × 25 mL), 10% NaHCO<sub>3</sub> soln (2 × 25 mL), and brine (25 mL). The organic phase was dried over Na<sub>2</sub>SO<sub>4</sub>, filtered, and concentrated. The crude product was purified using automated flash chromatography affording **4a** (2.47 g, 96%) as a white powder. <sup>1</sup>H NMR (400 MHz, CDCl<sub>3</sub>): δ 7.50 (d, *J* = 7.8 Hz, 4H), 7.20 (d, *J* = 8.0 Hz, 4H), 3.61 (t, *J* = 7.3 Hz, 4H), 3.51 (s, 4H), 3.31 (t, *J* = 6.5 Hz, 4H), 1.67–1.49 (m, 4H), 1.39 (p, *J* = 7.1 Hz, 4H). <sup>13</sup>C NMR (101 MHz, CDCl<sub>3</sub>): δ 170.2, 149.3, 138.8, 130.4 (q, <sup>2</sup>*J*<sub>C,F</sub> = 32.7 Hz), 130.1, 125.8 (q, <sup>3</sup>*J*<sub>C,F</sub> = 3.7 Hz), 123.9 (q, <sup>1</sup>*J*<sub>C,F</sub> = 272.2 Hz), 60.0, 45.2, 41.1, 32.7, 29.5, 26.4. HRMS-ESI: C<sub>28</sub>H<sub>28</sub><sup>79</sup>Br<sub>2</sub>F<sub>6</sub>KN<sub>2</sub>O<sub>3</sub><sup>+</sup> [M + K]<sup>+</sup> calcd, 751.0002; found, 751.0006.

**1,3-Bis(4-bromobutyl)-5,5-bis(naphthalen-2-yl-methyl)pyrimidine-2,4,6-(1H,3H,5H)-trione (4b)**. To a stirred suspension of **3b** (200 mg, 0.49 mmol) and K<sub>2</sub>CO<sub>3</sub> (273 mg, 1.95 mmol) in DMF (4 mL) was added 1,4-dibromobutane (0.57 mL, 4.9 mmol). The reaction was stirred for 18–48 h until completion was indicated by TLC (5% EtOAc in CHCl<sub>3</sub>). The reaction mixture was diluted with EtOAc (25 mL), and K<sub>2</sub>CO<sub>3</sub> was filtered off. The organic phase was washed with 10% citric acid solution (30 mL), 10% NaHCO<sub>3</sub> soln (30 mL), water (3 × 30 mL), and brine (30 mL); dried with Na<sub>2</sub>SO<sub>4</sub>, filtered; and concentrated. The crude product was dissolved in CHCl<sub>3</sub> (30 mL) and adsorbed onto Celite before purification on a silica column using 0–5% EtOAc in CHCl<sub>3</sub> to afford **4b** (347 mg, 80%) as a white powder. <sup>1</sup>H NMR (400 MHz, CDCl<sub>3</sub>): δ 7.75 (dd, *J* = 9.4, 6.4 Hz, 4H), 7.70 (d, *J* = 8.4 Hz, 2H), 7.57 (s, 2H), 7.48–7.42 (m, 4H), 7.18 (dd, *J* = 8.5, 1.7 Hz, 2H), 3.68 (s, 4H), 3.53 (t, *J* = 6.7 Hz, 4H), 2.99 (t, *J* = 6.2 Hz, 4H), 1.35–1.19 (m, 8H). <sup>13</sup>C NMR (101 MHz, CDCl<sub>3</sub>): δ 170.9, 149.6, 133.3, 132.7, 132.5, 128.8, 128.5, 127.8, 127.7, 127.2, 126.6, 126.3, 60.8, 45.8, 40.9, 32.8, 29.5, 26.3. HRMS-ESI: C<sub>34</sub>H<sub>34</sub><sup>79</sup>Br<sub>2</sub>N<sub>2</sub>NaO<sub>3</sub><sup>+</sup> [M + Na]<sup>+</sup> calcd, 699.0827; found, 699.0839.

**1,3-Bis(4-bromobutyl)-5,5-bis(4-F-naphthalene-1-yl-methyl)pyrimidine-2,4,6-(1H,3H,5H)-trione (4c)**. To a stirred suspension of **3c** (242 mg, 0.54 mmol) and K<sub>2</sub>CO<sub>3</sub> (300 mg, 2.17 mmol) in DMF (5 mL) was added 1,4-dibromobutane (0.64 mL, 5.4 mmol). The reaction was stirred for 18–48 h until completion was indicated by TLC (CHCl<sub>3</sub>, R<sub>f</sub> product: 0.74, R<sub>f</sub> starting material: 0.11). The reaction mixture was diluted with EtOAc (25 mL), and K<sub>2</sub>CO<sub>3</sub> filtered off. The organic phase was washed with 10% citric acid soln (30 mL), 10% NaHCO<sub>3</sub> soln (30 mL), water (3 × 30 mL), and brine (30 mL); dried with Na<sub>2</sub>SO<sub>4</sub>, filtered; and concentrated, yielding the crude as an oil. The crude product was dissolved in CHCl<sub>3</sub> (30 mL) and adsorbed onto Celite before purification on a silica column using CHCl<sub>3</sub> as the mobile phase to afford **4c** (237 mg, 61%) as a white solid. <sup>1</sup>H NMR (400 MHz, CDCl<sub>3</sub>): δ 8.23 (d, *J* = 8.6 Hz, 2H), 8.08 (d, *J* = 8.3 Hz, 2H), 7.63 (t, *J* = 7.7 Hz, 2H), 7.54 (t, *J* = 7.6 Hz, 2H), 7.23 (dd, *J* = 8.0, 5.5 Hz, 2H), 7.00 (dd, *J* = 9.8, 8.1 Hz, 2H), 4.06 (s, 4H), 3.33 (t, *J* = 7.2 Hz, 4H), 3.05 (t, *J* = 6.6 Hz, 4H), 1.34–1.12 (m, 4H), 1.08–0.90 (m, 4H). <sup>13</sup>C NMR (101 MHz, CDCl<sub>3</sub>): δ 178.0 (d, *J*<sub>C,F</sub> = 8.4 Hz), 158.5 (d, <sup>1</sup>*J*<sub>C,F</sub> = 253.3 Hz), 149.4, 133.2 (d, *J*<sub>C,F</sub> = 4.4 Hz), 129.0 (d, *J*<sub>C,F</sub> = 8.4 Hz), 127.4 (d, *J*<sub>C,F</sub> = 4.7 Hz), 127.2, 126.4 (d, *J*<sub>C,F</sub> = 2.1 Hz), 124.8 (d, *J*<sub>C,F</sub> = 2.7 Hz), 124.1 (d, *J*<sub>C,F</sub> = 15.7 Hz), 121.1 (d, *J*<sub>C,F</sub> = 6.0 Hz), 108.9 (d, *J*<sub>C,F</sub> = 20.0 Hz), 60.0, 40.9, 40.7, 32.7, 29.3, 25.9. HRMS-ESI: C<sub>34</sub>H<sub>32</sub><sup>79</sup>Br<sub>2</sub>F<sub>2</sub>N<sub>2</sub>NaO<sub>3</sub><sup>+</sup> [M + Na]<sup>+</sup> calcd, 735.0639; found, 735.0622.

**5,5-Bis(4-bromo-3-chlorobenzyl)-1,3-bis(4-bromobutyl)-pyrimidine-2,4,6-(1H,3H,5H)-trione (4d).** To a stirred suspension of **3d** (1.748 g, 3.267 mmol) and  $K_2CO_3$  (1.806 g, 13.07 mmol) in DMF (15 mL) was added 1,4-dibromobutane (4.46 mL, 37.3 mmol). The reaction was stirred for 14 days. The organic phase was washed with 10% citric acid soln (30 mL), 10%  $NaHCO_3$  soln (30 mL), water (3 × 30 mL), and brine (30 mL); dried with  $Na_2SO_4$ ; filtered; and concentrated, yielding the crude as an oil. The crude product was purified on an automated flash system silica column using DCM/MeOH as the mobile phase to afford **4d** (1.78 mg, 68%) as a white solid.  $^1H$  NMR (400 MHz,  $CDCl_3$ ):  $\delta$  7.47 (d,  $J$  = 8.2 Hz, 2H), 7.15 (d,  $J$  = 2.1 Hz, 2H), 6.80 (dd,  $J$  = 8.2, 2.1 Hz, 2H), 3.64 (t,  $J$  = 7.3 Hz, 4H), 3.41–3.28 (m, 8H), 1.65–1.55 (m, 4H), 1.51–1.40 (m, 4H).  $^{13}C$  NMR (101 MHz,  $CDCl_3$ ):  $\delta$  170.1, 149.2, 135.5, 134.9, 134.1, 131.4, 129.1, 122.2, 59.7, 44.3, 41.2, 32.7, 29.7, 26.5. HRMS-ESI:  $C_{26}H_{26}^{79}Br_4Cl_2N_2NaO_3^+$  [M + Na] $^+$  calcd, 822.7946; found, 822.7960.

**1,3-Bis(4-bromobutyl)-5,5-bis(3,5-dibromobenzyl)pyrimidine-2,4,6-(1H,3H,5H)-trione (4e).** To a stirred solution of **3e** (300 mg, 0.48 mmol) in DMF (6 mL) was added  $K_2CO_3$  (265 mg, 1.92 mmol) and 1,4-dibromobutane (0.57 mL, 4.81 mmol). The reaction was stirred for 18–48 h until completion was indicated by TLC (5% EtOAc in  $CHCl_3$ ). The reaction mixture was diluted with EtOAc (25 mL), and  $K_2CO_3$  was filtered off. The organic phase was washed with 10% citric acid soln (30 mL), 10%  $NaHCO_3$  soln (30 mL), water (3 × 30 mL), and brine (30 mL); dried with  $Na_2SO_4$ ; filtered; and concentrated, resulting in an oil that slowly turned into white crystals. The crude product was dissolved in  $CHCl_3$  (30 mL) and adsorbed onto Celite before purification on a silica column using pentane: $CH_2Cl_2$  (7:3 to 1:1) to afford **4e** (347 mg, 80%) as a white powder.  $^1H$  NMR (400 MHz,  $CDCl_3$ ):  $\delta$  7.54 (d,  $J$  = 1.8 Hz, 2H), 7.14 (d,  $J$  = 1.7 Hz, 4H), 3.65 (t,  $J$  = 7.4 Hz, 4H), 3.38 (t,  $J$  = 6.7 Hz, 4H), 3.33 (s, 4H), 1.77–1.61 (m, 4H), 1.58–1.43 (m, 4H).  $^{13}C$  NMR (101 MHz,  $CDCl_3$ ):  $\delta$  169.9, 149.1, 138.4, 133.9, 131.3, 123.4, 59.9, 44.2, 41.3, 32.7, 30.0, 26.7. HRMS-ESI:  $C_{26}H_{26}^{79}Br_3^{81}Br_3ClN_2O_3^-$  [M + Cl] $^-$  calcd, 928.6671; found, 928.6669.

**1,3-Bis(4-bromobutyl)-5,5-bis(3,5-bis(trifluoromethyl)benzyl)pyrimidine-2,4,6-(1H,3H,5H)-trione (4f).** To a stirred solution of **3f** (0.864 g, 1.57 mmol) in DMF (20 mL) were added  $K_2CO_3$  (1.233 g, 8.93 mmol) and 1,4-dibromobutane (1.76 mL, 14.9 mmol). The reaction mixture was stirred for 48 h, diluted with EtOAc (30 mL), and washed with water (3 × 20 mL), 5% LiCl soln (3 × 20), and brine (20 mL). The crude product was purified by automated flash chromatography to afford **4f** (0.64 g, 50%) as a white powder.  $^1H$  NMR (400 MHz,  $CDCl_3$ ):  $\delta$  7.79 (s, 2H), 7.53 (s, 4H), 3.59 (s, 4H), 3.57–3.51 (m, 4H), 3.26 (t,  $J$  = 6.8 Hz, 4H), 1.67–1.55 (m, 4H), 1.43–1.29 (m, 4H).  $^{13}C$  NMR (101 MHz,  $CDCl_3$ ):  $\delta$  169.4, 148.4, 136.9, 132.2 (q,  $^2J_{C,F}$  = 33.6 Hz), 130.0–129.4 (m), 122.9 (q,  $^1J_{C,F}$  = 272.9 Hz), 122.1 (p,  $^3J_{C,F}$  = 3.8 Hz), 59.7, 44.3, 41.1, 31.7, 29.6, 26.1. HRMS-ESI:  $C_{30}H_{26}^{79}Br_3F_{12}N_2O_3^-$  [M + Br] $^-$  calcd, 926.9308; found, 926.9308.

**1,3-Bis(4-bromobutyl)-5,5-bis(4-tert-butylbenzyl)pyrimidine-2,4,6-(1H,3H,5H)-trione (4g).** To a stirred solution of **3g** (3.88 g, 9.23 mmol) at room temperature in DMF (50 mL) were added  $K_2CO_3$  (5.12 g, 37 mmol) and 1,4-dibromobutane (10.9 mL, 92.5 mmol). The reaction mixture was stirred overnight. The reaction mixture was diluted with EtOAc (100 mL) and washed with water (100 mL). The crude product was purified by automated flash chromatography, affording the product **4g** (2.60 g, 40%) as a white powder.  $^1H$  NMR (400 MHz,  $CDCl_3$ ):  $\delta$  7.22 (d,  $J$  = 7.8 Hz, 4H), 6.98 (d,  $J$  = 7.9 Hz, 4H), 3.60 (t,  $J$  = 6.9 Hz, 4H), 3.41 (s, 4H), 3.33 (t,  $J$  = 6.4 Hz, 4H), 1.56 (p,  $J$  = 7.3 Hz, 4H), 1.42 (p,  $J$  = 7.7 Hz, 4H), 1.25 (s, 18H).  $^{13}C$  NMR (101 MHz,  $CDCl_3$ ):  $\delta$  170.9, 150.7, 149.9, 131.9, 129.2, 125.5, 60.7, 45.0, 40.7, 34.5, 32.9, 31.4, 29.5, 26.2. HRMS-ESI:  $C_{34}H_{46}^{79}Br_2N_3NaO_3^+$  [M + Na] $^+$  calcd, 711.1774; found, 711.1773.

**1,3-Bis(4-bromobutyl)-5,5-bis(3,5-di-tert-butylbenzyl)pyrimidine-2,4,6-(1H,3H,5H)-trione (4h).** To a stirred solution of **3h** (0.86 g, 1.62 mmol) in DMF was added  $K_2CO_3$  (1.2 g, 8.9 mmol). The reaction mixture was stirred for 5 min before addition of 1,4-

dibromobutane (1.76 mL, 14.8 mmol). The reaction was stirred for 18–48 h until completion was indicated by TLC (5% EtOAc in  $CHCl_3$ ). The reaction mixture was diluted with EtOAc (15 mL), and  $K_2CO_3$  was filtered off. The organic phase was washed with 10% citric acid soln (30 mL), 10%  $NaHCO_3$  soln (30 mL), water (3 × 30 mL), and brine (30 mL); dried with  $Na_2SO_4$ ; filtered; and concentrated. The crude was purified by automated flash chromatography to afford **4h** (0.64 g, 74%).  $^1H$  NMR (400 MHz,  $CDCl_3$ ):  $\delta$  7.26 (t,  $J$  = 1.9 Hz, 2H), 6.89 (d,  $J$  = 1.8 Hz, 4H), 3.59\* (t,  $J$  = 7.5 Hz, 4H), 3.46 (s, 4H), 3.23 (t,  $J$  = 6.7 Hz, 4H), 1.51 (p,  $J$  = 6.8 Hz, 4H), 1.35–1.23 (m, 40H).  $^{13}C$  NMR (101 MHz,  $CDCl_3$ ):  $\delta$  171.0, 151.1, 150.0, 134.4, 123.7, 121.5, 60.5, 46.5, 40.9, 34.8, 32.4, 31.6, 29.7, 26.5. \*Distorted triplet. HRMS-ESI:  $C_{42}H_{62}^{79}Br_2KN_2O_3^+$  [M + K] $^+$  calcd, 839.2759; found, 839.2755.

**Transformation to Azides (5).** **1,3-Bis(4-azidobutyl)-5,5-bis(4-trifluoromethylbenzyl)pyrimidine-2,4,6-(1H,3H,5H)-trione (5a).** To a stirred solution of **4a** (2.40 g, 3.35 mmol) in 5 mL of DMF was added  $NaN_3$  (762 mg, 11.7 mmol) and stirred for 18 h. The reaction mixture was diluted with EtOAc (30 mL) and washed with water (3 × 50 mL). The organic phase was dried over  $Na_2SO_4$ , filtered, and concentrated to afford the crude product **5a** as white crystals (1.91 g, 89%).  $^1H$  NMR (400 MHz,  $CDCl_3$ ):  $\delta$  7.49 (d,  $J$  = 7.8 Hz, 4H), 7.19 (d,  $J$  = 7.8 Hz, 4H), 3.67–3.58 (m, 4H), 3.51 (s, 4H), 3.27–3.15 (m, 4H), 1.38–1.23 (m, 8H).  $^{13}C$  NMR (101 MHz,  $CDCl_3$ ):  $\delta$  170.2, 149.3, 138.8, 130.4 (q,  $^2J_{C,F}$  = 32.7 Hz), 130.1, 126.0–125.6 (m), 123.9 (q,  $^1J_{C,F}$  = 272.2 Hz), 59.9, 50.8, 45.1, 41.4, 26.0, 24.9. HRMS-ESI:  $C_{28}H_{28}F_6N_8O_3Na^+$  [M + Na] $^+$  calcd, 661.2079; found, 661.2074.

**1,3-Bis(4-azidobutyl)-5,5-bis(naphthalen-2-yl)pyrimidine-2,4,6-(1H,3H,5H)-trione (5b).** To a stirred solution of **4b** (509 mg, 0.75 mmol) in DMF (3 mL) was added  $NaN_3$  (146 mg, 2.25 mmol). The reaction was stirred overnight until completion was indicated by TLC (5% EtOAc in  $CHCl_3$ ). The reaction mixture was diluted with EtOAc (20 mL) and washed with water (3 × 20 mL). The organic phase was dried over  $Na_2SO_4$ , filtered, and concentrated. The crude product was dissolved in  $CHCl_3$  and adsorbed onto Celite before purification on a silica column using 0–5% EtOAc in  $CHCl_3$  to afford **5b** (194 mg, 91%).  $^1H$  NMR (400 MHz,  $CDCl_3$ ):  $\delta$  7.80–7.71 (m, 4H), 7.68 (d,  $J$  = 8.4 Hz, 2H), 7.57 (s, 2H), 7.51–7.41 (m, 4H), 7.17 (d,  $J$  = 8.4 Hz, 2H), 3.68 (s, 4H), 3.52 (t,  $J$  = 7.0 Hz, 4H), 2.85 (t,  $J$  = 6.6 Hz, 4H), 1.14 (p,  $J$  = 7.4 Hz, 4H), 1.02 (p,  $J$  = 7.0 Hz, 4H).  $^{13}C$  NMR (101 MHz,  $CDCl_3$ ):  $\delta$  170.9, 149.6, 133.4, 132.7, 132.5, 128.8, 128.5, 127.8, 127.7, 127.2, 126.6, 126.3, 60.8, 50.7, 45.8, 41.2, 25.8, 24.9. HRMS-ESI:  $C_{34}H_{34}N_8NaO_3^+$  [M + Na] $^+$  calcd, 625.2646; found, 625.2647.

**1,3-Bis(4-azidobutyl)-5,5-bis(4-fluoronaphthalen-1-yl)methyl)pyrimidine-2,4,6-(1H,3H,5H)-trione (5c).** To a stirred solution of **4c** (166 mg, 0.23 mmol) in DMF (3 mL) was added  $NaN_3$  (45 mg, 0.69 mmol). The reaction was stirred overnight until completion was indicated by TLC ( $CHCl_3$ ). Then, the reaction mixture was diluted with EtOAc (20 mL) and washed with water (3 × 30 mL) and brine (30 mL). The organic phase was dried over  $Na_2SO_4$ , filtered, and concentrated to afford **5c** (142 mg, 95%).  $^1H$  NMR (400 MHz,  $CDCl_3$ ):  $\delta$  8.23 (d,  $J$  = 8.6 Hz, 2H), 8.08 (d,  $J$  = 8.3 Hz, 2H), 7.62 (t,  $J$  = 7.6 Hz, 2H), 7.54 (t,  $J$  = 7.5 Hz, 2H), 7.22 (t,  $J$  = 6.6 Hz, 2H), 6.98 (t,  $J$  = 9.0 Hz, 2H), 4.06 (s, 4H), 3.33 (t,  $J$  = 6.8 Hz, 4H), 2.94 (t,  $J$  = 6.4 Hz, 4H), 1.10–0.74 (m, 8H).  $^{13}C$  NMR (101 MHz,  $CDCl_3$ ):  $\delta$  170.9, 158.5 (d,  $^1J_{C,F}$  = 253.4 Hz), 149.4, 133.2 (d,  $J_{C,F}$  = 4.4 Hz), 127.9 (d,  $J_{C,F}$  = 8.5 Hz), 127.4 (d,  $J_{C,F}$  = 4.6 Hz), 127.2, 126.4 (d,  $J_{C,F}$  = 1.9 Hz), 124.8 (d,  $J_{C,F}$  = 2.6 Hz), 124.1 (d,  $J_{C,F}$  = 15.7 Hz), 121.1 (d,  $J_{C,F}$  = 6.1 Hz), 108.8 (d,  $J_{C,F}$  = 20.0 Hz), 60.0, 50.7, 41.1, 40.7, 25.6, 24.4. HRMS-ESI:  $C_{34}H_{32}ClF_2N_8O_3^-$  [M + Cl] $^-$  calcd, 673.2259; found, 673.2259.

**1,3-Bis(4-azidobutyl)-5,5-bis(4-bromo-3-chlorobenzyl)pyrimidine-2,4,6-(1H,3H,5H)-trione (5d).** To a stirred solution of **4d** (1.28 g, 1.58 mmol) in DMF (20 mL) was added  $NaN_3$  (0.29 g, 4.75 mmol). The reaction was stirred overnight until completion was indicated by TLC (5% EtOAc in  $CHCl_3$ ). Then, the reaction mixture was diluted with EtOAc (25 mL) and washed with water (2 × 20 mL). The organic phase was dried over  $Na_2SO_4$ , filtered, and concentrated to yield the crude product **5d** (1.153 g, 98%). The crude

product was used without further purification.  $^1\text{H}$  NMR (400 MHz,  $\text{CDCl}_3$ ):  $\delta$  7.46 (d,  $J = 8.2$  Hz, 2H), 7.15 (d,  $J = 2.0$  Hz, 2H), 6.80 (dd,  $J = 8.2, 2.1$  Hz, 2H), 3.63 (t,  $J = 6.7$  Hz, 4H), 3.35 (s, 4H), 3.30–3.21 (m, 4H), 1.36 (h,  $J = 3.2$  Hz, 8H).  $^{13}\text{C}$  NMR (101 MHz,  $\text{CDCl}_3$ ):  $\delta$  170.1, 149.2, 135.5, 134.9, 134.1, 131.4, 129.1, 122.2, 59.7, 50.9, 44.3, 41.5, 26.1, 25.1. HRMS-ESI:  $\text{C}_{26}\text{H}_{26}^{79}\text{Br}_2\text{Cl}_2\text{N}_8\text{NaO}_3^+ [\text{M} + \text{Na}]^+$  calcd, 748.9764; found, 748.9777.

**1,3-Bis(4-azidobutyl)-5,5-bis(3,5-dibromobenzyl)pyrimidine-2,4,6-(1H,3H,5H)-trione (5e).** To a stirred solution of **4e** (239 mg, 0.26 mmol) in DMF (3 mL) was added  $\text{NaN}_3$  (52 mg, 0.8 mmol). The reaction was stirred overnight until completion was indicated by TLC (5% EtOAc in  $\text{CHCl}_3$ ). Then, the reaction mixture was diluted with EtOAc (15 mL) and washed with water (2  $\times$  20 mL). The organic phase was dried over  $\text{Na}_2\text{SO}_4$ , filtered, and concentrated. The crude product was dissolved in  $\text{CHCl}_3$  and adsorbed onto Celite before purification on a silica column using 0–5% EtOAc in  $\text{CHCl}_3$  to afford **5e** (194 mg, 91%).  $^1\text{H}$  NMR (400 MHz,  $\text{CDCl}_3$ ):  $\delta$  7.54 (s, 2H), 7.14 (s, 4H), 3.73–3.58 (m, 4H), 3.33 (s, 4H), 3.31–3.22 (m, 4H), 1.58–1.29 (m, 8H).  $^{13}\text{C}$  NMR (101 MHz,  $\text{CDCl}_3$ ):  $\delta$  169.9, 149.1, 138.4, 133.8, 131.4, 123.3, 59.9, 50.9, 44.2, 41.6, 26.1, 25.3. HRMS-ESI:  $\text{C}_{26}\text{H}_{26}^{79}\text{Br}_4\text{ClN}_8\text{O}_3^- [\text{M} + \text{Cl}]^-$  calcd, 848.8555; found, 848.8564.

**1,3-Bis(4-azidobutyl)-5,5-bis(3,5-bis(trifluoromethyl)benzyl)pyrimidine-2,4,6-(1H,3H,5H)-trione (5f).** To a stirred solution of **4f** (101 mg, 0.12 mmol) in DMF (1 mL) was added  $\text{NaN}_3$  (23 mg, 0.35 mmol). The reaction was stirred overnight. When full conversion was reached according to MS analysis, the reaction mixture was diluted with EtOAc (15 mL) and washed with water (3  $\times$  20 mL). The organic phase was dried over  $\text{Na}_2\text{SO}_4$ , filtered, and concentrated to afford the crude of **5f** (63 mg, 68%) as a white powder.  $^1\text{H}$  NMR (400 MHz,  $\text{CDCl}_3$ ):  $\delta$  7.78 (s, 2H), 7.53 (s, 4H), 3.59 (s, 4H), 3.57–3.48 (m, 4H), 3.19 (t,  $J = 6.7$  Hz, 4H), 1.42–1.31 (m, 4H), 1.31–1.20 (m, 4H).  $^{13}\text{C}$  NMR (101 MHz,  $\text{CDCl}_3$ ):  $\delta$  169.6, 148.6, 137.0, 132.3 (q,  $^2J_{\text{C,F}} = 33.6$  Hz), 129.9, 123.0 (q,  $^3J_{\text{C,F}} = 272.9$  Hz), 122.8–121.9 (m), 59.8, 50.6, 44.5, 41.6, 26.0, 24.9. HRMS-ESI:  $\text{C}_{30}\text{H}_{26}\text{ClF}_{12}\text{N}_8\text{O}_3^- [\text{M} + \text{Cl}]^-$  calcd, 809.1630; found, 809.1622.

**1,3-Bis(4-azidobutyl)-5,5-bis(4-tert-butylbenzyl)pyrimidine-2,4,6-(1H,3H,5H)-trione (5g).** To a stirred solution of bromide **4g** (2.40 g, 3.47 mmol) in DMF (15 mL) was added  $\text{NaN}_3$  (678 mg, 10.4 mmol) and stirred for 18 h. The reaction mixture was diluted with EtOAc (50 mL) and washed with water (4  $\times$  50 mL). The organic phase was dried over  $\text{Na}_2\text{SO}_4$ , filtered, and concentrated. The crude product **5g** was isolated as a clear oil (2.16 g, 100%).  $^1\text{H}$  NMR (400 MHz,  $\text{CDCl}_3$ ):  $\delta$  7.20 (d,  $J = 7.7$  Hz, 4H), 6.97 (d,  $J = 7.8$  Hz, 4H), 3.59 (s, 4H), 3.40 (s, 4H), 3.21 (s, 4H), 1.37–1.28 (m, 8H), 1.24 (s, 18H).  $^{13}\text{C}$  NMR (101 MHz,  $\text{CDCl}_3$ ):  $\delta$  171.0, 150.8, 150.0, 132.0, 129.3, 125.5, 60.7, 50.9, 45.1, 41.1, 34.6, 31.4, 26.0, 24.8. HRMS-ESI:  $\text{C}_{34}\text{H}_{46}\text{N}_8\text{O}_3\text{Na}^+ [\text{M} + \text{Na}]^+$  calcd, 637.3577; found, 637.3583.

**1,3-Bis(4-azidobutyl)-5,5-bis(4-tert-butylbenzyl)pyrimidine-2,4,6-(1H,3H,5H)-trione (5h).** To a stirred solution of **4h** (630 mg, 0.78 mmol) in DMF (10 mL) was added  $\text{NaN}_3$  (140 mg, 2.15 mmol). The reaction was stirred overnight. When full conversion was reached according to MS analysis, the reaction mixture was diluted with EtOAc (50 mL) and washed with water 4  $\times$  50 mL. The organic phase was dried over  $\text{Na}_2\text{SO}_4$ , filtered, and concentrated, affording the crude product **5h** (463 mg, 80%).  $^1\text{H}$  NMR (400 MHz,  $\text{CDCl}_3$ ):  $\delta$  7.25 (t,  $J = 1.9$  Hz, 2H), 6.87 (d,  $J = 1.7$  Hz, 4H), 3.56 (t,  $J = 7.2$  Hz, 4H), 3.45 (s, 4H), 3.14 (t,  $J = 6.5$  Hz, 4H), 1.25 (s, 44H).  $^{13}\text{C}$  NMR (101 MHz,  $\text{CDCl}_3$ ):  $\delta$  171.1, 151.1, 150.0, 134.4, 123.8, 121.6, 60.6, 50.8, 46.5, 41.3, 34.8, 31.6, 25.9, 25.1. HRMS-ESI:  $\text{C}_{42}\text{H}_{62}\text{N}_8\text{NaO}_3^+ [\text{M} + \text{Na}]^+$  calcd, 749.4838; found, 749.4838.

**Reduction of Azides (5) to Amines (6).** **1,3-Bis(4-aminobutyl)-5,5-bis(4-(trifluoromethyl)benzyl)pyrimidin-2,4,6-(1H,3H,5H)-trione (6a).** To a stirred solution of **5a** (1.86 g, 2.90 mmol) and  $\text{Et}_3\text{N}$  (0.96 mL, 6.89 mmol) in *i*-PrOH/THF (1:1, 10 mL) was added 1,3-propanedithiol (0.1 mL, 0.99 mmol). The mixture was stirred for 5 min before addition of  $\text{NaBH}_4$  (316 mg, 8.35 mmol). After a 48 h reaction time,  $\text{Boc}_2\text{O}$  (1.75 g, 8.02 mmol) and  $\text{K}_2\text{CO}_3$  (1.91 g, 13.8 mmol) were added, and the reaction was stirred for 18 h and evaporated before adding EtOAc (20 mL) and water (15 mL) and

stirring for 1 h. The organic phase was washed with water (3  $\times$  15 mL) and brine (15 mL) and concentrated. The resulting crude was purified by automated flash chromatography and evaporated. The Boc-protected intermediate was deprotected with TFA (2 mL, 26 mmol) in  $\text{CH}_2\text{Cl}_2$  (5 mL) for 18 h. The reaction mixture was concentrated, and the crude product was purified by RP automated flash chromatography and lyophilized to afford **6a** (160 mg, 7%) as the TFA salt.  $^1\text{H}$  NMR (400 MHz,  $\text{CD}_3\text{OD}$ ):  $\delta$  7.58 (d,  $J = 8.1$  Hz, 4H), 7.28 (d,  $J = 8.1$  Hz, 4H), 3.71–3.58 (m, 4H), 3.57 (s, 4H), 2.96–2.75 (m, 4H), 1.42 (p,  $J = 7.3$  Hz, 4H), 1.30 (p,  $J = 7.3$  Hz, 4H).  $^{13}\text{C}$  NMR (101 MHz,  $\text{CD}_3\text{OD}$ ):  $\delta$  171.4, 162.9 (q,  $^2J_{\text{C,F}} = 34.7$  Hz, TFA), 150.7, 140.9, 131.5, 131.0 (q,  $^2J_{\text{C,F}} = 32.6$  Hz), 126.6 (q,  $^1J_{\text{C,F}} = 3.8$  Hz), 125.5 (q,  $^3J_{\text{C,F}} = 272.3$  Hz), 118.2 (q,  $^1J_{\text{C,F}} = 292.5$  Hz, TFA), 61.1, 45.8, 42.0, 40.0, 25.6 (overlap, two carbons). HRMS-ESI:  $\text{C}_{28}\text{H}_{33}\text{F}_6\text{N}_4\text{O}_3^+ [\text{M} + \text{H}]^+$  calcd, 587.2452; found, 587.2460.

**1,3-Bis(4-aminobutyl)-5,5-bis(naphthalen-2-yl-methyl)pyrimidin-2,4,6-(1H,3H,5H)-trione (6b).** To a stirred solution of **5b** (438 mg, 0.73 mmol) and  $\text{Et}_3\text{N}$  (0.22 mL, 1.59 mmol) in *i*-PrOH/THF (1:1, 4 mL) was added 1,3-propanedithiol (0.1 mL, 0.99 mmol). The mixture was stirred for 5 min before addition of  $\text{NaBH}_4$  (68 mg, 1.81 mmol). After a 72 h reaction time,  $\text{Boc}_2\text{O}$  (333 mg, 1.53 mmol) and  $\text{NaHCO}_3$  (244 mg, 2.90 mmol) were added, and the reaction was stirred for 18 h before being filtered through a pad of Celite and concentrated. The resulting crude was purified by automated flash chromatography and evaporated. The Boc-protected intermediate (305 mg) was deprotected with TFA (2 mL, 26.1 mmol) in  $\text{CH}_2\text{Cl}_2$  (5 mL) overnight. When MS analysis showed full deprotection, the reaction mixture was concentrated, and the crude product was purified by RP automated flash chromatography and lyophilized to afford **6b** (287 mg, 90%) as the TFA salt.  $^1\text{H}$  NMR (400 MHz,  $\text{CD}_3\text{OD}$ ):  $\delta$  7.90–7.68 (m, 6H), 7.60 (s, 2H), 7.52–7.43 (m, 4H), 7.19 (d,  $J = 8.3$  Hz, 2H), 3.70 (s, 4H), 3.59–3.50 (m, 4H), 2.56–2.37 (m, 4H), 1.30–0.96 (m, 8H).  $^{13}\text{C}$  NMR (101 MHz,  $\text{CD}_3\text{OD}$ ):  $\delta$  172.2, 162.8 (q,  $J = 35.2$  Hz, TFA), 151.0, 134.7, 134.1, 134.0, 129.9, 129.4, 128.8, 128.7, 128.2, 127.6, 127.3, 118.1 (d,  $J = 292.3$  Hz, TFA), 62.0, 46.6, 41.7, 39.8, 25.6, 25.5. HRMS-ESI:  $\text{C}_{34}\text{H}_{39}\text{N}_4\text{O}_3^+ [\text{M} + \text{H}]^+$  calcd, 551.3017; found, 551.3020.

**1,3-Bis(4-aminobutyl)-5,5-bis((4-fluoronaphthalen-1-yl)methyl)pyrimidin-2,4,6-(1H,3H,5H)-trione (6c).** To a stirred solution of **5c** (67 mg, 0.105 mmol) and  $\text{Et}_3\text{N}$  (0.03 mL, 0.21 mmol) in *i*-PrOH/THF (1:1, 4 mL) was added 1,3-propanedithiol (0.1 mL, 0.99 mmol). The mixture was stirred for 5 min before addition of  $\text{NaBH}_4$  (8 mg, 0.21 mmol). After a 72 h reaction time,  $\text{Boc}_2\text{O}$  (48 mg, 0.22 mmol) and  $\text{NaHCO}_3$  (35 mg, 0.42 mmol) were added, and the reaction was stirred for 18 h before being filtered through a pad of Celite and concentrated. The resulting crude was purified by automated flash chromatography and evaporated. The Boc-protected intermediate (72 mg) was deprotected with TFA (0.2 mL, 2.61 mmol) in  $\text{CH}_2\text{Cl}_2$  (5 mL) overnight. When MS analysis showed full deprotection, the reaction mixture was concentrated, and the crude product was purified by RP automated flash chromatography and lyophilized to yield **6c** (82 mg, 89%) as the TFA salt.  $^1\text{H}$  NMR (400 MHz,  $\text{CD}_3\text{OD}$ ):  $\delta$  8.34 (d,  $J = 7.9$  Hz, 2H), 8.07 (d,  $J = 7.7$  Hz, 2H), 7.74–7.53 (m, 4H), 7.38–7.19 (m, 2H), 7.08 (t,  $J = 8.9$  Hz, 2H), 4.13 (s, 4H), 3.39–3.33 (m, 4H), 2.60 (t,  $J = 6.8$  Hz, 4H), 1.20–1.00 (m, 4H), 0.94–0.71 (m, 4H).  $^{13}\text{C}$  NMR (101 MHz,  $\text{CDCl}_3$ ):  $\delta$  172.2, 163.11 (q,  $^2J_{\text{C,F}} = 34.1$  Hz, TFA), 159.6 (d,  $^1J_{\text{C,F}} = 251.5$  Hz), 150.8, 134.5 (d,  $J_{\text{C,F}} = 4.4$  Hz), 129.3 (d,  $J_{\text{C,F}} = 4.5$  Hz), 128.4 (d,  $J_{\text{C,F}} = 8.5$  Hz), 128.2, 127.6 (d,  $J_{\text{C,F}} = 1.1$  Hz), 126.3 (d,  $J_{\text{C,F}} = 2.4$  Hz), 125.2 (d,  $J_{\text{C,F}} = 15.6$  Hz), 121.5 (d,  $J_{\text{C,F}} = 6.2$  Hz), 118.23 (q,  $^1J_{\text{C,F}} = 292.8$  Hz, TFA), 109.76 (d,  $J_{\text{C,F}} = 20.2$  Hz), 61.0, 41.7, 41.3, 39.9, 25.3, 25.1. HRMS-ESI:  $\text{C}_{34}\text{H}_{37}\text{F}_2\text{N}_4\text{O}_3^+ [\text{M} + \text{H}]^+$  calcd, 587.2828; found, 587.2828.

**1,3-Bis(4-aminobutyl)-5,5-bis(4-bromo-3-chlorobenzyl)pyrimidine-2,4,6-(1H,3H,5H)-trione (6d).** To a stirred solution of **5d** (588 mg, 0.81 mmol) and  $\text{Et}_3\text{N}$  (0.23 mL, 1.69 mmol) in *i*-PrOH/THF (1:1, 10 mL) was added 1,3-propanedithiol (0.164 mL, 1.76 mmol). After a 48 h reaction time,  $\text{Boc}_2\text{O}$  (528 mg, 2.42 mmol) was added, and the reaction mixture was stirred for 18 h and evaporated. To the crude mixture was added EtOAc (20 mL) and water (15 mL)

and stirred for 30 min. The organic phase was washed with water (3 × 15 mL) and brine (15 mL) and concentrated. The resulting crude was purified by automated flash chromatography (EtOAc/heptane) and evaporated. The Boc-protected intermediate was deprotected with TFA (2 mL, 26 mmol) in CH<sub>2</sub>Cl<sub>2</sub> (5 mL) for 18 h. The reaction mixture was concentrated, and the crude product was purified by RP automated flash chromatography and lyophilized to afford **6d** (0.542 mg, 77%) as the TFA salt. <sup>1</sup>H NMR (400 MHz, CD<sub>3</sub>OD): δ 7.59 (d, *J* = 8.2 Hz, 2H), 7.24 (d, *J* = 2.1 Hz, 2H), 6.92 (dd, *J* = 8.3, 2.1 Hz, 2H), 3.73–3.59 (m, 4H), 3.43 (s, 4H), 3.01–2.76 (m, 4H), 1.59–1.43 (m, 4H), 1.36 (t, *J* = 9.3, 6.0 Hz, 4H). <sup>13</sup>C NMR (101 MHz, CD<sub>3</sub>OD): δ 171.4, 150.7, 137.7, 135.5, 135.3, 132.7, 130.7, 122.6, 61.0, 44.9, 42.1, 40.2, 26.0, 25.8. HRMS-ESI: C<sub>26</sub>H<sub>31</sub><sup>79</sup>Br<sub>2</sub>Cl<sub>2</sub>N<sub>4</sub>O<sub>3</sub><sup>+</sup> [M + H]<sup>+</sup> calcd, 675.0134; found, 675.0145.

**1,3-Bis(4-aminobutyl)-5,5-bis(3,5-dibromobenzyl)pyrimidin-2,4,6-(1H,3H,5H)-trione (6e).** To a stirred solution of **5e** (810 mg, 0.99 mmol) and Et<sub>3</sub>N (0.32 mL, 2.29 mmol) in *i*-PrOH/THF (1:1, 5 mL) was added 1,3-propanedithiol (0.20 mL, 1.99 mmol). The mixture was stirred for 5 min before addition of NaBH<sub>4</sub> (90 mg, 2.37 mmol). After a 48 h reaction time, Boc<sub>2</sub>O (650 mg, 2.97 mmol) was added, and the reaction mixture was stirred for 18 h and evaporated. To the crude mixture were added EtOAc (15 mL) and water (15 mL) and stirred for 30 min. The organic phase was washed with water (3 × 15 mL) and brine (15 mL) and concentrated. The resulting crude was purified by automated flash chromatography and evaporated. The Boc-protected intermediate was deprotected with TFA (2 mL, 26 mmol) in CH<sub>2</sub>Cl<sub>2</sub> (5 mL) for 18 h. The reaction mixture was concentrated, and the crude product was purified by RP automated flash chromatography and lyophilized to afford **6e** (374 mg, 38%) as the TFA salt. <sup>1</sup>H NMR (400 MHz, CD<sub>3</sub>OD): δ 7.66 (s, 2H), 7.23 (s, 4H), 3.68 (t, *J* = 7.7 Hz, 4H), 3.43 (s, 4H), 3.08–2.82 (m, 4H), 1.76–1.48 (m, 4H), 1.49–1.32 (m, 4H). <sup>13</sup>C NMR (101 MHz, CD<sub>3</sub>OD): δ 171.2, 163.01 (q, *J* = 34.4 Hz, TFA), 150.4, 140.5, 134.5, 132.7, 124.1, 118.2 (q, *J* = 293.3 Hz, TFA), 61.2, 44.8, 42.2, 40.3, 26.3, 25.8. HRMS-ESI: C<sub>26</sub>H<sub>31</sub><sup>79</sup>Br<sub>2</sub>N<sub>4</sub>O<sub>3</sub><sup>+</sup> [M + H]<sup>+</sup> calcd, 762.9124; found, 762.9124.

**1,3-Bis(4-aminobutyl)-5,5-bis(3,5-bis(trifluoromethyl)benzyl)pyrimidin-2,4,6-(1H,3H,5H)-trione (6f).** To a stirred solution of **5f** (63 mg, 0.81 mmol) and Et<sub>3</sub>N (0.034 mL, 0.24 mmol) in *i*-PrOH/THF (1:1, 2 mL) was added 1,3-propanedithiol (0.10 mL, 0.99 mmol). The mixture was stirred for 5 min before addition of NaBH<sub>4</sub> (92 mg, 0.24 mmol). After a 48 h reaction time, Boc<sub>2</sub>O (70 mg, 0.32 mmol) and K<sub>2</sub>CO<sub>3</sub> (45 mg, 0.33 mmol) were added, and the reaction was stirred for another night, before being diluted with EtOAc (10 mL) and water (10 mL) and stirred for 1 h. The organic phase was washed with water (3 × 15 mL) and brine (15 mL) and concentrated. The resulting crude was purified by automated flash chromatography and evaporated. The Boc-protected intermediate was deprotected with TFA (2 mL, 26 mmol) in CH<sub>2</sub>Cl<sub>2</sub> (5 mL) for 18 h. The reaction mixture was concentrated, and the crude product was purified by RP automated flash chromatography and lyophilized to afford **6f** (12 mg, 16%) as the TFA salt. <sup>1</sup>H NMR (400 MHz, CD<sub>3</sub>OD): δ 7.93 (s, 2H), 7.68 (s, 4H), 3.71 (s, 4H), 3.61–3.54 (m, 4H), 2.87–2.80 (m, 4H), 1.57–1.46 (m, 4H), 1.33–1.22 (m, 4H). <sup>13</sup>C NMR (101 MHz, CD<sub>3</sub>OD): δ 170.9, 150.1, 139.4, 133.0 (q, <sup>2</sup>J<sub>C,F</sub> = 33.4 Hz), 131.6–131.1 (m), 124.6 (q, <sup>1</sup>J<sub>C,F</sub> = 272.1 Hz), 123.0, 61.1, 44.8, 42.3, 40.0, 25.9, 25.7. HRMS-ESI: C<sub>30</sub>H<sub>31</sub>F<sub>12</sub>N<sub>4</sub>O<sub>3</sub><sup>+</sup> [M + H]<sup>+</sup> calcd, 723.2197; found, 723.2161.

**1,3-Bis(4-aminobutyl)-5,5-bis(4-tert-butylbenzyl)pyrimidin-2,4,6-(1H,3H,5H)-trione (6g).** To a stirred solution of **5g** (2.16 g, 3.52 mmol) and Et<sub>3</sub>N (0.98 mL, 7.05 mmol) in *i*-PrOH/THF (1:1, 10 mL) was added 1,3-propanedithiol (0.1 mL, 0.99 mmol). The mixture was stirred for 5 min before addition of NaBH<sub>4</sub> (270 mg, 7.14 mmol). After a 72 h reaction time, Boc<sub>2</sub>O (1.69 g, 7.74 mmol) and K<sub>2</sub>CO<sub>3</sub> (1.94 g, 14.0 mmol) were added, and the reaction was stirred for 18 h and evaporated before adding EtOAc (20 mL) and water (15 mL) and stirring for 30 min. The organic phase was washed with water (3 × 15 mL) and brine (15 mL) and concentrated. The resulting crude was purified by automated flash chromatography and evaporated. The Boc-protected intermediate was deprotected with TFA (2.2 mL, 28.7

mmol) in CH<sub>2</sub>Cl<sub>2</sub> (10 mL) for 18 h. The reaction mixture was concentrated, and the crude product was purified by RP automated flash chromatography and lyophilized to afford **6g** (367 mg, 85%) as the TFA salt. <sup>1</sup>H NMR (400 MHz, CD<sub>3</sub>OD): δ 7.25 (d, *J* = 7.1 Hz, 4H), 6.98 (d, *J* = 7.2 Hz, 4H), 3.62–3.53 (m, 4H), 3.39 (s, 4H), 2.87 (t, *J* = 7.4 Hz, 4H), 1.55–1.36 (m, 4H), 1.36–1.15 (m, 22H). <sup>13</sup>C NMR (101 MHz, CD<sub>3</sub>OD): δ 172.3, 163.0 (q, *J* = 34.4 Hz, TFA), 151.9, 151.0, 133.5, 130.3, 126.5, 118.2 (q, *J* = 292.8 Hz, TFA), 61.9, 45.9, 41.7, 40.0, 35.3, 31.7, 25.6, 25.5. HRMS-ESI: C<sub>34</sub>H<sub>51</sub>N<sub>4</sub>O<sub>3</sub><sup>+</sup> [M + H]<sup>+</sup> calcd, 563.3956; found, 563.3934.

**1,3-Bis(4-aminobutyl)-5,5-bis(3,5-di-tert-butylbenzyl)pyrimidin-2,4,6-(1H,3H,5H)-trione (6h).** To a stirred solution of **5h** (405 mg, 0.55 mol) and Et<sub>3</sub>N (0.16 mL, 1.15 mmol) in *i*-PrOH/THF (1:1, 6 mL) was added 1,3-propanedithiol (0.12 mL, 1.15 mmol). The mixture was stirred for 5 min before addition of NaBH<sub>4</sub> (44 mg, 1.16 mmol). After a 72 h reaction time, Boc<sub>2</sub>O (490 mg, 2.25 mmol) was added, and the reaction was stirred for another night before being diluted with EtOAc (10 mL) and water (10 mL) and stirred for 1 h. The organic phase was washed with water (3 × 15 mL) and brine (15 mL) and concentrated. The resulting crude was purified by automated flash chromatography and evaporated. The Boc-protected intermediate was deprotected with TFA (1.7 mL, 22.2 mmol) in CH<sub>2</sub>Cl<sub>2</sub> (5 mL) for 6 h. The reaction mixture was concentrated, and the crude product was purified by RP automated flash chromatography and lyophilized to afford **6h** (154 mg, 31%) as the TFA salt. <sup>1</sup>H NMR (400 MHz, CD<sub>3</sub>OD): δ 7.31 (t, *J* = 1.5 Hz, 2H), 6.89 (d, *J* = 1.6 Hz, 4H), 3.59 (t\*, 4H), 3.44 (s, 4H), 2.78 (t\*, 4H), 1.40 (p, *J* = 7.7 Hz, 4H), 1.26 (s, 36H), 1.17 (p, *J* = 7.6 Hz, 4H). <sup>13</sup>C NMR (101 MHz, CD<sub>3</sub>OD): δ 172.3, 162.8 (q, *J* = 34.7 Hz, TFA), 152.3, 151.1, 135.8, 124.7, 122.6, 118.1 (q, *J* = 292.5 Hz, TFA), 61.8, 47.3, 42.0, 39.9, 35.6, 31.9, 25.9, 25.5. \*Distorted triplets. HRMS-ESI: C<sub>42</sub>H<sub>67</sub>N<sub>4</sub>O<sub>3</sub><sup>+</sup> [M + H]<sup>+</sup> calcd, 675.5211; found, 675.5211.

**Guanylation of Amines (6) to Guanidines (7).** **1,1'-(2,4,6-Trioxo-5,5-bis(4-(trifluoromethyl)benzyl)dihydropyrimidine-1,3(2H,4H)-diyl)bis(butane-4,1-diyl)diguandine (7a).** To a stirred solution of the TFA salt of **6a** (33 mg, 0.41 μmol) in THF (3 mL) were added NaHCO<sub>3</sub> (27 mg, 0.31 mmol) and *N,N'*-bis-Boc-1-guanylpiperazine (27 mg, 0.86 mmol). The reaction was stirred at room temperature for 48 h until TLC (CH<sub>2</sub>Cl<sub>2</sub>) showed full guanylation of the diamine. The reaction mixture was concentrated, and the crude product was then dissolved in EtOAc (10 mL) and washed with 10% citric acid soln (2 × 10 mL), 10% NaHCO<sub>3</sub> soln (10 mL), and brine (10 mL). The organic phase was dried over Na<sub>2</sub>SO<sub>4</sub>, filtered, and concentrated. The crude product was purified by automated flash chromatography, and the resulting Boc-protected intermediate was deprotected with TFA (0.2 mL, 2.61 mmol) in CH<sub>2</sub>Cl<sub>2</sub> (2 mL) for 18 h. The reaction mixture was concentrated, and the crude was purified by RP automated flash chromatography and lyophilized to afford **7a** (24 mg, 65%) as a white powder. <sup>1</sup>H NMR (400 MHz, CD<sub>3</sub>OD): δ 7.56 (d, *J* = 8.1 Hz, 4H), 7.28 (d, *J* = 8.0 Hz, 4H), 3.62 (t, *J* = 6.7 Hz, 4H), 3.57 (s, 4H), 3.11 (t, *J* = 6.5 Hz, 4H), 1.37–1.28 (m, 8H). <sup>13</sup>C NMR (101 MHz, CD<sub>3</sub>OD): δ 171.5, 162.4 (q, <sup>2</sup>J<sub>C,F</sub> = 35.5 Hz, TFA), 158.7, 150.8, 140.9, 131.5, 131.1 (q, <sup>2</sup>J<sub>C,F</sub> = 32.4 Hz), 126.7–126.4 (m), 125.46 (q, <sup>1</sup>J<sub>C,F</sub> = 271.3 Hz), 117.9 (q, <sup>1</sup>J<sub>C,F</sub> = 291.1 Hz, TFA), 61.1, 45.9, 42.3, 41.8, 26.9, 25.8. HRMS-ESI: C<sub>30</sub>H<sub>37</sub>F<sub>6</sub>N<sub>8</sub>O<sub>3</sub><sup>+</sup> [M + H]<sup>+</sup> calcd, 671.2887; found, 671.2836.

**1,1'-(5,5-Bis(naphthalen-2-ylmethyl)-2,4,6-trioxodihydropyrimidine-1,3(2H,4H)-diyl)bis(butane-4,1-diyl)diguandine (7b).** To a stirred solution of the TFA salt of **6b** (54 mg, 0.069 mmol) in THF (4 mL) were added *N,N'*-bis-Boc-1-guanylpiperazine (63 mg, 0.20 mmol) and NaHCO<sub>3</sub> (41 mg, 0.48 mmol) and stirred at room temperature for 48 h until TLC (CHCl<sub>3</sub>) showed full conversion. The reaction mixture was diluted with EtOAc (5 mL), washed with 10% citric acid soln (2 × 10 mL) and brine (10 mL), dried over Na<sub>2</sub>SO<sub>4</sub>, filtered, and concentrated. The Boc-protected intermediate was dissolved in CHCl<sub>3</sub> and adsorbed onto Celite before purification on a silica column using CHCl<sub>3</sub> as the mobile phase. The Boc-protected intermediate (64 mg of a total of 104 mg, 0.057 mmol) was deprotected with TFA (0.2 mL) in CH<sub>2</sub>Cl<sub>2</sub> (4 mL) overnight. The reaction mixture was concentrated and purified by RP automated flash

chromatography and lyophilized to afford **7b** (60 mg, 99%) as a white powder.  $^1\text{H}$  NMR (400 MHz,  $\text{CD}_3\text{OD}$ ):  $\delta$  7.85–7.69 (m, 6H), 7.59 (s, 2H), 7.53–7.40 (m, 4H), 7.20 (dd,  $J = 8.4, 1.8$  Hz, 2H), 3.69 (s, 4H), 3.54 (t,  $J = 7.1$  Hz, 4H), 2.80 (t,  $J = 7.1$  Hz, 4H), 1.21–1.08 (m, 4H), 1.08–0.98 (m, 4H).  $^{13}\text{C}$  NMR (101 MHz,  $\text{CD}_3\text{OD}$ ):  $\delta$  172.3, 163.1 (q,  $J = 34.3$  Hz, TFA), 158.5, 151.0, 134.7, 134.1, 134.0, 129.8, 129.4, 128.7, 128.6, 128.3, 127.6, 127.3, 118.2 (q,  $J = 293.0$  Hz, TFA), 62.0, 46.6, 42.1, 41.8, 26.6, 25.9. HRMS-ESI:  $\text{C}_{36}\text{H}_{43}\text{N}_8\text{O}_3^+$  [ $\text{M} + \text{H}$ ] $^+$  calcd, 635.3450; found, 635.3448.

**1,1'-(5,5-Bis(4-fluoronaphthalen-1-yl)methyl)-2,4,6-trioxodihydropyrimidine-1,3(2H,4H)-diylbis(butane-4,1-diyl)diguandine (7c)**. To a stirred solution of the TFA salt of **6c** (35 mg, 43  $\mu\text{mol}$ ) in THF (3 mL) were added  $N,N'$ -bis-Boc-1-guanylpyrazole (38 mg, 122  $\mu\text{mol}$ ) and  $\text{NaHCO}_3$  (25 mg, 0.29 mmol) and stirred at room temperature for 48 h until TLC ( $\text{CHCl}_3$ ) showed full conversion. The reaction mixture was diluted with EtOAc (5 mL), washed with 10% citric acid soln and brine, dried over  $\text{Na}_2\text{SO}_4$ , filtered, and concentrated. The Boc-protected intermediate was dissolved in  $\text{CHCl}_3$  and adsorbed onto Celite before purification on a silica column using  $\text{CHCl}_3$  as the mobile phase. The Boc-protected intermediate (41 mg of a total of 95 mg, 0.038 mmol) was deprotected with TFA (0.1 mL) in  $\text{CH}_2\text{Cl}_2$  (4 mL) overnight. The reaction mixture was concentrated and purified by RP automated flash chromatography and lyophilized to afford **7c** (20 mg, 52%) as a white powder.  $^1\text{H}$  NMR (400 MHz,  $\text{CD}_3\text{OD}$ ):  $\delta$  8.32 (d,  $J = 8.6$  Hz, 2H), 8.06 (d,  $J = 7.9$  Hz, 2H), 7.71–7.55 (m, 4H), 7.25 (dd,  $J = 8.0, 5.5$  Hz, 2H), 7.06 (dd,  $J = 10.2, 8.1$  Hz, 2H), 4.12 (s, 4H), 3.35 (t,  $J = 7.2$  Hz, 4H), 2.87 (t,  $J = 7.1$  Hz, 4H), 1.00 (p,  $J = 7.2$  Hz, 4H), 0.86 (p,  $J = 7.4, 6.8$  Hz, 4H).  $^{13}\text{C}$  NMR (101 MHz,  $\text{CD}_3\text{OD}$ ):  $\delta$  172.2, 163.1 (q,  $^2J_{\text{C,F}} = 34.1$  Hz, TFA), 159.6 (d,  $^1J_{\text{C,F}} = 251.6$  Hz), 158.5, 150.9, 134.5 (d,  $^3J_{\text{C,F}} = 4.3$  Hz), 129.2 (d,  $J_{\text{C,F}} = 4.6$  Hz), 128.9 (d,  $J_{\text{C,F}} = 8.5$  Hz), 128.2, 127.6 (d,  $J_{\text{C,F}} = 1.6$  Hz), 126.2 (d,  $J_{\text{C,F}} = 2.5$  Hz), 125.2 (d,  $J_{\text{C,F}} = 15.8$  Hz), 121.5 (d,  $J_{\text{C,F}} = 6.2$  Hz), 118.2 (q,  $J_{\text{C,F}} = 292.8$  Hz, TFA), 109.7 (d,  $J_{\text{C,F}} = 20.2$  Hz), 60.9, 42.1, 41.8, 41.4, 26.5, 25.4. HRMS-ESI:  $\text{C}_{36}\text{H}_{41}\text{F}_2\text{N}_8\text{O}_3^+$  [ $\text{M} + \text{H}$ ] $^+$  calcd, 671.3264; found, 671.3244.

**1,1'-(5,5-Bis(4-bromo-3-chlorobenzyl)-2,4,6-trioxodihydropyrimidine-1,3(2H,4H)-diylbis(butane-4,1-diyl)diguandine (7d)**. To a stirred solution of the TFA salt of **6d** (203 mg, 0.299 mmol) in THF (20 mL) were added  $\text{NaHCO}_3$  (155 mg, 1.12 mmol) and  $N,N'$ -bis-Boc-1-guanylpyrazole (350 mg, 1.1 mmol) and stirred at room temperature for 48 h until MS analysis showed full guanylation. The reaction mixture was filtered and concentrated. The crude product was dissolved in EtOAc (15 mL) and washed with brine ( $2 \times 15$  mL). The organic phase was dried over  $\text{Na}_2\text{SO}_4$ , filtered, and concentrated. The crude product was purified by automated flash chromatography, and the resulting Boc-protected intermediate was deprotected with TFA (2 mL) in  $\text{CH}_2\text{Cl}_2$  (2 mL) for 18 h. The reaction mixture was concentrated, and the crude was purified by RP automated flash chromatography and lyophilized to afford **7d** as a white powder. The yield was not determined.  $^1\text{H}$  NMR (400 MHz,  $\text{CD}_3\text{OD}$ ):  $\delta$  7.57 (d,  $J = 8.2$  Hz, 2H), 7.22 (d,  $J = 2.1$  Hz, 2H), 6.92 (dd,  $J = 8.3, 2.1$  Hz, 2H), 3.74–3.61 (m, 4H), 3.43 (s, 4H), 3.23–3.12 (m, 4H), 1.47–1.29 (m, 8H).  $^{13}\text{C}$  NMR (101 MHz,  $\text{CD}_3\text{OD}$ ):  $\delta$  171.5, 158.6, 150.7, 137.7, 135.5, 135.3, 132.6, 130.7, 122.6, 61.0, 45.0, 42.5, 42.0, 26.9, 26.1. HRMS-ESI:  $\text{C}_{28}\text{H}_{35}^{79}\text{Br}_2\text{Cl}_2\text{N}_8\text{O}_3^+$  [ $\text{M} + \text{H}$ ] $^+$  calcd, 759.0570; found, 759.0578.

**1,1'-(5,5-Bis(3,5-dibromobenzyl)-2,4,6-trioxodihydropyrimidine-1,3(2H,4H)-diylbis(butane-4,1-diyl)diguandine (7e)**. To a stirred solution of the TFA salt of **6e** (360 mg, 0.362 mmol) in THF (5 mL) were added  $\text{NaHCO}_3$  (240 mg, 2.86 mmol) and  $N,N'$ -bis-Boc-1-guanylpyrazole (564 mg, 1.82 mmol) and stirred at room temperature for 48 h until MS analysis showed full guanylation. The reaction mixture was filtered and concentrated. The crude product was dissolved in EtOAc (20 mL) and washed with brine ( $2 \times 20$  mL). The organic phase was dried over  $\text{Na}_2\text{SO}_4$ , filtered, and concentrated. The crude product was purified by automated flash chromatography, and the resulting Boc-protected intermediate was deprotected with TFA (0.2 mL) in  $\text{CH}_2\text{Cl}_2$  (2 mL) for 18 h. The reaction mixture was concentrated, and the crude was purified by RP automated flash chromatography and lyophilized to afford **7e** (44 mg, 11%) as a white

powder.  $^1\text{H}$  NMR (400 MHz,  $\text{CD}_3\text{OD}$ ):  $\delta$  7.65 (t,  $J = 1.8$  Hz, 2H), 7.22 (d,  $J = 1.7$  Hz, 4H), 3.67 (t,  $J = 7.2$  Hz, 4H), 3.42 (s, 4H), 3.20 (t,  $J = 6.7$  Hz, 4H), 1.52–1.36 (m, 8H).  $^{13}\text{C}$  NMR (101 MHz,  $\text{CD}_3\text{OD}$ ):  $\delta$  171.3, 163.0 (q,  $J = 34.6$  Hz, TFA), 158.6, 150.5, 140.5, 134.5, 132.6, 124.1, 118.2 (q,  $J = 292.7$  Hz, TFA), 61.2, 44.9, 42.6, 42.1, 27.0, 26.4. HRMS-ESI:  $\text{C}_{28}\text{H}_{35}^{79}\text{Br}_2^{81}\text{Br}_2\text{N}_8\text{O}_3^+$  [ $\text{M} + \text{H}$ ] $^+$  calcd, 850.9525; found, 850.9532.

**1,1'-(5,5-Bis(3,5-bis(trifluoromethyl)benzyl)-2,4,6-trioxodihydropyrimidine-1,3(2H,4H)-diylbis(butane-4,1-diyl)diguandine (7f)**. To a stirred solution of the TFA salt of **6f** (21 mg, 0.02 mmol) in THF (1 mL) were added DIPEA (15.4  $\mu\text{L}$ , 0.09 mmol) and  $N,N'$ -bis-Boc-1-guanylpyrazole (17 mg, 0.06 mmol). The reaction was stirred at 45  $^\circ\text{C}$  for 2 h. The reaction mixture was concentrated, and the crude product was dissolved in EtOAc (10 mL) and washed with 10% citric acid soln ( $2 \times 10$  mL), 10%  $\text{NaHCO}_3$  soln (10 mL), and brine (10 mL). The organic phase was dried over  $\text{MgSO}_4$ , filtered, and concentrated. The crude product was purified by automated flash chromatography, and the resulting Boc-protected intermediate was deprotected with TFA (25  $\mu\text{L}$ ) in  $\text{CH}_2\text{Cl}_2$  for 18 h. The reaction mixture was concentrated, and the crude was purified by RP automated flash chromatography and lyophilized to afford **7f** (4 mg, 17%) as a white powder.  $^1\text{H}$  NMR (400 MHz,  $\text{CD}_3\text{OD}$ ):  $\delta$  7.91 (s, 2H), 7.67 (d,  $J = 1.7$  Hz, 4H), 3.71 (s, 4H), 3.63–3.53 (m, 4H), 3.10 (t,  $J = 7.1$  Hz, 4H), 1.40 (tt,  $J = 7.7, 4.0$  Hz, 4H), 1.36–1.24 (m, 4H).  $^{13}\text{C}$  NMR (101 MHz,  $\text{CD}_3\text{OD}$ ):  $\delta$  171.0, 158.7, 150.2, 139.4, 133.1 (q,  $^2J_{\text{C,F}} = 33.4$  Hz, 4C), 131.4–131.2 (m, 4C), 124.54 (q,  $^1J_{\text{C,F}} = 272.1$  Hz, 4C), 123.0–122.8 (m, 2C), 61.1, 44.9, 42.5, 41.7, 26.8, 26.0. HRMS-ESI:  $\text{C}_{30}\text{H}_{31}\text{F}_{12}\text{N}_4\text{O}_3^+$  [ $\text{M} + \text{H}$ ] $^+$  calcd 807.2635; found, 807.2632.

**1,1'-(5,5-Bis(4-tert-butylbenzyl)-2,4,6-trioxodihydropyrimidine-1,3(2H,4H)-diylbis(butane-4,1-diyl)diguandine (7g)**. To a stirred solution of the TFA salt of **6g** (129 mg, 0.16 mmol) in THF (2 mL) were added  $\text{NaHCO}_3$  (68 mg, 0.81 mmol) and  $N,N'$ -bis-Boc-1-guanylpyrazole (200 mg, 0.64 mmol). The reaction was stirred at room temperature for 48 h. The reaction mixture was concentrated, and the crude product was dissolved in EtOAc (20 mL) and washed with 10% citric acid soln ( $2 \times 20$  mL), 10%  $\text{NaHCO}_3$  soln (20 mL), and brine (20 mL). The organic phase was dried over  $\text{Na}_2\text{SO}_4$ , filtered, and concentrated. The crude product was purified by automated flash chromatography, and the resulting Boc-protected intermediate was deprotected with TFA (1 mL) in  $\text{CH}_2\text{Cl}_2$  for 18 h. The reaction mixture was concentrated, and the crude was purified by RP automated flash chromatography and lyophilized to afford **7g** (16 mg, 11%) as a white powder.  $^1\text{H}$  NMR (400 MHz,  $\text{CD}_3\text{OD}$ ):  $\delta$  7.24 (d,  $J = 8.3$  Hz, 4H), 6.98 (d,  $J = 8.3$  Hz, 4H), 3.58 (t,  $J = 6.7$  Hz, 4H), 3.39 (s, 4H), 3.13 (t,  $J = 6.6$  Hz, 4H), 1.39–1.29 (m, 8H), 1.24 (s, 18H).  $^{13}\text{C}$  NMR (101 MHz,  $\text{CD}_3\text{OD}$ ):  $\delta$  172.4, 162.4 (q,  $J = 35.6$  Hz, TFA), 158.7, 151.9, 151.2, 133.4, 130.3, 126.4, 117.9 (q,  $J = 291.5$  Hz, TFA), 61.9, 45.9, 42.0, 41.9, 35.3, 31.7, 26.8, 25.8. HRMS-ESI:  $\text{C}_{36}\text{H}_{55}\text{N}_8\text{O}_3^+$  [ $\text{M} + \text{H}$ ] $^+$  calcd, 647.4393; found, 647.4378.

**1,1'-(5,5-Bis(3,5-di-tert-butylbenzyl)-2,4,6-trioxodihydropyrimidine-1,3(2H,4H)-diylbis(butane-4,1-diyl)diguandine (7h)**. To a stirred solution of the TFA salt of **6h** (118 mg, 0.13 mmol) in THF (3 mL) were added  $N,N'$ -bis-Boc-1-guanylpyrazole (245 mg, 0.79 mmol) and  $\text{NaHCO}_3$  (49 mg, 0.59 mmol) and stirred at room temperature for 48 h until TLC ( $\text{CHCl}_3$ ) showed full conversion. The reaction mixture was diluted with EtOAc (5 mL), washed with 10% citric acid soln and brine, dried over  $\text{Na}_2\text{SO}_4$ , filtered, and concentrated. The crude was purified by automated flash chromatography, and the resulting Boc-protected intermediate was deprotected with TFA (1.5 mL) in  $\text{CH}_2\text{Cl}_2$  (1.5 mL) for 4 h. The reaction mixture was concentrated, and the crude was purified by RP automated flash chromatography and lyophilized to afford **7h** (44 mg, 34%) as a white powder.  $^1\text{H}$  NMR (400 MHz,  $\text{CD}_3\text{OD}$ ):  $\delta$  7.30 (t,  $J = 1.8$  Hz, 2H), 6.89 (d,  $J = 1.8$  Hz, 4H), 3.58\* (t,  $J = 7.5$  Hz, 4H), 3.44 (s, 4H), 3.06 (t,  $J = 7.0$  Hz, 4H), 1.38–1.14 (m, 44H).  $^{13}\text{C}$  NMR (101 MHz,  $\text{CD}_3\text{OD}$ ):  $\delta$  172.4, 162.8 (q,  $J = 35.2$  Hz, TFA), 158.6, 152.3, 151.3, 135.8, 124.6, 122.6, 118.0 (q,  $J = 292.3$  Hz, TFA), 61.7, 47.3, 42.4, 41.8, 35.6, 31.9, 26.7, 26.2. \*Distorted triplet. HRMS-ESI:  $\text{C}_{44}\text{H}_{71}\text{N}_8\text{O}_3^+$  [ $\text{M} + \text{H}$ ] $^+$  calcd, 759.5644; found, 759.5637.

**Biological Test Methods.** The bacterial reference strains are displayed in Table 1 for the first antimicrobial screening. The Norwegian National Advisory Unit on Detection of Antimicrobial Resistance (K-res), University Hospital of Northern-Norway (UNN), provided the collection of 30 multi-drug-resistant isolates in Table 2. All isolates were deposited at the Norwegian Organization for Surveillance of Resistant Microorganisms (NORM) in the period of 2012–2014.

**MIC Assay.** The working solutions of the test derivatives were prepared with up to 100% dimethyl sulfoxide (DMSO) and stored at  $-20\text{ }^{\circ}\text{C}$ . If necessary, the solutions were heated to  $40\text{--}80\text{ }^{\circ}\text{C}$  before testing to facilitate complete dissolution. Double-distilled water was used in all dilutions prepared. The final concentration of DMSO in the test series was  $\leq 1\%$  and did not affect the assay results. A microdilution susceptibility test was used for MIC determination according to CLSI M07-A9<sup>41</sup> with modifications as described by Igumnova *et al.*<sup>42</sup> Briefly, the bacterial inoculum was adjusted to approximately  $2.5\text{--}3 \times 10^4$  cells/mL in the Mueller–Hinton broth (MHB, Difco Laboratories, USA) and incubated in a ratio of 1:1 with test derivatives in polystyrene 96-well flat-bottomed microplates (NUNC, Roskilde, Denmark). The positive growth control (without test derivatives) and negative control (without bacteria) were included. The reference antibiotic was oxytetracycline hydrochloride (Sigma-Aldrich, Saint Louis, MO, USA). The microplates were incubated in an EnVision microplate reader (PerkinElmer, Turku, Finland) placed in an incubator set to  $35\text{ }^{\circ}\text{C}$  for 48 h. The MIC value was defined as the lowest concentration of the derivative resulting in no bacterial growth as determined by  $\text{OD}_{600}$  measurement. All derivatives were tested in three parallels.

**Antimicrobial Screening against Clinical Isolates.** The MIC assay was performed as explained above with some exceptions; the working solutions of the test derivatives were prepared from the concentrated DMSO stocks stored at room temperature, the density of the bacterial inoculum was increased  $40 \times$  to  $1\text{--}1.2 \times 10^6$  cells/mL, enterococci were incubated in the Brain Heart Infusion broth (BHIB, Difco Laboratories, USA), the polypropylene microplates (Greiner Bio-One, Frickenhausen, Germany) were incubated for 24 h, and the derivatives were tested in four parallels.

**Determination of Hemolytic Activity.** The protocol was adapted from Paulsen *et al.*<sup>17</sup> Hemolysis was determined using a heparinized fraction (10 IU/mL) of freshly drawn blood. The blood collected in ethylenediaminetetraacetic acid-containing test tubes (Vacutest, KIMA, Arzergande, Italy) was used for the determination of the hematocrit (hct). The heparinized blood was washed  $3 \times$  with pre-warmed phosphate-buffered saline (PBS) and adjusted to a final hct of 4%. Derivatives in DMSO (50 mM) were added to a 96-well polypropylene V-bottom plate (NUNC, Fisher Scientific, Oslo, Norway) and serially diluted. The test concentration range was  $500\text{--}4\text{ }\mu\text{M}$  with DMSO contents  $\leq 1\%$ . A solution of 1% triton X-100 was used as a positive control for 100% hemolysis. As a negative control, a solution of 1% DMSO in PBS was included. No signs of DMSO toxicity were detected. RBCs (1% v/v final concentration) were added to the well plate and incubated at  $37\text{ }^{\circ}\text{C}$  and 800 rpm for 1 h. After centrifugation (5 min, 3000g), 100  $\mu\text{L}$  of each well was transferred to a 96-well flat-bottomed microtiter plate, and absorbance was measured at 545 nm with a microplate reader (VersaMaxTM, Molecular Devices, Sunnyvale, CA, USA). The percentage of hemolysis was calculated as the ratio of the absorbance in the derivative-treated and surfactant-treated samples, corrected for the PBS background. Three independent experiments were performed, and  $\text{EC}_{50}$  values are presented as averages.

**Determination of Toxicity against MRC5 and HepG2.** Adherent, non-malignant lung fibroblasts MRC5 (ATCC CCL-171TM) and human hepatocellular carcinoma cells HepG2 (ATCC HB-8065) were used as toxicity control. MRC5 cells, suspended in Eagle's minimal essential medium (MEM) with 10% fetal bovine serum, 2 mM stable glutamine, 1% non-essential amino acids, 1% sodium pyruvate, 2%  $\text{NaHCO}_3$ , and 10  $\mu\text{g}/\text{mL}$  gentamicin, were seeded in 96-well microtiter plates at 15,000 cells/well. HepG2 cells, suspended in Eagle's MEM with 10% fetal bovine serum, 1 mM stable

glutamine, 1% non-essential amino acids, 1% sodium pyruvate, and 10  $\mu\text{g}/\text{mL}$  gentamicin, were seeded in 96-well microtiter plates at 20,000 cells/well (adherent cell lines). The adherent cell lines were incubated for 24 h before adding compounds 6a–h and 7a–h and were then incubated for 4 h. The cell viability was determined by a colorimetric 3-(4,5-dimethylthiazol-2-yl)-5-(3-carboxymethoxyphenyl)-2-(4-sulphophenyl)-2H-tetrazolium assay. At the end of the exposure time, 10  $\mu\text{L}$  of Cell Titer 96 Aqueous One Solution Reagent (Promega, Madison, WI, USA) was added to each well, and the plates were incubated for 1 h before absorbance was measured using a DTX 880 multimode detector (Beckman Coulter, CA, USA) at 485 nm. Cells in their respective growth medium were used as negative control, and cells treated with 10% DMSO were used as positive control. Growth inhibition was determined by using the measured optical density (OD) and was calculated as follows: cell survival (%) =  $(\text{OD treated well} - \text{OD positive control well}) / (\text{OD negative control well} - \text{OD positive control well}) \times 100$ .

**In Vivo Murine Neutropenic Peritonitis Model.** The MIC of 7e (3,5-di-Br) against *E. coli* (EC106-09) and *K. pneumoniae* (KP3010) was determined according to the CLSI guidelines. The concentration range used was  $0.032\text{--}32\text{ }\mu\text{g}/\text{mL}$ . Colistin was included as a comparator and quality control (QC), and *E. coli* (ATCC 25922) was included as a QC strain. The MIC of colistin against *E. coli* (ATCC 25922) was within the CLSI QC range  $0.25\text{--}2\text{ }\mu\text{g}/\text{mL}$ , indicating a correct procedure. Derivative 7e (3,5-di-Br) was dissolved in PEG400 to 10 mg/mL and further diluted in 0.0015 M Tris buffer to concentrations of 1 and 0.2 mg/mL. The *in vivo* efficacy of compound 7e (3,5-di-Br) against *E. coli* (EC106-09) and *K. pneumoniae* (KP3010) in 32 female neutropenic NMRI mice (weight 28–32 g) was investigated after i.p. injection of 1.4 and 2.8 mg/kg given 1 and 3 h post-infection at Statens Serum Institute (SSI) in Denmark.<sup>35</sup> Mice were first rendered neutropenic with injections of cyclophosphamide (day-4 and day-1) and on day 0 inoculated with *E. coli* (EC106-09) or *K. pneumoniae* (KP3010) before being treated with 7e (3,5-di-Br) and the control antibiotics colistin (5 mg/kg), ciprofloxacin (13 mg/kg), or vehicle 1 h post-infection. Mice were observed for clinical signs of infection for 4 h after injection. The bacterial loads in the peritoneum were thereafter determined by sampling peritoneal fluid for the determination of CFU 4 h after treatment. The colony counts in peritoneal fluid were determined 5 h post-inoculation. All animal experiments were conducted in compliance with the institutional guidelines of SSI.

**Bacterial Membrane Integrity Assay.** The real-time membrane integrity assay was modified from Virta *et al.*<sup>37</sup> The test strains were *B. subtilis* 168 (ATCC 23857) and *E. coli* HB101 carrying the plasmid pCSS962. Overnight cultures were grown in MHB with chloramphenicol (5  $\mu\text{g}/\text{mL}$  *B. subtilis* and 20  $\mu\text{g}/\text{mL}$  *E. coli*, Merck KGaA, Darmstadt, Germany). The bacteria were pelleted by centrifugation for 5 min at 4000g before they were resuspended in MHB to obtain an  $\text{OD}_{600}$  of 0.1. D-Luciferin potassium salt (pH 7.4, SynChem Inc, IL, USA) was added to a final concentration of 1 mM, and the background luminescence was measured. Black round-bottomed 96-well microplates (Nunc, Roskilde, Denmark), containing dilutions of the test compounds (5  $\mu\text{L}$  per well), were loaded into a Synergy H1 Hybrid Reader (BioTek, Winooski, VT, USA). The amine barbiturate 6e (3,5-di-Br) and the guanidine barbiturate 7e (3,5-di-Br) were screened for membrane activity by injecting 95  $\mu\text{L}$  of inoculum with D-luciferin successively (well by well) to the test wells by an automatic injector with tracking of the luminescence emission every second for 150 s at room temperature. CHX acetate (Fresenius Kabi, Halden, Norway) was used as a positive control.

**Bacterial Viability Assay.** The compounds 6e (3,5-di-Br) and 7e (3,5-di-Br) were also selected for the viability assay. The test strains were *B. subtilis* 168 and *E. coli* HB101 carrying a constitutively expressed *lux* operon as a chromosomal integration of the *lux* operon in the *sacA* locus (PliaG) or the plasmid pCGLS-1, respectively.<sup>43,44</sup> The bacterial suspension for the real-time viability assay was prepared as described for the membrane integrity assay with the exception that no external substrate was added and that 100  $\mu\text{g}/\text{mL}$  of ampicillin was used for selection of *E. coli* carrying the plasmid pCGLS-11. The assay

was performed using the same type of microplates and procedure as described in the membrane integrity assay.

**Structural Investigations. Electronic Structure Calculations.** Quantum electronic structure calculations were performed at the DFT level of theory with the Gaussian 16 package,<sup>45</sup> employing the B3LYP functional<sup>46,47</sup> with empirical dispersion corrections as formulated by Grimme<sup>48</sup> (B3LYP-GD3). Ground-state optimizations used the 6-31g basis set with additional diffuse (+) and polarization functions (d,p) for accurate description of neutral and charged species, 6-31 + g(d,p).<sup>49,50</sup> Solvent effects were included in all calculations *via* the polarized continuum method, with water as the solvent.<sup>51,52</sup> Additional single-point energy calculations were performed with the larger 6-311 ++ g(2d,2p) basis set. The larger basis set is expected to provide more accurate energies compared to the smaller 6-31 + g(d,p) by providing more flexibility to the electron density, especially in the case of charged groups. Calculated energy Hessians confirmed stationary points as minima (zero imaginary frequencies). The reported electronic energies are given in kcal/mol.

**Nuclear Magnetic Resonance.** All spectra were acquired on a Bruker Avance III HD spectrometer operating at 600 MHz for protons and equipped with an inverse TCI probe with cryogenic enhancement for <sup>1</sup>H, <sup>2</sup>H, and <sup>13</sup>C. NMR samples were prepared by dissolving 1 mg of **7e** in 500  $\mu$ L of H<sub>2</sub>O/D<sub>2</sub>O 9:1 in a 5 mm NMR tube. SDS was subsequently added to this sample in a 20:1 M ratio, resulting in a clear solution. Experiments were acquired using TopSpin 3.2, with gradient selection, adiabatic pulses, and excitation sculpting where applicable.

**MD Simulation.** An *E. coli* inner membrane model was adapted from Pandit and Klauda (2012) with a 4:1 PE/PG ratio.<sup>39</sup> Systems for MD simulations of the membrane and for each molecule **6a** (4-CF<sub>3</sub>), **6e** (3,5-di-Br), **6g** (4-tBu), **7e** (3,5-di-Br), and **7g** (4-tBu) were prepared in VMD.<sup>53</sup> Each molecule was placed approximately 8 Å from the membrane surface and oriented such that the direct interactions of the guanidine and lysine groups with the membrane surface were not favored. All membrane systems were solvated in a rectangular simulation box with a 0.15 mol/L KCl concentration. In addition to membrane simulations, each of the molecules **6a** (4-CF<sub>3</sub>), **6e** (3,5-di-Br), **6g** (4-tBu), **7e** (3,5-di-Br), and **7g** (4-tBu) were prepared for water simulations in rectangular simulation boxes. Cl<sup>-</sup> ions were added for counterions.

Molecules **6a** (4-CF<sub>3</sub>), **6e** (3,5-di-Br), **6g** (4-tBu), **7e** (3,5-di-Br), and **7g** (4-tBu) were built in PyMol.<sup>54</sup> Each of the compounds was given a starting structure where both phenyl groups are oriented in the up conformation. A simple minimization was performed in the builder tool of PyMol to clean the structures. Each molecule was assigned atom types, parameters, and charges with the CGenff online program.<sup>55,56</sup>

Three parallels of all-atom MD simulations were performed for all systems with the molecular modeling software NAMD and the CHARMM36 force field.<sup>57,58</sup> A 10,000 step conjugate gradient and line search minimization was performed to ensure a stable starting structure for the MD simulations. Each membrane system parallel was run for 260 ns, and each water system parallel was run for 100 ns. All simulations were run at 310.15 K with a 2 fs time step and periodic boundary conditions.

Particle Mesh Ewald was used for calculating the electrostatic interactions.<sup>59</sup> For non-bonded interactions, the scaled 1–4 principle was used for exclusion and 1.0 was used for scaling coefficient. A smoothing function was applied to the non-bonded forces with a cutoff of 12.0 Å and a switching distance of 10.0 Å. A pair list for the calculation of non-bonded interactions was updated every 20 steps, called one cycle, and the maximum distance for inclusion in the pair list for a pair of atoms was set to 16.0 Å. The pair list was regenerated twice every cycle. Bond lengths for hydrogen atoms were constrained with the SHAKE algorithm.<sup>60</sup> Both full electrostatic forces and the non-bonded forces were evaluated at every time step. The NPT ensemble was used for all simulations. Pressure control for the simulations was performed with Nosé-Hoover Langevin piston with a target pressure of 1 atm.<sup>61,62</sup> A flexible simulation cell was used for the membrane system. Langevin dynamics were used for temperature

control. Trajectory files were written every 1000 steps and energies were recorded every 125 steps.

Analysis of the MD trajectories was performed with the VMD GUI and VMD scripts. Figures were made with VMD and PyMol, and all graphs were generated with pandas, seaborn, and Matplotlib.<sup>63–65</sup>

**X-ray Crystallography.** A rod-like specimen of **7b** (2-Nal) was used for X-ray crystallographic analysis. The X-ray intensity data were measured with the Cu source ( $\lambda = 1.54178$  Å) of an in-house Bruker D8 Venture system. Frames were integrated using the Bruker SAINT software package, and the structure was solved and refined using the Bruker SHELXTL software package. The structure factors of **7b** have been deposited with the Cambridge Crystallographic Data Centre with deposition number 2026641. The integration of the data using a monoclinic unit cell yielded a total of 21874 reflections to a maximum  $\theta$  angle of 66.75° (0.84 Å resolution), of which 6692 were independent (average redundancy 3.269, completeness = 99.6%,  $R_{int} = 3.12\%$ , and  $R_{sig} = 2.71\%$ ) and 5846 (87.36%) were greater than  $2\sigma(F_2)$ . The final cell constants were 17.6014(15), 15.4212(12), and 16.0233(17) Å with  $\beta = 106.833(4)^\circ$ . The final anisotropic refinement converged with an  $R_1/wR_2$  of 6.8/21% with a GoF of 1.04. The structure of the asymmetric unit of **7b** (2-Nal) with thermal ellipsoids is shown in Figure S2.

## ■ ASSOCIATED CONTENT

### Supporting Information

The Supporting Information is available free of charge at <https://pubs.acs.org/doi/10.1021/acs.jmedchem.1c00734>.

(PDF)

<sup>1</sup>H and <sup>13</sup>C NMR spectra and SFC analysis data of the synthesized compounds; detailed description of the biosensor assays; comprehensive discussion of the conformational analysis; and molecular formula strings and MIC and toxicity data for compounds **6a–h** and **7a–h** (CSV)

## ■ AUTHOR INFORMATION

### Corresponding Authors

Annette Bayer – Department of Chemistry, UiT The Arctic University of Norway, NO-9037 Tromsø, Norway;

orcid.org/0000-0003-3481-200X;

Email: [annette.bayer@uit.no](mailto:annette.bayer@uit.no)

Morten B. Strøm – Department of Pharmacy, Faculty of Health Sciences, UiT The Arctic University of Norway, NO-9037 Tromsø, Norway; orcid.org/0000-0003-1973-0778; Email: [morten.strom@uit.no](mailto:morten.strom@uit.no)

### Authors

Marianne H. Paulsen – Department of Pharmacy, Faculty of Health Sciences, UiT The Arctic University of Norway, NO-9037 Tromsø, Norway

Magnus Engqvist – Department of Chemistry, UiT The Arctic University of Norway, NO-9037 Tromsø, Norway

Dominik Ausbacher – Department of Pharmacy, Faculty of Health Sciences, UiT The Arctic University of Norway, NO-9037 Tromsø, Norway

Trude Anderssen – Department of Pharmacy, Faculty of Health Sciences, UiT The Arctic University of Norway, NO-9037 Tromsø, Norway

Manuel K. Langer – Department of Chemistry, UiT The Arctic University of Norway, NO-9037 Tromsø, Norway

Tor Haug – The Norwegian College of Fishery Science, Faculty of Biosciences, Fisheries and Economics, UiT The Arctic University of Norway, NO-9037 Tromsø, Norway;

orcid.org/0000-0003-1104-5813

Glenn R. Morello – Department of Chemistry, UiT The Arctic University of Norway, NO-9037 Tromsø, Norway; Department of Science, Valley City State University, Valley City 58072 North Dakota, United States

Laura E. Liikanen – Department of Chemistry, UiT The Arctic University of Norway, NO-9037 Tromsø, Norway

Hans-Matti Blencke – The Norwegian College of Fishery Science, Faculty of Biosciences, Fisheries and Economics, UiT The Arctic University of Norway, NO-9037 Tromsø, Norway

Johan Isaksson – Department of Chemistry, UiT The Arctic University of Norway, NO-9037 Tromsø, Norway;

[orcid.org/0000-0001-6287-7594](https://orcid.org/0000-0001-6287-7594)

Eric Juskewitz – Department of Medical Biology, Faculty of Health Sciences, UiT The Arctic University of Norway, NO-9037 Tromsø, Norway

Complete contact information is available at:

<https://pubs.acs.org/10.1021/acs.jmedchem.1c00734>

## Notes

The authors declare no competing financial interest.

## ACKNOWLEDGMENTS

This study was funded by the Research Council of Norway (RCN) (grant nos. 214493/F20 and 224790/O30), UiT—The Arctic University of Norway (project nos. A23260 and 235560), pre-seed grant from Novo Nordisk Fonden (grant no. NNF17OC0030098), and the MABIT programme (grant no. BS0079). The computational work has furthermore received funding from the RCN (grant no. 231706/F20), the Norwegian supercomputing program NOTUR (grant nos. NN4654K and NN9330K), and assistance of computational resources at the Center for Computationally Assisted Science and Technology (CCAST) at North Dakota State University, US. The authors thank professor Ørjan Samuelsen (K-Res/UNN) for giving us access to multi-drug-resistant clinical isolates. We also thank engineers Alena Didriksen (UNN) and Hege Devold (UiT) for their technical assistance with MIC screening, engineer Elizaveta M. Igumnova (UNN/UiT) for providing compound **3h**, Dr. Bjarte Aarmo Lund (UiT) for X-ray crystallographic analysis, *in vivo* studies at Statens Serum Institute (SSI, DK), and MIC studies at the Advanced Microscopy Core Facility (AMCF, UiT).

## ABBREVIATIONS

*A. baumannii*, *Acinetobacter baumannii*; *B. subtilis*, *Bacillus subtilis*; *C. glutamicum*, *Corynebacterium glutamicum*; *E. coli*, *Escherichia coli*; *E. faecium*, *Enterococcus faecium*; *K. pneumoniae*, *Klebsiella pneumoniae*; MRSA, methicillin-resistant *S. aureus*; *P. aeruginosa*, *Pseudomonas aeruginosa*; *S. aureus*, *Staphylococcus aureus*; VRE, vancomycin-resistant *Enterococcus*; AMPs, antimicrobial peptides; Boc<sub>2</sub>O, di-*tert*-butyl dicarbonate; CFU, colony-forming units; CHX, chlorhexidine; DBU, 1,8-diazabicyclo[5.4.0]undec-7-ene; DFT, density functional theory; DMF, dimethylformamide; DMSO, dimethyl sulfoxide; ESBL–CARBA, extended spectrum  $\beta$ -lactamase–carbapenemase; HCTU, (2-(6-chloro-1*H*-benzotriazol-1-yl)-1,1,3,3-tetramethylammonium-hexafluorophosphate); i.p., intraperitoneal; LPS, lipopolysaccharide; MD, molecular dynamics; MIC, minimum inhibitory concentration; MTD, maximal tolerated dose; NMR, nuclear magnetic resonance; PL, phospholipid; PMA, phosphomolybdic acid; RBCs, red blood cells; RLU,

relative light units; SMAMPs, synthetic mimics of antimicrobial peptides; TFA, trifluoroacetic acid; THF, tetrahydrofuran

## REFERENCES

- (1) World Health Organization. *2019 Antibacterial Agents in Clinical Development: An Analysis of the Antibacterial Clinical Development Pipeline*; World Health Organization: Geneva, 2019.
- (2) O'Neill, J. *Tackling Drug-Resistant Infections Globally: Final Report and Recommendations*; [www.amr-reveiw.org](http://www.amr-reveiw.org), 2016.report
- (3) Cassini, A.; Högberg, L. D.; Plachouras, D.; Quattrocchi, A.; Hoxha, A.; Simonsen, G. S.; Colomb-Cotinat, M.; Kretzschmar, M. E.; Devleeschauwer, B.; Cecchini, M.; Ouakrim, D. A.; Oliveira, T. C.; Struelens, M. J.; Suetens, C.; Monnet, D. L.; Strauss, R.; Mertens, K.; Struyf, T.; Catry, B.; Latour, K.; Ivanov, I. N.; Dobрева, E. G.; Tambic Andrašević, A.; Soprek, S.; Budimir, A.; Paphitou, N.; Zemlicková, H.; Schytte Olsen, S.; Wolff Sönksen, U.; Martin, P.; Ivanova, M.; Lyytikäinen, O.; Jalava, J.; Coignard, B.; Eckmanns, T.; Abu Sin, M.; Haller, S.; Daikos, G. L.; Gikas, A.; Tsiodras, S.; Kontopidou, F.; Tóth, A.; Hajdu, A.; Guólaugsson, O.; Kristinsson, K. G.; Murchan, S.; Burns, K.; Pezzotti, P.; Gagliotti, C.; Dumpis, U.; Liuimiene, A.; Perrin, M.; Borg, M. A.; de Greeff, S. C.; Monen, J. C.; Koek, M. B.; Elström, P.; Zabicka, D.; Deptula, A.; Hryniewicz, W.; Caniça, M.; Nogueira, P. J.; Fernandes, P. A.; Manageiro, V.; Popescu, G. A.; Serban, R. I.; Schréterová, E.; Litvová, S.; Stefkovicová, M.; Kolman, J.; Klavs, I.; Korošec, A.; Aracil, B.; Asensio, A.; Pérez-Vázquez, M.; Billström, H.; Larsson, S.; Reilly, J. S.; Johnson, A.; Hopkins, S. Attributable deaths and disability-adjusted life-years caused by infections with antibiotic-resistant bacteria in the EU and the European Economic Area in 2015: a population-level modelling analysis. *Lancet Infect. Dis.* **2019**, *19*, 56–66.
- (4) World Health Organization. *Global Action Plan on Antimicrobial Resistance* (accessed 04 02 2017).
- (5) Tadesse, M.; Tabudravu, J. N.; Jaspars, M.; Strøm, M. B.; Hansen, E.; Andersen, J. H.; Kristiansen, P. E.; Haug, T. The antibacterial ent-eusynstyelamide B and eusynstyelamides D, E, and F from the Arctic bryozoan tegella cf. spitzbergensis. *J. Nat. Prod.* **2011**, *74*, 837–841.
- (6) Tapiolas, D. M.; Bowden, B. F.; Abou-Mansour, E.; Willis, R. H.; Doyle, J. R.; Muirhead, A. N.; Liprot, C.; Llewellyn, L. E.; Wolff, C. W. W.; Wright, A. D.; Motti, C. A. Eusynstyelamides A, B, and C, nNOS Inhibitors, from the Ascidian Eusynstyla latericus. *J. Nat. Prod.* **2009**, *72*, 1115–1120.
- (7) Barykina, O. V.; Snider, B. B. Synthesis of (+/-)-eusynstyelamide A. *Org. Lett.* **2010**, *12*, 2664–2667.
- (8) Strøm, M. B.; Haug, B. E.; Skar, M. L.; Stensen, W.; Stiberg, T.; Svendsen, J. S. The pharmacophore of short cationic antibacterial peptides. *J. Med. Chem.* **2003**, *46*, 1567–1570.
- (9) Ghosh, C.; Haldar, J. Membrane-active small molecules: designs inspired by antimicrobial peptides. *ChemMedChem* **2015**, *10*, 1606–1624.
- (10) Gunasekaran, P.; Rajasekaran, G.; Han, E. H.; Chung, Y.-H.; Choi, Y.-J.; Yang, Y. J.; Lee, J. E.; Kim, H. N.; Lee, K.; Kim, J.-S.; Lee, H.-J.; Choi, E.-J.; Kim, E.-K.; Shin, S. Y.; Bang, J. K. Cationic amphipathic triazines with potent anti-bacterial, anti-inflammatory and anti-atopic dermatitis properties. *Sci. Rep.* **2019**, *9*, 1292.
- (11) Jiang, Y.; Chen, Y.; Song, Z.; Tan, Z.; Cheng, J. Recent advances in design of antimicrobial peptides and polypeptides toward clinical translation. *Adv. Drug Deliv. Rev.* **2021**, *170*, 261–280.
- (12) Giuliani, A.; Pirri, G.; Nicoletto, S. Antimicrobial peptides: an overview of a promising class of therapeutics. *Cent. Eur. J. Biol.* **2007**, *2*, 1–33.
- (13) Zasloff, M. Antimicrobial peptides of multicellular organisms. *Nature* **2002**, *415*, 389–395.
- (14) Hancock, R. E. W.; Haney, E. F.; Gill, E. E. The immunology of host defence peptides: beyond antimicrobial activity. *Nat. Rev. Immunol.* **2016**, *16*, 321–334.
- (15) Powers, J.-P. S.; Hancock, R. E. W. The relationship between peptide structure and antibacterial activity. *Peptides* **2003**, *24*, 1681–1691.



- (16) Latham, P. W. Therapeutic peptides revisited. *Nat. Biotechnol.* **1999**, *17*, 755–757.
- (17) Paulsen, M. H.; Ausbacher, D.; Bayer, A.; Engqvist, M.; Hansen, T.; Haug, T.; Anderssen, T.; Andersen, J. H.; Sollid, J. U. E.; Strøm, M. B. Antimicrobial activity of amphipathic  $\alpha,\alpha$ -disubstituted  $\beta$ -amino amide derivatives against ESBL - CARBA producing multi-resistant bacteria; effect of halogenation, lipophilicity and cationic character. *Eur. J. Med. Chem.* **2019**, *183*, 111671.
- (18) Hansen, T.; Ausbacher, D.; Flaten, G. E.; Havelkova, M.; Strøm, M. B. Synthesis of cationic antimicrobial  $\beta(2,2)$ -amino acid derivatives with potential for oral administration. *J. Med. Chem.* **2011**, *54*, 858–868.
- (19) Wong, O.; McKeown, R. H. Substituent effects on partition coefficients of barbituric acids. *J. Pharm. Sci.* **1988**, *77*, 926–932.
- (20) Ashnagar, A.; Naseri, N. G.; Sheeri, B. Novel synthesis of barbiturates. *Chin. J. Chem.* **2007**, *25*, 382–384.
- (21) Huang, H.-M.; Procter, D. J. Radical-radical cyclization cascades of barbiturates triggered by electron-transfer reduction of amide-type carbonyls. *J. Am. Chem. Soc.* **2016**, *138*, 7770–7775.
- (22) Neumann, D. M.; Cammarata, A.; Backes, G.; Palmer, G. E.; Jursic, B. S. Synthesis and antifungal activity of substituted 2,4,6-pyrimidinetrione carbaldehyde hydrazones. *Bioorg. Med. Chem.* **2014**, *22*, 813–826.
- (23) Gunasekaran, P.; Yim, M. S.; Ahn, M.; Soung, N.-K.; Park, J.-E.; Kim, J.; Bang, G.; Shin, S. C.; Choi, J.; Kim, M.; Kim, H. N.; Lee, Y.-H.; Chung, Y.-H.; Lee, K.; EunKyeong Kim, E.; Jeon, Y.-H.; Kim, M. J.; Lee, K.-R.; Kim, B.-Y.; Lee, K. S.; Ryu, E. K.; Bang, J. K. Development of a polo-like kinase-1 polo-box domain inhibitor as a tumor growth suppressor in mice models. *J. Med. Chem.* **2020**, *63*, 14905–14920.
- (24) Jursic, B. S. A simple method for Knoevenagel condensation of  $\alpha,\beta$ -conjugated and aromatic aldehydes with barbituric acid. *J. Heterocycl. Chem.* **2001**, *38*, 655–657.
- (25) Jursic, B. S.; Neumann, D. M. Reductive C-alkylation of barbituric acid derivatives with carbonyl compounds in the presence of platinum and palladium catalysts. *Tetrahedron Lett.* **2001**, *42*, 4103–4107.
- (26) Kotha, S.; Deb, A. C.; Kumar, R. V. Spiro-annulation of barbituric acid derivatives and its analogs by ring-closing metathesis reaction. *Bioorg. Med. Chem. Lett.* **2005**, *15*, 1039–1043.
- (27) Pei, Y.; Wickham, B. O. S. Regioselective syntheses of 3-aminomethyl-5-substituted isoxazoles: A facile and chemoselective reduction of azide to amine by sodium borohydride using 1,3-propanedithiol as a catalyst. *Tetrahedron Lett.* **1993**, *34*, 7509–7512.
- (28) Hansen, T.; Moe, M. K.; Anderssen, T.; Strøm, M. B. Metabolism of small antimicrobial  $\beta(2,2)$ -amino acid derivatives by murine liver microsomes. *Eur. J. Drug Metab. Pharmacokinet.* **2012**, *37*, 191–201.
- (29) Gillis, E. P.; Eastman, K. J.; Hill, M. D.; Donnelly, D. J.; Meanwell, N. A. Applications of fluorine in medicinal chemistry. *J. Med. Chem.* **2015**, *58*, 8315–8359.
- (30) Kim, S.-H.; Semanya, D.; Castagnolo, D. Antimicrobial drugs bearing guanidine moieties: A review. *Eur. J. Med. Chem.* **2021**, *216*, 113293.
- (31) Andreev, K.; Bianchi, C.; Laursen, J. S.; Citterio, L.; Hein-Kristensen, L.; Gram, L.; Kuzmenko, I.; Olsen, C. A.; Gidalevitz, D. Guanidino groups greatly enhance the action of antimicrobial peptidomimetics against bacterial cytoplasmic membranes. *Biochim. Biophys. Acta* **2014**, *1838*, 2492–2502.
- (32) Gabriel, G. J.; Madkour, A. E.; Dabkowski, J. M.; Nelson, C. F.; Nüsslein, K.; Tew, G. N. Synthetic mimic of antimicrobial peptide with nonmembrane-disrupting antibacterial properties. *Biomacromolecules* **2008**, *9*, 2980–2983.
- (33) Locock, K. E. S.; Michl, T. D.; Valentin, J. D. P.; Vasilev, K.; Hayball, J. D.; Qu, Y.; Traven, A.; Griesser, H. J.; Meagher, L.; Haeussler, M. Guanlylated polymethacrylates: a class of potent antimicrobial polymers with low hemolytic activity. *Biomacromolecules* **2013**, *14*, 4021–4031.
- (34) Yang, S.-T.; Shin, S. Y.; Lee, C. W.; Kim, Y.-C.; Hahm, K.-S.; Kim, J. I. Selective cytotoxicity following Arg-to-Lys substitution in tritrypticin adopting a unique amphipathic turn structure. *FEBS Lett.* **2003**, *540*, 229–233.
- (35) SSI Novel Polymyxin Derivatives Effective in Treating Experimental Peritoneal E. coli Infection in Mice. <https://en.ssi.dk/-/media/arkiv/uk/products-and-services/contract-research-organization/antimicrobial-evaluation/poster---efficacy-study-in-the-peritonitis-model.pdf?la=en> (accessed 18 02 2021).
- (36) Galluzzi, L.; Karp, M. Intracellular redox equilibrium and growth phase affect the performance of luciferase-based biosensors. *J. Biotechnol.* **2007**, *127*, 188–198.
- (37) Virta, M.; Åkerman, K. E. O.; Saviranta, P.; Oker-Blom, C.; Karp, M. T. Real-time measurement of cell permeabilization with low-molecular-weight membranolytic agents. *J. Antimicrob. Chemother.* **1995**, *36*, 303–315.
- (38) Kuyyakonond, T.; Quesnel, L. B. The mechanism of action of chlorhexidine. *FEMS Microbiol. Lett.* **1992**, *100*, 211–215.
- (39) Pandit, K. R.; Klauda, J. B. Membrane models of E. coli containing cyclic moieties in the aliphatic lipid chain. *Biochim. Biophys. Acta* **2012**, *1818*, 1205–1210.
- (40) Dixon, E. A.; Fischer, A.; Robinson, F. P. Preparation of a series of substituted fluoromethylnaphthalenes. *Can. J. Chem.* **1981**, *59*, 2629–2641.
- (41) Clinical and Laboratory Standards Institute. *Methods for Dilution Antimicrobial Susceptibility Tests for Bacteria that Grow Aerobically*. Approved Standard, M07-A9, 9; CLSI: Wayne, PA, 2012.
- (42) Igumnova, E. M.; Mishchenko, E.; Haug, T.; Blencke, H.-M.; Sollid, J. U. E.; Fredheim, E. G. A.; Lauksund, S.; Stensvåg, K.; Strøm, M. B. Synthesis and antimicrobial activity of small cationic amphipathic aminobenzamide marine natural product mimics and evaluation of relevance against clinical isolates including ESBL-CARBA producing multi-resistant bacteria. *Bioorg. Med. Chem.* **2016**, *24*, 5884–5894.
- (43) Radeck, J.; Kraft, K.; Bartels, J.; Cikovic, T.; Dürr, F.; Emenegger, J.; Kelterborn, S.; Sauer, C.; Fritz, G.; Gebhard, S.; Mascher, T. The Bacillus BioBrick Box: generation and evaluation of essential genetic building blocks for standardized work with *Bacillus subtilis*. *J. Biol. Eng.* **2013**, *7*, 29.
- (44) Frackman, S.; Anhalt, M.; Neelson, K. H. Cloning, organization, and expression of the bioluminescence genes of *Xenorhabdus luminescens*. *J. Bacteriol.* **1990**, *172*, 5767–5773.
- (45) Frisch, M. J.; Trucks, G. W.; Schlegel, H. B.; Scuseria, G. E.; Robb, M. A.; Cheeseman, J. R.; Scalmani, G.; Barone, V.; Mennucci, B.; Petersson, G. A.; Nakatsuji, H.; Caricato, M.; Li, X.; Hratchian, H. A.; Izmaylov, A. F.; Bloino, G. Z.; Sonnenberg, J. L.; Hada, M.; Ehara, M.; Toyota, K.; Fukuda, R.; Hasegawa, J.; Ishida, M.; Nakajima, T.; Honda, Y.; Kitao, O.; Nakai, H.; Vreven, T.; Montgomery, J.; Peralta, J. E.; Ogliaro, F.; Bearpark, M.; Heyd, J. J.; Brothers, E.; Kudin, K. N.; Staroverov, V. N.; Keith, T.; Kobayashi, R.; Normand, J.; Raghavachari, K.; Rendell, A.; Burant, J. C.; Iyengar, S. S.; Tomasi, J.; Cossi, M.; Rega, N.; Millam, J. M.; Klene, M.; Knox, J. E.; Cross, J. B.; Bakken, V.; Adamo, C.; Jaramillo, J.; Gomperts, R.; Stratmann, R. E.; Yazyev, O.; Austin, A. J.; Cammi, R.; Pomelli, C.; Ochterski, J. W.; Martin, R. L.; Morokuma, K.; Zakrzewski, V. G.; Voth, G. A.; Salvador, P.; Dannenberg, J. J.; Dapprich, S.; Daniels, A. D.; Farkas, O.; Foresman, J. B.; Ortiz, J. V.; Cioslowski, J.; Fox, D. J. *Gaussian 09*, Revision D.01; Gaussian Inc.: Wallingford, CT, 2013.
- (46) Becke, A. D. A new mixing of Hartree-Fock and local density-functional theories. *J. Chem. Phys.* **1993**, *98*, 1372–1377.
- (47) Lee, C.; Yang, W.; Parr, R. G. Development of the Colle-Salvetti correlation-energy formula into a functional of the electron density. *Phys. Rev. B: Condens. Matter Mater. Phys.* **1988**, *37*, 785–789.
- (48) Grimme, S.; Antony, J.; Ehrlich, S.; Krieg, H. A consistent and accurate ab initio parametrization of density functional dispersion correction (DFT-D) for the 94 elements H-Pu. *J. Chem. Phys.* **2010**, *132*, 154104.





- (49) McLean, A. D.; Chandler, G. S. Contracted Gaussian basis sets for molecular calculations. I. Second row atoms, Z=11-18. *J. Chem. Phys.* **1980**, *72*, 5639–5648.
- (50) Krishnan, R.; Binkley, J. S.; Seeger, R.; Pople, J. A. Self-consistent molecular orbital methods. XX. A basis set for correlated wave functions. *J. Chem. Phys.* **1980**, *72*, 650–654.
- (51) Tomasi, J.; Mennucci, B.; Cancès, E. The IEF version of the PCM solvation method: an overview of a new method addressed to study molecular solutes at the QM ab initio level. *J. Mol. Struct.* **1999**, *464*, 211–226.
- (52) Cancès, E.; Mennucci, B.; Tomasi, J. A new integral equation formalism for the polarizable continuum model: Theoretical background and applications to isotropic and anisotropic dielectrics. *Chem. Phys.* **1997**, *107*, 3032–3041.
- (53) Humphrey, W.; Dalke, A.; Schulten, K. VMD: visual molecular dynamics. *J. Mol. Graph.* **1996**, *14*, 33–38.
- (54) *The PyMOL Molecular Graphics System, Version 2.0*; Schrödinger, LLC.
- (55) Vanommeslaeghe, K.; MacKerell, A. D., Jr. Automation of the CHARMM General Force Field (CGenFF) I: bond perception and atom typing. *J. Chem. Inf. Model.* **2012**, *52*, 3144–3154.
- (56) Vanommeslaeghe, K.; Raman, E. P.; MacKerell, A. D., Jr. Automation of the CHARMM General Force Field (CGenFF) II: assignment of bonded parameters and partial atomic charges. *J. Chem. Inf. Model.* **2012**, *52*, 3155–3168.
- (57) Phillips, J. C.; Braun, R.; Wang, W.; Gumbart, J.; Tajkhorshid, E.; Villa, E.; Chipot, C.; Skeel, R. D.; Kalé, L.; Schulten, K. Scalable molecular dynamics with NAMD. *J. Comput. Chem.* **2005**, *26*, 1781–1802.
- (58) Klauda, J. B.; Venable, R. M.; Freites, J. A.; O'Connor, J. W.; Tobias, D. J.; Mondragon-Ramirez, C.; Vorobyov, I.; MacKerell, A. D., Jr.; Pastor, R. W. Update of the CHARMM all-atom additive force field for lipids: validation on six lipid types. *J. Phys. Chem. B* **2010**, *114*, 7830–7843.
- (59) Darden, T.; York, D.; Pedersen, L. Particle mesh Ewald: an N·log(N) method for Ewald sums in large systems. *J. Chem. Phys.* **1993**, *98*, 10089–10092.
- (60) Ryckaert, J.-P.; Ciccotti, G.; Berendsen, H. J. C. Numerical integration of the cartesian equations of motion of a system with constraints: molecular dynamics of n-alkanes. *J. Comput. Phys.* **1977**, *23*, 327–341.
- (61) Feller, S. E.; Zhang, Y.; Pastor, R. W.; Brooks, B. R. Constant pressure molecular dynamics simulation: the Langevin piston method. *J. Chem. Phys.* **1995**, *103*, 4613–4621.
- (62) Martyna, G. J.; Tobias, D. J.; Klein, M. L. Constant pressure molecular dynamics algorithms. *J. Chem. Phys.* **1994**, *101*, 4177–4189.
- (63) McKinney, W. In *Data structures for statistical computing in python. Proceedings of the 9th Python in Science Conference*: Austin, TX, 2010; pp 51–56.
- (64) Michael, W.; The Seaborn Development Team. *Mwaskom/Seaborn, 0.11.0*; Zenodo, 2020.
- (65) Hunter, J. D. Matplotlib: A 2D graphics environment. *Comput. Sci. Eng.* **2007**, *9*, 90–95.



## Paper IV

## Article

# Anti-Colonization Effect of Au Surfaces with Self-Assembled Molecular Monolayers Functionalized with Antimicrobial Peptides on *S. epidermidis*

Eskil André Karlsen <sup>1,2</sup>, Wenche Stensen <sup>1,2</sup> , Eric Juskewitz <sup>3</sup> , Johan Svenson <sup>4</sup> , Mattias Berglin <sup>4</sup> and John Sigurd Mjøsén Svendsen <sup>1,2,\*</sup> 

<sup>1</sup> Amicoat AS, Sykehusvegen 23, 9019 Tromsø, Norway; eskil.a.karlsen@uit.no (E.A.K.); wenche.stensen@uit.no (W.S.)

<sup>2</sup> Department of Chemistry, Faculty of Science and Technology, UiT—The Arctic University of Norway, 9037 Tromsø, Norway

<sup>3</sup> Department of Medical Biology, Faculty of Health Sciences, UiT—The Arctic University of Norway, 9037 Tromsø, Norway; eric.juskewitz@uit.no

<sup>4</sup> RISE Research Institutes of Sweden, Brinellgatan 4, 504 62 Borås, Sweden; johan.svenson@cawthron.org.nz (J.S.); mattias.berglin@ri.se (M.B.)

\* Correspondence: john-sigurd.svendsen@uit.no; Tel.: +47-7764-4086



**Citation:** Karlsen, E.A.; Stensen, W.; Juskewitz, E.; Svenson, J.; Berglin, M.; Svendsen, J.S.M. Anti-Colonization Effect of Au Surfaces with Self-Assembled Molecular Monolayers Functionalized with Antimicrobial Peptides on *S. epidermidis*. *Antibiotics* **2021**, *10*, 1516. <https://doi.org/10.3390/antibiotics10121516>

Academic Editors: Marc Maresca, Catherine Lefay and Vincent Humblot

Received: 28 November 2021

Accepted: 8 December 2021

Published: 10 December 2021

**Publisher's Note:** MDPI stays neutral with regard to jurisdictional claims in published maps and institutional affiliations.



**Copyright:** © 2021 by the authors. Licensee MDPI, Basel, Switzerland. This article is an open access article distributed under the terms and conditions of the Creative Commons Attribution (CC BY) license (<https://creativecommons.org/licenses/by/4.0/>).

**Abstract:** Medical devices with an effective anti-colonization surface are important tools for combatting healthcare-associated infections. Here, we investigated the anti-colonization efficacy of antimicrobial peptides covalently attached to a gold model surface. The gold surface was modified by a self-assembled polyethylene glycol monolayer with an acetylene terminus. The peptides were covalently connected to the surface through a copper-catalyzed [3 + 2] azide-acetylene coupling (CuAAC). The anti-colonization efficacy of the surfaces varied as a function of the antimicrobial activity of the peptides, and very effective surfaces could be prepared with a 6 log unit reduction in bacterial colonization.

**Keywords:** antimicrobial surface; antimicrobial peptide; self-assembled monolayer; antifouling; anti-colonization; ToF-SIMS imaging; Certika

## 1. Introduction

In the rich parts of the world, healthcare-associated infections (HAI) hit 1 of 14 hospitalized patients, often requiring additional treatment and extended hospitalization [1]. The highest frequency of HAI is associated with the use of invasive devices, in particular central lines, urinary catheters, and ventilators [2]. A device-associated infection accounts for up to 23% out of all healthcare-associated infections, including central line-associated bloodstream infections (CLABSI), catheter-associated urinary tract infections (CAUTI), and ventilator-associated pneumonia [2]. There is a goal to limit the number of HAIs, and in 2015, the U.S. Department of Health and Human Services set a target to reduce the infection rate by 25–50% by 2020 through stricter regulations and guidelines regarding the use of the devices [3,4]. Despite the progress of reducing CLABSIs and CAUTIs through best practice, the underlying problem remains—the surfaces of medical devices are still prone to bacterial growth and biofilm formation.

Bacteria can adhere irreversibly to living and non-living surfaces, colonize, and subsequently develop into an enclosed structured society of both Gram-positive and/or Gram-negative bacteria that adhere to a surface, forming a protective matrix known as a biofilm [5]. The most common bacteria found in biofilms are *E. faecalis*, *S. aureus*, *S. epidermidis*, *E. coli*, *K. pneumoniae*, and *P. aeruginosa* [6]. Biofilms are challenging to eradicate due to the extracellular polymeric material that creates a “slime-like” matrix, which acts as a protective barrier for the bacteria [5].

Indwelling medical devices (e.g., catheters) are particularly prone to bacterial colonization on the surface and subsequent biofilm formation, leading to infections in the patient [6]. Biofilm-associated infections on indwelling medical devices prolong initial treatment regimens, increase antibiotic use, and add additional healthcare expenses for the hospital and society. As an example, a central line-associated bloodstream infection can cost up to USD 46,000 per case and the patient can be hospitalized for an additional 7 days or more, depending on the type and severity of infection [7]. In addition, patients are at risk of sepsis and the mortality rate can be up to 25% [7]. A study conducted from 2015 to 2017 showed the most common bacteria reported on indwelling devices were *Escherichia coli* (18%), *Staphylococcus aureus* (12%), and *Klebsiella* spp. (9%) [8]. Another study conducted from 2008 to 2017 showed that 22% (48 out of 213 patients) of the device-associated infections were caused by multidrug-resistant bacteria [9].

If medical device-associated infections can be avoided, it would reduce antibiotic use and cost, and hence, contribute to alleviating the antimicrobial resistance crisis. Manufacturers of medical devices have worked intensely to create technologies that would diminish the infection risk originating from the use of such devices. Several techniques have been tried, and the use of heavy metals (like silver or copper in metal or ionic form [10–12]) or antibiotics (gentamicin, nitrofurazone, norfloxacin, minocycline-rifampicin, and more [13]) integrated into the devices, creating anti-colonization (antifouling) surfaces, are currently the most common solutions. However, limited efficacy, unwanted toxicity, and the non-degradability of silver and other heavy metals have kept the medical device industry looking for better alternatives [12,14,15]. Another issue with antibiotic-coated surfaces is the risk of contributing to the development of antibiotic resistance. As an example, the widespread use of triclosan as an antibacterial agent in medical devices and a variety of consumer products has not only triggered resistance against triclosan [16,17] but also against ciprofloxacin [18].

Coating the surface with covalently attached antimicrobial peptides (AMPs) can be an alternative solution to the problem of medical device-associated infections [19,20]. AMPs [21] have many advantages over the current antimicrobial agents used in medical devices. Antimicrobial peptides intrinsically biodegrade into amino acids, and hence, the problem with antibiotic persistence is limited. Furthermore, AMPs generally have negligible side effects, a broad action spectrum against both Gram-positive and Gram-negative bacteria, and they may even eradicate established biofilms [22–24]. The mechanism of action of AMPs is generally believed to involve microbial membrane destabilization or lysis [25], and hence, the risk of promoting resistance development is low compared to classic antibiotics that address a specific drug target [26]. An additional advantage of AMPs is the information of pharmacophores, that is, the minimum content of essential features, enabling a de novo design of synthetic peptides with pre-determined antibacterial activities [27]. AMPs and mimics of antimicrobial peptides have been shown to inhibit bacteria from colonizing on the surface either by releasing active agents or by covalently attaching to surfaces [20,28], although the surface immobilization of AMPs may lower the activity of the peptides [29].

In the present study, the quantitative effect of antimicrobial peptides covalently attached to a surface upon the colonization of an avidly biofilm-forming bacterium, *Staphylococcus epidermidis*, was investigated. A gold surface with a polyethylene glycol (PEG) self-assembled molecular monolayer (SAM) was chosen as the model system since its preparation is a versatile and established technique [30]. A chemically addressable SAM monolayer composed of  $\alpha$ -thio-PEG- $\omega$ -alkyne monolayers that spontaneously form on the Au (111) surface was used as the experimental platform because the peptides could be introduced as azide derivatives on the alkyne-molecular monolayer through a copper(I)-catalyzed alkyne-azide cycloaddition (CuAAC) reaction [31]. The use of a common surface where the peptides were covalently linked through the same chemical reaction allows for the preparation of a set of similar surfaces that differ only in the presence of an additional

PEG linker and the type of peptide, and subsequently allows for the determination of a structure–activity relationship involving these features (Figure 1).

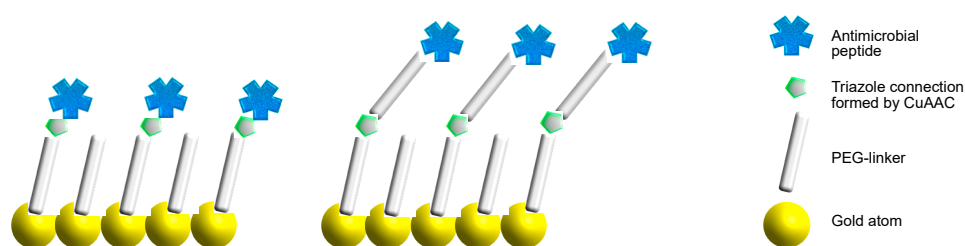


**Figure 1.** The design of the peptide-functionalized self-assembled monolayer (SAM) gold surface. The peptides were connected by a CuAAC reaction either directly to the terminus of the SAM (peptides **1c**, **1d**, **2c**, and **2d**, left), or through an additional PEG linker (peptides **1a**, **1b**, **2a**, and **2b**, right).

## 2. Results

### 2.1. Surface Design and Preparation

A quantitative investigation of the anti-colonization effect of antimicrobial peptides covalently attached to a model surface requires the restriction of uncontrolled parameters as much as possible. Hence, the functionalized surfaces were prepared using well-established and reliable methods. The peptides were connected to the surface through a Cu(I)-catalyzed [3 + 2] acetylene-azide cycloaddition (CuAAC, click) reaction between the surface-bound acetylene group and an azide functional group connected to the peptide, which is a reliable, high-yielding, and bioorthogonal method [31]. The selection of the CuAAC reaction for the peptide connection requires the surface to have an acetylene terminus. Hence, the Au–SAM surface was constructed through the self-assembly of  $\alpha$ -thio-PEG600- $\omega$ -alkyne on an Au(111) substrate (Figure 2, left) through a self-assembled monolayer (Figure 2, middle), terminating in the required alkyne functional group. Furthermore, a PEG-based SAM surface was chosen to ensure the hydrophilic surface interacted well with the aqueous environment. The CuAAC-linking of the peptide effector molecules to the Au–SAM surface generates a stable covalent connection through a 1,2,3-triazole moiety (Figure 2, right) [32].

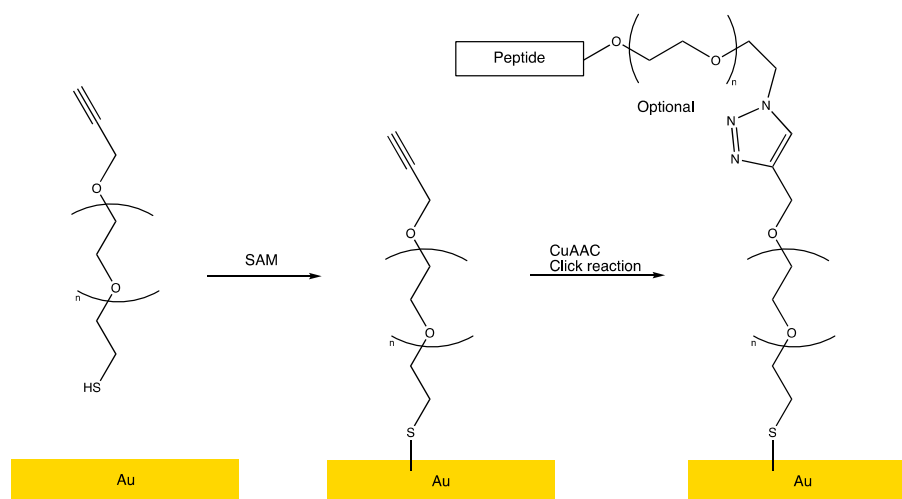


**Figure 2.** The preparation of the peptide-functionalized Au(-SAM) surface. A hydrophilic Au–SAM surface was made by reacting an Au(111) substrate with  $\alpha$ -thio-PEG600- $\omega$ -alkyne (**left**→**middle** panel). The peptide-functionalized surface was created by a CuAAC reaction between the acetylene terminated Au–SAM surface and an azide-functionalized peptide (**middle**→**right** panel).

## 2.2. Peptide Design

The peptides were designed according to the pharmacophore of cationic antimicrobial peptides [27,33], with five or six residues containing two arginine residues and three bulky and lipophilic moieties in the form of tryptophan, phenylalanine, and 4'-phenyl-phenylalanine (biphenylalanine, B) [34,35]. Series 1 (**1a–d**) contains tryptophan as the major hydrophobic group, while Series 2 (**2a–d**) contains biphenylalanine as the main hydrophobic amino acid. The selection of tryptophan and biphenylalanine as bulky and lipophilic residues in the peptides was made to ensure a wide distribution of antimicrobial activity. All peptides adhere to the minimum motif for antimicrobial activity, and the increased bulkiness and lipophilicity of biphenylalanine over tryptophan ensures a higher antimicrobial efficacy of the Series 2 peptides compared to the Series 1 counterparts [34–37]. All peptides had a phenylalanine residue close to the amidated C-terminus. One peptide from each series was cyclized to investigate whether the anti-colonization efficacy was affected by the decrease in conformational freedom resulting from cyclization. Half of the peptides, **1c**, **1d**, **2c**, and **2d**, contained an azido-lysine residue used for a direct surface connection. The effect of linking the peptide directly to the Au–SAM or through an additional PEG linker was also included in the study using PEG200-linked peptides (**1a** and **2a**) and PEG400-linked peptides (**1b** and **2b**). An overview of the peptides prepared for the study is shown in Figure 3.

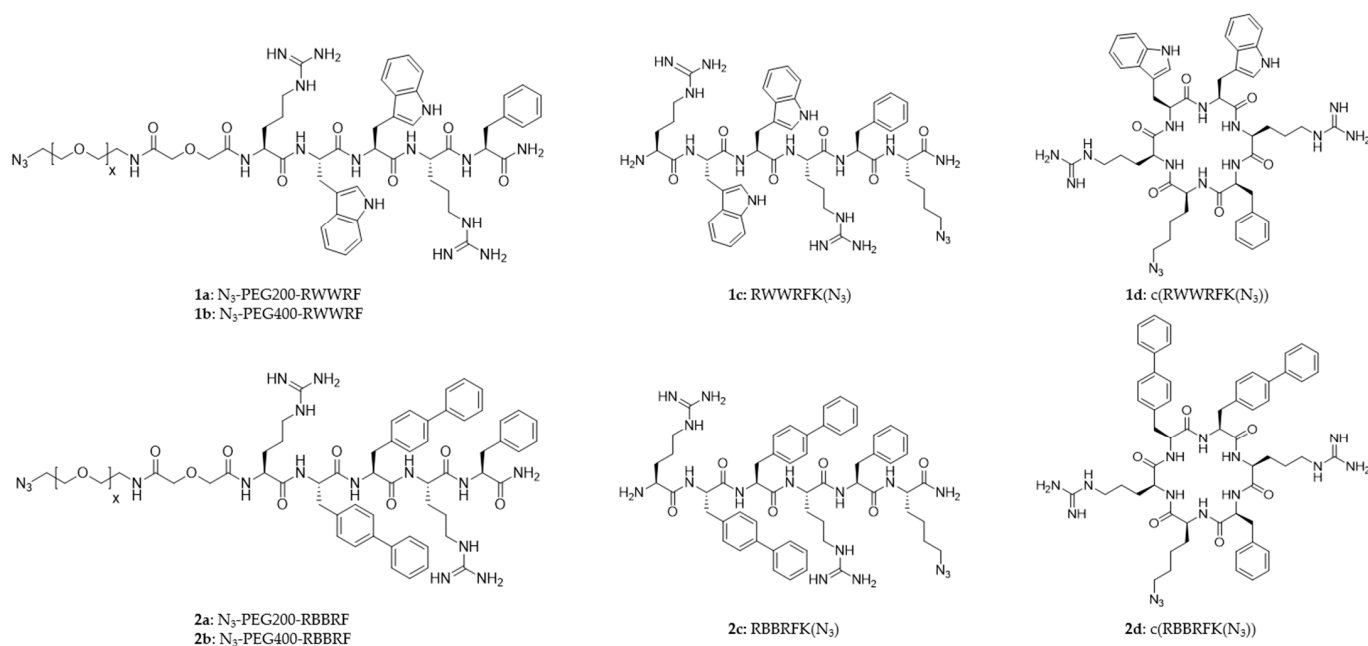


**Figure 3.** Eight azidopeptides with different hydrophobic groups (Series 1: tryptophan, Series 2: biphenylalanine).

## 2.3. Intrinsic Antimicrobial Activity of the Peptides

The eight azidopeptide analogs designed for this study were screened against the Gram-positive bacteria *S. aureus* and *S. epidermidis* and the Gram-negative *E. coli* and *P. aeruginosa* reference strains to determine the intrinsic antimicrobial activity of the peptides as the minimum inhibitory concentration (MIC) (Table 1). The bacterial strains represent typical pathogens found in medical device-related biofilms.



**Table 1.** Antimicrobial activity of eight clickable peptides against four selected bacterial reference strains.

Entry	Sequence	Net Charge	Mw	Antimicrobial Activity (MIC in µg/mL)			
				<i>S. aureus</i>	<i>S. epidermidis</i>	<i>E. coli</i>	<i>P. aeruginosa</i>
<b>1a</b>	N <sub>3</sub> -PEG200-RWWRWF	2+	1188.49	64	32	256	256
<b>1b</b>	N <sub>3</sub> -PEG400-RWWRWF	2+	1388.49	128	128	>256	>256
<b>1c</b>	RWWRWFK(N <sub>3</sub> )	3+	1003.19	32	16	64	64
<b>1d</b>	c(RWWRWFK(N <sub>3</sub> ))	2+	986.16	8	8	64	128
<b>2a</b>	N <sub>3</sub> -PEG200-RBBRF	2+	1262.53	8	8	64	64
<b>2b</b>	N <sub>3</sub> -PEG400-RBBRF	2+	1462.53	32	16	128	256
<b>2c</b>	RBBRFK(N <sub>3</sub> )	3+	1077.31	8	4	8	16
<b>2d</b>	c(RBBRFK(N <sub>3</sub> ))	2+	1060.28	4	2	64	256

Bacterial reference strains: *Staphylococcus aureus* ATCC 9144; *Staphylococcus epidermidis* 1457; *Escherichia coli* ATCC 25922; *Pseudomonas aeruginosa* ATCC 27853. Full data set can be found in Supplementary Information Table S3.

The eight peptides displayed a substantial spread in MIC values, with the Gram-positive bacteria being more susceptible than the Gram-negatives. Some peptides, like **1c** and **2c**, displayed similar antimicrobial efficacy against all four bacteria in the panel, whereas other peptides (e.g., **1d**, **2a**, and **2d**) were quite selective against Gram-positive bacteria. The PEGylated tryptophan peptides **1a** (PEG200) and **1b** (PEG400) were modestly active against Gram-positive and inactive against Gram-negative bacteria. The linear peptide, **1c**, despite being modestly active against Gram-positive (MIC: 16–32 µg/mL) and Gram-negative (MIC: 64 µg/mL) bacteria, was more active than **1a** and **1b**, indicating that PEGylation slightly decreased the activity. The cyclization of **1c** to give **1d** improved the antimicrobial activity to 8 µg/mL against Gram-positive bacteria but remained the same as **1c** against *E. coli* (MIC: 64 µg/mL) and gave 128 µg/mL against *P. aeruginosa*.

Replacing the tryptophan residues in Series 1 with biphenylalanine residues increased the activity, as expected [36]. Peptide **2a** showed good activity against Gram-positive (MIC: 8 µg/mL) but was less active against the Gram-negative (MIC: 64 µg/mL) bacteria. Substituting PEG200 with PEG400 in peptide **2b** diminished activity similarly as in Series 1. Removing the PEG chain increased activity, as observed for **2c**. The cyclization of **2c** to give **2d** improved the activity against Gram-positive bacteria but became less active against Gram-negative bacteria. Peptide **2d** had potent activity against *S. aureus* (MIC: 4 µg/mL) and *S. epidermidis* (MIC: 2 µg/mL), but less activity against *E. coli* (MIC: 64 µg/mL) and was not active against *P. aeruginosa* (MIC: 256 µg/mL).

#### 2.4. Characterization of Peptide Surfaces

The preparation of peptide-functionalized Au-SAM surfaces took place in two steps—self-assembly of the acetylene-terminated PEG monolayer and the CuAAC functionalization with the antimicrobial peptides (Figure 2). To be able to reliably interpret the biological efficacy data, it is important to assess the integrity (the presence of the correct peptide) and the homogeneity of the surface. In the present study, two surface characterization methods were used—the measurement of the contact angle and spatially resolved ToF-SIMS mass spectrometry (ToF-SIMS imaging).

##### 2.4.1. Contact Angle

The contact angle is a measurement of the wettability of a surface, and as peptide functionalization of the Au-SAM surface is expected to alter the hydrophobicity of the surface, the contact angle is, hence, expected to be altered. A larger contact angle indicates a more hydrophobic surface (low surface energy), and the opposite indicates a hydrophilic surface (high surface energy) (Figure S25) [38]. To assess the homogeneity of the surface, the contact angle was determined for five droplets tested per peptide surface to get an average value and a standard deviation. The measured contact angles for the functionalized surfaces are shown in Table 2.

**Table 2.** The average contact angles  $\theta$  (standard deviation) of **1a–d**, **2a–d** covalently linked to Au surface. Control is Au surface treated with peptide, without the CuAAC reaction.

<b>1a</b>	<b>1b</b>	<b>1c</b>	<b>1d</b>	<b>2a</b>	<b>2b</b>	<b>2c</b>	<b>2d</b>	<b>Control</b>
49.1 (2.7)	52.2 (2.5)	50.0 (3.2)	49.6 (2.1)	54.7 (2.4)	53.5 (2.3)	54.9 (3.4)	54.0 (2.5)	39.6 (2.8)

The observed contact angles did not vary significantly between the five droplets applied on each surface specimen, indicating that the surface was homogenous on the scale of the specimens. The contact angle,  $\theta$ , of the control surface—the Au–SAM PEG-alkyne surface with no peptide functionalization—was 39.6°. The surfaces functionalized with the AMPs **1a–d** and **2a–d** showed a considerably higher  $\theta$  than the control surface, verifying a significant increase in surface lipophilicity. This lipophilicity change is compatible with the AMPs being covalently linked to the surface by the CuAAC reaction. There were small differences between the peptides themselves with the same hydrophobic amino acids, but the biphenylalanine peptides (**2a–d**) showed an overall higher contact angle than the tryptophan peptides (**1a–d**) due to biphenylalanine being more hydrophobic than tryptophan [39].

#### 2.4.2. Surface Characterization by Spatially Resolved ToF-SIMS Mass Spectrometry

Spatially resolved time-of-flight secondary ion mass spectrometry (ToF-SIMS imaging) is a powerful technique for the characterization of surfaces that are modified by organic molecules in nanoscale layers, and it has successfully been used to verify surface attachment [40]. In this technique, a specimen is introduced into the ion source of a ToF-mass spectrometer, and the SIMS ion beam is scanned over the surface, providing spatially resolved SIMS mass spectra of the surface. In this manner, both the chemical composition and the homogeneity of the surface can be verified.

For the Trp-containing peptides **1a–d**, the SIMS mass spectra of the corresponding surfaces revealed the presence of signals due to the arginine and tryptophan residues. Arginine residues gave rise to ions originating from the side chain with  $\text{CH}_6\text{N}_3^+$  (the guanidinium group), as well as two additional ions,  $\text{C}_3\text{H}_9\text{N}_3^+$  and  $\text{C}_4\text{H}_{10}\text{N}_3^+$ , including the carbon atoms of the arginine side chain. The tryptophan residues provided the side chain methyleneindole ion  $\text{C}_9\text{H}_8\text{N}^+$ . The ToF-SIMS images of the peptide-modified surfaces were compared to the control Au–SAM surfaces, which had only the thiol-PEG-alkyne linked on the surface. As an example, Figure 4a shows the ToF-SIMS image of the Au–SAM surface functionalized with peptide **1a** when observing the arginine-specific ions. Figure 4b shows the image of the same surface when observed the tryptophan-specific ions. Figure 4c, on the other hand, shows the ToF-SIMS image when imaging the naïve (no peptide) Au–SAM surface by searching for the tryptophan-specific  $\text{C}_9\text{H}_8\text{N}^+$  ion. Arginine side chains and the indole group of tryptophan were observed on all the peptide surfaces, displaying high-intensity images by ToF-SIMS. Typical arginine and tryptophan surface data of peptide **1a** with the control group are displayed in Figure 4. Surface ToF-SIMS images for peptides **1b–d** are found in the Supplementary Material, Figure S26.

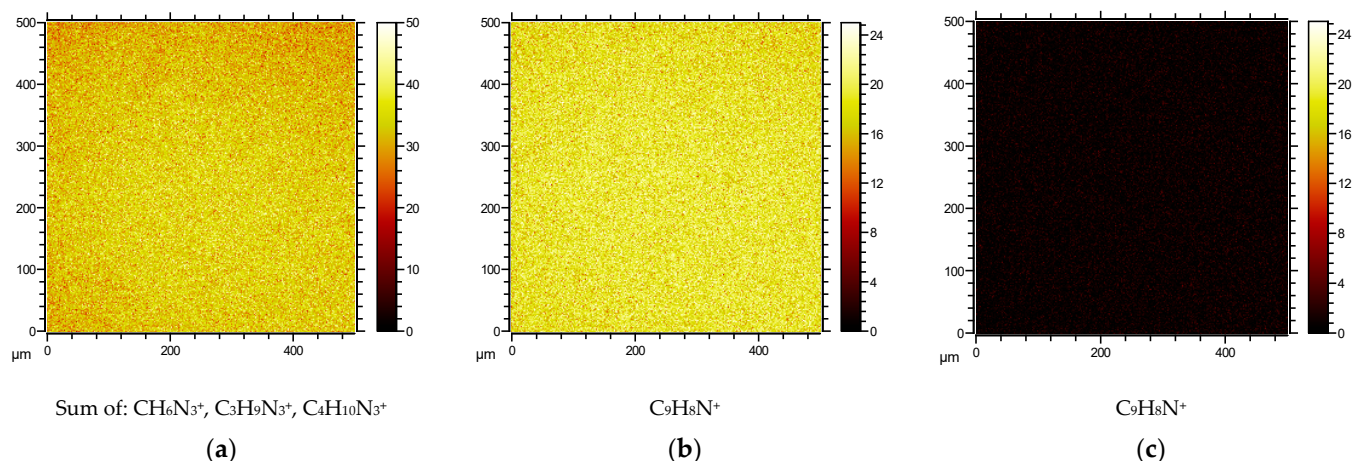


**Figure 4.** Typical ToF-SIMS images of an Au-SAM surface coated with azido-peptide-containing tryptophan, **1a**: (a) ion intensities for  $\text{CH}_6\text{N}_3^+$ ,  $\text{C}_3\text{H}_9\text{N}_3^+$ , and  $\text{C}_4\text{H}_{10}\text{N}_3^+$  of arginine; (b) ion intensity of tryptophan indole-ion  $\text{C}_9\text{H}_8\text{N}^+$ ; (c) ion intensity image of control Au-SAM surface observed at the tryptophan-specific ion  $\text{C}_9\text{H}_8\text{N}^+$ .

For biphenylalanine peptides **2a–d** linked to the Au-SAM surface, arginine and biphenylalanine moieties on the surface were located through ToF-SIMS imaging. The biphenylalanine residue was identified by the  $\text{C}_{13}\text{H}_{11}^+$  ion, which forms with a lower ionization efficiency than the arginine ions (Figure 5a,b). Figure 5c shows the control Au-SAM surface observed through the biphenylalanine ion, confirming the absence of a biphenylalanine peptide. Surface ToF-SIMS images for peptides **2b–d** are found in the Supplementary Material, Figure S27.

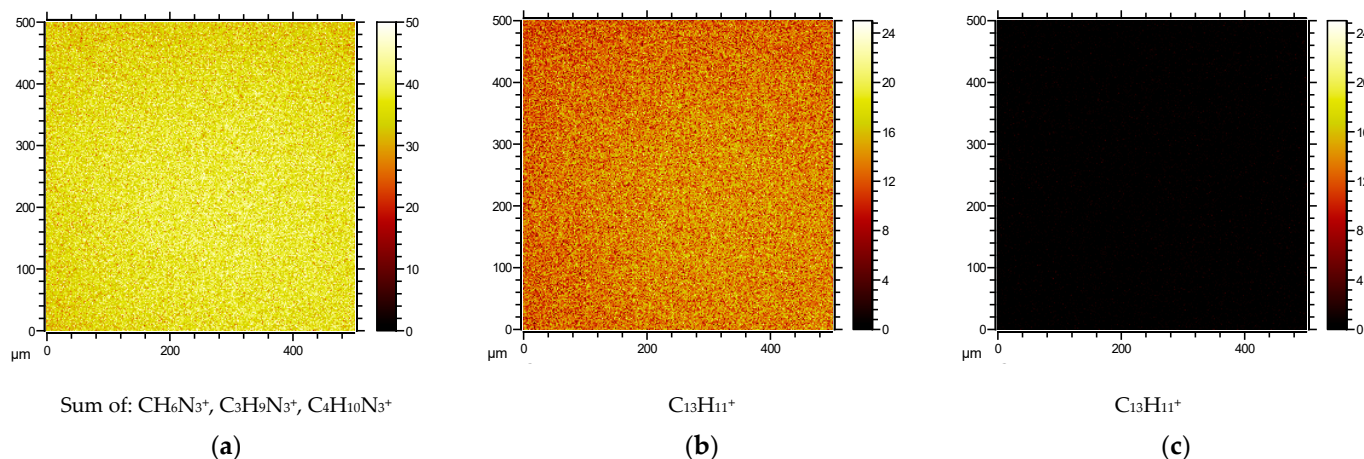


**Figure 5.** Typical ToF-SIMS images of an Au-SAM surface coated with azido-peptide-containing biphenylalanine, **2a**: (a) ion intensities for  $\text{CH}_6\text{N}_3^+$ ,  $\text{C}_3\text{H}_9\text{N}_3^+$ , and  $\text{C}_4\text{H}_{10}\text{N}_3^+$  of arginine; (b) ion intensity of biphenylalanine-ion  $\text{C}_{13}\text{H}_{11}^+$ ; (c) ion intensity image of control Au-SAM surface observed at the biphenylalanine-specific ion  $\text{C}_{13}\text{H}_{11}^+$ .

### 2.5. Anti-Colonization Efficacy of Peptide Modified Gold Surfaces Certika

The antibacterial effectiveness of active surfaces can be tested with the proliferation assay Certika [41]. In short, this method consisted of the samples being washed in phosphate-buffered saline (PBS) in a 24-well plate before the test strains were added to each sample and incubated at 37 °C for 1 h to allow bacterial cells to adhere to the sample surface. Loosely bound bacteria were subsequently removed by washing in PBS before the samples were incubated in a minimum medium. After removal of the test samples, each well was supplemented with TSB complete medium. The bacterial growth (of the daughter

cells) at 37 °C was recorded every 30 min for a period of 48 h by optical density (OD) measurements in a microtiter plate reader at a wavelength of 578 nm. Thus, the Certika method measured the anti-colonization efficacy of the surface as a prolonged onset time of bacterial growth. The antimicrobial effectiveness of an antimicrobial-coated surface is measured as the difference in the time required to reach the onset OD value of the active surface and the time needed to reach the onset OD value for the control surface, and hence, a prolonged time difference indicates an active surface. In the present study, the non-peptide Au-SAM surface was used as the inactive control, the onset OD value was set to 0.2, and the test bacterium, *S. epidermidis*, was assumed to divide once every 30 min. As an example, a time difference of 5 h in the net onset OD (in comparison to a blank sample) can be translated into the fact that it takes ten duplications/divisions (two duplications per hour) before the bacteria present on the active surface reaches the number of bacteria on the control surface. In 10 duplications, a single bacterium will give rise to  $2^{10}$  bacteria, and hence, a time difference of 5 h equates to a reduction of  $2^{10}:1$  (=1024:1) and/or  $\approx 0.1\%$  of the formed daughter cells on the active surface compared to the control.

The Au-SAM surfaces functionalized with peptides **1a–d** and **2a–d** were tested against *S. epidermidis* RP62A using the Certika assay to determine their anti-colonization effect on the surfaces (Table S2). These peptide surfaces were compared to the non-peptide Au-SAM surface as the control group, shown in Figure 6.

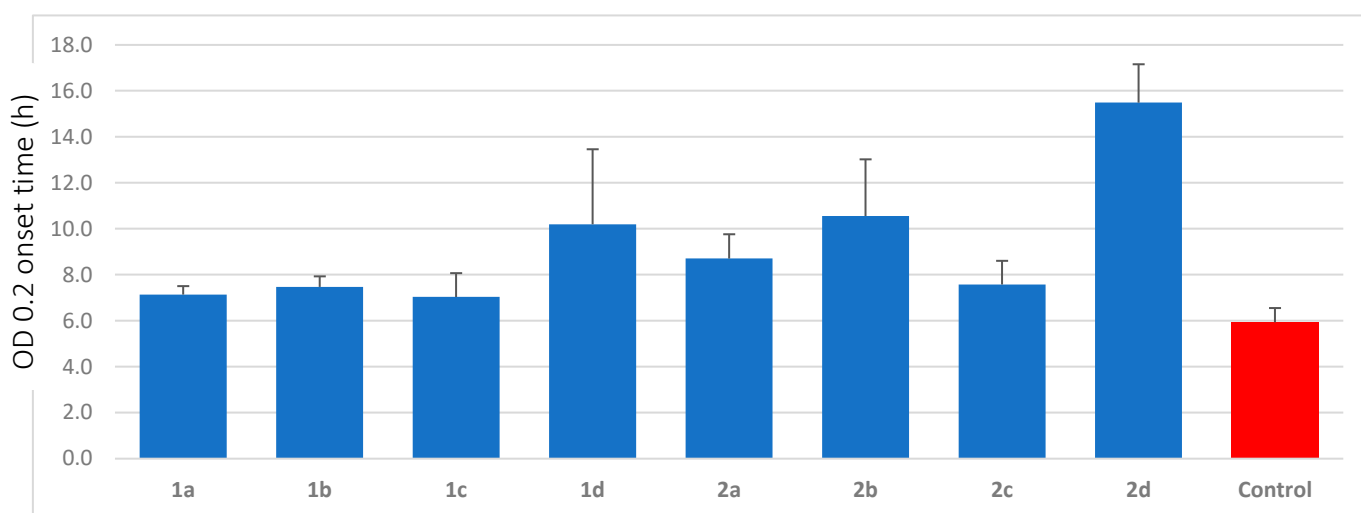


**Figure 6.** Certika assay with Au-SAM surfaces functionalized with peptides **1a–d** and **2a–d** as well as the control using the biofilm-forming bacterium *S. epidermidis* RP62A as a challenge. The diagram shows the OD 0.2 onset time in hours for all surfaces.

Series 1 surfaces showed lower anti-colonization efficacy against *S. epidermidis* compared to the corresponding peptides belonging to Series 2. The best anti-colonization effect of the tryptophan series was observed for the cyclic peptide **1d**, with a prolonged onset time of 4 h, corresponding to  $2^8:1$ , that is, a 256:1 reduction of colonization. There was no difference between **1a** (PEG200) and **1c** (no PEG), while there was a slight increase in the onset time compared to that for **1b** (PEG400).

The anti-colonization efficacy pattern observed in the tryptophan peptides was also observed for the corresponding biphenylalanine peptides, although the anti-colonization efficacy was much higher. The cyclic biphenylalanine peptide **2d** displayed the highest activity of the entire panel of peptide-functionalized surfaces with a delayed net onset time of 10 h. Under the assumption of a generation time of 30 min, this delay corresponds to a reduction in the colonizing ability of  $2^{20}:1$ , or 1,048,576:1 (6 log scales). The PEG-length on the peptides also showed a correlation with enhanced activity, with PEG400 (**2b**) having the highest activity, followed by PEG200 (**2a**) and then non-PEGylated linear peptide **2c**.

### 3. Discussion

#### 3.1. The Intrinsic Antimicrobial Activity of the Peptide Library

The antimicrobial peptides used in this study were designed based on the pharmacophore for short cationic antimicrobial peptides [27] to span a wide efficacy range from weak to very active peptides. Furthermore, the effect of cyclization of a linear peptide and the aspect of linking the peptides to the surface through an additional PEG tether or linking the peptides directly to the molecular monolayer were also investigated.

The pharmacophore predicts that all peptides prepared with at least two cationic charges and three bulky and lipophilic residues should have a minimum of antibacterial activity which is also observed in the present library. In some of the peptides, the tryptophan residues were substituted with biphenylalanine, with a subsequent change in bulk, geometry, and lipophilicity that favors enhanced antibacterial efficacy [34,35], an effect also observed in the present library, where the peptides in Series 2 were more effective than their Series 1 analogs. The effect of cyclization represents a loss of the N-terminal charge in the linear peptide as well as a substantial restriction on the conformational freedom of the peptide backbone, effects that turned out to be positive for the Gram-positive efficacy, but negative, activity-wise, against the Gram-negative bacteria. A general increase in antimicrobial activity upon cyclization has previously been reported for a small set of bacteria, however, the increase was the largest for *E. coli* [42], which is the opposite of what we observed. The effect of PEGylation upon the intrinsic antimicrobial activity was marginal when considering the mass increase connected with PEGylation. Overall, the library designed and prepared for the study represented a variety in antimicrobial efficacy from the very active peptides **1d**, **2c**, and **2d** to almost inactive peptides **1a**, **1b**, **2a**, and **2b**, as well as including structural diversity in the peptide library.

#### 3.2. Surface Attachment of the Peptides

##### 3.2.1. Contact Angle and Surface Lipophilicity

The Cu(I)-catalyzed [3 + 2] cycloaddition (CuAAC) between the acetylenic terminus of the Au-SAM monolayer and the azide functionality of the peptides created a covalent, non-leaching peptide surface. The self-assembled monolayer is PEG-based; hence, the Au-SAM surface is hydrophilic in nature. The hydrophilicity of the SAM surface is evident in the low measured contact angle of 39.6°. The contact angle increased significantly to 49–55° upon the covalent attachment of the antimicrobial peptides. This increase in contact angle is a measurement of the increase in lipophilicity of the surface caused by attaching the amphipathic peptides to the surface. While the increase in contact angle of the surface upon peptide functionalization is substantial, the variation within the peptide series is smaller; the Series 1 tryptophan peptides varied between 49.1° and 52.2°, whereas the Series 2 biphenylalanine peptides were more lipophilic, with contact angles between 53.5° and 54.9°. Although the Series 2 peptides were more efficacious against the bacteria than those in Series 1—fitting the general picture that lipophilic peptides are more active than their less lipophilic counterpart—there is seemingly no correlation between the contact angle and the peptide activity within each group.

##### 3.2.2. Verification of Surface Integrity and Homogeneity by Spatially Resolved ToF-SIMS Mass Spectrometry

The interpretation of the anti-colonization efficacy of the various peptide-modified surfaces is highly dependent on verifying the integrity—whether the peptide is present on the surface—and the homogeneity of the surface—that the peptides coupled to the surface are evenly spread. ToF-SIMS imaging is a premier method for such an analysis [40]. The technique provides a mass resolved 2D-map (image) of the surface specimen. When the masses selected for the imaging are among the characteristic ions for each amino acid in the sequence, the combined maps provide the spatial distribution of the peptides, as shown in Figures 4 and 5. The data unequivocally shows the presence of the specific peptides on the surface, and the surfaces are homogenous in nature. A drawback with the method is

that it is not quantitative, making comparisons between specimens difficult [43]. However, the homogeneity within a sample is a good indication that we can consider that there are no gross differences in the surface density of the peptides between the different surfaces, but that the absolute surface density is an unknown factor. On this basis, that is, that the peptides are connected to the Au-SAM surfaces in a manner that is similar for all peptides, we could start interpreting the anti-colonization activity of the different surfaces.

### 3.3. Anti-Colonization Efficacy

The Certika test that was selected to assay the anti-colonization efficacy of the peptide-modified surfaces is a rigorous quantitative test that is based on measuring the quantitative regrowth of surface adherent bacteria after a bacterial challenge. The Certika method is particularly valuable as it can measure a wide variation of anti-colonization efficacy without the dilution of the assay material.

The Certika test was applied to all eight surfaces using *S. epidermidis* as the challenge organism. *S. epidermidis* was selected because it is a bacterium with a large potential for surface colonization and subsequent biofilm formation [44]. The Certika test confirmed that the anti-colonization of all surfaces increased after peptide linkage, but the efficacy varied to a large degree. The trends in the anti-colonization efficacy of the peptide-functionalized surfaces grossly followed the intrinsic MIC values for the individual peptides. The major break in the correlation was that the PEG400 peptides became more efficacious than the shorter PEG200 peptides, a result suggesting that the increased motional freedom of the peptides with a longer tether to the surface was beneficial for the anti-colonization efficacy. The trend was even extended to the **1c** and **2c** peptides, where the peptides were connected directly to the SAM surface without the use of an additional PEG tether, although a direct comparison is more difficult, as the **1c** and **2c** peptides were connected close to the C-terminus and had an additional charge compared to the peptides **1a**, **2a**, **1b**, and **2b**, which were linked to the surface through a PEG unit connected to the N-terminus.

The most surprising result, however, was the large difference observed in the anti-colonization efficacy compared to the relatively narrow span of the intrinsic antimicrobial efficacy of the non-coupled peptides. While the antibacterial efficacy of the eight peptides in the library covered a range of 2–128 µg/mL, the anti-colonization efficacy varied from 2<sup>2</sup>:1 for surfaces with **1a** and **1c** to 2<sup>10</sup>:1 for a surface prepared with **2d**, or, in log sales, a variation between 0.6 log and 6 log.

An anti-colonization efficacy in the order of 6 log units is well within what would be needed for practical utilization of covalently anchored peptides to create an anti-colonization surface. Admittedly, the surface used here was a model surface, and more work is needed to translate these promising results into a practical and general method for peptide functionalization of surfaces. Furthermore, the analytical techniques used in the present study do not provide a quantification of the surface density of the peptides. On the other hand, the AMP-functionalized Au-SAM method provides a surface with high homogeneity and chemical integrity, allowing for the determination of the influence of the intrinsic antimicrobial efficacy of the attached peptides and the anti-colonization efficacy they provide on a surface. The results, so far, have revealed a surprising effect where modest differences in antimicrobial efficacy translated into large changes in anti-colonization activity.

## 4. Materials and Methods

### 4.1. Materials

Rink amide HL resin, 2-chlorotrityl chloride resin, and natural Fmoc-protected amino acids were bought from Novabiochem. Fmoc-Bip-OH was purchased from Iris Biotech. Other chemicals used in standard Fmoc solid phase peptide synthesis (SPPS) were bought from Sigma-Aldrich. The starting material, reactants, and solvents for the synthesis of the PEG linker were purchased from Sigma-Aldrich. Pre-diced gold (Au)-coated Si-wafers (10 × 10 × 0.5 mm) were purchased from ConScience AB, Gothenburg, Sweden. The Au

surface was protected by polymer S1813 during shipment and handling.  $\alpha$ -Thio-PEG600- $\omega$ -alkyne was purchased from Nanocs, NY, USA, while the rest of the chemicals for CuAAC were bought from Sigma-Aldrich.

#### 4.2. Experimental Method

##### 4.2.1. Synthesis of Azide and Carboxylic Acid Terminal-Conjugated Polyethylene Glycol

The preparation of the  $\alpha$ -carboxyl-PEG- $\omega$ -alkynes **6a** and **b** were prepared from PEG200 and PEG400, respectively, through a four-step sequence (a–d) outlined in Figure 7.

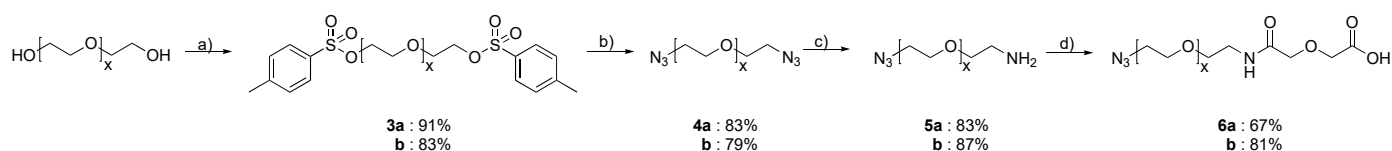


**Figure 7.** Synthesis of a modified PEG (average Mw: 200 (Series a) and 400 (Series b)) moiety with azido and carboxylic acid terminals: (a). TsCl and KOH in DCM at rt overnight; (b) NaN<sub>3</sub> in Et<sub>2</sub>O at 80 °C overnight; (c) PPh<sub>3</sub> in Et<sub>2</sub>O:1M HCl (1:1) rt overnight; (d) 2.0 eq. diglycolic anhydride and 0.2 eq. DMAP in DCM rt overnight. The chemical yield is given under each compound.

#### *O,O'*-Bis(tosyloxy)polyethylene glycols

Polyethylene glycol (PEG, average Mw 200) (0.5 g, 0.0025 mol) was dissolved in 50 mL dichloromethane (DCM) and cooled on an ice bath for 15 min. Powdered KOH (8.0 eq., 1.1221 g, 0.02 mol) was added slowly before adding 4-toluenesulfonyl chloride (3.0 eq., 1.4298 g, 0.0075 mol) to the ice-cold solution. The reaction was carried out overnight at room temperature before quenching with 15 mL of ice-cold water. The reaction mixture was extracted with 10 mL of DCM three times, dried over MgSO<sub>4</sub>, filtered, and concentrated under vacuum. The crude product was purified by silica column chromatography (MeOH/DCM, 1:10) to give **3a** (1.157 g, 91%) as a transparent colorless oil. <sup>1</sup>H NMR (400 MHz, CDCl<sub>3</sub>):  $\delta$  7.83 (dd,  $J$  = 8.3, 1.4 Hz, 4H), 7.37 (d,  $J$  = 8.0 Hz, 4H), 4.20–4.15 (m, 4H), 3.74–3.54 (m, 14H), 2.48 (s, 6H) (Figure S1). HRMS (ESI): calculated for C<sub>22</sub>H<sub>30</sub>O<sub>9</sub>S<sub>2</sub>Na<sup>+</sup> [M + Na]<sup>+</sup> 525.1229; found 525.1226.

Synthesis of PEG average Mw 400 (1.0 g, 0.0025 mol) was synthesized using the same method as above to give **3b** (1.468 g, 83%) as a transparent colorless oil. <sup>1</sup>H NMR (400 MHz, CDCl<sub>3</sub>):  $\delta$  7.82–7.75 (m, 4H), 7.33 (d,  $J$  = 8.1 Hz, 4H), 4.14 (dd,  $J$  = 5.7, 4.0 Hz, 4H), 3.67 (dd,  $J$  = 5.6, 4.1 Hz, 4H), 3.65–3.58 (m, 17H), 3.57 (s, 8H), 2.44 (s, 6H) (Figure S2). HRMS (ESI): calculated for C<sub>34</sub>H<sub>54</sub>O<sub>15</sub>S<sub>2</sub>Na<sup>+</sup> [M + Na]<sup>+</sup> 789.2802; found 789.2796

#### *O,O'*-Bis(2-azidoethyl)polyethylene glycols

Compound **3a** (15.957 g, 0.031 mol) was dissolved in 80 mL dimethylformamide (DMF). To the stirred solution, sodium azide (3.0 eq., 6.125 g, 0.093 mol) was added slowly and the mixture refluxed at 80 °C overnight. Excess sodium azide was quenched with 100 mL of ice-cold water. The product was extracted with diethyl ether, dried over MgSO<sub>4</sub>, filtered, and concentrated under vacuum to give crude **4a** (6.535 g, 83%) as a transparent colorless oil. The product was used without further purification. <sup>1</sup>H NMR (400 MHz, CDCl<sub>3</sub>):  $\delta$  3.71–3.64 (m, 14H), 3.39 (td,  $J$  = 5.1, 2.4 Hz, 4H) (Figure S3). HRMS (ESI): calculated for C<sub>14</sub>H<sub>28</sub>N<sub>6</sub>O<sub>6</sub>Na<sup>+</sup> [M + Na]<sup>+</sup> 399.1968; found 399.1954

The same method was applied for the preparation of **4b** from **3b** (4.843 g, 0.0068 mol) to give **4b** (2.441 g, 79%) as a transparent colorless oil. <sup>1</sup>H NMR (400 MHz, CDCl<sub>3</sub>)  $\delta$  3.69–3.63 (m, 30H), 3.38 (t,  $J$  = 5.1 Hz, 4H) (Figure S4). HRMS (ESI): calculated for C<sub>24</sub>H<sub>48</sub>N<sub>6</sub>O<sub>11</sub>K<sup>+</sup> [M + K]<sup>+</sup> 635.3018; found 635.3006

#### *O*-(2-Aminoethyl)-*O'*-(2-azidoethyl)polyethylene glycols

To a stirred solution of **4a** (5.537 g, 0.022 mol) in 50 mL diethyl ether, 1M HCl (50 mL) and triphenylphosphine (1.0 eq., 5.804 g, 0.022 mol) were added and the resulting mixture was stirred overnight at room temperature. White solids of triphenylphosphine oxide were removed by filtration, and the filtrate was extracted with diethyl ether to remove residues

of triphenylphosphine oxide. The pH of the aqueous phase was adjusted by KOH until pH ~12, extracted with 15 mL DCM, dried over MgSO<sub>4</sub>, filtered, and concentrated under vacuum to give crude **5a** (4.157 g, 83%) as a transparent colorless oil. <sup>1</sup>H NMR (400 MHz, CDCl<sub>3</sub>): δ 3.72–3.61 (m, 14H), 3.52 (ddd, *J* = 8.7, 5.7, 4.2 Hz, 2H), 3.40 (dt, *J* = 8.4, 4.9 Hz, 2H), 2.88 (q, *J* = 5.3 Hz, 2H), 1.91 (s, 2H) (Figure S5). HRMS (ESI): calculated for C<sub>14</sub>H<sub>31</sub>N<sub>4</sub>O<sub>6</sub><sup>+</sup> [M + H]<sup>+</sup> 351.2238; found 351.2245.

The same method was applied for the preparation of **5b** from **4b** (2.441 g, 0.0054 mol). Compound **5b** (1.999 g, 87%) was obtained as a yellow oil. <sup>1</sup>H NMR (400 MHz, CDCl<sub>3</sub>): δ 3.61–3.46 (m, 28H), 3.39 (t, *J* = 5.2 Hz, 2H), 3.26 (t, *J* = 5.0 Hz, 2H), 2.73 (t, *J* = 5.2 Hz, 2H), 2.08 (s, 3H) (Figure S6). HRMS (ESI): calculated for C<sub>24</sub>H<sub>51</sub>N<sub>4</sub>O<sub>11</sub><sup>+</sup> [M + H]<sup>+</sup> 571.3549; found 571.3532

#### **O-(2-Azidoethyl)-O-[2-(diglycolyl-amino)ethyl]polyethylene glycols**

To a stirred solution of **5a** (3.516 g, 0.016 mol) in 35 mL DCM, diglycolic anhydride (2.0 eq., 3.643 g, 0.032 mol) and 4-dimethylaminopyridine (0.2 eq., 0.352 g, 0.0032 mol) were added and the reaction mixture was stirred for 4 h. Ethylenediamine (2.0 eq., 1.886 g, 0.032 mol) was added and stirring was continued overnight to remove the excess diglycolic anhydride. DCM (30 mL) was added before washing the organic phase with 15 mL of 1M HCl three times. The combined acidic aqueous phase was extracted with 5x15 mL dichloromethane. The organic layer was dried over MgSO<sub>4</sub>, filtered and concentrated under vacuum to give **6a** (3.615 g, 67%) as a pink oil. <sup>1</sup>H NMR (400 MHz, CDCl<sub>3</sub>): δ 10.15 (s, 1H), 4.08 (s, 2H), 4.05 (s, 2H), 3.65–3.51 (m, 14H), 3.49 (t, *J* = 5.4 Hz, 2H), 3.41 (q, *J* = 5.3 Hz, 2H), 3.30 (t, *J* = 4.9 Hz, 2H) (Figure S7). HRMS (ESI): calculated for C<sub>16</sub>H<sub>30</sub>N<sub>4</sub>O<sub>9</sub>Na<sup>+</sup> [M + Na]<sup>+</sup> 445.1910; found 445.1925.

The same method was applied for the preparation of **6b** from **5b** (1.979 g, 0.005 mol). Compound **6b** (2.060 g, 81%) was obtained as a pink oil. <sup>1</sup>H NMR (400 MHz, CDCl<sub>3</sub>): δ 7.66 (s, 1H), 4.16 (s, 2H), 4.11 (s, 2H), 3.71–3.60 (m, 33H), 3.58–3.54 (m, 2H), 3.51 (q, *J* = 5.1 Hz, 2H), 3.38 (t, *J* = 5.1 Hz, 2H) (Figure S8). HRMS (ESI): calculated for C<sub>22</sub>H<sub>42</sub>N<sub>4</sub>O<sub>12</sub>Na<sup>+</sup> [M + Na]<sup>+</sup> 577.2697; found 577.2689.

#### 4.2.2. Synthesis of Linear Azidopeptides and Azido PEG Peptides

The linear azidopeptides were assembled on a Rink Amide HL 100–200 mesh (loading: 0.98 mmol/g) based on an Fmoc solid-phase peptide synthesis technique. The scale varied from 0.18 mmol to 0.21 mmol.

Loading of Rink Amide resin and coupling: Rink Amide HL (0.98 mmol/g) was swelled at 70 °C for 20 min. A solution of 20% piperidine in DMF was added to the resin to remove the Fmoc group from the resin. Fmoc amino acids (4.00 eq.) were coupled with *O*-(benzotriazol-1-yl)-*N,N,N',N'*-tetramethyluronium hexafluorophosphate (HBTU, 3.92 eq.), 1-hydroxybenzotriazole hydrate (HOBt, 4.00 eq.), and *N,N*-diisopropylethylamine (DIPEA, 8.0 eq.). The removal of N-terminal Fmoc was carried out with piperidine (20%) in DMF before coupling the next amino acid. Fmoc-Phe-OH (4.0 eq.) and Fmoc-Trp(Boc)-OH (4.0 eq.) were coupled at 70 °C for 5 min and Fmoc-Bip-OH (4.0 eq.) was coupled at 70 °C for 15 min. Fmoc-Arg(Pbf)-OH (4.0 eq.) was coupled at room temperature for 60 min and Fmoc-Lys(N<sub>3</sub>) was coupled at room temperature for 16 h. N<sub>3</sub>-PEG200-COOH (4.0 eq.) or N<sub>3</sub>-PEG400-COOH (4.0 eq.) were coupled with HBTU (3.92 eq.) and HOBt (4.0 eq.) at room temperature for 16 h. After the last coupling, non-PEGylated peptides were removed from the Fmoc group, and the resin was washed with MeOH and DCM before being placed in a desiccator to dry overnight.

Cleavage from the resin and side-chain deprotection: A solution of TFA (trifluoroacetic acid)/TIS (triisopropylsilane)/H<sub>2</sub>O (95:2.5:2.5, 10 mL) was added to the resin twice to remove the protecting groups. The combined solutions were evaporated under reduced pressure before adding ice-cold diethyl ether to precipitate the peptide. The crude peptides were washed 3 times with diethyl ether before purifying the peptides by reversed-phase high-performance liquid chromatography (RP-HPLC) to achieve a purity of ≥95%.



Following the procedure in Section 4.2.2 at a 0.21 mmol scale, **1a** was isolated as a white powder (44.4 mg, 17.2%) (Figure S17).  $^1\text{H}$  NMR (400 MHz, DMSO- $d_6$ )  $\delta$  10.80 (d,  $J = 2.3$  Hz, 2H), 8.13 (dd,  $J = 9.9, 7.5$  Hz, 2H), 8.05 (td,  $J = 7.2, 6.0, 3.7$  Hz, 2H), 7.98 (d,  $J = 8.2$  Hz, 1H), 7.91 (d,  $J = 8.1$  Hz, 1H), 7.61 (q,  $J = 5.3$  Hz, 2H), 7.57 (d,  $J = 7.9$  Hz, 2H), 7.45–7.41 (m, 1H), 7.32 (dd,  $J = 8.0, 6.3$  Hz, 3H), 7.25–7.19 (m, 6H), 7.15 (dt,  $J = 5.7, 3.2$  Hz, 5H), 7.09 (d,  $J = 2.4$  Hz, 2H), 7.08–7.02 (m, 4H), 6.95 (t,  $J = 7.4$  Hz, 3H), 4.55 (dq,  $J = 8.4, 4.7, 3.9$  Hz, 2H), 4.47 (td,  $J = 8.4, 5.2$  Hz, 2H), 4.34–4.20 (m, 7H), 3.96 (s, 4H), 3.61–3.55 (m, 2H), 3.55–3.48 (m, 8H), 3.43 (td,  $J = 6.0, 4.4$  Hz, 2H), 3.40–3.35 (m, 2H), 3.30–3.23 (m, 2H), 3.13 (dd,  $J = 15.2, 4.4$  Hz, 2H), 3.03 (dt,  $J = 19.7, 7.7$  Hz, 8H), 2.96–2.79 (m, 3H), 1.62 (ddd,  $J = 13.7, 9.5, 6.3$  Hz, 2H), 1.55–1.32 (m, 8H) (Figure S9). HRMS (ESI): calculated for  $\text{C}_{57}\text{H}_{82}\text{N}_{18}\text{O}_{12}^{2+}$  [ $\text{M} + 2\text{H}$ ] $^{2+}$  605.3175; found 605.3186.

Following the procedure in Section 4.2.2 at a 0.21 mmol scale, **1b** was isolated as a white powder (31.5 mg, 18.3%) (Figure S18).  $^1\text{H}$  NMR (600 MHz, DMSO- $d_6$ ):  $\delta$  10.79 (d,  $J = 2.4$  Hz, 2H), 8.14 (d,  $J = 7.4$  Hz, 1H), 8.11 (d,  $J = 7.5$  Hz, 1H), 8.07–8.03 (m, 2H), 7.98 (d,  $J = 8.1$  Hz, 1H), 7.91 (d,  $J = 8.1$  Hz, 1H), 7.57 (dd,  $J = 11.2, 7.0$  Hz, 4H), 7.44–7.42 (m, 1H), 7.32 (t,  $J = 8.7$  Hz, 3H), 7.23 (q,  $J = 5.9, 4.7$  Hz, 6H), 7.15 (ddd,  $J = 13.9, 6.1, 2.1$  Hz, 4H), 7.09 (d,  $J = 2.4$  Hz, 1H), 7.05 (td,  $J = 7.3, 4.0$  Hz, 3H), 6.95 (t,  $J = 7.4$  Hz, 3H), 4.55 (tt,  $J = 8.4, 3.8$  Hz, 2H), 4.47 (td,  $J = 8.4, 5.2$  Hz, 1H), 4.31 (td,  $J = 8.4, 5.4$  Hz, 1H), 4.23 (q,  $J = 7.2$  Hz, 1H), 3.97–3.94 (m, 4H), 3.59 (q,  $J = 3.9, 2.9$  Hz, 2H), 3.57–3.46 (m, 33H), 3.42 (t,  $J = 6.0$  Hz, 3H), 3.38 (t,  $J = 5.0$  Hz, 3H), 3.26 (q,  $J = 6.0$  Hz, 3H), 3.15–3.10 (m, 2H), 3.02 (tq,  $J = 19.9, 6.1$  Hz, 8H), 2.91 (dd,  $J = 15.0, 9.4$  Hz, 1H), 2.83 (dd,  $J = 13.9, 8.7$  Hz, 1H), 1.66–1.58 (m, 2H), 1.49 (tdd,  $J = 13.7, 9.9, 5.9$  Hz, 3H), 1.38 (tdd,  $J = 15.6, 11.6, 6.7$  Hz, 5H) (Figure S10). HRMS (ESI): calculated for  $\text{C}_{69}\text{H}_{106}\text{N}_{18}\text{O}_{18}^{2+}$  [ $\text{M} + 2\text{H}$ ] $^{2+}$  737.3961; found 737.3957.

Following the procedure in Section 4.2.2 at a 0.18 mmol scale, **1c** was isolated as a white powder (18.0 mg, 9.9%) (Figure S19).  $^1\text{H}$  NMR (400 MHz, DMSO- $d_6$ )  $\delta$  10.85 (d,  $J = 2.4$  Hz, 1H), 10.78 (d,  $J = 2.4$  Hz, 1H), 8.54 (d,  $J = 7.7$  Hz, 1H), 8.35 (d,  $J = 7.7$  Hz, 1H), 8.14–8.01 (m, 6H), 7.71 (t,  $J = 5.9$  Hz, 1H), 7.66 (d,  $J = 7.8$  Hz, 1H), 7.63–7.55 (m, 2H), 7.33 (dd,  $J = 8.1, 2.7$  Hz, 3H), 7.28–7.19 (m, 7H), 7.17–7.10 (m, 4H), 7.09–7.02 (m, 4H), 6.95 (dt,  $J = 12.8, 7.5$  Hz, 3H), 4.69–4.60 (m, 1H), 4.57 (tt,  $J = 7.6, 3.7$  Hz, 2H), 4.30 (q,  $J = 7.1$  Hz, 1H), 4.18 (td,  $J = 8.2, 5.3$  Hz, 1H), 3.73 (dt,  $J = 11.4, 4.8$  Hz, 1H), 3.53–3.46 (m, 2H), 3.26 (t,  $J = 6.9$  Hz, 2H), 3.18–3.10 (m, 1H), 3.11–2.99 (m, 6H), 2.94 (td,  $J = 15.3, 9.3$  Hz, 2H), 2.83 (dd,  $J = 14.0, 8.8$  Hz, 1H), 1.66 (tt,  $J = 13.7, 6.6$  Hz, 4H), 1.47 (qd,  $J = 13.1, 10.7, 6.3$  Hz, 8H), 1.29 (tt,  $J = 15.4, 6.5$  Hz, 2H) (Figure S11). HRMS (ESI): calculated for  $\text{C}_{49}\text{H}_{67}\text{N}_{18}\text{O}_6^+$  [ $\text{M} + \text{H}$ ] $^+$  1003.5485; found 1003.5492.

Following the procedure in Section 4.2.2 at a 0.21 mmol scale, **2a** was isolated as a white powder (33.6 mg, 12.8%) (Figure S21).  $^1\text{H}$  NMR (400 MHz, DMSO- $d_6$ ):  $\delta$  8.28 (d,  $J = 7.8$  Hz, 2H), 8.09–7.97 (m, 4H), 7.69 (t,  $J = 5.7$  Hz, 1H), 7.61 (t,  $J = 8.2$  Hz, 6H), 7.55 (d,  $J = 8.0$  Hz, 3H), 7.50 (d,  $J = 7.9$  Hz, 3H), 7.45 (qd,  $J = 7.9, 6.3, 1.9$  Hz, 7H), 7.38–7.30 (m, 6H), 7.28 (d,  $J = 8.1$  Hz, 3H), 7.23 (d,  $J = 4.5$  Hz, 6H), 7.18–7.11 (m, 3H), 4.58 (dtd,  $J = 13.2, 8.4, 4.2$  Hz, 2H), 4.50 (td,  $J = 8.2, 5.3$  Hz, 1H), 4.30 (dq,  $J = 14.2, 7.8, 7.3$  Hz, 2H), 3.96 (s, 2H), 3.94 (s, 2H), 3.60–3.54 (m, 3H), 3.50 (ddd,  $J = 14.7, 7.5, 4.0$  Hz, 9H), 3.44–3.33 (m, 5H), 3.24 (q,  $J = 5.9$  Hz, 2H), 3.12–2.97 (m, 8H), 2.84 (dp,  $J = 13.8, 9.3, 7.9$  Hz, 3H), 1.71–1.59 (m, 2H), 1.59–1.31 (m, 7H) (Figure S13). HRMS (ESI): calculated for  $\text{C}_{63}\text{H}_{84}\text{N}_{16}\text{O}_{11}^{2+}$  [ $\text{M} + 2\text{H}$ ] $^{2+}$  620.3247; found 620.3240.

Following the procedure in Section 4.2.2 at a 0.21 mmol scale, **2b** was isolated as a white powder (44.0 mg, 14.7%) (Figure S22).  $^1\text{H}$  NMR (600 MHz, DMSO- $d_6$ ):  $\delta$  8.30–8.26 (m, 2H), 8.06 (d,  $J = 8.2$  Hz, 1H), 8.05–8.02 (m, 2H), 7.99 (d,  $J = 8.1$  Hz, 1H), 7.68 (t,  $J = 5.7$  Hz, 1H), 7.64–7.59 (m, 5H), 7.55 (d,  $J = 8.0$  Hz, 2H), 7.50 (d,  $J = 8.0$  Hz, 2H), 7.44 (ddd,  $J = 15.6, 8.5, 2.5$  Hz, 6H), 7.37–7.32 (m, 5H), 7.28 (d,  $J = 8.0$  Hz, 3H), 7.23 (d,  $J = 5.2$  Hz, 5H), 7.15 (td,  $J = 5.4, 3.0$  Hz, 2H), 7.13 (t,  $J = 2.9$  Hz, 1H), 4.58 (dtd,  $J = 19.2, 8.5, 4.5$  Hz, 2H), 4.50 (td,  $J = 8.3, 5.3$  Hz, 1H), 4.31 (ddt,  $J = 21.4, 14.3, 6.3$  Hz, 2H), 3.96 (s, 2H), 3.94 (d,  $J = 1.7$  Hz, 2H), 3.59 (dtd,  $J = 4.8, 3.5, 2.0$  Hz, 3H), 3.57–3.45 (m, 30H), 3.41 (t,  $J = 6.0$  Hz, 2H), 3.38 (t,  $J = 4.9$  Hz, 2H), 3.27–3.22 (m, 2H), 3.07 (q,  $J = 6.7$  Hz, 3H), 3.04 (d,  $J = 5.0$  Hz, 2H), 3.01 (dt,  $J = 12.7,$

5.8 Hz, 3H), 2.89–2.77 (m, 3H), 1.70–1.61 (m, 2H), 1.59–1.31 (m, 7H) (Figure S14). HRMS (ESI): calculated for  $C_{73}H_{104}N_{16}O_{16}^{2+}$   $[M + 2H]^{2+}$  730.3903; found 730.3900.

Following the procedure in Section 4.2.2 at a 0.18 mmol scale, **2c** was isolated as a white powder (98.0 mg, 50.5%) (Figure S23).  $^1H$  NMR (400 MHz, DMSO- $d_6$ )  $\delta$  8.63 (d,  $J = 7.9$  Hz, 1H), 8.47 (d,  $J = 7.9$  Hz, 1H), 8.28 (d,  $J = 7.8$  Hz, 1H), 8.11 (d,  $J = 7.9$  Hz, 3H), 8.05 (d,  $J = 8.1$  Hz, 1H), 7.76 (t,  $J = 5.8$  Hz, 1H), 7.71 (t,  $J = 5.6$  Hz, 1H), 7.66–7.60 (m, 4H), 7.54 (dd,  $J = 8.3, 2.4$  Hz, 4H), 7.45 (dd,  $J = 8.4, 6.9$  Hz, 5H), 7.39–7.32 (m, 7H), 7.28 (d,  $J = 2.2$  Hz, 2H), 7.26–7.18 (m, 6H), 7.16–7.10 (m, 2H), 7.10–7.05 (m, 1H), 4.70–4.56 (m, 3H), 4.31 (q,  $J = 7.2$  Hz, 1H), 4.19 (td,  $J = 8.2, 5.3$  Hz, 1H), 3.82–3.73 (m, 1H), 3.27 (t,  $J = 6.9$  Hz, 2H), 3.05 (dq,  $J = 18.3, 7.6, 5.9$  Hz, 7H), 2.91–2.76 (m, 3H), 1.66 (qd,  $J = 9.1, 8.6, 3.8$  Hz, 4H), 1.59–1.39 (m, 8H), 1.38–1.23 (m, 2H) (Figure S15). HRMS (ESI): calculated for  $C_{57}H_{73}N_{16}O_6^+$   $[M + H]^+$  1077.5894; found 1077.5907.

#### 4.2.3. Synthesis of Cyclic Azidopeptides

The cyclic azidopeptides were prepared from the fully protected linear analogs assembled on 2-chlorotrityl chloride resin.

Activation and loading of 2-chlorotrityl chloride resin: 2-chlorotrityl chloride resin (1.63 mmol/g, 0.18 mmol scale) was swelled for an hour in DCM. A solution of thionyl chloride (1.2 eq.) was added to the resin under argon and stirred slowly for 2 h before washing the resin thoroughly with DCM. Fmoc-Phe-OH (3.00 eq.) was coupled to the resin with DIPEA (6.0 eq.) in DCM and stirred slowly overnight at room temperature.

Capping, removal of Fmoc, and amino acid coupling: The remaining uncoupled sites were capped with DCM/MeOH/DIPEA (80:15:5, 10 mL) for 30 min. The Fmoc group was removed using a solution of 20% piperidine in DMF. The amino acids (4.0 eq.) were coupled with HBTU (3.92 eq.), HOBT (4.0 eq.), and DIPEA (8.0 eq.) at 70 °C for 5 min (Fmoc-Bip-OH: 15 min) with the exception of Fmoc-Arg(Pbf)-OH and Fmoc-Lys(N<sub>3</sub>)-OH. Fmoc-Arg(Pbf)-OH and Fmoc-Lys(N<sub>3</sub>)-OH were coupled at room temperature for 1 h and 16 h, respectively. After coupling the final amino acid, the N-terminal Fmoc group was removed, and the resin was washed with MeOH and DCM before being left to dry overnight in a desiccator.

Cleavage from the resin and cyclization: Hexafluoroisopropanol (HFIP) in DCM (3:7, 5 mL) was added to the resin and stirred slowly for 45 min. The process was repeated two times. The combined solution was evaporated under vacuum. The resulting peptide was dissolved in 10 mL of DMF, and DIPEA (6.0 eq.) was added. Benzotriazole-1-yl-oxytrispyrrolidino-phosphonium hexafluorophosphat (PyBOP, 3.0 eq.) was dissolved in 200 mL of DMF and stirred rapidly before adding the peptide dropwise. The reaction was monitored by MS until completion. The solvents were evaporated under reduced pressure.

Side-chain deprotection and diethyl ether precipitation: A solution of TFA/TIS/H<sub>2</sub>O (95:2.5:2.5, 10 mL) was added to the peptide and stirred for 3 h. The solvents were evaporated under reduced pressure before ice-cold diethyl ether was added. The precipitate was washed three times with diethyl ether and the crude peptide was purified by RP-HPLC.

Following the procedure in Section 4.2.3 at a 0.18 mmol scale, **1d** was isolated as a white powder (22 mg, 12.3%) (Figure S20).  $^1H$  NMR (400 MHz, DMSO- $d_6$ )  $\delta$  10.74 (d,  $J = 2.3$  Hz, 1H), 10.69 (s, 1H), 8.11–7.96 (m, 4H), 7.90 (d,  $J = 7.7$  Hz, 1H), 7.52 (d,  $J = 7.8$  Hz, 1H), 7.48–7.38 (m, 3H), 7.35 (d,  $J = 5.8$  Hz, 1H), 7.32–7.09 (m, 11H), 7.07 (d,  $J = 2.3$  Hz, 2H), 7.05–6.95 (m, 4H), 6.91 (q,  $J = 7.2$  Hz, 3H), 4.31–4.18 (m, 3H), 3.95 (s, 1H), 3.85–3.73 (m, 2H), 3.22 (td,  $J = 6.9, 1.9$  Hz, 3H), 3.17–3.10 (m, 2H), 3.09–2.85 (m, 9H), 1.70–1.37 (m, 9H), 1.34–1.07 (m, 6H) (Figure S12).

Following the procedure in Section 4.2.3 at a 0.18 mmol scale, **2d** was isolated as a white powder (65 mg, 34.0%) (Figure S24).  $^1H$  NMR (400 MHz, DMSO- $d_6$ )  $\delta$  8.28 (d,  $J = 7.6$  Hz, 1H), 8.20 (q,  $J = 7.5, 6.5$  Hz, 4H), 8.13 (d,  $J = 7.1$  Hz, 1H), 7.67–7.50 (m, 11H), 7.43 (td,  $J = 7.7, 3.1$  Hz, 5H), 7.37–7.24 (m, 10H), 7.24–7.18 (m, 4H), 4.40–4.28 (m, 2H), 4.21 (q,  $J = 7.6$  Hz, 1H), 4.06 (q,  $J = 7.1$  Hz, 1H), 3.92 (q,  $J = 7.1$  Hz, 2H), 3.28 (td,  $J = 6.8, 2.5$  Hz, 2H), 3.25–3.17 (m, 2H), 3.13–2.93 (m, 8H), 1.89–1.44 (m, 9H), 1.27 (tdd,  $J = 27.7, 16.1, 7.1$  Hz,

7H) (Figure S16). HRMS (ESI): calculated for  $C_{57}H_{70}N_{18}O_5^+$   $[M + H]^+$  1060.5628; found 1060.5637.

#### 4.2.4. HPLC

Peptides **1a–b** and **2a–b** were purified using RP-HPLC on a Supelco Ascentis  $C_{18}$  column (10  $\mu$ m, 10 cm  $\times$  21.2 mm, flow rate 7 mL/min) and peptides **1c–d** and **2c–d** were purified using RP-HPLC on a YMC-Triart  $C_{18}$  column (5  $\mu$ m, 20  $\times$  150 mm, flow rate of 11 mL/min) with a mixture of water and acetonitrile (both containing 0.1% TFA) as eluent. The peptides were analyzed by RP-HPLC using a Supelco Ascentis Express  $C_{18}$  column (2.7  $\mu$ m, 10 cm  $\times$  3.0 mm, flow rate of 1 mL/min) and positive ion electrospray mass spectrometry.

#### 4.2.5. Preparation of Au Surface and Copper(I)-Catalyzed Alkyne-Azide Cycloaddition

The Au surfaces were washed with MeOH (50 mL  $\times$  4), dried with  $N_2$ , placed in a UV oven for 20 min, and then washed with Milli-Q<sup>®</sup>  $H_2O$ . A beaker with 25 mL Milli-Q<sup>®</sup>  $H_2O$  and 5 mL ammonia (33% solution) was heated to 75 °C before adding the Au surfaces. After 5 min, 5 mL of hydrogen peroxide was added before simmering for 12 min. Each surface was washed thoroughly with Milli-Q<sup>®</sup>  $H_2O$  before adding 3 mL of an ethanolic solution of HS-PEG-Alkyne (Mw600, 0.08 mg/mL) and left to react overnight at room temperature. The following day, each surface was washed thoroughly with EtOH (5 mL  $\times$  5), and Milli-Q<sup>®</sup>  $H_2O$  (5 mL  $\times$  5) and dried with  $N_2$ . Solutions of the peptides (100  $\mu$ M) in Dulbecco's phosphate-buffered saline (DPBS), ascorbic acid (1 mM) in DPBS, and the copper ( $CuSO_4$ , 150  $\mu$ M) with tris-hydroxypropyltriazolymethylamine (750  $\mu$ M) and HCl (1 mM) in DPBS were prepared. To the tubes with the dried Au surfaces, 700  $\mu$ L of peptide solution, 700  $\mu$ L of copper solution, and 700  $\mu$ L of ascorbic acid solution were added and left to react overnight at room temperature. The control surfaces received 700  $\mu$ L of peptide solution and 1400  $\mu$ L of DPBS.

Upon completion of the copper(I)-catalyzed alkyne-azide cycloaddition, each surface was washed thoroughly with Milli-Q<sup>®</sup>  $H_2O$  (25 mL  $\times$  5) and then dried with  $N_2$ .

#### 4.2.6. Minimal Inhibitory Concentration Determinations

The minimal inhibitory concentration (MIC) of peptides **1a**, **1b**, **2a**, and **2b** were determined by broth microdilution according to the Clinical Laboratory Standard Institute (CLSI) method M07-A9. The MICs of the peptides **1c**, **1d**, **2c**, and **2d** were determined by broth dilution according to the European Committee for Antimicrobial Susceptibility Testing (EUCAST) [45]. Final concentrations of 0.5–256  $\mu$ g/mL were tested against a panel of reference bacteria—*S. aureus* (ATCC 9144), *S. epidermidis* (1457), *E. coli* (ATCC 25922), and *P. aeruginosa* (ATCC 27853).

Each strain was tested in biological triplicate. The MIC values were defined as the lowest concentration of the peptides resulting in no visual growth.

#### 4.2.7. Certika Assay

The Certika assay was adopted from Bruenke et al. [41] Bacterial test strains (200  $\mu$ L,  $1 \times 10^6$  colony-forming units (CFU)  $mL^{-1}$ ) were added to the Au-SAM peptide surface samples and incubated at 37 °C for 1 h to allow bacterial cells to adhere to the sample surface. Loosely bound bacteria were then removed by washing in PBS pH 7.2 for 10 min before the samples were incubated in 200  $\mu$ L of minimum medium (PBS with 1% tryptic soy broth (TSB)) at 37 °C for 18 h (challenge time). After the removal of the test samples, each well was supplemented with 50  $\mu$ L of TSB complete medium. The bacterial growth (of the daughter cells) at 37 °C was recorded every 30 min (readout time, Software KC4 3.4, BioTek) for a period of 48 h by OD measurements in a microtiter plate reader at a wavelength of 578 nm. The onset OD value was defined as 0.2.

#### 4.2.8. ToF-SIMS Mass Spectrometry Imaging

The coupling efficacy/homogeneity was evaluated by imaging mass spectroscopy following the presence of peptide-specific fragments on the surface. The ToF-SIMS analysis was carried out in a ToFSIMS IV instrument (IONToF GmbH, Germany), using 25 keV Bi<sup>3+</sup> primary ions at a pulsed current of 0.1 pA (cycle time 150  $\mu$ s, width 1.2 ns). Each sample was analyzed in the bunched mode at an analysis area of 500  $\times$  500  $\mu$ m<sup>2</sup> (resolution of 256 pixels). The average of 25 scans at an acquisition time of 100 s was used when acquiring data.

Reference spectra of pure peptides were measured by placing a drop of peptide dissolved in EtOH at 1% (*w/v*) on a clean silica wafer. After the evaporation of the EtOH, the peptide was analyzed and specific mass fragments from each peptide were identified, such as arginine (100,09 *m/z*) and tryptophan (130, 07 *m/z*). The distribution of coupled peptides on the Au/PEG/alkyne surfaces was then determined by following the presence of these fragments.

#### 4.2.9. Contact Angle Measurements

The static water contact angle before and after peptide coupling was measured using the sessile drop method. A DSA100 instrument from Krüss GmbH (Hamburg, Germany) was used for the deposition and image evaluation of drop shape. A drop volume of 5  $\mu$ L was deposited using ultrapure and deionized water (resistivity > 18.2 M $\Omega$ <sup>-1</sup> cm) and the drop shape was measured 10 s after surface deposition. The analysis was performed under ambient temperature and humidity. The contact angles were obtained through ten independent measurements (Table S1).

**Supplementary Materials:** The following are available online at <https://www.mdpi.com/article/10.3390/antibiotics10121516/s1>, Figures S1–S8: <sup>1</sup>H NMR spectra of compounds **3a** and **b**, **4a** and **b**, **5a** and **b**, and **6a** and **b**, Figures S9–S16: <sup>1</sup>H NMR spectra of compounds **1a–d**, and **2a–d**, Figures S17–S24: HPLC of compounds **1a–d**, and **2a–d**, Figure S25: Contact angle images of **1a–d** and **2a–d** covalently linked to an Au surface, Figure S26: ToF-SIMS images of **1a–d** covalently linked to an Au surface, Figure S27: ToF-SIMS images of **2a–d** covalently linked to an Au surface, Table S1: Contact Angle of **1a–d** and **2a–d** covalently linked to an Au surface, Table S2: Certika data of **1a–d** and **2a–d** covalently linked to an Au surface, Table S3: Overview of MIC data.

**Author Contributions:** Conceptualization, J.S.M.S. and E.A.K.; methodology, W.S., J.S. and M.B.; validation, E.A.K., W.S. and M.B.; formal analysis, M.B.; investigation, E.A.K. and E.J.; resources, J.S.M.S.; data curation, E.A.K., E.J. and M.B.; writing—original draft preparation, J.S.M.S. and E.A.K.; writing—review and editing, W.S.; visualization, E.A.K.; supervision, J.S.M.S.; project administration, J.S.M.S.; funding acquisition, J.S.M.S. All authors have read and agreed to the published version of the manuscript.

**Funding:** This research was funded by Amicoat AS and the Research Council of Norway, grant number 283272.

**Institutional Review Board Statement:** Not applicable.

**Informed Consent Statement:** Not applicable.

**Data Availability Statement:** The data presented in this study are available in Supplementary Material.

**Acknowledgments:** E.A.K. thanks DigiBiotics for support and scientific guidance. Therese Andersson and Karin Agrenius is acknowledged for laboratory assistance during Certika tests.

**Conflicts of Interest:** The authors declare no conflict of interest.

## References

1. Health Care-Associated Infections FACT SHEET. Available online: [https://www.who.int/gpsc/country\\_work/gpsc\\_ccisc\\_fact\\_sheet\\_en.pdf](https://www.who.int/gpsc/country_work/gpsc_ccisc_fact_sheet_en.pdf) (accessed on 28 November 2021).
2. Centers for Disease Control and Prevention. *Types of Healthcare-Associated Infections*; Centers for Disease Control and Prevention: Atlanta, GA, USA, 2014. Available online: <https://www.cdc.gov/hai/infectiontypes.html> (accessed on 28 November 2021).

3. U.S. Department of Health and Human Services. *National HAI Targets & Metrics*; U.S. Department of Health and Human Services: Washington, DC, USA, 2020. Available online: <https://health.gov/our-work/health-care-quality/health-care-associated-infections/targets-metrics> (accessed on 28 November 2021).
4. U.S. Department of Health and Human Services. *National Action Plan to Prevent Health Care-Associated Infections: Road Map to Elimination*; U.S. Department of Health and Human Services: Washington, DC, USA, 2020. Available online: <https://health.gov/our-work/health-care-quality/health-care-associated-infections/national-hai-action-plan> (accessed on 1 December 2021).
5. Chandki, R.; Banthia, P.; Banthia, R. Biofilms: A microbial home. *J. Indian Soc. Periodontol.* **2011**, *15*, 111–114.
6. Donlan, R.M. Biofilms and device-associated infections. *Emerg. Infect. Dis.* **2001**, *7*, 277–281. [[CrossRef](#)] [[PubMed](#)]
7. Haddadin, Y.; Annamaraju, P.; Regunath, H. *Central Line Associated Blood Stream Infections (CLABSI)*; StatPearls Publishing: Treasure Island, FL, USA, 2019.
8. Weiner-Lastinger, L.M.; Abner, S.; Edwards, J.R.; Kallen, A.J.; Karlsson, M.; Magill, S.S.; Pollock, D.; See, I.; Soe, M.M.; Walters, M.S.; et al. Antimicrobial-resistant pathogens associated with adult healthcare-associated infections: Summary of data reported to the National Healthcare Safety Network, 2015–2017. *Infect. Control. Hosp. Epidemiol.* **2019**, *41*, 1–18. [[CrossRef](#)]
9. Girona-Alarcón, M.; Fresán, E.; Garcia-Garcia, A.; Bobillo-Perez, S.; Balaguer, M.; Felipe, A.; Esteban, M.E.; Jordan, I. Device-associated multidrug-resistant bacteria surveillance in critically ill children: 10 years of experience. *Acta Paediatr.* **2020**, *110*, 203–209. [[CrossRef](#)]
10. Rupp, M.E.; Fitzgerald, T.; Marion, N.; Helget, V.; Puumala, S.; Anderson, J.R.; Fey, P.D. Effect of silver-coated urinary catheters: Efficacy, cost-effectiveness, and antimicrobial resistance. *Am. J. Infect. Control.* **2004**, *32*, 445–450. [[CrossRef](#)] [[PubMed](#)]
11. Montero, D.A.; Arellano, C.; Pardo, M.; Vera, R.; Gálvez, R.; Cifuentes, M.; Berasain, M.A.; Gómez, M.; Ramírez, C.; Vidal, R.M. Antimicrobial properties of a novel copper-based composite coating with potential for use in healthcare facilities. *Antimicrob. Resist. Infect. Control* **2019**, *8*, 3. [[CrossRef](#)]
12. Choi, Y.J.; Lim, J.K.; Park, J.J.; Huh, H.; Kim, D.-J.; Gong, C.-H.; Yoon, S.Z. Chlorhexidine and silver sulfadiazine coating on central venous catheters is not sufficient for protection against catheter-related infection: Simulation-based laboratory research with clinical validation. *J. Int. Med. Res.* **2017**, *45*, 1042–1053. [[CrossRef](#)] [[PubMed](#)]
13. Dave, R.N.; Joshi, H.; Venugopalan, V.P. Novel Biocatalytic Polymer-Based Antimicrobial Coatings as Potential Ureteral Biomaterial: Preparation and In Vitro Performance Evaluation. *Antimicrob. Agents Chemother.* **2010**, *55*, 845–853. [[CrossRef](#)]
14. Trop, M.; Novak, M.; Rodl, S.; Hellbom, B.; Kroell, W.; Goessler, W. Silver-Coated Dressing Acticoat Caused Raised Liver Enzymes and Argyria-like Symptoms in Burn Patient. *J. Trauma Inj. Infect. Crit. Care* **2006**, *60*, 648–652. [[CrossRef](#)]
15. Wan, A.T.; Conyers, R.A.; Coombs, C.J.; Masterton, J.P. Determination of silver in blood, urine, and tissues of volunteers and burn patients. *Clin. Chem.* **1991**, *37*, 1683–1687. [[CrossRef](#)] [[PubMed](#)]
16. Wesgate, R.; Grasha, P.; Maillard, J.-Y. Use of a predictive protocol to measure the antimicrobial resistance risks associated with biocidal product usage. *Am. J. Infect. Control* **2016**, *44*, 458–464. [[CrossRef](#)] [[PubMed](#)]
17. Yazdankhah, S.P.; Scheie, A.A.; Høiby, E.A.; Lunestad, B.-T.; Heir, E.; Fotland, T.; Naterstad, K.; Kruse, H. Triclosan and Antimicrobial Resistance in Bacteria: An Overview. *Microb. Drug Resist.* **2006**, *12*, 83–90. [[CrossRef](#)] [[PubMed](#)]
18. Chuanchuen, R.; Beinlich, K.; Hoang, T.T.; Becher, A.; Karkhoff-Schweizer, R.R.; Schweizer, H.P. Cross-resistance between triclosan and antibiotics in *Pseudomonas aeruginosa* is mediated by multidrug efflux pumps: Exposure of a susceptible mutant strain to triclosan selects nfxB mutants overexpressing MexCD-OprJ. *Antimicrob. Agents Chemother.* **2001**, *45*, 428–432. [[CrossRef](#)] [[PubMed](#)]
19. Costa, F.; Carvalho, I.F.; Montelaro, R.C.; Gomes, P.; Martins, M.C.L. Covalent immobilization of antimicrobial peptides (AMPs) onto biomaterial surfaces. *Acta Biomater.* **2011**, *7*, 1431–1440. [[CrossRef](#)]
20. Riool, M.; De Breij, A.; Drijfhout, J.W.; Nibbering, P.H.; Zaat, S.A.J. Antimicrobial Peptides in Biomedical Device Manufacturing. *Front. Chem.* **2017**, *5*, 63. [[CrossRef](#)]
21. Zasloff, M. Antimicrobial peptides of multicellular organisms. *Nature* **2002**, *415*, 389–395. [[CrossRef](#)]
22. Fjell, C.; Hiss, J.A.; Hancock, R.; Schneider, G. Designing antimicrobial peptides: Form follows function. *Nat. Rev. Drug Discov.* **2011**, *11*, 37–51. [[CrossRef](#)] [[PubMed](#)]
23. Giuliani, A.; Pirri, G.; Nicoletto, S. Antimicrobial peptides: An overview of a promising class of therapeutics. *Open Life Sci.* **2007**, *2*, 1–33. [[CrossRef](#)]
24. Lei, J.; Sun, L.; Huang, S.; Zhu, C.; Li, P.; He, J.; Mackey, V.; Coy, D.H.; He, Q. The antimicrobial peptides and their potential clinical applications. *Am. J. Transl. Res.* **2019**, *11*, 3919–3931.
25. Raheem, N.; Straus, S.K. Mechanisms of Action for Antimicrobial Peptides with Antibacterial and Antibiofilm Functions. *Front. Microbiol.* **2019**, *10*, 2866. [[CrossRef](#)]
26. Assoni, L.; Milani, B.; Carvalho, M.R.; Nepomuceno, L.N.; Waz, N.T.; Guerra, M.E.S.; Converso, T.R.; Darrieux, M. Resistance Mechanisms to Antimicrobial Peptides in Gram-Positive Bacteria. *Front. Microbiol.* **2020**, *11*, 593215. [[CrossRef](#)]
27. Strøm, M.B.; Haug, B.E.; Skar, M.L.; Stensen, W.; Stiberg, T.; Svendsen, J.S. The Pharmacophore of Short Cationic Antibacterial Peptides. *J. Med. Chem.* **2003**, *46*, 1567–1570. [[CrossRef](#)]
28. Francolini, I.; Donelli, G. Prevention and control of biofilm-based medical-device-related infections. *FEMS Immunol. Med. Microbiol.* **2010**, *59*, 227–238. [[CrossRef](#)] [[PubMed](#)]
29. Bagheri, M.; Beyermann, M.; Dathe, M. Immobilization Reduces the Activity of Surface-Bound Cationic Antimicrobial Peptides with No Influence upon the Activity Spectrum. *Antimicrob. Agents Chemother.* **2009**, *53*, 1132–1141. [[CrossRef](#)]

30. Cerruti, M.; Fissolo, S.; Carraro, C.; Ricciardi, C.; Majumdar, A.; Maboudian, R. Poly(ethylene glycol) Monolayer Formation and Stability on Gold and Silicon Nitride Substrates. *Langmuir* **2008**, *24*, 10646–10653. [[CrossRef](#)]
31. Castro, V.; Rodríguez, H.; Albericio, F. CuAAC: An Efficient Click Chemistry Reaction on Solid Phase. *ACS Comb. Sci.* **2016**, *18*, 1–14. [[CrossRef](#)]
32. Tornøe, C.W.; Christensen, C.; Meldal, M. Peptidotriazoles on Solid Phase: [1,2,3]-Triazoles by Regiospecific Copper(I)-Catalyzed 1,3-Dipolar Cycloadditions of Terminal Alkynes to Azides. *J. Org. Chem.* **2002**, *67*, 3057–3064. [[CrossRef](#)]
33. Strøm, M.B.; Rekdal, Ø.; Svendsen, J.S. Antimicrobial activity of short arginine- and tryptophan-rich peptides. *J. Pept. Sci.* **2002**, *8*, 431–437. [[CrossRef](#)] [[PubMed](#)]
34. Haug, B.E.; Skar, M.L.; Svendsen, J.S. Bulky aromatic amino acids increase the antibacterial activity of 15-residue bovine lactoferricin derivatives. *J. Pept. Sci.* **2001**, *7*, 425–432. [[CrossRef](#)]
35. Haug, B.E.; Svendsen, J.S. The role of tryptophan in the antibacterial activity of a 15-residue bovine lactoferricin peptide. *J. Pept. Sci.* **2001**, *7*, 190–196. [[CrossRef](#)] [[PubMed](#)]
36. Haug, B.E.; Stensen, W.; Stiberg, T.; Svendsen, J.S. Bulky Nonproteinogenic Amino Acids Permit the Design of Very Small and Effective Cationic Antibacterial Peptides. *J. Med. Chem.* **2004**, *47*, 4159–4162. [[CrossRef](#)] [[PubMed](#)]
37. Haug, B.E.; Stensen, W.; Svendsen, J.S. Application of the Suzuki–Miyaura cross-coupling to increase antimicrobial potency generates promising novel antibacterials. *Bioorg. Med. Chem. Lett.* **2007**, *17*, 2361–2364. [[CrossRef](#)] [[PubMed](#)]
38. Förch, R.; Schönherr, H.; Jenkins, A.T.A. *Surface Design: Applications in Bioscience and Nanotechnology*; Wiley-VCH: Weinheim, Germany, 2009.
39. Jones, C.W.; Morales, C.G.; Eltiste, S.L.; Yanchik-Slade, F.E.; Lee, N.R.; Nilsson, B.L. Capacity for increased surface area in the hydrophobic core of  $\beta$ -sheet peptide bilayer nanoribbons. *J. Pept. Sci.* **2021**, *27*, e3334. [[CrossRef](#)] [[PubMed](#)]
40. Paulöehrl, T.; Welle, A.; Bruns, M.; Linkert, K.; Börner, H.G.; Bastmeyer, M.; Delaittre, G.; Barner-Kowollik, C. Spatially Controlled Surface Immobilization of Nonmodified Peptides. *Angew. Chem. Int. Ed.* **2013**, *52*, 9714–9718. [[CrossRef](#)] [[PubMed](#)]
41. Bruenke, J.; Roschke, I.; Agarwal, S.; Riemann, T.; Greiner, A. Quantitative Comparison of the Antimicrobial Efficiency of Leaching versus Nonleaching Polymer Materials. *Macromol. Biosci.* **2016**, *16*, 647–654. [[CrossRef](#)] [[PubMed](#)]
42. Dathe, M.; Nikolenko, H.; Klose, J.; Bienert, M. Cyclization Increases the Antimicrobial Activity and Selectivity of Arginine- and Tryptophan-Containing Hexapeptides. *Biochemistry* **2004**, *43*, 9140–9150. [[CrossRef](#)]
43. Herzberg, M.; Berglin, M.; Eliahu, S.; Bodin, L.; Agrenius, K.; Zlotkin, A.; Svenson, J. Efficient Prevention of Marine Biofilm Formation Employing a Surface-Grafted Repellent Marine Peptide. *ACS Appl. Bio Mater.* **2021**, *4*, 3360–3373. [[CrossRef](#)]
44. Flemming, K.; Klingenberg, C.; Cavanagh, P.; Sletteng, M.; Stensen, W.; Svendsen, J.S.; Flaegstad, T.; Flaegstad, T. High in vitro antimicrobial activity of synthetic antimicrobial peptidomimetics against staphylococcal biofilms. *J. Antimicrob. Chemother.* **2008**, *63*, 136–145. [[CrossRef](#)]
45. European Committee for Antimicrobial Susceptibility Testing (EUCAST) of the European Society of Clinical Microbiology and Infectious Diseases (ESCMID). *Determination of minimum inhibitory concentrations (MICs) of antibacterial agents by broth dilution.* *Clin. Microbiol. Infect.* **2003**, *9*, ix–xv.

